



**SAPIENZA**  
UNIVERSITÀ DI ROMA

BIOCHEMISTRY PhD PROGRAMME

CYCLE XXX (2014-2017)

**Unravelling the molecular mechanism of Sorcin  
(SOluble Resistance-related Calcium binding  
proteIN)-dependent resistance to chemotherapeutic  
drugs in cancer and its network of interaction**

**Supervisor**

Dott. Gianni Colotti

**PhD Coordinator**

Prof. Francesco Malatesta

**PhD student**

Ilaria Genovese

## Index

<b>1. Intruduction</b>	<b>5</b>
1.1 Calcium importance in cells and the role of Ca <sup>2+</sup> storages	6
1.2 Sorcin: a Penta EF-hand (PEF) protein that handles calcium intracellular concentration in cells (structure, activation, localization)	10
1.2.1 Sorcin role in cardiomyocytes	22
1.2.2 Sorcin role in brain	26
1.2.3 Sorcin role in cancer and MultiDrug Resistance (MDR)	28
1.3 MultiDrug Resistance	31
1.3.1 MDR1 and its amplicon	36
1.4 Function of doxorubicin and retinoic acid in chemotherapy	40
1.5 Proteomic Peptide Phage Display (ProP-PD): a novel technique to dissect binding motifs and protein-protein interactions (PPIs)	42
<b>2. Aim of the thesis</b>	<b>46</b>
<b>3. Results</b>	<b>51</b>
3.1 Overall structure, calcium coordination and comparison of human sorcin structures: conformational changes induced by calcium binding	52
3.2 Analysis of sorcin solvent-accessible surface areas	56
3.3 Sorcin binds doxorubicin and other chemotherapeutic drugs with high affinity	59
3.4 Crystal structure of the sorcin-doxorubicin complex	62
3.5 Sorcin localization responds to doxorubicin treatment	65
3.6 Effect of sorcin expression on doxorubicin uptake and toxicity, and cell death	66
3.7 Effect of sorcin expression on MDR1 expression and activity	70

3.8 Sorcin binds to Retinoic acid and changes localization	72
3.9 Analysis of N-terminal peptide-sorcin interaction	74
3.10 Phage display selection in presence of EDTA and calcium	75
3.11 Proteomic peptide phage display (ProP-PD) calcium selection and dataset analysis (pipeline)	77
3.12 Mutagenesis of putative crucial residues involved in sorcin-target interaction and binding affinity analysis through SPR and MicroScale Thermophoresis (MST) experiments	88
3.13 Selective calcium-dependent interactions between sorcin and targets	92
Supplementary material	94
<b>4 Discussion</b>	<b>108</b>
<b>5 Conclusion and future perspectives</b>	<b>115</b>
<b>6 Materials and Methods</b>	<b>118</b>
6.1 Cell cultures and western blots	119
6.2 Retinoic Acid, Doxorubicin treatment and silencing for sorcin	120
6.3 Doxorubicin uptake (confocal microscopy and FACS)	121
6.4 Sytox blue assay and cell counts	122
6.5 Sorcin localization, confocal microscopy	123
6.6 Rhodamine 123 incorporation	123
6.7 Differentiation and morphology	124
6.8 Human sorcin wild-type, SCBD and A2C mutant recombinant protein cloning, mutagenesis and purification	124
6.9 Surface Plasmon Resonance (SPR) experiments	126
6.10 Fluorescence titrations	129
6.11 Crystallization, data collection and structure solution and refinement of Apo, calcium-bound and doxorubicin-bound sorcin	130

6.11.1 Apo and calcium-bound Sorcin X-Ray crystal structure	130
6.11.2 Doxorubicin-bound Sorcin X-Ray crystal structure	132
6.12 Combinatorial Phage Display	134
6.13 Proteomic peptide phage display selection	134
6.14 Pooled phage ELISA assay	136
6.15 Clonal phage ELISA and sequencing of binding clones	137
6.16 Data set analysis	138
6.17 Phage clones analysis	140
6.18 Phage clones mutants	140
6.19 Sorcin A2C cysteine labeling with Cy5 and Microscale Thermophoresis (MST)	142
<b>References</b>	<b>145</b>
<b>Acknowledgments</b>	<b>164</b>
<b>List of published papers</b>	<b>165</b>
<b>Attachments</b>	<b>166</b>



# **1.Introduction**

## 1.1 Calcium importance in cells and the role of Ca<sup>2+</sup> storage

Calcium (Ca<sup>2+</sup>) has multifaceted role in cell since it is capable to regulate many biological processes. The versatility of calcium signaling is achieved in several fashions enabling it to operate in a wide dynamic range.

Ca<sup>2+</sup> is involved in cytoskeletal assembly/disassembly, protein folding, cell signaling, vesicle trafficking, muscle contraction, neurotransmission, apoptosis and necrosis etc.; thus its intracellular concentration ([Ca<sup>2+</sup>]<sub>i</sub>) has to be fine-tuned in order to control every cellular process.

[Ca<sup>2+</sup>]<sub>i</sub> at rest is generally kept at about 100 nM concentration, in contrast to the extracellular space and the subcellular compartments or calcium stores, where the concentration of the ion are respectively about 1 mM and 100 μM. For this reason the interplay between these compartments is essential for cell functions (Kaufman RJ et al. 2014).

To this end the cells take advantage of different calcium binding proteins (CaBP) that cooperate to regulate intracellular calcium concentration and to modulate several cellular functions.

Among these proteins there are:

- calcium channels or voltage operated channels (VOCs),
- calcium pumps and exchangers (SERCA, PMCA and Na<sup>+</sup>/Ca<sup>2+</sup> exchangers),
- calcium buffers (parvalbumin, calbinding, calretinin, calsequestin, calreticulin),

-calcium sensors (mostly EF-hand proteins, Calmodulin)

Besides proteins that binds directly this ion, with higher or lower affinity, there are also a large number of cell receptors as G-protein coupled receptors (GPCRs) and protein tyrosine kinase-linked receptors (PTKRs) that are coupled to different isoforms of phospholipase C (PLC), that generates inositol 1,4,5-triphosphate (InsP<sub>3</sub>), able to mobilize calcium as second messenger; as well as calmodulin-dependent kinases (CaMKs) and phosphatases as calcineurin, involved in calcium-dependent cell processes and gene regulation (Berridge MJ, 2011; Berridge MJ 2003).

Therefore it has been largely reported that the unbalance in calcium signaling and intracellular concentration can bring to several diseases, as cardio-pathological and neurodegenerative conditions (Carafoli E. et al, 2003).

The most interesting interplay in the regulation of  $[Ca^{2+}]_i$  is played by subcellular compartments also known as cell calcium storages: in particular, mitochondrion and endo/sarcoplasmic reticulum (ER/SR).

Mitochondria have two membrane layers. The outer membrane is generally more permeable to ions and small molecules and has voltage-dependent anion-selective channels (VDACs), whom role in calcium flux is still under debate, but together with IP<sub>3</sub>-receptors (IP3R) and a protein chaperone called GRP75 can regulate the ion flux between the mitochondrion and ER, through the so called mitochondria-associated membranes (MAMs). MAMs consist of proteins and lipid biosynthetic enzymes connected reversibly to mitochondrion (Vance JE, 2014). They include calcium transfer channels, IP3R, VDAC and the chaperone

GRP75, and allow efficient calcium transfer from ER to mitochondrion (Poston CN et al., 2011).

In contrast, the inner membrane needs specific transporters to ensure the intake of calcium in the matrix, the mitochondrial calcium uniporter (MCU).

The endoplasmic reticulum regulates calcium concentration through a variety of proteins that bind calcium with low affinity but high binding-capacity, i.e. the calcium buffers. These proteins are mostly protein chaperones: calreticulin (CRT), calnexin (CNX), protein disulfide isomerase (PDI), BiP/GRP78.

Ion influx is regulated by the sarco/endoplasmic reticulum calcium ATPase (SERCA), while calcium efflux from the ER can be driven by ryanodine receptors (RYRs) (Kaufman RJ et al. 2014).

The physiological  $[Ca^{2+}]_{ER}$  allows protein folding process to work properly in the ER, and  $[Ca^{2+}]_{mit}$  is essential for the oxidative phosphorylation and mitochondrion bioenergetics; indeed the ion flux between the two compartments is crucial.

Conditions that prevent  $Ca^{2+}$  transfer from the ER to mitochondria include overexpression of anti-apoptotic proteins such as BCL-2 and BCL-XL and constitute survival signaling. In case of protein misfolding, the mitochondrion can be overloaded with calcium, leading to the stimulation of respiration and thus the production of reactive oxygen species (ROS), together with the activation of the pro-apoptotic signal.

As summarized by Kaufman in 2014 (Figure 1) calcium homeostasis is central to all cellular functions and the tuning of its concentration has a pivotal role in the balance between cell survival and death.

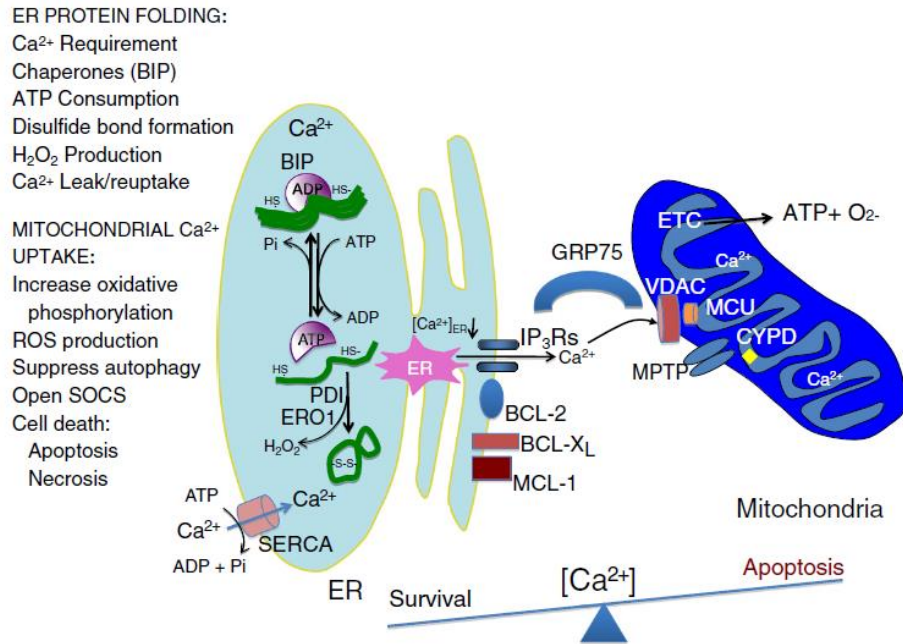


**Figure 1:** Schematic representation of how [Ca<sup>2+</sup>] can influence protein folding in the ER that modulates mitochondrial ATP and ROS production. Protein folding in the ER requires Ca<sup>2+</sup> and ATP for chaperone function. Misfolded proteins may sequester protein chaperones, which facilitate the opening of Ca<sup>2+</sup> channels to initiate Ca<sup>2+</sup> transfer to mitochondria or to stimulate oxidative phosphorylation. Ca<sup>2+</sup> transfer occurs through the activity of several Ca<sup>2+</sup> channels that include the ER localized inositol-1,4,5-triphosphate receptors (IP<sub>3</sub>Rs), as well as the ryanodine receptors (RyRs) and the mitochondrial-localized voltage-dependent anion channel (VDAC) and the mitochondrial Ca<sup>2+</sup> uniporter complex MCU. Once Ca<sup>2+</sup> crosses the outer mitochondrial membrane (OMM), it can cause depolarization of the inner mitochondrial permeability transition pore (MPTP) and induction of apoptotic stimuli. As Ca<sup>2+</sup> accumulates in mitochondria, cells are predisposed to disruption of the electron transport chain (ETC) to produce ROS, Mitochondrial permeability transition pore (MPTP), mitochondrial swelling, disruption of the OMM, release of cytochrome c and apoptosome components leading to caspase activation and apoptosis. Finally, in addition to superoxide production from the ETC, disulfide bond formation mediated by the protein thiol-disulfide isomerases (PDI) and ER oxidase 1 (ERO1) generates hydrogen peroxide upon electron transport to molecular O<sub>2</sub> as the acceptor. The balance between the amount of Ca<sup>2+</sup> stored in the ER lumen and the amount loaded into the mitochondrial matrix may be a determinant in the decision between survival and death. (Kaufman et al.2014)

## **1.2 Sorcin, a Penta EF-hand (PEF) protein that handles calcium intracellular concentration in cells: structure, activation, localization**

The EF-hand is a helix-loop-helix structural motif where the two  $\alpha$ -helices are connected by a loop that contains negatively charged residues, as aspartate and glutamate, to coordinate calcium (Kawasaki H et al., 1995). Canonical EF-hand proteins have a loop of 12 aminoacids and the coordination of the ion takes place with a symmetry of a pentagonal bipyramid. The residues responsible for the coordination of calcium ions are well conserved and correspond to the positions X, Y, Z, -Y, -X, -Z (Figure 2).

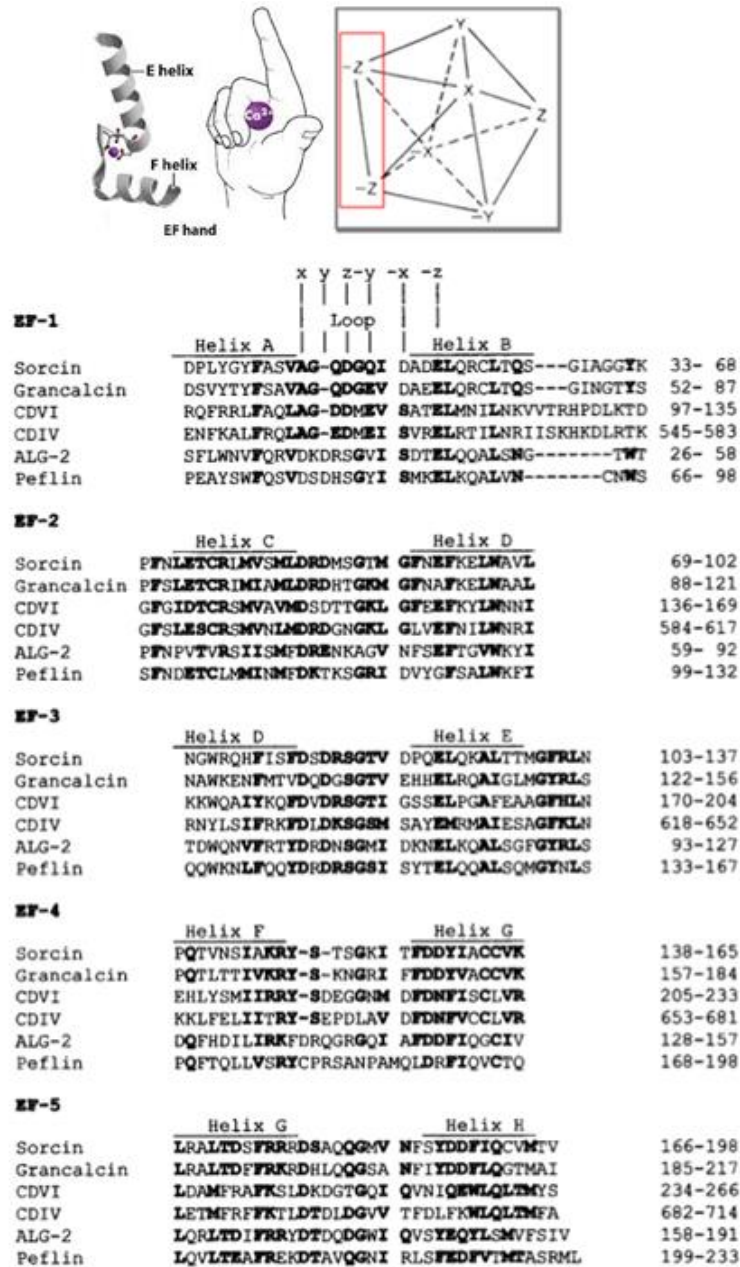


**Figure 2: EF-hand structural motif.** (Top) Schematic representation of the helix-loop-helix EF-hand motif and a scheme of how the coordination of the ion takes place. The residues in the loop are generally conserved among the proteins containing this motif, and generally the -Z positions contain acidic residues (D, E) able to coordinate calcium. (Bottom) The position of these residues is highlighted

on a sequence alignment of Penta-EF hand proteins; identical or similar residues are in bold. (Ilari A et al. 2002).

Usually the proteins that utilize this motif present an even number of EF-hands, that are structurally and functionally paired. The most known example of EF-hand protein is calmodulin (CaM), which has two pairs of EF-hands; an EF-hand couple is located at the N-terminal and another one is at the C-terminal. Both motifs are able to bind calcium, although the C-terminal region has higher affinity for calcium (Meador et al., 1992; Meador et al., 1993; Andersson et al., 1983; Crouch and Klee, 1980).

Sorcin, i.e. SOLuble Resistance-related Calcium binding proteIN, is a small globular 22 KDa protein belonging to the Penta EF-hand (PEF) protein family, able to bind calcium through EF-hand motifs. This family includes: Sorcin, calpains, PDCD6 (or ALG-2), grancalcin and peflin (Maki M., et al. 2002). The PEF proteins are involved in different cellular processes, they exert different functions but they share quite high sequence identity; Sorcin is 30% identical to calpain domain VI, 36% to PDCD6 and 60% to grancalcin. This sequence conservation indicates that these proteins can share a similar overall fold. Besides the sequence and structural similarity, PEF proteins share other common features, as:

- a flexible and hydrophobic Gly/Pro-rich N-terminal domain,
- a C-terminal domain containing the five EF-hand motifs;
- functional and structural pairing occurs in EF1-EF2 hands and EF3-EF4 hands;
- PEF proteins are dimers, in which monomer-monomer association occurs through the unpaired C-terminal EF5 hand;



- PEF proteins share the same mechanism of activation: upon calcium binding, a conformational change occurs enabling the translocation of the protein to the membrane.

The N-terminal domain is often short and flexible, although, in the case of the large subunit of calpains, it can be rather complex, and include a protease domain. The C-terminal, calcium-binding domain, is rather well conserved among the PEF proteins (Figure 3).

```

-----N-terminal domain-----          -A helix-  EF1  -B helix
sorcin      1  -maypghpgagggy---ypgygggap-----ggpafp---gqtQDPLYGYFAAV-AGQDQIDADLQRCL  58
grancalcin  1  -maypyggqgfqnfsiqvpmqmqgpvpbtgpailldgysqpaysdtyssaGDSVYTYPSAV-AGQDGEVDAELQRCL  77
PDCD6      1  maaysyrpq-----pqagppa-----aqaalp-----QSFLWNVQRVDRKDRSGVISDTLQQAL  52
s-calpain  1  -----THYSNIEANE--SEEVQRRLPAQL-AGEDMEVSATELMNIL  40
l-calpain  483 lvpstfepnkdgdfcirvfsekkady--qavddeieanleefdis--DDIDDGVRRLPAQL-AGEDAEISAFELQTIL  556

---          -C helix--  EF2  -----D helix-----  EF3  -E helix-
sorcin      59  TQSGIAGG---YKPFNLETCLMLVSMLDRDMSGTMGFNFKELWAVLNGWRQHFISFDTDRSGTVDPQLQKALTTMGF  134
grancalcin  78  TQSGINGT---YSPFLETCLRIMIAMLRDDHDTGKMGFNAFKELWAALNAWKENFMTVDQDGSSTVEHHLRQAIGLMGY  153
PDCD6      53  S---NCT---WTPFNPTVRSIISMFDRENKAGVNFSEFTGVWYITDWQNVPRTYDRDNSGMIDKNELKALSGFY  124
s-calpain  41  NKVVTRHPDLKTDGFGIDTCRSMVAVMDSDTTGKLGFEEFKYLWNNIKRWQAIYKQFDTRSGTICSSELPGAFEAAGF  119
l-calpain  557  RRVLAKRQDIKSDGFSIETCKIMVDMLSDSGSGLGLKEFYILWTKIQKYQKIYREIDVDRSGTMNSYEMRKALEEAGF  635

-F helix--  EF4  -----G helix-----  EF5  -H helix
sorcin      135  RLSPQAVNSIAKRYSTNGK--ITFDDYIACCVKLRALTDSFRRRDTAQQGVVNFYDDFIQCVMSV-  198
grancalcin  154  RLSPQTLTTIVKRYSKNGR--IPDDYVACCVKLRALTDFFRKRDHLQQSSANFIYDDFLQGTMAI-  217
PDCD6      125  RLSDQFHDLIRKFDRQGRGIAFDDFIQGCIVLQRLTDIFRRYDTDQGWIQVSYEQYLSMVFSIV  191
s-calpain  120  HLNEHLYNMIIRRYSDESG-NMDFNFISCLVRLDAMFRAFKSLDKDGTQIQVNIQEWLQLTMYS-  184
l-calpain  636  KMPQLHQVIVARFADDQL-IDFDNFVRCLVRLETLFKIFKQLDPENTGTELDLISWLCFSVL--  699

```

**Figure 3: Sequence alignment of human PEF proteins of known crystal structures.** Sorcin (NP\_003121), grancalcin (NP\_036330), PDCD6 (NP\_037364), and small and large M-calpain chains are shown. The residues in the N-terminal domain are indicated as lowercase; the residues of the C-terminal calcium binding domain are indicated as uppercase. Structural alignment of EF-hands and of alpha-helices is reported. Glu53, Glu94, Trp99, Trp105, Phe112 and Glu124 are indicated in bold and blue (Colotti et al. 2014).

However, despite the sequence and structural conservation, there is no common mode of information transfer within the PEF family, which exert diverse cellular function, even if an overall mechanism of action can be proposed: upon calcium binding, PEF proteins translocate to the membranes where the proteins usually exhibit their different functions.

The intrinsic ability of the EF-hand motifs to have different binding affinities for calcium make these proteins highly versatile calcium sensors, able to

carry out many different functions and regulate a wide range of cell processes.

To better understand the role of Sorcin in calcium handling in cellular processes it is worthy to better present the relationship between its structure and mechanism of activation, together with its localization in the cell.

### **Sorcin structure and mechanism of activation**

As the name suggest, Sorcin (SOluble Resistance-related Calcium binding proteIN) has been firstly studied for its role in drug resistance in cancer, because of its co-amplification with the pump P-gp (Van der Bliet et al. 1986) and it is well known as a calcium binding protein.

Sorcin gene (*SRI*) is located in the chromosome 7q21 and the transcription gives rise to four alternative isoforms, where the isoform A is the primary transcript, while B, C and D are shorter forms lacking of parts of the N-terminal domain and/or the final residues of the C-terminal domain (Colotti G et al., 2014). It is still unclear whether these different forms can have additional function and localization as reported by Maddalena F. and coworkers (2013) and Landriscina M (2010).

Sorcin is largely distributed among the vertebrates and the sequence conservation appears to be quite high among the species; for example, the mouse protein has just 8 aminoacidic differences compared to the human one. Furthermore, Sorcin can nearly be considered ubiquitous, since it is expressed in every human tissue (MOPED, PaxDb), with particular spikes in brain, heart, bone, B- and T-lymphocytes, monocytes, kidney, breast and skin. It has to be noted that the majority of those tissues require calcium for their physiology and cell signaling.

From a structural point of view, Sorcin belongs to the small family PEF proteins, and it is a homodimer (Xie X. et al., 2001; Ilari A et al., 2002), although heterodimerization with grancalcin is reported (Hansen C et al., 2003).

The first Sorcin structure was solved by Xie X and coworkers in 2001, and it was the calcium-free human protein, obtained at a resolution of 2.2 Å.

Each Sorcin monomer is composed by two domains, i.e. the flexible N-terminal domain (1-32) rich in glycines and prolines residues, and the C-terminal domain (33-198) containing the five EF-hands and thus called Sorcin calcium binding domain (SCBD). Only the last five residues (28-32) of the N-terminal domain appear to be structured in the apo form of the protein (Xie X et al., 2001; Franceschini S et al., 2008). The SCBD has a globular fold and contains 8  $\alpha$ -helices (A-H) which form 5 EF-hand motifs (EF1-5). The EF-hands pair via short  $\beta$ -sheets: EF1 is associated with EF2, EF3 pairs with EF4, and the odd EF5 pairs with another EF5, belonging to another Sorcin monomer, forming a large part of the dimerization interface. The Sorcin dimer is thus the structural protein unit, containing five EF pairs. Helices D and G are long and rigid structures that connect different pairs of EF-hands (helix D belongs to both EF2 and EF3; helix G is part of EF4 and EF5), and serve to propagate the conformational change, induced by the binding of calcium, to the whole protein (Figure 4).

**a** N-terminal domain  
MAYPGHPGAGGGYYPGGYGGAPGGPAFPGQTQ 1-32

C-terminal domain

Helix A EF1 Helix B  
EF1: DPLYGYFAAVAGQDGQIDADELQRCLTQSGIAGG 33-58

Helix C EF2 Helix D  
EF2: YKPFNLETCLMVSMMLDRDMSGTMGFNEFKELWAV 59-101

Helix D EF3 Helix E  
EF3: LNGWRQHFISEDTDRSGTVDPQELQKALTMGFR 102-135

Helix F EF4 Helix G  
EF4: LSPQAVNSIAKRYSTNGKITFDDYIACCVKLR 136-167

Helix G EF5 Helix H  
EF5: ALTDSFRRRDTAQQGVVNFPYDDFIQCVMSV 168-198

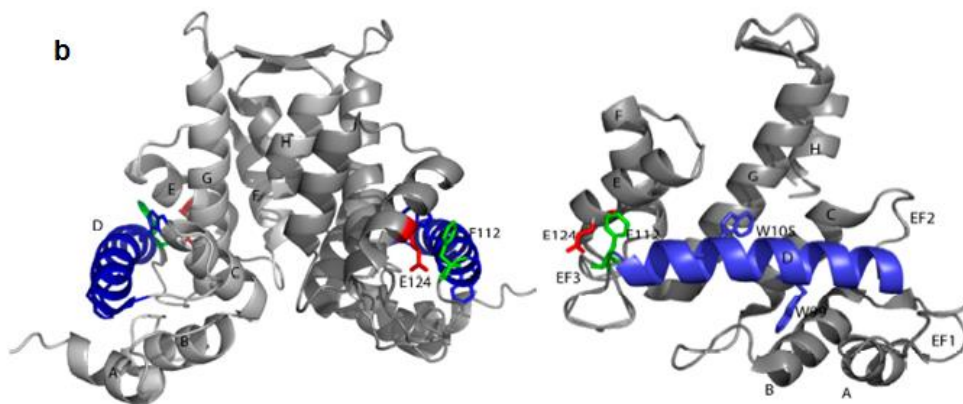


**Figure 4: Sorcin sequence and structure.** (a) Sorcin aminoacidic sequence showing the structural EF-hand motifs in the SCBD and the flexible Pro-Gly-rich N-terminal region. (b) X-ray crystal structure of the human apo-SCBD homodimer (left) vs monomer structure (right) (PDB:1JUO). In both the panels the residues involved in the interactions with targets are colored in blue (Ilari A et al. 2002). The residues mutated to study the mechanism of action of Sorcin are underlined (W99, W105, E53, E94, E124, F112). The D helix is colored in blue as the W residues, while F112 is green and E124 is in red. (Colotti et al. 2014)

SCBD can be divided in two subdomains: EF1-3 (residues 33–134), composed by three EF-hands that bind calcium at micromolar concentration (Mella M et al., 2003), and EF4-5 (residues 135–198), which does not bind calcium with high affinity, but mediates dimerization. Sedimentation

equilibrium analysis showed that Sorcin forms dimers in the absence of calcium (Zamparelli et al. 2000).

In EF-hand proteins, calcium binding determines the transition from a “closed” conformation to an “open” conformation (Kawasaki H et al., 1995). Addition of calcium quenches tryptophan fluorescence (Meyers et al. 1995), indicating that calcium binding produces a conformational change that results in the exposure of buried hydrophobic residues, increases exposure of hydrophobic surfaces and induces aggregation (Zamparelli et al. 1997).

Binding of calcium to EF3, the highest-affinity calcium-binding motif, EF2 and EF1, activates Sorcin: Ca<sup>2+</sup> binding at the EF3 site generates a change in the conformation of the loop containing Glu124, that appears to be crucial, since its mutation alters both calcium affinity and the capability of the protein to interact with targets (Mella M et al., 2003). This conformational change is transmitted then to EF2 via the long and rigid D helix (Ilari A et al., 2002; Franceschini S et al. 2008). The canonical structural coupling between EF2 and EF1 allows information transfer to the N-terminus. These organized movements determine exposure to solvent of hydrophobic residues of the D-helix (in particular Trp99 and Trp105; see Figure 4), of the EF loop and of the G-helix, with a consequent dramatic decrease of solubility, thus allowing Sorcin to translocate from cytosol to membranes, and to bind and regulate a series of target proteins (Franceschini S et al., 2008; Mella M et al., 2003; Colotti G et al., 2006).

It is conceivable that information of Ca<sup>2+</sup> binding to EF3 is transferred to the rest of the molecule by taking advantage of the specific hydrogen-bonding interactions established by the EF3 Ca<sup>2+</sup> binding loop and of the long D helix that connects EF3 to EF2, and in particular by Phe112, located at the end of the D-helix (see Figure 4), whose natural mutant (F112L) disrupts the

hydrogen bonding network provoking alteration in EF3 and EF1 hands (Franceschini S et al., 2008).

Importantly, the long D helix contains the two tryptophan residues of the protein. Trp99 is close to the EF2 Ca<sup>2+</sup>-binding loop (4 Å), whereas Trp105 is close to EF3 (7 Å), one and one-half helical turns apart from Trp99. The side chain of Trp99 lies on the outer surface of the SCBD, in contact with residues that join N-terminal and C-terminal domains, whereas the Trp105 side chain points toward the core of the SCBD, where it interacts primarily with residues of the D and G helices (see Figure 4). The different localization of the two tryptophan residues within the D helix and the different type of interactions they establish suggest that their substitution may affect differently the functional coupling of EF3 and EF2 and the interaction with target proteins. In particular, Trp105 is involved in the network of hydrophobic and hydrogen bonding interactions thus expecting to render this residue of highly important for the transmission of the Ca<sup>2+</sup>-dependent conformational change. This was confirmed with Trp105Gly mutagenesis experiments, whereas mutation of solvent-facing Trp99 has little effect. In both cases, Ca<sup>2+</sup> affinity is substantially unaltered in the two mutants with respect to the wild-type protein (Colotti et al., 2006).

Further details of Sorcin structure for the prediction of its mechanism of activation and the modulation of its activity were obtained by Ilari et al. in 2002, with the resolution of the crystal structure of apo-SCBD. The study provided insights into the phosphorylation, dimerization and tetramerization processes specific to Sorcin and confirms the general characteristics of the PEF family. The association of the EF5 hands through the G and H helices of two monomers forms a four-helix bundle, while the loops between them give rise to an antiparallel  $\beta$ -sheet. The interface thus created buries about 20% of

the surface of each monomer and the dimer interface is stabilized primarily by hydrophobic interactions between side-chains, which include three phenylalanine residues of both subunits (Phe186, Phe191, Phe173).

### **Sorcin Localization**

Sorcin is a globular cytosolic protein and, as mentioned before, can dynamically localize to membranes upon calcium binding. From databases annotated information (MOPED, PaxDb) it is known that Sorcin is one of the most expressed calcium-binding proteins, and is ubiquitously expressed in human tissues, with particularly high expression levels in those tissue that require calcium for their working principles; as brain, heart, bone, kidney etc. Furthermore, Sorcin is overexpressed in several tumors, especially those who resist to chemotherapy (see below).

Speaking of its dynamic localization, it was reported by Lalioti VS and collaborators in 2014 that Sorcin changes its localization throughout the mitosis and links calcium signaling to vesicle trafficking in cells. In detail, during the interphase Sorcin localizes in the nucleus, in the cytosol, in the plasma membranes, at the endoplasmic reticulum (ER) and in ER-derived vesicles localized along the microtubules, whereas during mitosis, it concentrates in the cleavage furrow during late telophase, and at the midbody before cytokinesis (Lalioti VS et al., 2014). These ER-derived vesicles also contain RyRs, SERCA, calreticulin and Rab10. In addition, as mentioned, an 18 kDa Sorcin variant has been found to be localized at the mitochondrion, probably exerting anti-apoptotic function (Landriscina M et al., 2010; Maddalena F et al., 2013).

In the cytosol Sorcin is engaged as a calcium sensor, with the role of keeping the  $[Ca^{2+}]_i$  in the range of 10-100nM cooperating with pumps, channels and other proteins involved in calcium buffering.

Sorcin takes part to the regulation of calcium homeostasis in different fashions, since it binds the ion itself at micromolar range (Mella M et al., 2003; Zamparelli C et al., 2000), and upon calcium binding it can bind calcium channels and pumps, regulating them. Indeed Sorcin is able to interact with RyR and SERCA, located in the ER, and with L-type calcium channel and  $Na^+-Ca^{2+}$  exchangers (NCX), located in the plasma membrane, regulating them (Meyers MB et al., 1995; Lokuta AJ et al., 1997; Seidler T et al., 2003; Matsumoto T et al., 2005, Zamparelli C et al., 2010). In particular, Sorcin increases calcium accumulation in the ER by activating SERCA and by inhibiting RyR (see also below) (Figure 5), increases dimensions and calcium load of ER-derived vesicles, and is also able to increase mitochondrial calcium concentration (Lalioti VS et al., 2014; Suarez J et al., 2013).



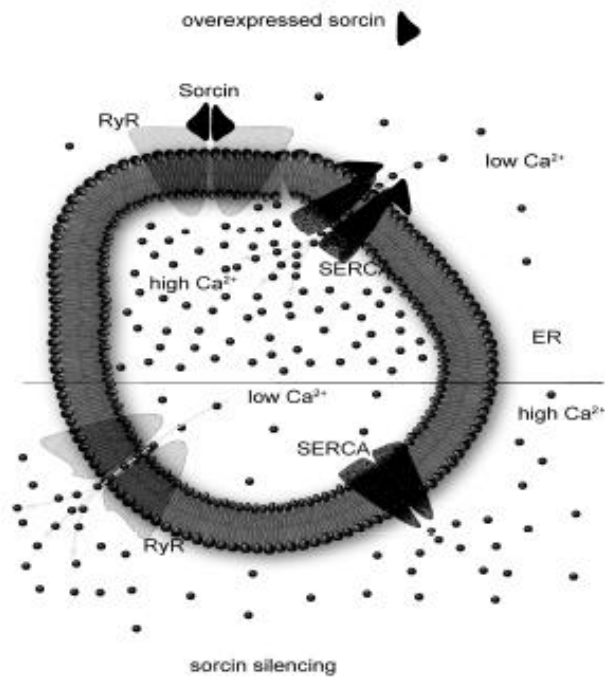


**Figure 5: Schematic representation of Sorcin  $[Ca^{2+}]_i$  regulation.** When Sorcin is upregulated it can activate SERCA pumps and inhibit RYRs increasing calcium concentration in the ER lumen; while if Sorcin is silenced,  $Ca^{2+}$  storage in the ER lumen is decreased (Colotti et al.,2014).

Therefore high Sorcin expression increases ER calcium concentration, in this way it can prevent ER stress and the unfolded protein response, and increases escape from apoptosis (Lalioti VS et al., 2014; Maddalena F et al., 2013, Maddalena F et al., 2011). On the contrary, Sorcin silencing activates apoptotic proteases as caspase-3, caspase-12 and GRP78/BiP (Maddalena F et al., 2011), results in severe defects in mitosis and cytokinesis, blocks cell cycle progression in mitosis, increases the number of rounded polynucleated cells and induces apoptosis and cell death (Lalioti VS et al., 2014).

As a multifaceted protein it can also interact with serine-threonine kinases, which participate in the regulation of mitosis progression (Lalioti VS et al., 2014). Sorcin contains several potential phosphorylation sites and

phosphorylation contributes to regulate Sorcin activity. Sorcin can be phosphorylated by Polo-like kinase 1 (Plk1), induces Plk1 autophosphorylation, and contributes to Plk1 regulation (Lalioi VS et al., 2014). Also cAMP-dependent protein kinase (PKA) and calcium-calmodulin dependent kinase II (CaMKII) phosphorylate Sorcin (Ilari A et al., 2002; Anthony DF et al., 2007), altering its binding to RyRs and SERCA, and therefore calcium homeostasis.

Sorcin has been found in other vesicles than the ER-dependent ones, as such: nanovesicles containing Annexin A7, released in a calcium-dependent fashion from the erythrocytes (Salzer U et al., 2002), and in exosomes from different sources, such as B-cell exosomes (Buschow SI et al., 2010), mesenchymal stem cell exosomes (Lai RC et al., 2011), exosomes from human urine (Pisitkun T et al., 2004; Gonzales PA et al., 2004).

Furthermore, it has been reported that Sorcin binds and sequesters the carbohydrate-responsive element binding protein (ChREBP) in the cytosol at low glucose concentration, by interacting with the N-terminal glucose-sensing domain of ChREBP (Noordeen NA et al., 2012). Following glucose stimulation and calcium influx, Sorcin releases ChREBP, which becomes free to translocate to the nucleus.

### **1.2.1 Sorcin role in cardiomyocytes**

Sorcin role was first dissected in tissues or cells with calcium-dependent functions, as heart and cardiomyocytes.

Given the importance of  $\text{Ca}^{2+}$  in the excitation-contraction-relaxation processes, it has been crucial to characterize how calcium was mobilized between cytoplasm, calcium intra-cellular storages and extra-cellular space during the process. Indeed in the cardiomyocyte the alteration of calcium

homeostasis is the primary cause of arrhythmia and contractile dysfunctions in physio-pathological conditions.

Sorcini acts as a regulator of the contraction-relaxation process in cardiomyocytes, due to its calcium sensing capability and the ability to bind calcium channels, exchanger and pumps in a calcium-dependent manner, and to regulate them.

Heart contraction is a complex and fast process. Located in the wall of the right atrium is a group of specialized cells, called the sinoatrial node. These cells, unlike most other cells within the heart, can spontaneously produce action potentials. These action potentials travel along the cell membrane (sarcolemma), as impulses, passing from one cell to the next through channels, in structures known as gap junctions. The speed of conduction of the action potential varies at different parts of the heart, and once the atria have contracted, there is a slight delay, which enables the ventricles to fill with blood before they contract. Certain regions of the sarcolemma penetrate deep into the cell. These are known as transverse-tubules (T-tubules), also found in skeletal muscle cells, and allow for the action potential to travel into the centre of the cell. Upon the action potential triggers the wave of depolarization reaches a cardiomyocyte, voltage-dependent  $\text{Na}^+$  channels open, which results in a rapid cell depolarization. During depolarization, calcium enters the cell via voltage-dependent  $\text{Ca}^{2+}$  channels (VOCC, mainly L-type channels). L-Type  $\text{Ca}^{2+}$  channels are located primarily in the T-tubule, in the dyadic space, juxtaposed to sarcoplasmic reticulum (SR) calcium release channels, the ryanodine receptors (RyRs). Calcium entry via VOCC and locally increases  $\text{Ca}^{2+}$  concentration near RyRs, triggering  $\text{Ca}^{2+}$  release from the SR, a specialized calcium store similar to ER. This calcium-activated process is called calcium-induced calcium release (CICR). The  $\text{Ca}^{2+}$

flux further raises the free  $[Ca^{2+}]_i$ , allowing the binding of the ion to troponin C thus triggering the contraction.

To stop the stimulus and let the relaxation occur, cytosolic  $[Ca^{2+}]$  has to decrease, allowing calcium dissociation from the myofilaments. Thus, RyR has to be closed, and calcium has to be transported out of the cytosol, mainly via the SERCA pumps, which brings  $Ca^{2+}$  back into the SR, the sarcolemmal  $Na^+/Ca^{2+}$  exchanger (NCX) and mitochondrial  $Ca^{2+}$  uniporter (MCU) (Bers DM et al., 2006) (Figure 6).

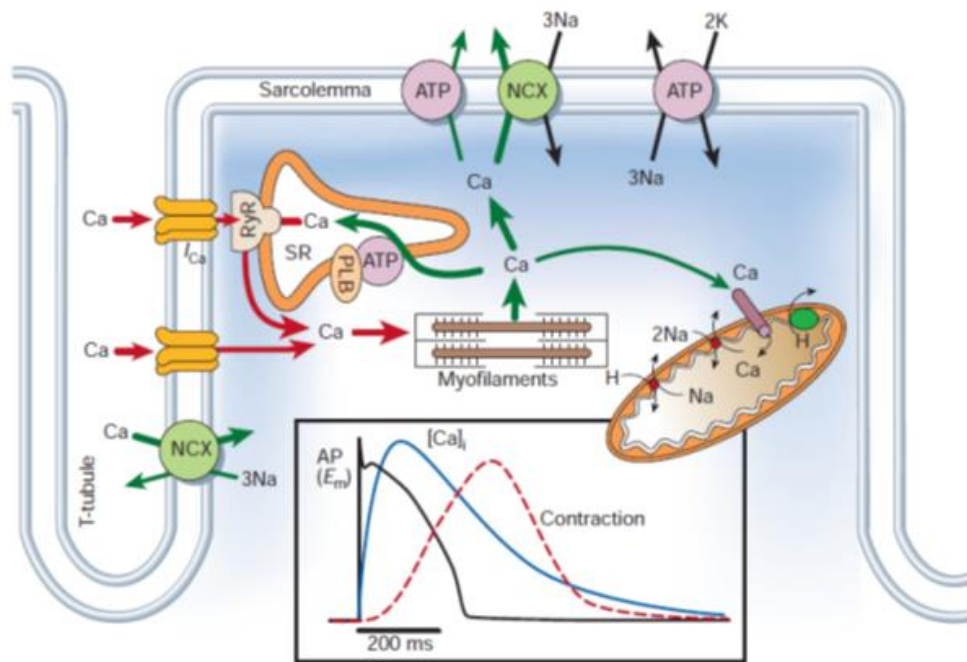


**Figure 6: Schematic representation of excitation-contraction-relaxation coupling in cardiomyocytes.** The red arrows represent the calcium fluxes activated upon contraction stimulus and depolarization. The green arrows represent the calcium fluxes activated once the contraction occurs on myofilaments and intracellular calcium concentration has to be restored. The panel in the figure puts together the wave of the action potential during the depolarization, followed, in a time-scale of 200 msec, by the increase of  $[Ca^{2+}]_i$  and subsequently the contraction event.

Sorcin plays a crucial role in the regulation of cardiac contraction, being able to interact with all the main calcium channels-exchangers, above mentioned, and to regulate them. Sorcin modulates the L-type VOCC, by interacting with its alpha-1C subunit with its SCBD, slowing  $\text{Ca}^{2+}$ -dependent inactivation and stimulating voltage-dependent inactivation of the calcium currents of the channel (Fowler MR et al., 2008 2009).

Moreover, Sorcin is able to interact with RyR2, the cardiac isoform, and to strongly inhibit it, in a calcium-dependent manner (Lokuta AJ et al., 1997; Farrell EF et al., 2003). In the cardiomyocyte, such RyR inhibition takes place when the local calcium concentration at the surface of SR is increased by CICR from the calcium store, bringing a decreased localized calcium release events and reducing global calcium transients. Sorcin reduces calcium flow from RyR2 by decreasing the mean open time and the frequency of open event (Franceschini S et al., 2008; Lokuta AJ et al., 1997; Farrell EF et al., 2003).

On the other hand Sorcin also interacts with SERCA, activating it (Matsumoto T et al. 2005). All these interactions make Sorcin able to increase calcium intake of SR and to determine negative regulation of its release, in a dose-dependent and calcium-dependent fashion. Sorcin also activates NCX through a calcium-dependent interaction of the respective C-terminal domains. It has been reported that the overexpression of Sorcin in cardiomyocytes has also been associated with increased activity of the  $\text{Na}^+$ - $\text{Ca}^{2+}$  exchanger (Seidler T et al., 2003; Zamparelli C et al., 2010).

Overall, Sorcin regulates the excitation-contraction-relaxation process in the heart, by terminating the calcium-induced calcium release by the SR, and favoring relaxation, by decreasing the cytosolic calcium concentration, with at least three different modalities:

- it inhibits calcium release from the SR by inhibiting RyR2,
- it increases calcium uptake to SR by activating SERCA2a,
- it enables calcium extrusion from the sarcolemma by increasing NCX activity.

As mentioned in the previous section phosphorylation by PKA alters  $\text{Ca}^{2+}$  sensitivity of Sorcin and calcium-dependent interaction with RyR2. Moreover, in the failing heart, Sorcin is found hyper-phosphorylated and translocation to the SR membrane is increased, suggesting a preservation of the SR  $\text{Ca}^{2+}$  content together with an improved cardiac relaxation (Lokuta AJ et al., 1997; Matsumoto T et al., 2005; Maddalena F et al., 2011).

The natural mutant Phe112Leu in Sorcin EF3-hand was associated with hypertrophic cardiomyopathy and hypertension. This mutation, as described in the previous section, decreases the ability of Sorcin to interact with its cardiac targets and to negatively regulate calcium storages release, resulting in complex cardiac alterations (Franceschini S et al., 2008; Collis LP et al., 2007).

Sorcin overexpression in mice is associated with an increase in cardiac contractility of the normal heart and with a dramatic rescue of the abnormal contractile function of the diabetic heart; this might be explained with the improved calcium transient found in cardiomyocytes upon Sorcin overexpression (Frank KF et al., 2005; Suarez J et al., 2004)

### **1.2.2 Sorcin role in the brain**

The expression level of Sorcin in the brain is quite high, i.e. about 5-10 times higher than that in the heart. Particularly Sorcin is well expressed in the amygdala, in the prefrontal cortex, in the hypothalamus as well as in many

brain cancers (GeneAtlas U133A, gcrma); Sorcin was found as one of the most expressed calcium-binding proteins in these tissues.

Sorcin is considered a histological marker for malignant glioma (Yokota T et al., 2006), and is one of the most expressed proteins in anaplastic astrocytoma, oligodendroglioma and glioblastoma (French PJ et al., 2005; Shai R et al., 2003; Sun L et al., 2006). Moreover Sorcin has been found as one of the main markers of poor outcome in embryonal tumors of central nervous system (Pomeroy SL et al., 2002).

Besides, dysfunction of calcium-mediated signaling has been implicated in many neurodegenerative diseases including Alzheimer's disease (AD) and Parkinson disease (PD), where it was found that perturbed ER calcium homeostasis, ER stress, and the consequent accumulation of unfolded protein, are involved in the accumulation of misfolded proteins, etiology of these pathologies. As mentioned, Sorcin is able to interact directly with RyR and SERCA (inhibiting RyR and activating SERCA), thus maintaining calcium load in ER; this feature could possibly be linked to the ability of Sorcin to decrease the unfolded protein response in the brain. Several studies reported alteration in regulation and function of RyR in human AD-affected brains, in brains of transgenic AD mice models and in cells expressing familiar AD-linked mutation to  $\beta$  amyloid precursor protein ( $\beta$ APP) and presenilins (Del Prete D et al., 2014), suggesting a possible implication of Sorcin. Moreover Sorcin directly interacts in a calcium-dependent fashion with alpha-synuclein (AS) and presenilin 2 (PS2), two proteins involved in the pathogenesis of PD and AD, respectively, *in vitro*, in cultured cells and in human brain (Pack-Chung E et al., 2000; Woods WS et al., 2007). Sorcin binds to the C-terminal region of PS2, a protein whose interaction with RyR upon calcium binding

and regulation of calcium homeostasis in the cells has been reported (Takeda T et al., 2005).

In addition, Sorcin is overexpressed in a PD cell model induced by 1-methyl-4-phenylpyridinium ion (MPP<sup>+</sup>) in SH-SY5Y cells (Xie H et al., 2011), and is one of the most differentially expressed proteins in PD vs. normal human substantia nigra (Werner CJ et al., 2008). Sorcin interacts with the N-methyl-D-aspartate receptor 1 in caudate-putamen nucleus (Gracy KN et al., 1999). Further, it interacts with annexins A7 and A11, which affect functions of primary astrocytes (Clemen CS et al., 2003).

### **1.2.3 Sorcin role in cancer and MultiDrug Resistance (MDR)**

Sorcin was firstly isolated by Meyers and Biedler in 1981 as a soluble, low molecular weight protein in hamster lung cancer cell line resistant to vincristine, and this feature was used to give Sorcin the name now used (Meyer MB and Biedler JL 1981).

As aforementioned, Sorcin exerts several biological functions, as binding and regulating Ca<sup>2+</sup> pumps and channels playing a key role in calcium sensing, being phosphorylated by several kinases involved in cell cycle progression or calcium homeostasis, regulating calcium load in storage organelles and vesicle trafficking. Beside all these calcium-related processes, it has been largely reported throughout the years that Sorcin is overexpressed in many cancer types, especially the ones with a MultiDrug Resistance (MDR) phenotype (see below).

MDR is the major cause of chemotherapy failure and this phenotype in cells can arise in different fashions, that will be further dissected in the following section.



One of these features is the increased expression of energy-dependent ABC (ATP binding cassette) transporters, that results in an increased extrusion of the drugs outside the cell.

*Sorcin* (*SRI*) gene, located in chromosome 7, shares the same amplicon with other genes, some of them involved in resistance to chemotherapeutics as ABC transporters, as such: ABCB4 and ABCB1 (Mdr1, or P-glycoprotein P), both in humans and rodent genomes.

These energy-dependent pumps have a broad substrate specificity and they are physiologically engaged in the extrusion of xenobiotics out of the cell, and they are reported to be overexpressed in cancer cells that develop resistance towards different chemotherapeutic drugs.

Sorcin was identified as resistance-related because its gene was co-amplified with P-glycoproteins in cancer cells with MDR phenotype (Van der Blik AM et al., 1986). For years Sorcin overexpression was thought to be an accidental by-product of this co-amplification process (Van der Blik AM et al., 1988). Sorcin is found overexpressed in many human tumors, as: lymphoma, leukemia, gastric cancer, lung cancer, adenocarcinoma, breast cancer, nasopharyngeal cancer and ovarian cancer, particularly in the MDR cancers (Deng L et al., 2010; Padar S et al., 2004; Qi J et al., 2006; Qu Y et al., 2010; Tan Y et al., 2003; Yamagishi N et al., 2014; Yang YX et al., 2014; Zhou Y et al., 2006).

Lately many studies have dissected the role of Sorcin in MDR cancer types, indicating its role as an oncoprotein. For example, in K562/A02 leukemia doxorubicin-induced resistant cell lines Sorcin was found consistently up-regulated compared to the parental cell line, and the overexpression in resistant line conferred MDR phenotype. Furthermore leukemia cell lines showed an up-regulation in anti-apoptotic and survival pathways and a

decrease in the pro-apoptotic ones (Qi J et al., 2006). The level of Sorcin expression in leukemia patients generally correlates with patients low-response to chemotherapies and poor prognosis.

Moreover Sorcin overexpression by gene transfection resulted in increased drug resistance to a variety of chemotherapeutic agents, including doxorubicin, etoposide, homoharringtonine and vincristine in K562 cells; and determined drug resistance to vincristine, adriamycin, taxol and 5-fluorouracil in SGC7901 cells, ovarian and breast cancer; confirming the ability to generate additional drug resistance. On the contrary the inhibition of Sorcin expression by Sorcin-targeting RNA interference techniques led to reversal of drug resistance in the following cell lines: MDR K562/A02 and Sorcin-transfected K562; MCF-7/A02; HeLa; colorectal cancer; and CNE2/DDPIs (Zhou Y et al., 2006; Hamada H et al., 1988; He Q et al., 2011; Hu Y et al.; 2013; Kawakami M et al., 2007; Liu X et al., 2014; Parekh HK et al., 2002).

Sorcin silencing inhibits the epithelial-to-mesenchymal transition in the breast cancer MDA-MB-213 cell line, possibly via E-cadherin and VEGF expression, and reduces breast cancer metastasis, while Sorcin overexpression increases migration and invasion *in vitro* (Hu Y et al., 2014). Even though this findings demonstrate that Sorcin is clearly a marker of MDR and may represent a therapeutic target for reversing tumor multidrug resistance, conflicting results are still present in literature on the effect of Sorcin overexpression and silencing on MDR1 expression and activity (see Lee WP et al., 1996; Wang SL et al., 1995; Xu P et al., 2015; Yamagishi N et al., 2014) and many efforts still have to be done to understand the molecular mechanism that make Sorcin a crucial actor in cancer cells with MDR phenotype.

Several groups are currently studying Sorcin role in the development of MDR in cancer cells, disclosing intriguing findings.

Yamagishi and his collaborators found that Sorcin expression correlates with ABCB1 up-regulation; in fact Sorcin induces ABCB1 expression through cAMP response element (CRE) situated within -716 and -709 basepairs of *mdr1* gene. Additionally they found that Sorcin up-regulation induces ABCB1 expression through the activation of CREB (cAMP response element-binding protein) pathway increasing the phosphorylation of CREB1 and its binding to the CRE sequence on *mdr1* promoter (Yamagishi N et al., 2014).

A shorter isoform (18KDa) of Sorcin, identified as mitochondrial, is the object of the quality control operated by ER-associated TRAP1. This protein is up-regulated in several human tumors and can modulate apoptosis; indeed transfection experiments of TRAP1 deletion mutant in TRAP1-silenced cells increases the expression of mitochondrial Sorcin and protects from apoptosis upon treatment with ER stress agents and paclitaxel (Maddalena F et al., 2013).

Sorcin thus participates in the prevention of ER stress and of the unfolded protein response, and increases escape from apoptosis (Lalioi VS et al., 2014; Maddalena F et al., 2013; Maddalena F et al., 2011), shifting the equilibrium between cell life and cell death towards proliferation in MDR cancer cells overexpressing Sorcin.

### **1.3 MultiDrug Resistance**

MultiDrug Resistance (MDR) is the ability of cells to develop resistance to several pharmaceutical treatments. This process was firstly discovered in bacteria, where the strategy is exploited to resist to antibiotics. Even though

some mechanisms of drug-resistance are disease-specific, cancer cells and bacteria share drug efflux among these mechanisms, suggesting its highly evolutionary conservation (Housman G et al., 2014).

MDR appears to be the major cause of chemotherapy failure and subsequent cancer relapse after surgical removal. This happens because there are two types of MDR development (Longley DB and Johnston PG 2005; Holohan C et al., 2013):

- Intrinsic resistance (before receiving chemotherapy), due to pre-existing resistance-mediating factors in the bulk of tumor cells, that impede the effectiveness of the drugs;
- Acquired resistance (after receiving chemotherapy), caused by mutations and/or increase of adaptive response, ranging from increasing expression of therapeutic targets to activation of alternative pathways.

An additional feature to this scenario is cell heterogeneity, inherent in tumors, that permits the co-existence of different cell populations at the same time (including the above mentioned) and is involved in the development of drug resistance.

Recent studies report that inside a cancer heterogeneous population, some cells with stem cell properties are drug-resistant, but also a small fraction of adult cells might have this ability. Since the treatment affects only the sensitive population, the drug-resistant cell pools survive and possibly spread to other organs, making the treatment ineffective (Housman G et al., 2014).

Focusing our attention on cancer cells, there are several mechanisms by which cells can develop MDR (Figure 7):

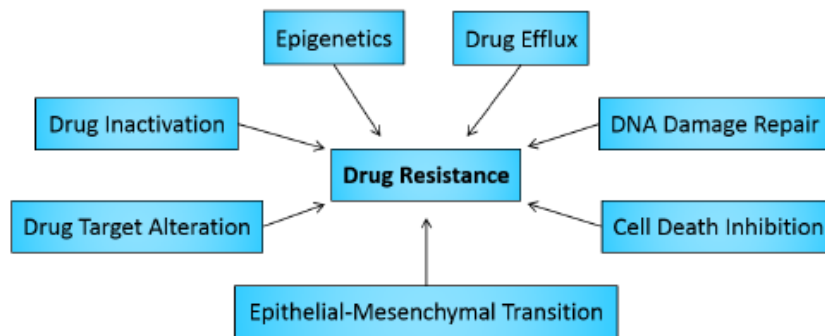


**Figure 7: Summary of mechanisms activated in the development of Drug resistance.** These mechanisms can promote direct or indirect MDR and can act independently or together, through various signal transduction pathways (Housman G et al., 2014).

In details,

(i) *Drug inactivation*: in some cases the drug undergoes a process of activation in vivo, that includes the collaboration of different proteins to modify, partially degrade, and/or complex the drug to other molecules or proteins. Many drugs need this activation to be effective on tumors, thus one of the resistance-strategies engaged is the decrease or block of drug activation mechanisms.

(ii) *Drug target alteration*: the effectiveness of the therapy depends on its target as well; for this reason some tumors develop mechanisms of alteration of the drug targets, as mutation or changes in their expression levels.

(iii) *DNA damage repair*: many drugs can act directly or indirectly on DNA stability, so the DNA damage response (DDR) can reverse the damage induced by the therapy. Indeed the effectiveness of a cytotoxic DNA-damaging drug strictly depends on the inefficacy of DDR. To this end a combined therapeutic strategy of inhibition of damage response effectors together with the DNA-damaging drugs can increase the sensitivity and thus the efficacy of the therapy.

(iv) *Cell death inhibition*: in many cancer types anti-apoptotic proteins (BCL-2 proteins, Akt etc.) are overexpressed and their downstream transcription modulators (STAT, NFκB) are highly active, leading to the cell death escape. However, these can represent good targets to revert drug resistance. Autophagy can contribute to cell death as well; it is exerted by phagolysosomal death at acidic pH. Some drugs, as chloroquines, can raise the pH in the lysosome, preventing this process to occur and inactivating digestive enzymes in the lysosome.

(v) *Epithelial-mesenchymal transition (EMT) and metastasis*: the EMT is a complex mechanism by which tumor cells can develop metastasis. A change in cancer cells, stromal cells and the microenvironment occur, where the expression pattern of cell adhesion receptors, integrins and cadherins changes. The attention on this aspect in the development of drug resistance is increasing (Shang Y et al., 2013; Singh A et al., 2010).

Some studies focus the attention on cancer stem cells, i.e. the cell population that initiate the metastatic event, that survive the surgical removal or chemotherapy (Chaffer C et al., 2011; Chaffer C et al., 2011; Sarkar S et al., 2013; Byler S et al., 2014; Byler S and Sarkar S 2014), and on the signaling process activated during differentiation, essential for EMT to occur (Bates RC et al., 2015); both mechanisms can lead to MDR.

Stromal cells may play an important role as well. Recent findings on drug resistance in cancer-fibroblast co-cultured cells indicates their involvement in MDR and may explain the failure of the therapy in animal model despite cultured tumor cells (Staussman R et al., 2012).

(vi) *Epigenetics*; the role of epigenetics in carcinogenesis and drug-resistance has been investigated recently. Epigenetic modifications occur on DNA binding proteins, the histones, that govern the degree of DNA coiling to facilitate or inhibit DNA transcription. The modifications consist in the addition of certain chemical groups on specific aminoacidic residues of histones; these are mainly acetyl and methyl groups, that usually correspond to an activation and repression of transcription, respectively.

Recent findings showed that epigenetic modifications can influence resistance development. As reported by Kantharidis and collaborators, the demethylation of MDR1 promoter is strongly correlated to increase of drug resistance in cancer cells (Kantharidis P et al., 1997). It has been proposed that demethylation associated to the re-expression of tumor suppressor genes make resistant cancer cells sensitive to cytotoxic agents (Sarkar S et al., 2013; Byler S et al., 2014; Byler S and Sarkar S 2014; Sarkar S et al., 2013).

To this end, epigenetics can be a powerful strategy to develop new treatments because the modification are reversible, the methylation of MDR1 promoter render it a good therapeutic target, cancer cells can be sensitized by the combination of methylation agents and cytotoxic drugs, and recent clinical studies demonstrated that the pre-treatment of cancer cells with epigenetic drugs reduces cancer relapse and make the treatment of resistance more effective (Juergens R et al., 2011).

(vii) *Drug efflux*: drug efflux represents the most studied mechanism of resistance (also shared with bacteria), consisting in the ability of enhance the extrusion of the drug outside the cell thanks to the up-regulation of specific

transporters. These are ATP binding cassette (ABC) transporters involved in the physiological extrusion of xenobiotics from the cells (see below).

Deregulation of signaling pathways and kinases can act on the expression of these proteins as well, leading to an overexpression and, consequently, to the development of the MDR phenotype.

As presented, MDR appears to be a mosaic of features that can occur together or independently, often rendering the therapeutic strategies ineffective. The deep understanding of the causes behind this mechanism is fundamental to overcome this problem; for this reason, combined therapy and molecularly-targeted therapies represent the future perspectives of this challenge.

### **1.3.1 MDR1 and its amplicon**

MDR1, also known as P-gp (permeability glycoprotein) and ABCB1 (ATP binding cassette member B1), belongs to a family of large membrane proteins that transport against steep concentration gradient neutral amphipathic compounds at the cost of ATP hydrolysis.

The human genome contains 48 ABC genes, where 16 of these have a known function and 14 are associated to a specific disease; physiologically, these proteins transport lipids, bile salts, toxic compounds, and peptides (Borst P and Elferink RO 2002).

Among all of these members, only three have been studied extensively due to their role in MDR: MDR1, MDR-associated protein 1 (MRP1 or ABCC1) and breast cancer resistance protein (BCRP or ABCG2) (Gottesman MM et al., 2002). The three ABC transporters have partially overlapping substrate specificities, and promote the extrusion of hydrophobic compounds from the



cell, including major cancer therapeutic drugs (taxanes, topoisomerases inhibitors and antimetabolites).

Overexpression of MDR1 is associated with chemotherapy failure in many cancer types (Holohan C et al., 2013). MDR1 is expressed in most of the tissues at low levels but found at higher levels on the surface of epithelial cells belonging to tissues with an excretory function as, colon, small intestine, pancreatic ductules, bile ductules and kidney proximal tubules (Ambudkar SV et al., 1999; Choi CH 2005), as well as blood-brain barrier, testis-blood barrier and placenta (Borst P and Schinkel AH, 2013) (Figure 8).

Furthermore, some studies reported that the normal expression of MDR1 in tissues with excretory function as kidney, liver, intestine is increased whether the tissue become cancerous (Housman G et al., 2014). It has been reported that lung cancer cells treated with doxorubicin increased MDR1 expression, while the same treatment in normal cells does not have the same effect in MDR1 protein level, suggesting that there is a concurrence of acquired and intrinsic mechanism of MDR1-overexpression (Hilgendorf C et al., 2007).

Conflicting opinions exist on MDR1 exclusive contribution to drug efflux in MDR. Although its role in pharmacokinetics is uncontested, recent studies highlighted that its role in drug resistance of human tumors has turned out to be smaller than expected; whether a small amount of MDR1 can completely protect mouse tumors from chemotherapy drugs, it seems effective on human tumors in a smaller extent (Borst P, 2012).

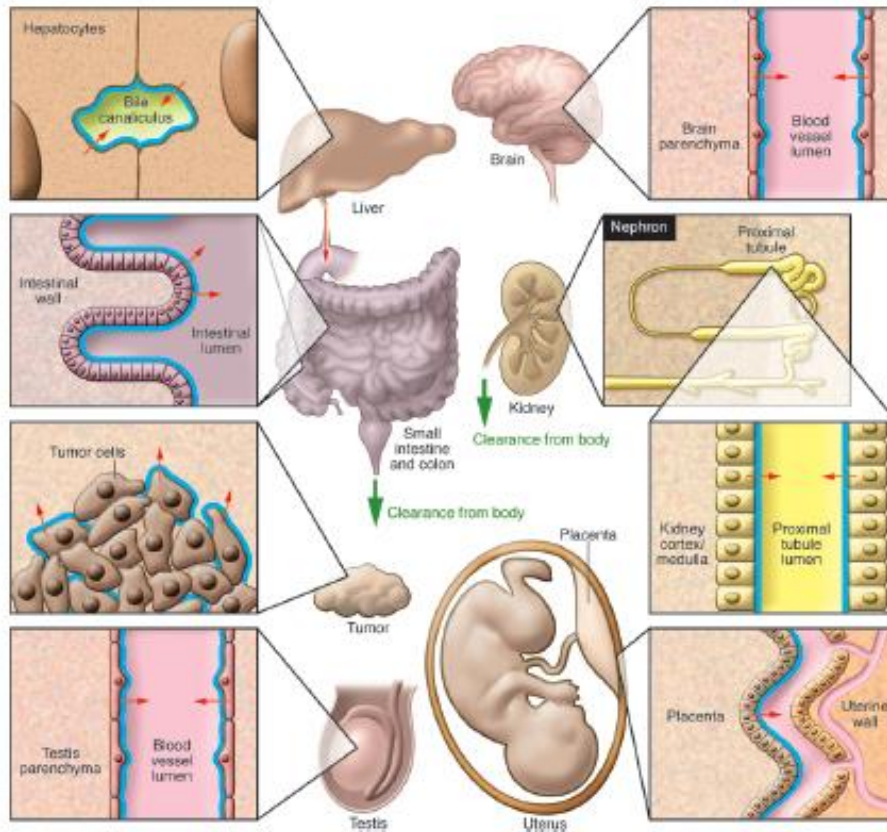


**Figure 8: MDR1 functional expression throughout the body.** The blue lines indicate the location of MDR1, the red arrows indicate the direction of MDR1-mediated transport, green arrows indicate net body excretion of MDR1 substrates. MDR1 protects the tissue from its specific substrate in the blood-brain barrier, testis-blood barrier and placenta; mediates substrate excretion in intestine, and mediates hepatobiliary and renal substrate excretion; while it mediates MDR in tumor cells (Borst P and Schinkel AH, 2013).

As mentioned in the previous section, MDR drug efflux strategy is shared with bacteria as well, suggesting a highly conserved evolutionary mechanism, confirmed by the fact that ABC transporters are present in all existing phyla (Housman G et al., 2014). Although proteins structures vary inside the family, they overall share the common presence of two distinct domains: the highly conserved nucleotide binding domain and the variable transmembrane domain (Chang G et al., 2001).

Hence the mechanism of activation and transport is basically the same; upon substrate binding on the transmembrane portion, ATP hydrolysis is activated on the other domain. The hydrolysis then provokes a change in conformation that drives the extrusion of the substrate outside the cell (Sauna Z et al., 2001).

The role of MDR1 in drug resistance is also intriguing because of its co-amplification with Sorcin (see 1.2.3 section, Van der Bliet AM et al., 1986), since the genes are located close in 7q 21 chromosome portion (Figure 9).

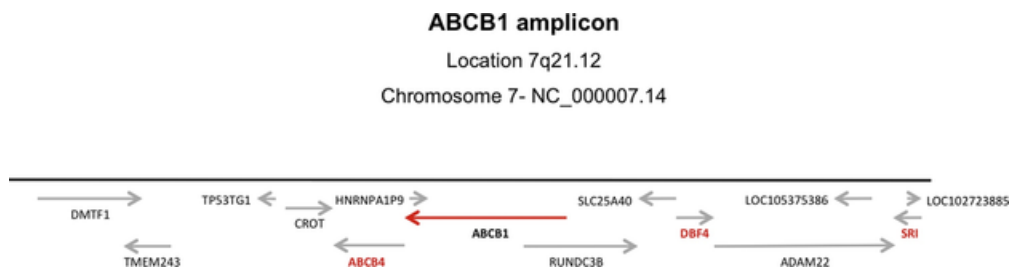


**Figure 9: ABCB1 and SRI amplicon.** ABCB1 gene sequence resides on chromosome 7, region 7q21.12 as Sorcin (SRI) gene. Highlighted genes are over-expressed in cells with MDR phenotype, red arrow (ABCB1) or red names (SRI, ABCB4, DBF4) (Source: NCBI gene).

It is possible to notice that the amplicon contains genes as *ABCB4*, *ADAM22*, *SLC25A40*, *TP53TG1* and *DBF4*, involved in cancer or other pathologies, and reported to have a role also in MDR (Rosenthal EA et al., 2013; Kwon NS et al., 2017; Bonte D et al., 2008; Varrin AE et al. 2005; Diaz-Lagarez et al. 2016; Chao et al. 1991; Van der Bliet et al. 1987; Januchowski et al. 2013; Nemcova-Furstova et al. 2016).

What is known about MDR1 gene is that it can undergo chromosomal rearrangements that can explain its abnormal regulation in cancer and drug resistant cells (Duesberg P et al., 2007) and the up-regulation of Sorcin as well. Nevertheless the molecular reasons that explain those over-expressions

is still under investigation and many questions still have to be tackled. For example, do the rearrangements affect the expression of MDR1 and Sorcin only? Is there the involvement or the contribution of other genes of the locus? The answer to these questions may shed light on MDR complex phenotype development.

#### 1.4 Function of doxorubicin and retinoic acid in chemotherapy

Doxorubicin and retinoic acid (Figure 10) are chemotherapeutic drugs largely utilized in the treatment of mainly solid tumors and leukemia, respectively.

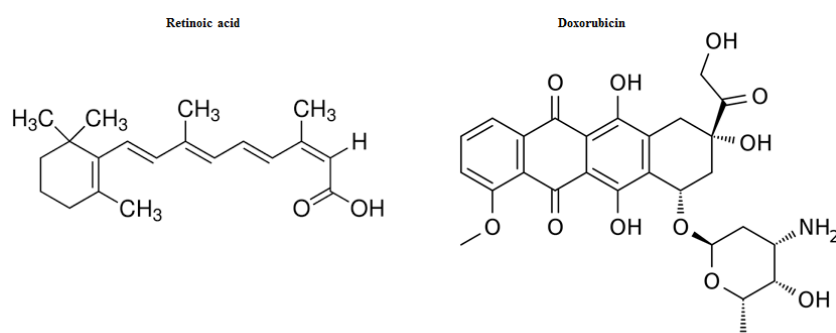


**Figure 10:** Structures of Retinoic Acid on the left side and Doxorubicin on the right side.

**Doxorubicin:** also known as Adriamycin, it is generally used for the treatment of breast and bladder cancers, sarcoma and lymphoma. Doxorubicin is the 14-hydroxylated version of daunomycin, which is quite abundant in nature as a product of several wild-type species of *Streptomyces*; one non wild-type variant (*Streptomyces peucetius* subspecies *cesius*, ATCC 27952) is known to produce the most commonly used doxorubicin (Lomovskaya N et al., 1999).

Its mechanism of action involves DNA intercalation (Tacar O et al., 2013; Fornari FA et al., 1994) and inhibition of DNA and other macromolecules biosynthesis (Mompalmer RL et al., 1976). DNA intercalation, through its planar aromatic rings, causes the blockage of topoisomerase II, the enzyme involved in DNA coils relaxation. Indeed the planar aromatic chromophore intercalates between two base pair of DNA, while the six-membered daunosamine sugar interacts with flanking base pairs, immediately after the intercalation site, in the minor groove (Frederick CA et al., 1990; Pigram WJ et al., 1972). Furthermore, doxorubicin stabilizes the topoisomerase II complex after it has broken the double helix; this complex prevents the release of the double helix of DNA, thus interrupting the replication process (Tacar O et al., 2013). Thanks to the intercalation strategy, doxorubicin can also induce histone loss from transcriptionally active chromatin (Pang B et al., 2013; Pang B et al., 2015), resulting in transcription deregulation. Among the other functions, it can increase quinone-type free radicals production, that can contribute to its cytotoxic effect (Rossi S 2013). Overall, DNA damage response, transcription and epigenetic processes are affected in doxorubicin-exposed cells (Pang B et al., 2013).

**Retinoic acid (RA):** a metabolite of vitamin A or retinol, it is the mediator of vitamin A function during development and differentiation. Retinoic acid is required by chordata, from fish to humans, for early embryonic development of the posterior portion of the embryo along the anterior-posterior axis (Duester G, 2008); during this process it acts through the Hox genes, which control the ultimately development of embryo anterior-posterior axis (Holland LZ, 2007).

Despite its well-known role as a teratogen agent, RA has been also employed successfully as a chemotherapeutic agent in the treatment of Acute Promyelocytic Leukemia (APL) and Acute Myeloid Leukemia (AML) or as a co-adjuvant of cytotoxic agents, as arsenic, in solid tumors (Degos L and Wang ZY, 2001; Su M et al., 2015; Le-Min Lin et al., 2005).

APL is caused by a chromosome translocation involving the gene coding for RAR $\alpha$  fused, in most of the cases, with the promyelocytic leukemia gene (PML) resulting in an abnormal control of myeloid differentiation and a subsequent accumulation of granulocytes precursors, the promyelocytes. The treatment with RA makes these cells responsive again to the differentiation stimulus, such that good prognosis has drastically improved to 77% (Coombs CC et al., 2015).

The AML scenario is more complex though, because different causes can cooperate for the etiopathology; generally RA can be used for chemotherapy because of its ability to induce differentiation. Its mechanism of action consists in its binding to the nuclear heterodimeric receptor RAR/RXR that, upon retinoic acid binding, changes its conformation driving the transcription activation or repression of specific genes on retinoic acid response elements (RARE). Retinoic acid can mediate the transcription of several gene sets, generally involved in differentiation, of various cell type; so the regulated target genes depends strictly on the cellular target (Venkatesh K et al., 2013).

### **1.5 Proteomic Peptide Phage Display (ProP-PD): a novel technique to dissect binding motifs and protein-protein interactions (PPIs)**

Proteomic Peptide-Phage Display (ProP-PD) is a novel high-throughput method used to characterize protein-protein interactions (PPIs; Davey NE et

al., 2017). In ProP-PD, peptides derived from the human proteome are displayed on the major coat protein pVIII of the M13 phage. M13 is a bacteriophage that contains a circular single stranded DNA (ssDNA) sheltered by five different coat proteins. The whole surface of M13 is covered by the major coat protein pVIII, expressed in ~ 2.700 copies. This strain is easy to handle and manipulate (Sundell GN and Ivarsson Y 2014). Moreover using the major coat protein a high valency display (up to 1.000 copies) is accomplished (Marvin DA et al., 2014).

ProP-PD differs from combinatorial phage display because the library is specifically designed to display peptides of the human proteome. The power of this technique resides in the high versatility that peptides libraries can achieve, indeed they can be designed on specific protein domains (as PDZ, Ivarsson Y et al., 2014), intrinsically disordered regions (Davey NE et al., 2017) of proteins or whatever region of interest. Intrinsically disordered regions are highly interesting because are enriched in SLiMs (Short Linear Motifs), 3-10 aminoacidic stretches which are generally involved in interactions that are crucial for cell signaling.

The versatility of the designed peptides library can thus give crucial and novel information about previously unknown networks of interaction, and combine this information to the preferred binding motifs or residues involved in those interaction.

In comparison to other methods to study PPIs, as peptide and protein array, yeast surface display and yeast-two-hybrids, the main advantages of ProP-PD are that it does not require labor-intense set up or high affinity interactions (as protein arrays), or have a quite low throughput (as yeast surface display),

or high number of false positive and negative read-outs (as peptide array and yeast-two-hybrids) (Blikstad C and Ivarsson Y, 2015). The main disadvantage of phage display has typically been the sequencing costs, but these days, next-generation sequencing (NGS) has conferred a reduced sequencing cost and a less laborious analysis.

ProP-PD process is based on selection steps, where the phage pools displaying single peptides are selected each day based on their interaction with the bait protein, so that every selection day the pool of bound phages is enriched (Figure 11).

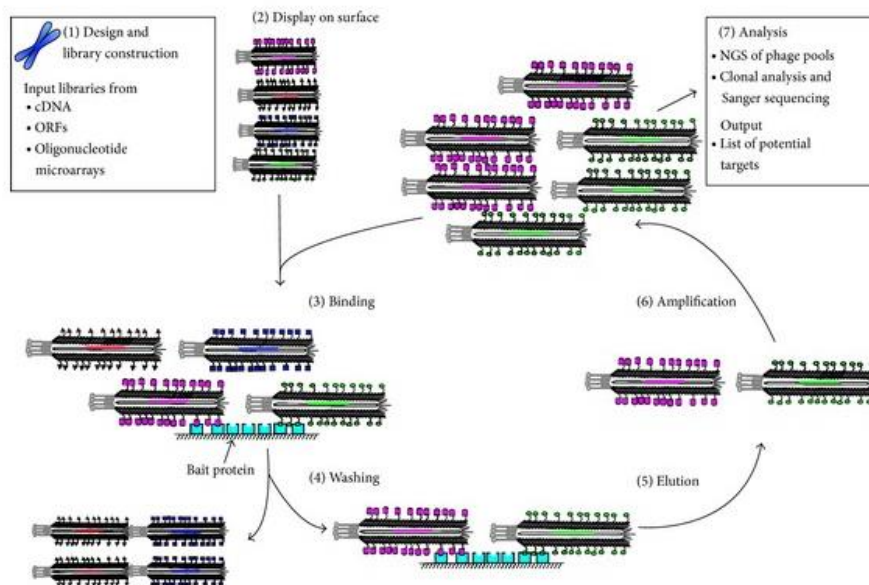


**Figure 11: Representation of Proteomic Peptide Phage Display, using M13 phage:** Starting from the top-left square, a library is designed, then peptides from the library are displayed on M13 surface, the bound phages are eluted after washing steps and finally they are amplified and sequenced (Sundell GN and Ivarsson Ylva, 2014).



Overall, the major power of this technique resides in the libraries versatility, the high throughput readout together with the information on preferred motifs and/or residues involved in the binding between the bait protein and the displayed peptides.

## **2. Aim of the thesis**

The present work aims to shed light on Sorcin activation upon calcium binding, to dissect the molecular role of Sorcin in the MultiDrug Resistance (MDR) process in cancer cell lines, together with the characterization of Sorcin interactome and preferred binding motifs using a cutting-edge technique called Proteomic-Peptide Phage display (ProP-PD).

As mentioned in Chapter one, Sorcin is a calcium-binding penta EF-hand protein whose overexpression in various cancer types goes along with MDR phenotype and poor prognosis. This feature may be due to its simultaneous expression with glycoprotein-P (P-gp or MDR1), which gene is in the same amplicon of Sorcin and physiologically involved in the extrusion of xenobiotics from cells. The lack of information concerning the molecular relationship between Sorcin and MDR phenotype brought us to investigate the process in cancer cell lines.

To tackle this question we performed the cell biology experiments with a cell line that expresses high level of Sorcin in order to get an MDR-like model, and then treated it with doxorubicin, a chemotherapeutic drug that inhibits cell cycle progression intercalating the DNA.

Thus the experimental plan consisted in:

- testing different tumor cell lines (MDA-MD231, MDA-MD468, H1299, HeLa, CALU, A549) for endogenous Sorcin expression;
- testing the survival rate of those cell lines upon doxorubicin treatment and comparing the readout to Sorcin expression levels in each cell line;

- performing direct Sorcin-silencing through a specific siRNA in the cell line with MDR-like phenotype (high Sorcin expression level; high survival rate upon treatment) and then test the drug-sensitivity rate;
- evaluating localization of Sorcin in untreated cells and upon doxorubicin treatment through confocal microscopy;
- evaluating the uptake of doxorubicin upon silencing, *via* confocal microscopy and Fluorescence-Associated Cell Sorting (FACS);
- testing MDR1 expression level upon Sorcin silencing;
- testing the capability of MDR1 in pumping out drugs in control cells and upon Sorcin silencing.

Besides cell biology experiments, we studied the interaction of Sorcin with chemotherapeutic drugs such paclitaxel, vinblastine, cisplatin, retinoic acid and doxorubicin, through Surface Plasmon Resonance (SPR) experiments.

Starting from this information we:

- tested Sorcin-doxorubicin binding by spectrofluorometry, measuring tryptophan quenching during titration experiments with the chemotherapeutic drug;
- grew crystals of Sorcin, and of Sorcin-doxorubicin complex, and performed experiments of soaking of Sorcin crystals with doxorubicin;
- measured fluorescence spectra on crystals of Sorcin-doxorubicin complex;
- solved the crystal structure of Sorcin-doxorubicin complex.

Furthermore, starting from Sorcin-retinoic acid binding information, preliminary data about on the relationship between Sorcin and retinoic acid-dependent Acute Promyelocytic Leukemia (APL) differentiation were obtained.

Moreover, we solved the crystal structures of apo and calcium-bound Sorcin, that enabled us to understand its activation and subsequent interaction with binding partners upon ion binding. To this end, we took advantage of ProP-PD to better understand Sorcin preferred binding motifs involved in Sorcin-protein interaction in presence of calcium.

As described in the previous section, ProP-PD is a novel high-throughput technique that allows the dissection of preferred binding motifs to a bait protein. We used a 16-mer peptide library, displayed on M13 phage surface, designed on intrinsically disordered regions of human proteins containing SLiMs (Short Linear Motifs), about 6 aminoacids stretches generally involved in protein-protein interaction.

We thus performed two Pro-PPD selections, in presence and absence of calcium; we then analyzed the resulting dataset with bioinformatics tools and with *in vitro* binding experiments.

As a list of potential peptide binders was obtained, we then proceeded with *in vitro* validation of binding through SPR experiments and MicroScale Thermophoresis (MST), and indeed achieved important information about preferred binding motifs involved in protein-protein interaction upon calcium binding and we found new potential Sorcin molecular partners.

Altogether these experiments have given us a better understanding of the relationship between Sorcin activation upon calcium binding, interaction with its cellular binding partners and its role in MDR process, making it an intriguing target for cancer therapy.

## **3. Results**

### **3.1 Overall structure, calcium coordination and comparison of human Sorcin structures: conformational changes induced by calcium binding**

We solved structures of Sorcin in complex with calcium (CaSor) and in the apo form (apoSor), at a higher resolution than the one solved by Xie et al. (Xie et al. 2001). Structures statistics are reported in Table 1. All the structures have the typical fold of the PEF proteins family. Briefly, the monomer is formed by two domains: a Gly-rich N-terminal domain (residues 1–32), partially visible in both apo and calcium-bound structures (residues 30–32 and 26–32, respectively), and a calcium binding domain (SCBD), containing eight  $\alpha$ -helices (A-H) organized in five calcium binding motifs (EF1-EF5). Two helices are very long and connect two adjacent EF hands: the D-helix (hD) is common to EF2 and EF3, while the G-helix is common to EF4 and EF5 (Figure 12 a,b). EF1 is structurally coupled with EF2, and EF3 is paired with EF4. Sorcin dimerization occurs by pairing of the EF5 of two monomers. In CaSor,  $\text{Ca}^{2+}$  is bound at EF1, EF2 and EF3 and it is hepta-coordinated in a classical pentagonal bipyramidal configuration (Figure 12 c,d,e). EF1 and EF2 are coupled by Gln48, which coordinates the EF1-bound  $\text{Ca}^{2+}$ , whereas in EF2 is hydrogen-bound to Thr89.



PDB code	apoSor	CaSor
	4UPG	4USL
Space group	I422	C222 <sub>1</sub>
Cell parameters (Å)	a = b = 106.4, c = 77.5 Å	a = 52.4, b = 111.6, c = 60.5
Asymmetric unit (residues)	Monomer (30–198)	Monomer(12–17, 26–198)
N° of bound ions	—	3 Ca <sup>2+</sup>
Resolution ranges (Å)	2.1–50.0 (2.1–2.2)	1.65–50 (1.65–1.69)
Unique reflections	23604 (4375)	41040 (3051)
Completeness (%)	99.7 (98.2)	99.5 (99.6)
Redundancy	6.8 (7)	3.4 (3.3)
R <sub>merge</sub> (%)	11 (59)	4 (66)
CC(1/2)	99.8 (88.2)	99.9 (83.3)
I/σ(I)	14.8 (3.6)	21.57 (3.0)
Resolution ranges (Å)	2.10–40.59 (2.10–2.15)	1.65–37.34 (1.65–1.69)
R <sub>cryst</sub> (%)	18.1 (23.4)	19.1 (32.9)
R <sub>free</sub> (%)	21.9 (30.0)	22.1 (33.3)
rms (angles) (°)	1.46	1.32
Rms (bonds) (Å)	0.01	0.01
Wilson B-factor (Å <sup>2</sup> )	29.3	21.6
Residues in core regions of the Ramachandran plot (%)	98.8	99.4
Residues in allowed regions of the Ramachandran plot (%)	1.2	0.6

**Table 1: Crystal parameters, data collection statistics and refinement statistics of Sorcin in the apoform (apoSor) and in complex with Ca<sup>2+</sup> (CaSor).** Values in parentheses are for the highest-resolution shell.

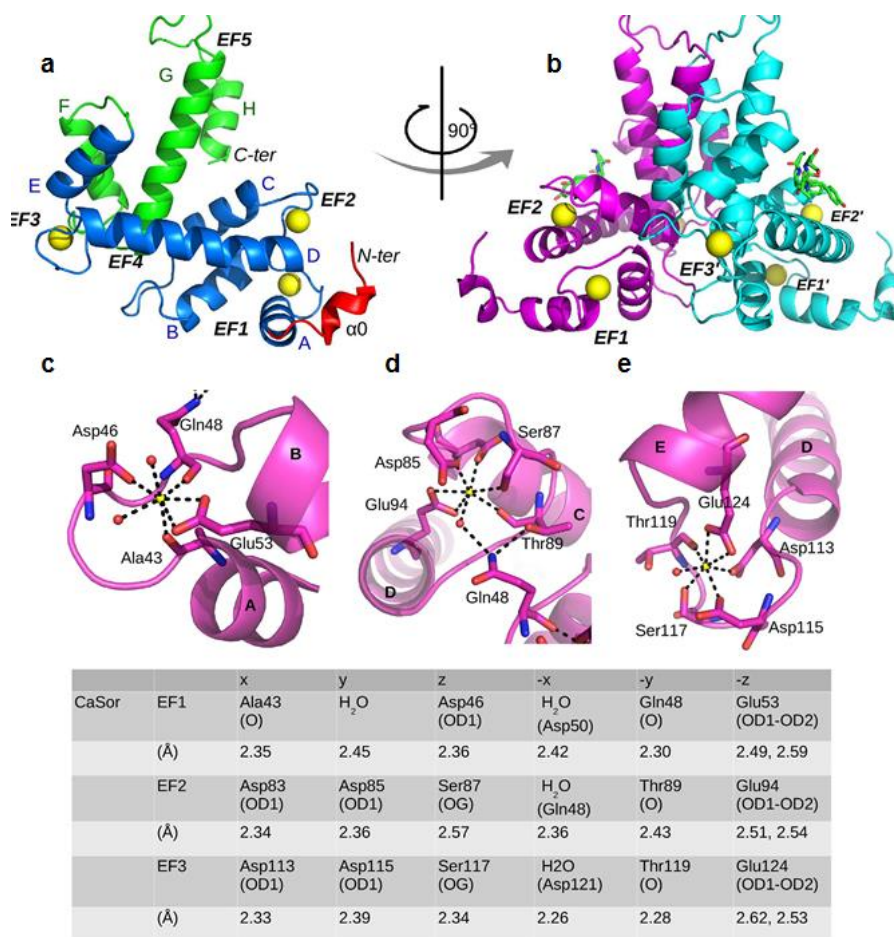


**Figure 12: Overall structure of calcium-bound human Sorcin and calcium coordination in Sorcin** (a) The monomer comprises part of the flexible N-terminal domain containing an alpha helical region designated  $\alpha 0$  (red) and a calcium-binding domain (SCBD) that can be divided in two regions: EF1-3 (blue) and EF4-5 (green). Calcium ions (yellow spheres) are bound at EF1, EF2 and EF3. The helices (A-H) and the EF-hands (EF1-5) are indicated. (b) Dimerization occurs through the pairing of EF4-5 of two monomers (cyan and magenta). The N-terminal hexapeptide modeled in the structure is shown as green sticks. Close-up of Ca<sup>2+</sup> binding sites in EF1 (c), EF2 (d) and EF3 (e) reveals the classical pentagonal bipyramidal geometry. The involved residues are shown as sticks, water molecules as red spheres and calcium ions as yellow spheres. Ligand positions and coordination distances are listed.

The comparison between all the known human Sorcin structures (apo human Sorcin, PDB code: 1JUO; apo-F112L human Sorcin mutant, PDB code: 2JC2; apoSor, PDB code: 4UPG; CaSor, PDB code: 4USL) shows that the

EF1–3 region is more flexible than the EF4-EF5 region and that a large conformational change in the EF1-EF2 subdomain and EF3 is visible upon calcium binding to the first three EF hand motifs (Franceschini S et al. 2008; Xie et al. 2001). Indeed, the rmsd values (Table 2) measured by superimposing CaSor to the apoSor clearly indicate that upon calcium binding Sorcin undergoes a large conformational change, mainly involving EF1, EF2 and EF3 (Table 2, Figure 13).

	Whole structure (SSM)	112-198 (LSQ)
CaSor	3.13	1.52
F112L	-	0.73
1JUO,A	1.05	0.73
1JUO,B	2.38	1.30

**Table 2:** Rmsd of known structures of Sorcin with respect to apoSor. The structures have been superimposed, both using the C $\alpha$  atoms of residues 112-198 (LSQ method) and the C $\alpha$  atoms of all the protein residues (SSM method) by the program COOT, apoSor has been used as reference structure.

As shown in Figure 13, calcium binding to EF1, EF2 and EF3, i.e. the three EF hands with the highest affinity for the cation (Mella M et al. 2003), induces a large displacement (of about 21°) of the D-helix. The comparison between apoSor and the calcium-bound Sorcin structures sheds light on the mechanism of cation-mediated structural changes of Sorcin, which is fundamental for the comprehension of its function. The binding of calcium at the EF3 loop causes the movement of the three ligands Asp113, Asp115 and Ser117 towards the bidentate Glu124 ligand in the E-helix. Thus, the loop undergoes a rearrangement and may act as a lever dragging the long and rigid D-helix away from the E-helix. As a result, EF3 acts as a pivot: the first half of the calcium binding domain (formed by A-, B-, C- and D-helices) rotates

and moves away from the second half (formed by the E-, F-, G- and H-helices), which is the dimerization subdomain and forms the stable Sorcin dimeric interface.

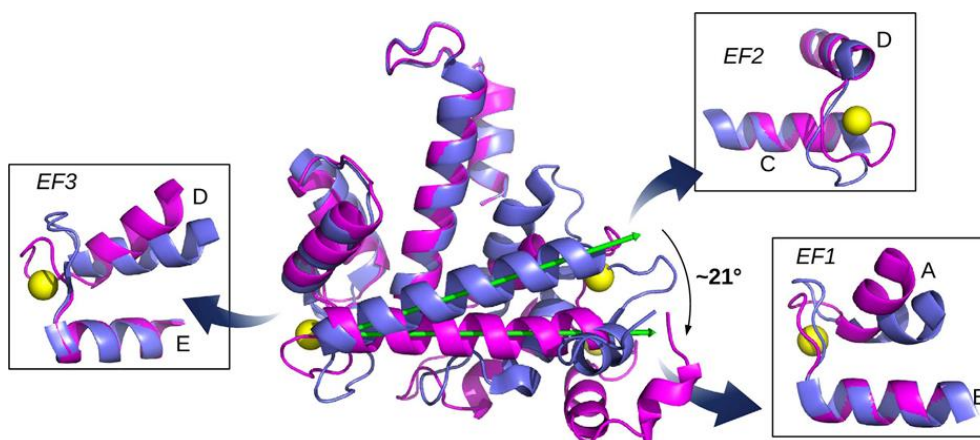


**Figure 13: Conformational changes induced by ion binding.** The superposition of CaSor (magenta) and apoSor (blue) reveals the conformational variation induced by calcium (yellow spheres). The green arrows represent the axis of the D helix in the two structures: the binding of three  $\text{Ca}^{2+}$  to each Sorcin monomer causes a large movement of the D helix that drags the EF1-EF2 region. The panels illustrate the changes of EF1, EF2 and EF3 taken alone, analyzed aligning the C-terminal helix for each EF-hand: EF1 and EF3 open upon  $\text{Ca}^{2+}$ -binding, while EF2 is almost unchanged.

### 3.2 Analysis of Sorcin solvent-accessible surface areas

The analysis of solvent accessible surface areas has been performed with areaimol (CCP4 suite, <http://www.ccp4.ac.uk/html/areaimol.html>) and shows that upon calcium binding there is an increase in the exposed surface areas of several residues. The residues with a difference in SASA (Solvent Accessible Surface Areas) higher than 30% between the apo and the calcium bound form of Sorcin are Tyr67, Ser80, Met81, Met86, Ile110, Arg116, Gly118, Ser143 and Ser197 (Figure 14).

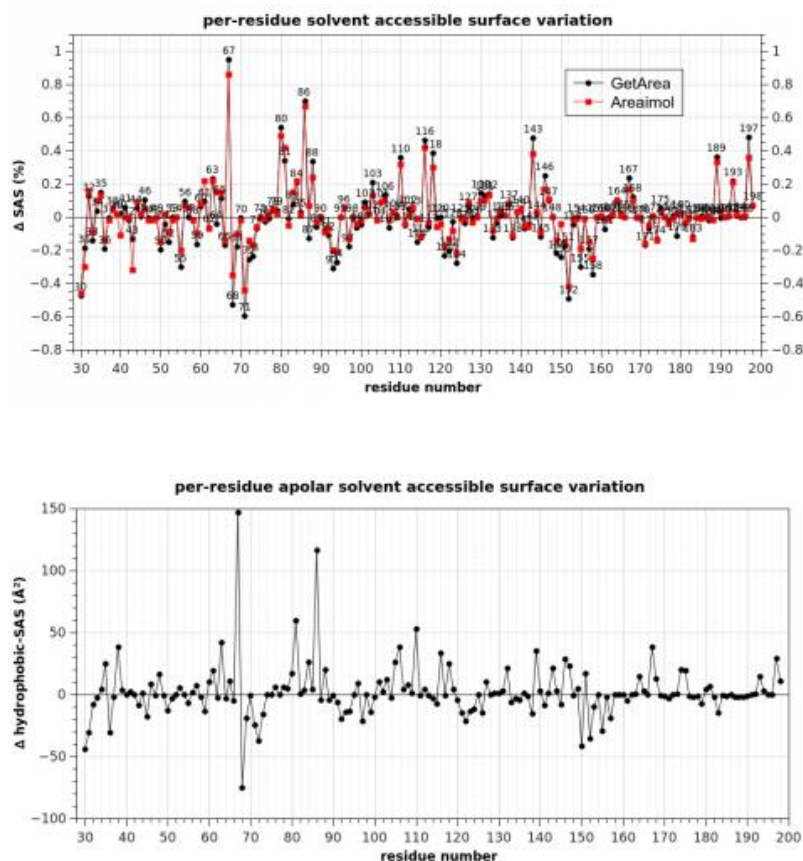


**Figure 14: Residues exposure variation upon calcium binding.** (top) GetArea and Areaimol give the value of percentage of SAS (%SAS) per-residue, calculated as the ratio between SAS area of a residue X in its three-dimensional structure and SAS of its extended tripeptide Gly-X-Gly conformation. For each residue the difference of %SAS between CaSor and apoSor has been calculated and plotted to identify the surface regions with the main variations. Positive values indicate that the residue is more exposed in CaSor than in apoSor and vice versa. (bottom) Only the hydrophobic component of the surface is taken into account. Some artifact has arisen from the absence of side chains in the model (Arg175, Gln107).

As shown in Figure 15a, the residues displaying the highest SASA (higher than 30%) are located in the loop preceding the C helix (hC), in the EF2 loop (which follows the hC), in the C-terminal part of the D-helix and in the EF3 loop; all these structural features present a wide calcium-dependent rearrangement. Even if ion binding has almost no effect on the

relative position of helices C and D of EF2 hand, upon ion binding there is a reorganization of the last part of the helix C containing Met81 and of the loop 83–91 containing Met86, which become exposed to the solvent. Tyr67 is placed on the loop between helices B and C, and in apoSor it is hydrogen bonded to Asp113 of the EF3 loop and is partially covered by it. Upon calcium binding this interaction is broken since Asp113 participates in ion coordination; the rearrangement of the EF3 loop causes also the exposure of Arg116 (Figure 15b). We further analyzed the CaSor structure using the Hotpatch server (<http://hotpatch.mbi.ucla.edu/>) in order to identify unusual hydrophobic patches likely mediating protein-protein interactions between Sorcin and its molecular partners (Pettit F et al. 2007). The Hotpatch analysis highlights that besides Met86 (cyan) and Tyr67 (green), each Sorcin monomer has two significant regions consisting of three different zones, shown in Figure 15c. The pink one includes His108 and Met132 (pocket 1), the red one Met81, Val101, Trp105, Val164 (pocket 2) and the orange one Ala26, Phe27, Pro28, Pro34, Leu35, Tyr36, Gly37, Tyr38, Ser61, Trp99 (pocket 3). Interestingly, these clusters are found in the areas most affected by calcium dependent structural changes, namely EF1 (orange residues) and EF3 (red and pink residues). Moreover, both areas include tryptophan residues (Trp99 and Trp105) strongly conserved among the PEF protein family members. Supporting the importance of these regions in ligands binding, Colotti and coworkers previously demonstrated that mutation of Trp105 impairs the capacity of Sorcin to recognize and interact with RyR2 and annexin 7 at physiological calcium concentrations (Partha SK et al. 2014).

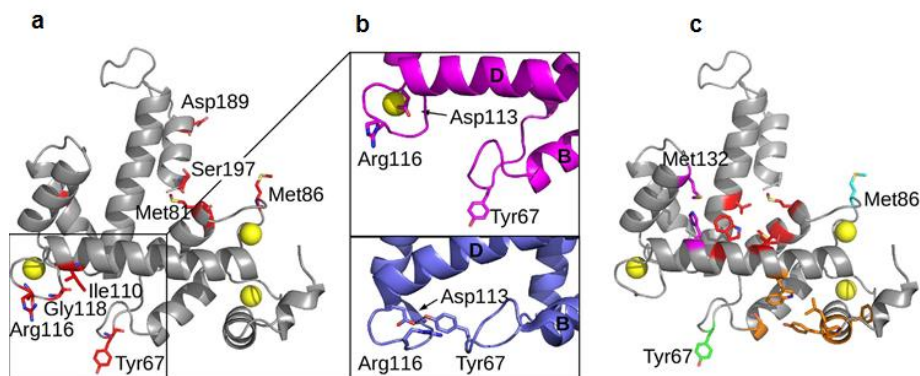


**Figure 15: Solvent accessible surface analysis and hot-spots prediction.** (a) The residues that upon calcium binding become more accessible (SASA increase higher than 30%) are mapped as red sticks on CaSor structure; Tyr67 and Met86 show the strongest variation. (b) In apoSor (blue) Tyr67 forms a hydrogen bond with Asp113. In CaSor (magenta) the hydrogen bond is broken and the loop moves away together with helix B and the EF1-EF2 region. (c) Hotpatch analysis identified 3 pockets (pocket 1, magenta; pocket 2, red; pocket 3, orange) likely mediating protein-protein interactions.

### 3.3 Sorcin binds doxorubicin and other chemotherapeutic drugs with high affinity

For Surface Plasmon Resonance (SPR) experiments, two types of sensorgrams have been measured. OneStep-SPR experiments show that Sorcin is able to bind doxorubicin, paclitaxel and vinblastine, with high affinity, in the submicromolar range (Figure 16d); FastStep-SPR experiments (Figure 16a) can be fitted with two binding sites, one in the nanomolar range and one in the low micromolar range ( $K_{D1} = 10$  nM;  $K_{D2} = 1$   $\mu$ M in the presence of calcium;  $K_{D1} = 22$  nM;  $K_{D2} = 2$   $\mu$ M in the presence of EDTA Figure 17a). Sorcin also binds cisplatin, with a  $K_D = 1.7$   $\mu$ M (one binding site, Figure 16e).

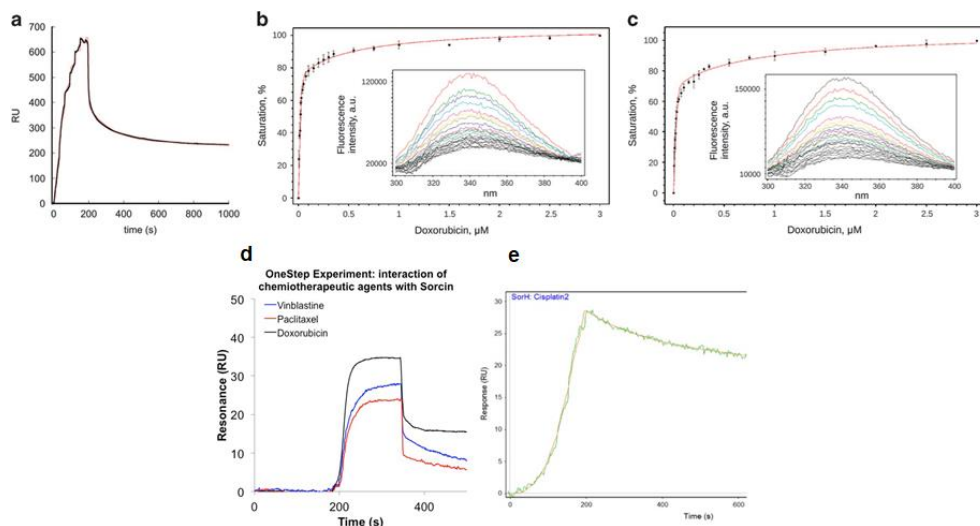
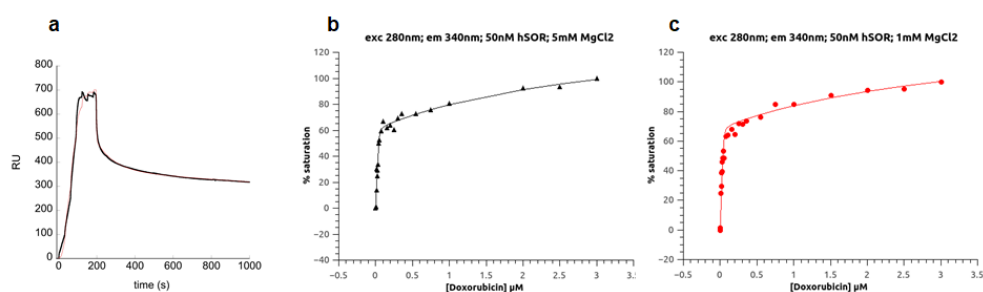


**Figure 16: Sorcin binds doxorubicin and chemotherapeutic drugs with high affinity in vitro.** (a) SPR titration experiments in the presence of 500  $\mu\text{M}$   $\text{CaCl}_2$  and (b,c) fluorescence titration experiments in the presence of 0.5  $\mu\text{M}$  EDTA: Doxorubicin binding to Sorcin (b) and SCBD (c) monitored by intrinsic fluorescence quenching. Each protein was incubated for 3 min at 25  $^\circ\text{C}$  in the presence of increasing concentration of ligand. The bars indicate the standard deviation for three independent experiments. The insets show the whole emission peak for each sample from one representative experiment. Both Sorcin and SCBD contain two binding sites for doxorubicin, with affinities in the nanomolar and low micromolar range. (d) SPR OneStep Experiment: Sorcin binds vinblastine, paclitaxel and doxorubicin directly and with high affinity; (e) SPR FastStep experiment: Sorcin binds cisplatin with high affinity.

Fluorescence titrations (Figure 16b,c; Figure 17) were carried out by measuring the fluorescence at 280 nm upon stepwise doxorubicin addition to Sorcin (Figure 16b) and to the Sorcin calcium-binding domain (SCBD, Figure 16c), comprising residues 32–198 of Sorcin. The fitting of fluorescence titrations for both Sorcin and SCBD are compatible with 2 doxorubicin binding sites (Figure 16; Figure 17), with affinity constants in the same order of magnitude with respect to those measured by SPR experiments, that is,  $1.4 \pm 1$  and  $734 \pm 396$  nM for SCBD and  $0.9 \pm 0.5$  and  $511 \pm 140$  nM for Sorcin in the presence of EDTA (1.2 and 360 nM; 0.9 and 318 nM for Sorcin, in the presence of 1 and 5 mM magnesium, respectively): doxorubicin binding occurs at the C-terminal calcium-binding domain, since SCBD retains the binding sites. Signal shift was not detected, indicating that



the environment of fluorophores did not change upon doxorubicin binding. The value obtained for  $K_{D1}$  is lower than protein concentration, condition that can cause an overestimation of the constant and large errors. We could not lower protein concentration due to the signal/noise ratio; however it can be assessed that  $K_{D1}$  is not greater than estimated. Therefore, Sorcin, which was previously shown to increase resistance to a variety of chemotherapeutic agents, is able to bind directly and with high affinity doxorubicin and other chemotherapeutic drugs in vitro; this prompted further experiments to understand how such binding may contribute to increase drug resistance in cells as a function of its expression in the cell.



Sorcin-doxorubicin	SPR		Fluorescence	
	Site 1 (KD1)	Site 2 (KD2)	Site 1 (KD1)	Site 2 (KD2)
EDTA	22nM	2μM	0.9 ± 0.5 nM	511±140nM
+0,5 mM CaCl <sub>2</sub>	10nM	1μM		
+1mM MgCl <sub>2</sub>			1.2 ± 2.7 nM	360 ± 950 nM
+5mM MgCl <sub>2</sub>			0.9 ± 1.2 nM	318 ± 280 nM

**Figure 17:** Doxorubicin binding to Sorcin monitored by (a) SPR titration experiments in the presence of 500 μM EDTA and (b, c) fluorescence titration experiments in the presence of 1 mM (c) and 5 mM MgCl<sub>2</sub> (b). Each protein was incubated for 3 minutes at 25°C in the presence of increasing concentration of ligand. Sorcin contains two binding sites for doxorubicin, with affinities in the nanomolar and low micromolar range.

### **3.4 Crystal structure of the Sorcin-doxorubicin complex**

Addition of 4:1 molar excess of doxorubicin to a clear, transparent solution of concentrated apo-Sorcin determines clouding of the solution, aggregation and precipitation of the protein (similar to the precipitation observed upon calcium addition), with formation of a red precipitate and the slow growth of red-colored crystals (Figure 18a). Crystals of different intensity of red color grew depending on the amount of doxorubicin used for crystallization, ranging from 0.5:1 (colorless) to 2:1 (pink) to 15:1 (red) molar excesses. Emission spectra of the crystals grown from these solutions were recorded at 100 K in the Bessy facility, exciting at 473 nm. Changes in peaks intensity and a 25nm red shift of the bands in high-amount doxorubicin (red crystals) were observed with respect to low-amount doxorubicin Sorcin crystals (Figure 18d). These changes are likely due to doxorubicin stacking to aromatic residues of the protein or doxorubicin dimerization, once bound (Changenet-Barret P et al. 2013). We solved the structure of the complex between SCBD and doxorubicin (doxo-SCBD) at quite low resolution (3.74 Å, PDB accession: 5MRA). The asymmetric unit contains two dimers (A–B and C–D). The structure contains 10 Mg<sup>2+</sup> ions (3 bound to monomer A, 2 to monomer B, 3 to monomer C, 2 to monomer D). Doxorubicin is bound to the B monomer. The protein structure is similar to apo-Sorcin and apo-SCBD (PDB accessions: 4UPG, 1 GJY (Ilari A et al. 2002) (Figure 18b).

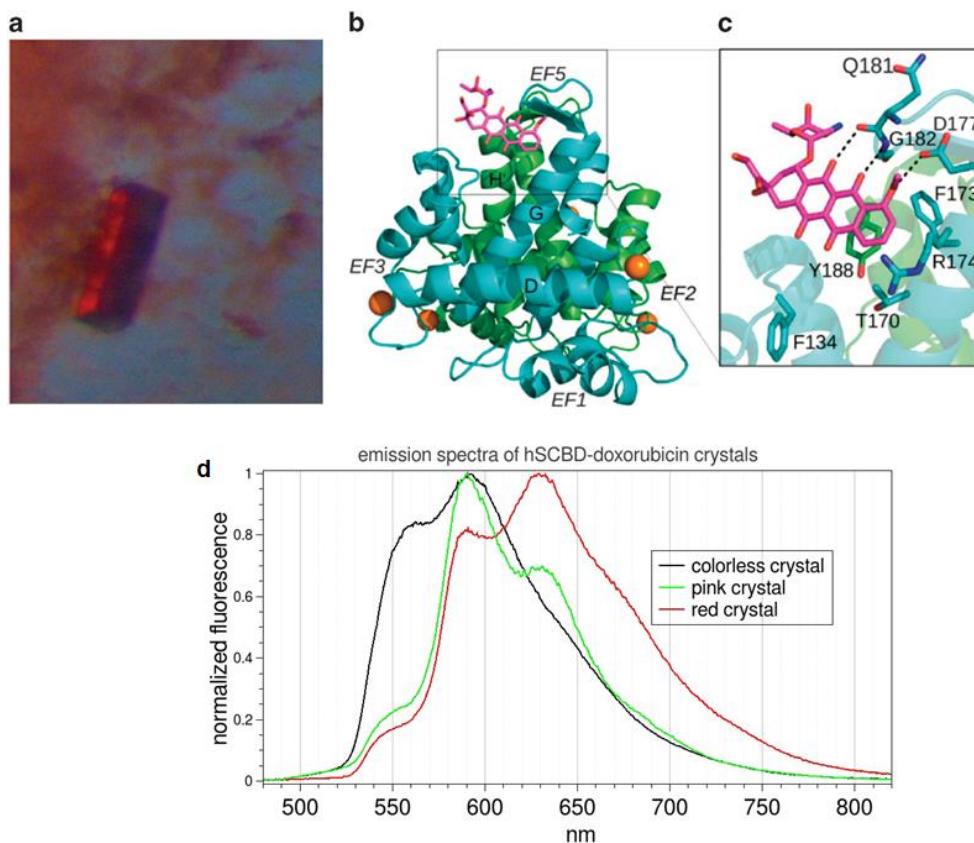


**Figure 18: Sorcin calcium binding domain-doxorubicin complex.** (a) Crystal and (b) crystal structure of Sorcin calcium binding domain-doxorubicin complex; (c) doxorubicin binding site at EF5 (pocket 1), stacked to Tyr188. (d) Emission spectra at 100K ( $\lambda_{exc} = 473$  nm) of Sorcin crystals containing different amounts of doxorubicin. Changes in peaks intensity and a 25nm red shift are likely due to doxorubicin stacking to aromatic residues or dimerization, once bound to Sorcin.

The superimposition between the  $C\alpha$  trace of doxo-SCBD with the  $C\alpha$  trace of apo-Sorcin yields an rmsd of 1.11 Å, indicating that the structures are similar and therefore neither  $Mg^{2+}$  ions binding nor doxorubicin binding are able to promote the conformational changes induced by calcium ions in Sorcin. In accordance with binding experiments, doxorubicin binding occurs at two sites. Inspection of the  $F_o - F_c$  electronic density map allowed the identification of two peaks (Figure 19): one close to the EF5 hand, which does not bind calcium in Sorcin and is responsible for dimer formation, and

the other close to the D-helix connecting the EF2 and EF3 sites at the interface between the two dimers.

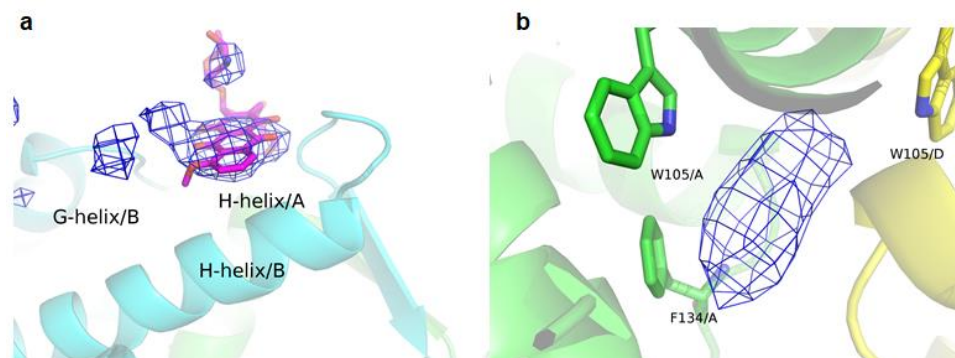


**Figure 19: Fo-FC omit maps of doxorubicin binding sites.** (a) Fo-FC omit map contoured at  $3\sigma$  (blue), calculated in the absence of doxorubicin, showing doxorubicin binding to EF5; the helices surrounding doxorubicin are indicated. (b) blow up of the Fo-FC omit map contoured at  $3\sigma$ , showing the peak of density at pocket 2, at the interface between two dimers of the asymmetric unit.

We succeeded in modeling the doxorubicin molecule in the first site (close to the EF5) whereas it was not possible to model the doxorubicin molecule in the second site (close to the D helix) indicating both the low occupancy of the site and the flexibility of the doxorubicin molecule (Figure 19). These sites have been previously identified as Pocket 1 and Pocket 2, able to bind protein targets, in another PEF protein, that is, PDCD6 (ALG-2) (Suzuki H et al. 2008). The binding of doxorubicin to SCBD in pocket 1 involves a stacking interaction of the drug with the aryl ring of Tyr188 of one monomer and interaction with Asp177, Gly182, Phe173 and Phe134 of the two-fold symmetry related monomer at the dimeric interface (Figures 18b,c). In the second putative site (pocket 2) doxorubicin likely interacts with Trp105 and Phe134 (Figure 19b). Probably doxorubicin binding to the second site would be facilitated by the binding of calcium ions which, as previously described, induce a conformational change promoting the movement of the D-helix and the exposure of hydrophobic interfaces. In the structure, magnesium is bound

to EF3 and to part of EF1 and EF2 sites, showing that in Sorcin the first three EF-hands can bind not only calcium, but also magnesium, with rather high affinity, and that EF3 is the site endowed with the highest affinity for divalent cations, responsible for Sorcin cation-dependent activation.

### 3.5 Sorcin localization responds to doxorubicin treatment

In H1299 lung cancer cell line, Sorcin (green fluorescence) localizes to cell membrane, nucleus, ER and cytosol, as already observed in other cellular systems (Laloti VS et al. 2014). Upon treatment with doxorubicin, Sorcin localization changes with respect to control: after 1-h doxorubicin treatment, cytosolic Sorcin localization increases and nuclear, ER and membrane localization decreases; the ratio of cytosol/(nucleus+ER) Sorcin fluorescence increases by 77% (from 0.278 to 0.491, number of cells= 60,  $P<0.01$ , Figure 20). This is a clear indication that Sorcin localization responds to doxorubicin treatment and that Sorcin presumably binds doxorubicin also in the cell, upon drug entry.

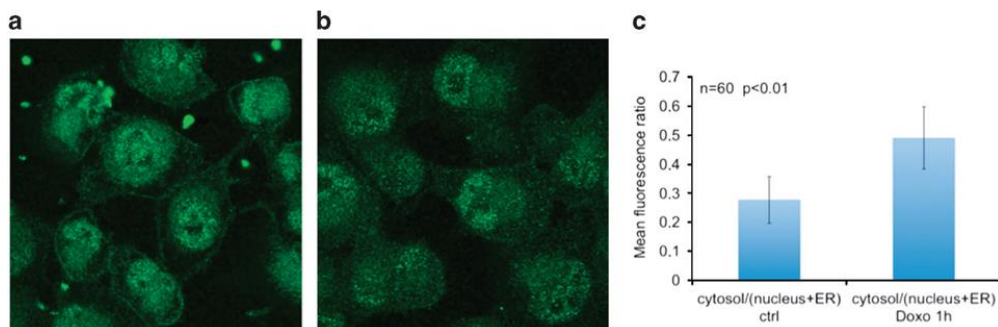


**Figure 20: Sorcin localization changes upon doxorubicin treatment.** Sorcin localization (green fluorescence) in (a) control H1299 cells and in (b) H1299 cells treated for 1 h with 0.6 μM doxorubicin. (c) ratio between cytosol/(nucleus+ER) fluorescence (n=60 cells;  $P<0.01$ ).

### **3.6 Effect of Sorcin expression on doxorubicin uptake and toxicity, and cell death**

Sorcin is expressed at high levels in human and in many cell lines (PaxDB). We have analyzed Sorcin expression in different cell lines from lung, cervix and breast cancers and we evidenced that Sorcin is expressed in all tested cell lines, but the levels differ even by more than one order of magnitude between different lines. In particular, Sorcin is highly expressed in lung cancer cell lines Calu-1 and H1299, that we have selected for further studies, and in breast cancer cell lines MDA-MB-231 and MDA-MB-468, while low Sorcin expression levels were observed in lung A549 and in cervical cancer HeLa cells (Figure 21a). Sorcin high level of expression occurs in cell lines rather resistant to cell death upon treatment with doxorubicin, as H1299, Calu-1 and MDA-MB-468 cells, while A549 and HeLa cell lines, where Sorcin expression is lower by about 90%, are more sensitive to doxorubicin treatment (Figure 21a).

To support the relevance of Sorcin in doxorubicin treatment response, we proceeded with Sorcin silencing experiments. In all tested cell lines, siRNA cds3 effectively silences Sorcin expression, by at least 85% after 24–48 h (Figure 21b). In the H1299 line,  $94\pm 3\%$  silencing occurs. Interestingly the silencing of Sorcin expression is also maintained upon doxorubicin treatment (Figure 21c).

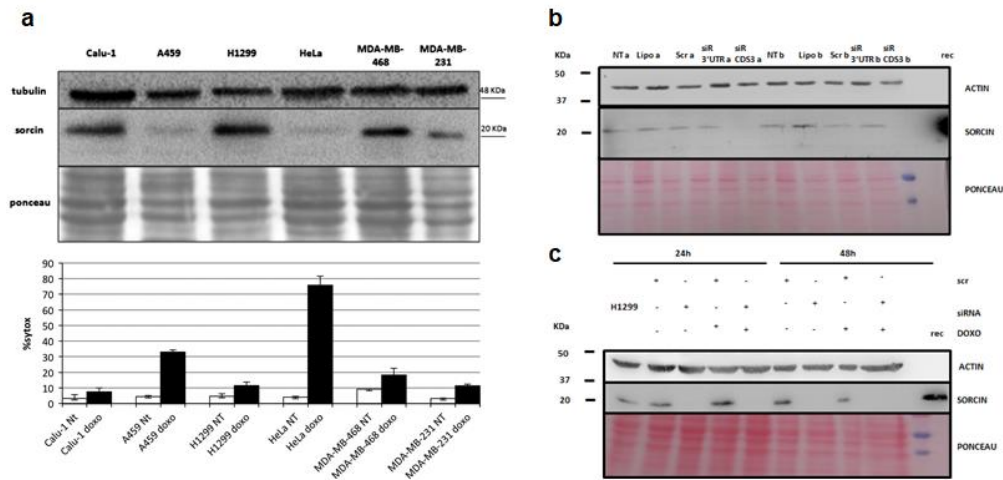


**Figure 21: Sorcin expression versus cell death, and Sorcin silencing in H1299 cells.** (a) (Top) Western blot experiment showing the expression of Sorcin in lung carcinoma Calu-1, A459 and H1299 cells; cervix adenocarcinoma HeLa; breast adenocarcinoma MDA-MB-468 and MDA-MB-231 (bottom). Cell death is increased upon 24 h doxorubicin (0.6  $\mu$ M) treatment in A549 and HeLa cells, where Sorcin expression level is reduced by 480% with respect to H1299 cells. (b) Experiment showing efficiency of Sorcin silencing in control experiments (+Lipofectamine;+scrambled siRNA; + siRNA 3'UTR) vs. silencing using CD53 siRNA. (a and b represent duplicate experiments). (c) Silencing level using CD53 siRNA= -94 $\pm$ 3%. Controls vs. 24 and 48 hours treatment with 0.6  $\mu$ M doxorubicin.

Sorcin silencing by siRNA *cds3* (versus control experiments with scrambled siRNA) slightly increases cell death (Figure 22), as shown by both cell count and by flow cytometry experiments on cells stained with Sytox blue, a cyanine dye that is completely excluded from live eukaryotic cells.

Upon Sorcin silencing, doxorubicin-dependent cell death is markedly increased in H1299 cells (Figure 22b,c): upon treatment with scrambled siRNA and 0.6  $\mu$ M doxorubicin, the percentage of dead H1299 cells increases from 3.4% (control) to 4.6% and 16.3% (24 and 48 h after doxorubicin treatment, respectively), while upon treatment with Sorcin-directed siRNA and 0.6  $\mu$ M doxorubicin, the percentage of dead H1299 cells increases from 4.5% (control) to 10.3% and 29.7% (+124% and +82%, 24 and 48 h after doxorubicin treatment, respectively).

Further, Sorcin silencing increases doxorubicin entry in H1299 cell nuclei by 140% as shown by analysis of confocal microscopy experiments (Figures 23a,b). FACS experiments (Figure 23c) show that upon treatment with scrambled siRNA and 0.6  $\mu$ M doxorubicin, the percentage of doxorubicin incorporation increases from 0.4% after 30 min to 3.4% after 1 h to 49.6% after 3 h doxorubicin treatments, while upon treatment with Sorcin-directed siRNA and 0.6  $\mu$ M doxorubicin, the percentage of doxorubicin incorporation increases from 0.8% after 30 min to 7.1% after 1 h to 72.7% after 3 h doxorubicin treatments (+100%, +109%, +47%, respectively). After 5 h incubation with doxorubicin, the buffering capacity of Sorcin is almost lost (Figure 23d).

In the presence of high levels of Sorcin, doxorubicin is therefore prevented from entering the nuclei of H1299 cells, and the cells are protected from drug-dependent DNA damages.

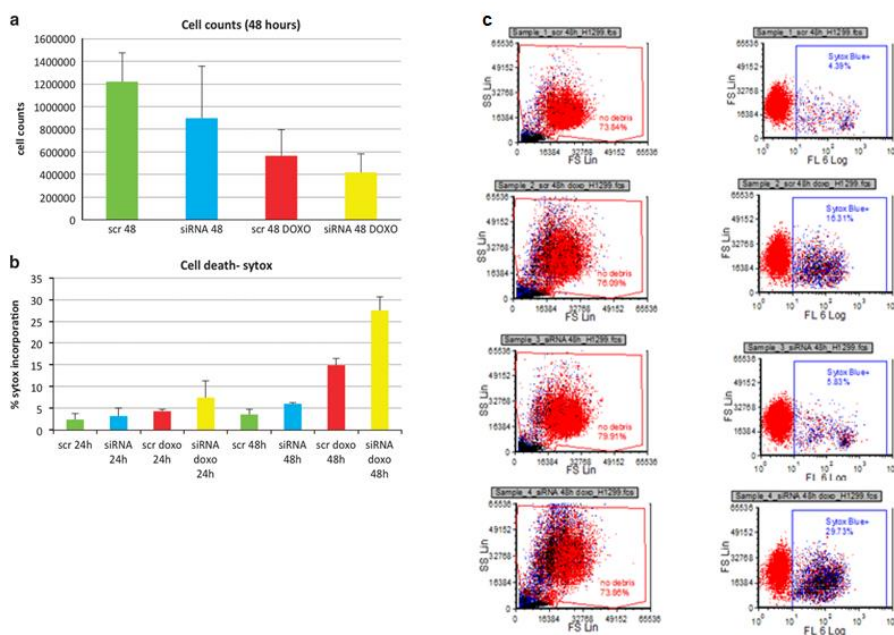


**Figure 22: Sorcin silencing increases cell death upon treatment of H1299 cells with 0.6  $\mu$ M doxorubicin, cell counts and Sytox Blue incorporation (a) Cell count and (b) cell death percentage**



upon treatment of H1299 cells with scrambled siRNA or Sorcin siRNA in control and doxorubicin-treated cells. (c) Cell death percentage upon H1299 cells transfection with scrambled siRNA or Sorcin siRNA in control and 0.6  $\mu\text{M}$  48 hours doxorubicin-treated cells.

Sorcin protects cells, while Sorcin silencing increases doxorubicin-dependent Poly(ADP-ribose)polymerase (PARP) cleavage (Figure 24), an apoptotic marker. In cells treated with Sorcin-directed siRNA, 48 h after treatment with 0.6  $\mu\text{M}$  doxorubicin, the levels of cleaved PARP are higher than in control cells. An even higher increase of doxorubicin-dependent PARP cleavage upon Sorcin silencing in doxorubicin-treated cells can be measured by calculating the ratio between the intensities of cleaved versus full-length PARP.

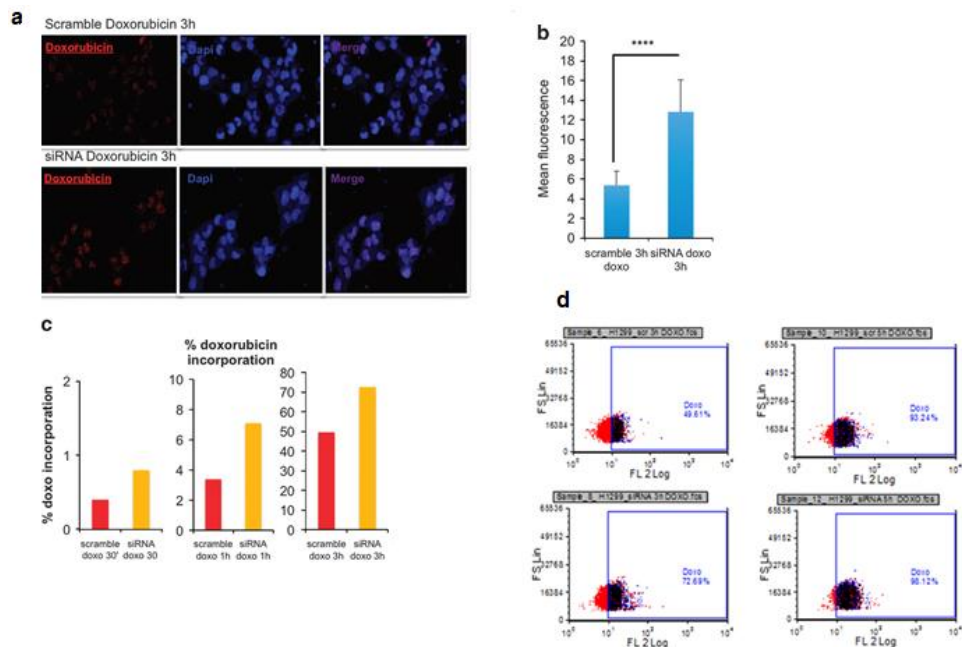


**Figure 23: Sorcin silencing increases doxorubicin accumulation in H1299 cells.** (a) Confocal microscopy images, showing the nuclear accumulation of doxorubicin upon 3 h treatment in H1299 cells treated with scrambled siRNA or with Sorcin siRNA; (b) nuclear doxorubicin incorporation by fluorescence quantification (n=60 cells;  $P < 0.0001$ ); (c) time-dependent quantification of doxorubicin

incorporation in H1299 cells by FACS; (d) doxorubicin accumulation in H1299 cells upon Sorcin silencing (bottom) with respect to scrambled RNA (top), after 3 hour- (left) and 5-hour treatment (right).

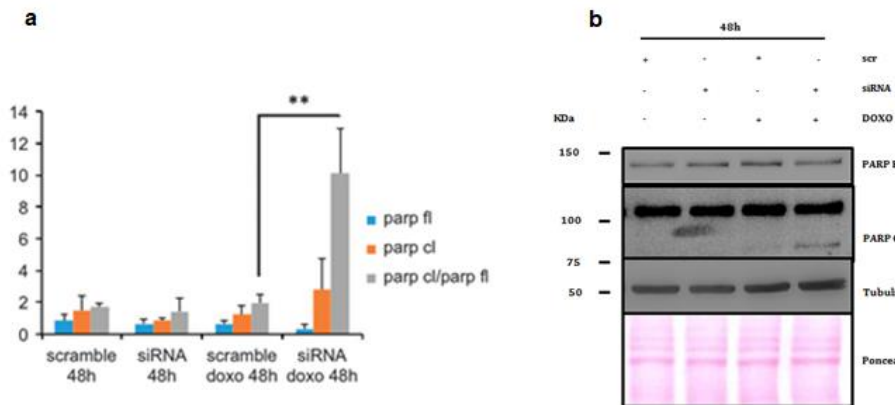


**Figure 24: PARP cleavage experiment upon 48 hours 0.6  $\mu$ M doxorubicin treatment.** (a) upon 48 h doxorubicin treatment, in Sorcin-silenced cells PARP cleavage is increased with respect to control cells (n=3, P<0.01). (b) Western blot analysis showing that upon Sorcin silencing, there is a negligible cleavage of PARP, compared to the combination of Sorcin-directed-silencing and doxorubicin treatment (PARP FL: PARP full length; PARP CL: PARP cleaved).

### 3.7 Effect of Sorcin expression on MDR1 expression and activity

The effect of Sorcin expression on doxorubicin uptake and toxicity can be explained in part by the direct binding of doxorubicin by Sorcin, that may prevent the drug entry in the nucleus. However, doxorubicin is also a substrate of the efflux pump MDR1 (Borst P, Elferink RO 2002) whose gene is located in the same amplicon of Sorcin gene (van der Blik AM et al. 1986). Conflicting results are in literature on the effect of Sorcin expression on MDR1 expression and activity (Lee WP et al. 1996; Wang SL et al. 1995; Xu P et al. 2015; Yamagishi N et al. 2014).

Figure 25 shows that Sorcin silencing decreases both MDR1 expression and activity in H1299 cells, as already demonstrated in A549 cells (Gao Y et al. 2015) by about 40%. In cells treated with Sorcin-directed siRNA the MDR1-mediated efflux of rhodamine123 is substantially decreased with respect to

control cells treated with scrambled siRNA, showing a decrease of the activity of MDR1 in Sorcin-silenced cells (Figure 25a,b): the level of intracellular rhodamine123 in H1299 cells treated with Sorcin-directed siRNA is increased by 27, 51 and 67% (upon 30 min, 1 h and 2 h incubation with the MDR1 substrate, respectively) with respect to control cells. MDR1 expression level is also strongly decreased by Sorcin silencing: in cells treated with Sorcin-directed siRNA, a 45% decrease in MDR1 level occurs with respect to H1299 control cells (Figure 25c,d), with no relevant contribution of doxorubicin.

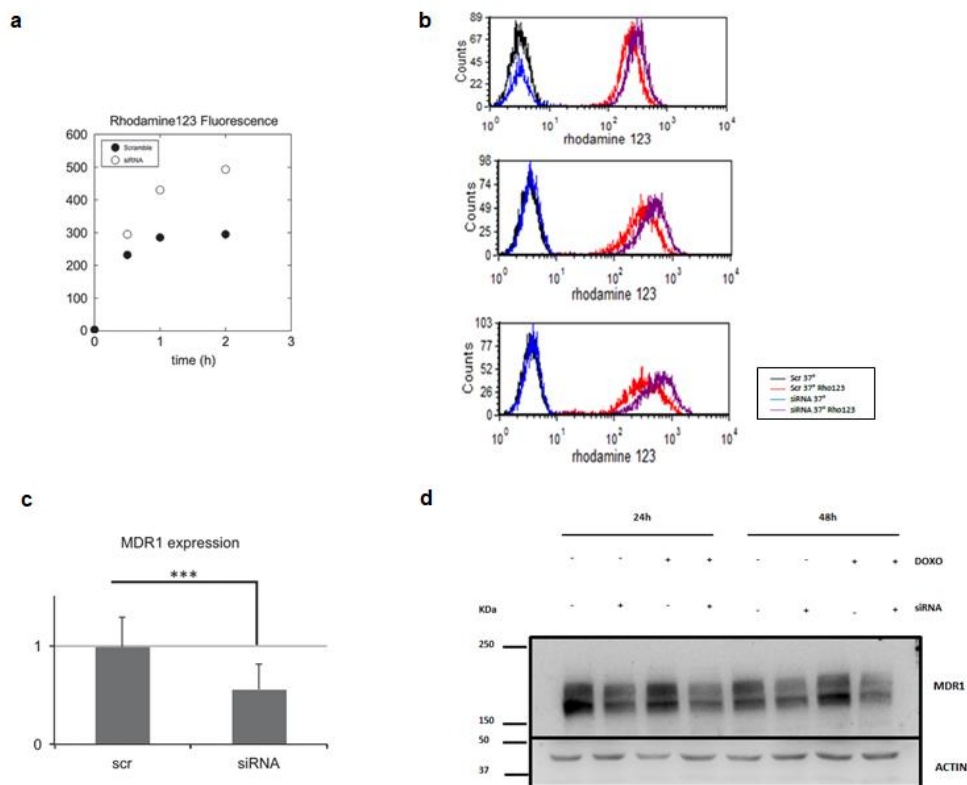


**Figure 25: Sorcin silencing decreases MDR1 expression and activity in H1299 cells.** (a) Rhodamine123 fluorescence is increased (and therefore its efflux is decreased) and (b) the incorporation of rhodamine123, in a time-course experiment performed at 37°C, (top) 30', (center) 1h, (bottom) 2h after incubation with the dye. Black and blue curves represent the non-treated cells (in the presence of scrambled siRNA and upon Sorcin silencing, respectively), while red and purple curves

represent the cells treated with rhodamine123 (in the presence of scrambled siRNA and upon Sorcin silencing, respectively). (c) MDR1 expression is decreased in Sorcin-silenced H1299 cells with respect to control cells (n= 3, P<0.001), (d) western blot experiment showing a decrease in MDR1 protein level upon Sorcin silencing, both 24h and at 48h after treatment with siRNA.

### 3.8 Sorcin binds to Retinoic acid and changes localization

Differentiation is a complex rearrangement of cellular physiology and it is used as a strategy to treat Acute Promyelocytic Leukemia (APL) to induce cell growth arrest (Degos L, Wang ZY, 2001).

Since Sorcin is an important calcium sensor oncoprotein, overexpressed in many leukemias (see the Chapter 1), we wondered whether it might exert a role in differentiation induction upon retinoic acid (RA) treatment.

To this end, NB4 promyelocytic cell line was treated with RA to induce granulocytic differentiation, checked in a time course experiment (Figure 26), in order to dissect the role of Sorcin in this process.

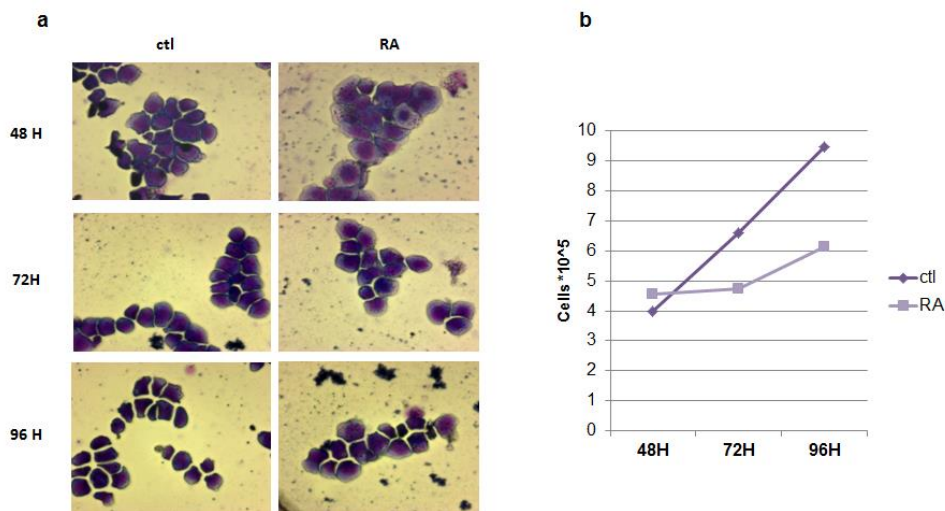


**Figure 26: NB4 differentiation time-course treatment with 1µM RA:** (a) Optical microscopy 40X images giemsa-stained used to check for the cell morphology and differentiation; upon RA treatment promyelocytic cells undergo a cellular rearrangements where the cytoplasm become larger and clear-

stained than nuclear portion compared to controls, and the nuclei lose their typical rounded shape. (b) Cells were counted in a burker chamber in triplicates to assess the growth arrest.

Then, the mRNA and protein expression were checked by RT-PCR and western blot respectively and no changes in mRNA levels (data not shown) were detected, while a little (1.5 fold) increase in Sorcin expression was observed (Figure 27b).

Nucleus/cytoplasm fractioning experiments revealed that Sorcin expression does not increase consistently upon RA treatment but rather the protein changes its localization. Indeed, confocal microscopy investigation shows that Sorcin, 72 hours after RA treatment, migrates towards cell membranes or insoluble fraction as shown in figure 27 a and b.

These preliminary data need further experiments to shed light on the role of Sorcin in granulocytic differentiation; indeed we observed that Sorcin interacts directly with RA, with a single binding site.  $K_D$  values in the low micromolar range were obtained by fitting OneStep experiments ( $K_D=2.5 \mu\text{M}$ ), and FastStep SPR experiments ( $K_D=5 \mu\text{M}$ ) (Figure 27c). These investigations bring insights on novel Sorcin roles and molecular partners so far un-dissected.

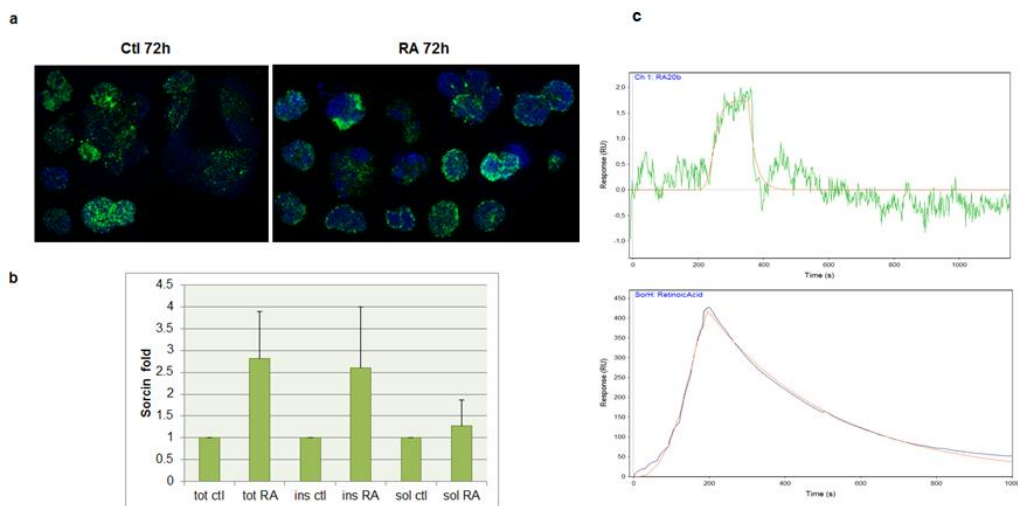


**Figure 27: Sorcin binds to RA and migrates to cell membranes.** (a) Confocal microscopy images of NB4 cells upon 72 hours RA treatment, TO-PRO-3 stain for the nucleus is in blue, Sorcin antibody is in green, notice that Sorcin migrates to membranes (cellular or nuclear membranes) after treatment. (b) Western blot quantification of NB4 total, insoluble and soluble fractions; as shown, the contribute to the total fraction is given by the insoluble portion (n=4). (c) SPR experiments OneStep (top) and FastStep (bottom) revealed a single site Sorcin-RA interaction with a  $K_D$  in the range of low micromolar. The OneStep experiment was performed using a gradient of analyte concentration reaching a maximum of 20 $\mu$ M RA, while the FastStep experiment was performed using 7 serial dilutions (1:2) of analyte from 3.12 to 200  $\mu$ M RA.

### 3.9 Analysis of N-terminal peptide-Sorcin interaction

The analysis of the CaSor structure reveals the presence of an electron density peak in the cavity formed upon calcium binding and the consequent tilt of the D-helix. We fitted this electronic density map with the GYYPPGG hexapeptide belonging to the N-terminal region of Sorcin (residues 12–17). The same region was thought to interact with PDCD6 N-terminal peptide by Jia J et al.; Suzuki et al. demonstrated that it probably was PEG demonstrated that it probably was PEG. We can exclude PEG binding to Sorcin structure: the Fo-Fc and 2Fo-Fc electron density maps shows clearly the presence of a short peptide containing side chains with a very well resolved proline residue clearly visible in the structure (12-GYYPPGG-17; Figure 28), belonging to a different dimer. The interacting surface between the N-terminal peptide and Sorcin was analysed using the program ePISA ([http://www.ebi.ac.uk/msd-srv/prot\\_int/cgi-bin/piserver](http://www.ebi.ac.uk/msd-srv/prot_int/cgi-bin/piserver)). The residues buried at the interface between peptide and Sorcin are: Met78, Met81, Leu82, Glu97, Ala100, Val101, Gly104, Trp105, His108 placed on the D helix; Phe112 on the EF3 loop; Thr131, Met132, on the EF4 loop; Val164, Arg167, and Asp171 on the G helix. Trp105, Glu97 and Arg167 form hydrogen bonds with Tyr13 and Tyr14 of the peptide (OH Tyr13-OE2 Glu97 = 2.78 Å; O Tyr13-NE1 Trp35 = 2.74 Å; O Tyr14-OE2 Glu97 = 2.90 Å) (Figure 28b). The residues laying on the D helix play a major role in interacting with the N-terminal peptide; in

particular, Trp105 establishes a strong stacking interaction with Pro15 and is hydrogen bonded to the carbonyl group of Tyr13, determining the orientation of the peptide into the pocket which is opposite to that of Alix in PDCD6. These residues belong to pockets 1 and 2, identified by Hotpatch analysis (Figure 15C).

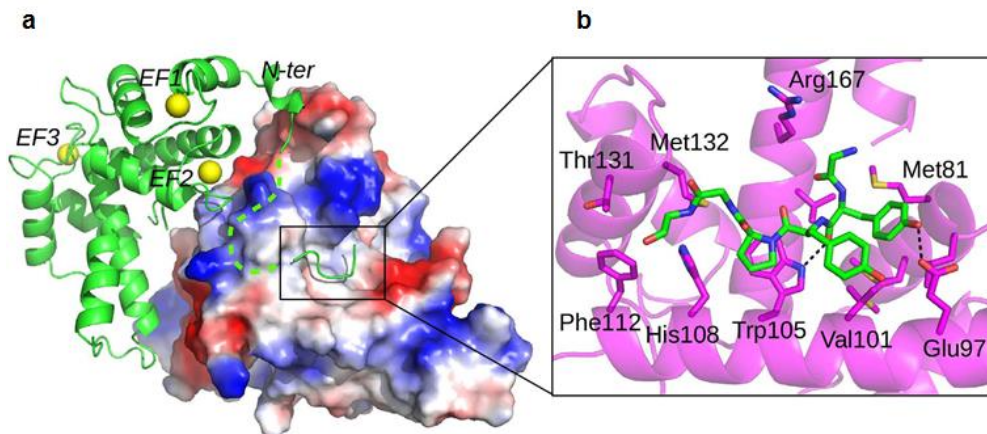


**Figure 28: Interaction between Sorcin and the N-terminal peptide.** (a) The electrostatic surface potential (blue-positive, red-negative) of CaSor dimer is shown. The hydrophobic surface corresponding to pockets 1–2 accommodates the 12-GYYPPGG-17 peptide (green) plausibly belonging to an adjacent Sorcin molecule in the crystal (green cartoon); the residues 11–25 are not visible (green dashes). (b) Close-up of the peptide binding region: the peptide is shown as green sticks, the residues interacting with the peptide are depicted as magenta sticks, and the hydrogen bonds between Trp105-Tyr13 and Glu97-Tyr13 are indicated as black dashes.

### 3.10 Phage display selection in presence of EDTA and calcium

To investigate if the structural changes conferred by  $\text{Ca}^{2+}$  binding translate into specificity changes, we used Sorcin as a bait protein against a highly diverse M13 phage display library that displays 16mer peptides on the major coat protein p8.

Selections were performed in the presence of EDTA (1 mM) or  $\text{Ca}^{2+}$  (1 mM) and were in both cases successful as judged by pooled phage ELISAs (i.e. signal to background > 2). Sequencing of individual clones (38 and 20 clones from the selections in presence or  $\text{Ca}^{2+}$  and EDTA, respectively) revealed

that the majority of ligands contains a conserved Pro and that the main consensus motif under both conditions is a relaxed  $\Phi$ /Gly/Met- $\Phi$ /Gly/Met-x-P, where  $\Phi$ /Gly/Met is an aromatic residue (Trp, Tyr or Phe) or a Gly or Met residue, and x is any amino acid (Figure 29, top). The consensus sequence agrees with the GYYPG peptide belonging to the Sorcin N-terminal domain, identified in the Sorcin binding site in our crystal structure. In addition, there is a set of peptides that lack a clear  $\Phi$  /Gly/Met- $\Phi$ /Gly/Met-x-P motif but instead contains an acidic- $\Phi$  motif (Figure 29, bottom).

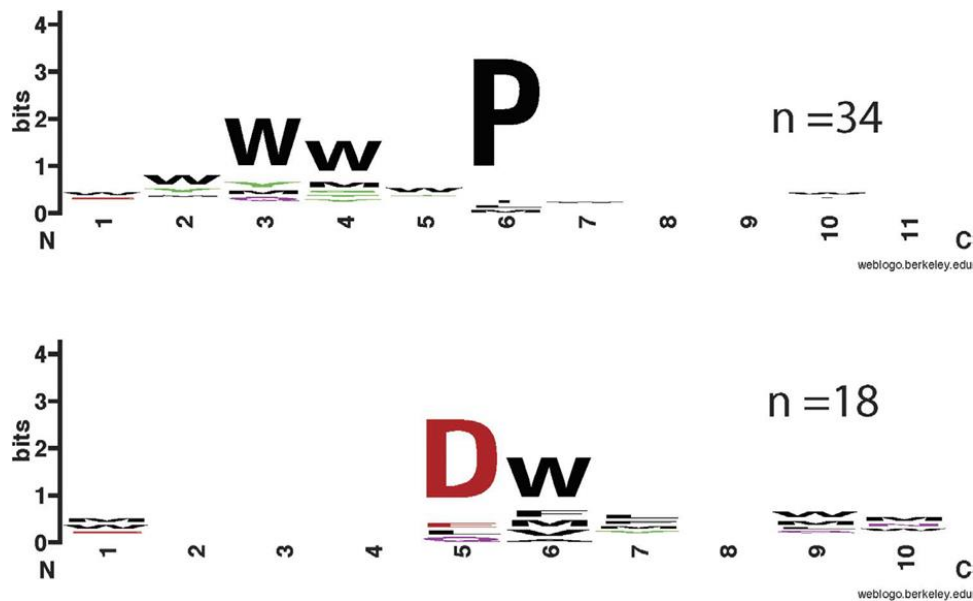


**Figure 29: WebLogo outputs of consensus peptide motifs identified through peptide phage display.** (top) The  $\Phi$ /Gly/Met- $\Phi$ /Gly/Met-x-P motif is based on 34 unique peptide sequences, of which 20 were obtained from a phage selection performed in the presence of 1 mM  $\text{Ca}^{2+}$ . (bottom) The acidic- $\Phi$  motif is from 18 unique peptides of which 16 were selected in presence of  $\text{Ca}^{2+}$ .

Such peptides are more frequently observed in presence of  $\text{Ca}^{2+}$  (47% of sequenced peptides) than in the presence of EDTA (15% of sequenced peptides). In a cellular context, likely Sorcin can establish interactions with a variety of ligands containing the main  $\Phi$ /Gly/Met- $\Phi$ /Gly/Met-x-P motif, or the acidic- $\Phi$  motif found in intrinsically disordered regions of target proteins.



Such interactions might be facilitated by the exposure of hydrophobic binding surface in Sorcin upon  $\text{Ca}^{2+}$  binding, as suggested by the structure. However, peptide binding might occur also in absence of  $\text{Ca}^{2+}$  if the preferred target is readily available as in the high avidity p8 phage display. Indeed, the presence of a high affinity ligand might shift the equilibrium towards the open conformation. Further detailed mechanistic studies should shed light on this issue.

### **3.11 Proteomic peptide phage display (ProP-PD) selection in the presence of calcium, and dataset analysis (pipeline)**

The phage selection in presence of 1 mM EDTA did not result in any significant enrichment of binding motifs (data not shown), thus we focused on the 1 mM calcium selection. In this selection there was an enrichment of binding clones throughout the selection (see Methods). Significant enrichment of selected phages was obtained on the 4<sup>th</sup> round of selection as determined by pooled phage ELISA (signal to background > 2). This pool was then subjected to clonal sequencing analysis and Next Generation Sequencing. This resulted in a list of potential binding clones, as shown in Figure 30 and Appendix 1.

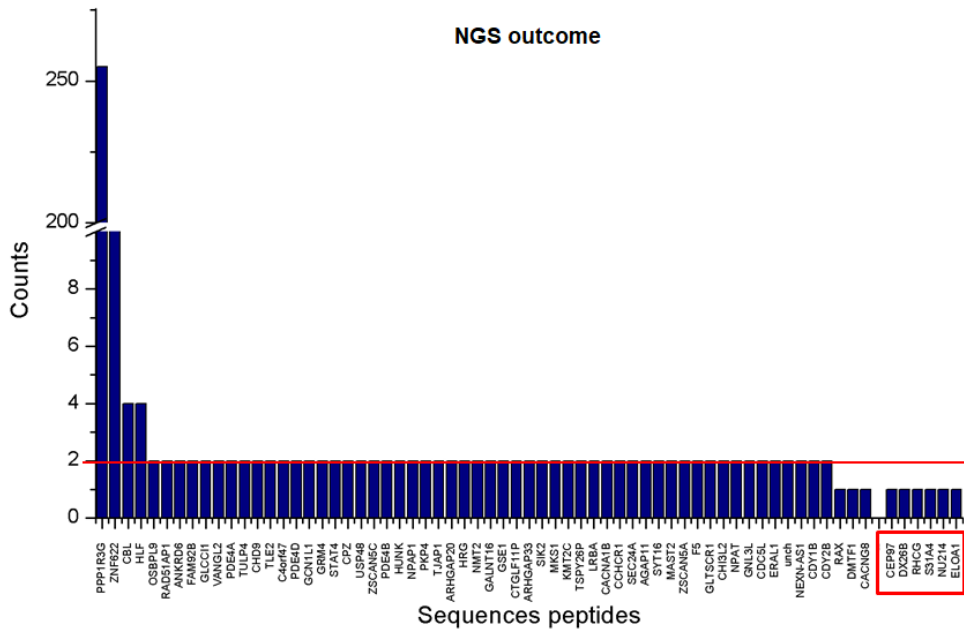


**Figure 30: Next generation sequencing outcome on 4<sup>th</sup> round of phage selection.** Selected bound phages from the 4<sup>th</sup> round of selection underwent NGS analysis that resulted in a list (dataset) of peptide sequences. Each peptide sequence is associated to a count number that corresponds to how many times it has been found in the sequencing analysis. A preliminary sorting was based on counts number, and a threshold of minimum 2 counts was set. In the red squares there are the peptide sequences derived from the clonal analysis.

Once the dataset was obtained, we established a pipeline to sort out unspecific binding clones, based on bioinformatics tools.

The pipeline consists in:

- Counts in NGS
- Enrichment in binding motif/s based on combinatorial phage display
- Biological function (GO TERM)
- Sequence conservation (Ensembl, PepTool, Consurf)
- Bait protein interaction with binding partners (Cytoscape on BioGrid and INTACT networks of interaction)

- Bait protein cellular/subcellular/tissue colocalization with binding partners (Compartments, PaxDB, Human Protein Atlas)

Based on the NGS counts: PPP1R3G, ZNF622, CBL and HLF were selected (>2 counts); if the other dataset peptides are comprised in one or more of pipeline steps they can be included in the final list of targets.

The GO TERM biological function was evaluated with PepTools, DAVID and Generic GO TERM finder (Figure 31 a,b; Appendix 2), highlighting an enrichment in proteins involved in negative regulation of relaxation in skeletal and cardiac muscle, as well as nucleotide metabolism, calcium-related processes and biological regulation. Furthermore, a preferred motif was found in the dataset with WebLogo (Figure 31c). The motif is [FILMPV].[DEST] quite comparable to the motifs derived from combinatorial phage display selections ( $\phi\phi\text{xP}$ ; E/D $\phi$ ).

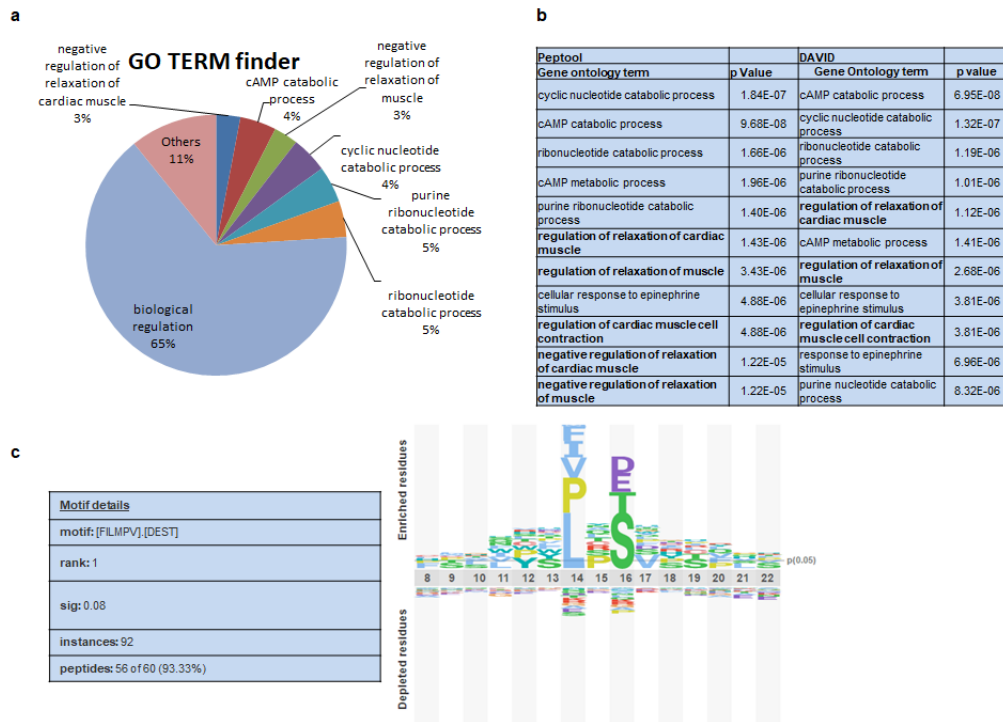


**Figure 31: GO TERM enrichment and preferred motif.** (a) GO TERM finder tool reported an enrichment in peptides belonging to proteins involved in cardiac/skeletal muscle relaxation process, biological regulation and nucleic acids metabolism. (b) Table ranking the biological functions found with PepTool and DAVID, p-value-based. (c) the WebLogo analysis of the dataset showed an enrichment in the FILMPV.DEST motif, with a coverage of 93% of peptide's dataset.

Further, the dataset peptides were analyzed with software as Compartments (<http://compartments.jensenlab.org/Search>) (Table 3), for subcellular localization, and PaxDb (<http://pax-db.org/>) and Human Protein Atlas (<http://www.proteinatlas.org/>) for tissue localization (Table 4 and Figure 32); the targets that shared tissue localization using both tools are PDE4D, PDE4B, OSBPL9, TLE2, PKP4, NMT2, LRBA, MAST2, CEP97.

SORCIN (COMPARTMENTS)	
<b>Knowledge</b>	
	<a href="#">Extracellular exosome</a> , <a href="#">Cytoplasm</a> , <a href="#">Sarcoplasmic reticulum membrane</a> , <a href="#">Z disc</a> , <a href="#">T-tubule</a> , <a href="#">Membrane</a> , <a href="#">ER membrane</a> , <a href="#">Cytosol</a>
<b>Experiments</b>	
	<a href="#">Cytosol</a> , <a href="#">Nucleus</a>
<b>Text mining</b>	
	Sarcoplasmic reticulum, ER membrane, Plasma membrane, Cytosol, Membrane microdomain, cAMP-dependent protein kinase complex, PSI associated light-harvesting complex I, Nucleus, Gas vesicle, PSII associated light-harvesting complex II
<b>Predictions</b>	
	Cytosol, Extracellular region, Cytosol, Nucleus

CBL PDE4A PDE4D PDE4B SEC24A
<ul style="list-style-type: none"> <li>• cytoplasm,</li> <li>• membrane microdomain,</li> <li>• Sarcoplasmic Reticulum,</li> <li>• Endoplasmic Reticulum membrane,</li> <li>• nucleus,</li> <li>• cAMP-dependent protein kinase complex,</li> <li>• plasma membrane,</li> <li>• Z disc</li> </ul>

**Table 3: Compartments results for subcellular localization.** The output of the Compartments tool gives the subcellular localization information based on experimental knowledge, literature and prediction. Five peptides co-localize with Sorcin in the compartments listed in the square in the right

Sorcin tissue expression in PaxDb	
tissue	ppm
<a href="#">H.sapiens - Whole organism, IBAQ (Khan,Science,2013)</a>	1637 ppm
<a href="#">H.sapiens - Gut, Fetal, SC (Kim,Nature,2014)</a>	721 ppm
<a href="#">H.sapiens - Spinalcord, SC (Kim,Nature,2014)</a>	694 ppm
<a href="#">H.sapiens - Female gonad, Fetal, SC (Kim,Nature,2014)</a>	623 ppm
<a href="#">H.sapiens - Placenta, SC (Wilhelm,Nature,2014)</a>	621 ppm
<a href="#">H.sapiens - Heart, normalized data APEX (Ave,Mol. Bio. Syst,2010)</a>	588 ppm
<a href="#">H.sapiens - Colon, SC (Wilhelm,Nature,2014)</a>	559 ppm
<a href="#">H.sapiens - Rectum, SC (Kim,Nature,2014)</a>	545 ppm
<a href="#">H.sapiens - Testis, Fetal, SC (Kim,Nature,2014)</a>	508 ppm
<a href="#">H.sapiens - Cerebral cortex, SC (Wilhelm,Nature,2014)</a>	503 ppm
<a href="#">H.sapiens - Female gonad (Integrated)</a>	462 ppm
<a href="#">H.sapiens - Prostate gland, SC (Kim,Nature,2014)</a>	453 ppm
<a href="#">H.sapiens - Platelet, SC (Kim,Nature,2014)</a>	453 ppm
<a href="#">H.sapiens - Uterus, Post-menopause, SC (Wilhelm,Nature,2014)</a>	441 ppm
<a href="#">H.sapiens - Pancreas, SC (Kim,Nature,2014)</a>	419 ppm
<a href="#">H.sapiens - Placenta (Integrated)</a>	419 ppm
<a href="#">H.sapiens - Uterus (Integrated)</a>	410 ppm
<a href="#">H.sapiens - Fallopian tube, SC (Wilhelm,Nature,2014)</a>	407 ppm
<a href="#">H.sapiens - Uterine cervix, SC (Wilhelm,Nature,2014)</a>	396 ppm
<a href="#">H.sapiens - Oral cavity, SC (Wilhelm,Nature,2014)</a>	390 ppm
<a href="#">H.sapiens - Lymph node, SC (Wilhelm,Nature,2014)</a>	383 ppm
<a href="#">H.sapiens - Kidney, SC (Kim,Nature,2014)</a>	377 ppm
<a href="#">H.sapiens - Liver, Fetal, SC (Kim,Nature,2014)</a>	373 ppm
<a href="#">H.sapiens - Frontal cortex, SC (Kim,Nature,2014)</a>	366 ppm
<a href="#">H.sapiens - Spleen, SC (Wilhelm,Nature,2014)</a>	363 ppm

**23 hits in common with sorcin:**  
 PPP13RG, CBL, OSBP1S, FAM92B, PDE4A, TLE2, Corf47, PDE4D, GCN1L1, STAT4, CPZ, USP48, PDE4B, HUNK, PKP4, TJAP1, HRG, NMT2, LRBA, CCHCR1, SEC24A, MAST2, F5, CDC5L, ERAL1, CEP97, NUP214, ELOA1

**Table 4: PaxDb Sorcin tissue expression.** Sorcin is well expressed in the whole body as in many organs and tissues (here listed some of them). Proteins from the dataset that shares  $\geq 3$  hits in common with Sorcin are listed in the square at the right side.

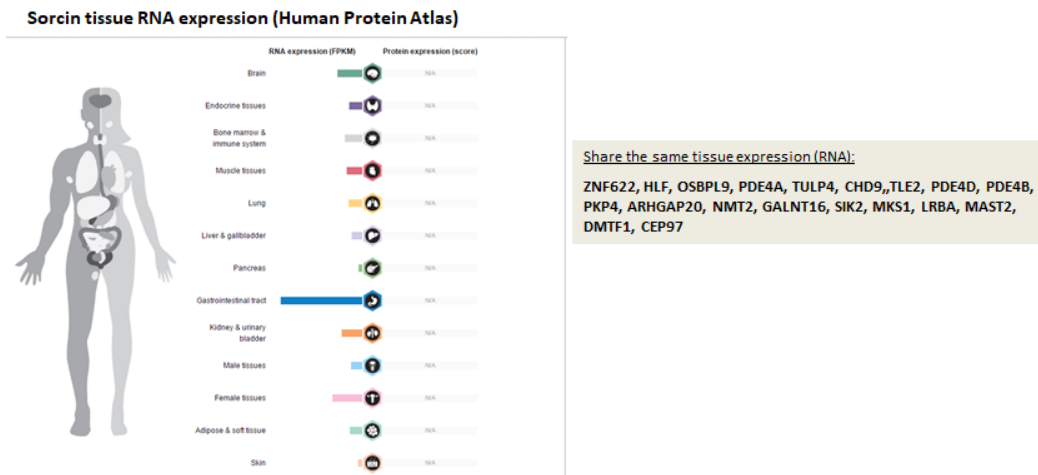


**Figure 32: Sorcin tissue RNA expression in Human Protein Atlas.** Human Protein Atlas gives only Sorcin RNA expression information, in the right-side square are listed the dataset peptides that share with Sorcin the same RNA tissue expression.

Beside the cellular and tissue localization, in order to evaluate whether the proteins from the dataset share common binding partners with Sorcin, a protein-protein interaction network was performed using Cytoscape.

Information of binders listed in the BioGrid and INTACT databases were used as inputs for each protein of the selected dataset. These networks were then merged with Sorcin network and only the first of first neighbour network was selected resulting in the networks shown in Figure 33.

The green squares are the matches between the BioGrid/Intact networks of targets and Sorcin. Biogrid network has: NMT2, OSBPL9, STAT4, GSE1, LRBA, F5, HRG, MAST2, GCNC1, CBL, NUP214; while Intact network has: NMT2, CBL, NUP214, LRBA, HRG, CACN1B, GNL3L, CDC5L, MSK1. Interestingly some are shared in both networks.

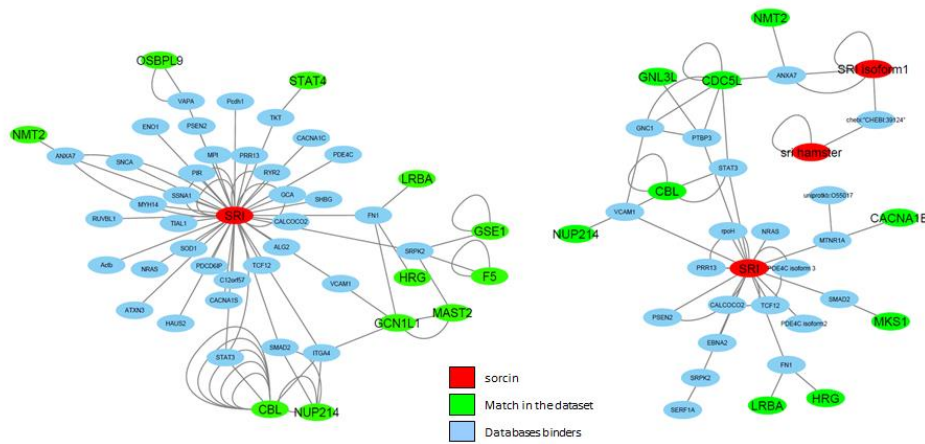


**Figure 33: Cytoscape networks built on BioGrid and Intact interaction databases.** Both networks (BioGrid left; Intact right) have matches in the peptide dataset, meaning that some proteins might be in networks related to the bait protein.

The abovementioned findings were applied as a filter on the dataset and a first list of targets was generated combining these information with the protein functions (Table 5, source Uniprot). Several peptides contained Pro flanked by hydrophobic residues ( $\phi$ ) and/or hydrophobic residues flanked by acidic residues (D, E) e.g:  $\phi\phi xP$  and  $E/D\phi$ , consistent with previous results. However some of the positively filtered peptides (SYT16, MAST2, CAC1B) did not contain aforementioned motifs although they may potentially use different binding ways. Based on the sequences, the counts, the cellular/tissue localization, related interaction networks and biological relevance (e.g: involvement in same biological processes) following peptides were chosen for further analysis (Table 5).

<p><b>PP13G (255) YTFTEWRSFLDVPAEL</b> Glycogen-targeting subunit for protein phosphatase 1 (PP1). Involved in the regulation of hepatic glycogenesis in a manner coupled to the fasting-feeding cycle and distinct from other glycogen-targeting subunits</p>
<p><b>ZNF622 (14) LEFADFYDFRSSYPDH</b> May behave as an activator of the bound transcription factor, MYBL2, and be involved in embryonic development</p>



<b>CBL (4) <u>PRDLLPQRVAVPSSA</u></b> Adapter protein that functions as a negative regulator of many signaling pathways that are triggered by activation of cell surface receptors. Acts as an E3 ubiquitin-protein ligase promoting protein degradation by the proteasome. Recognizes activated receptor tyrosine kinases and terminates signaling.
<b>HLF (4): <u>HPGIPSPNCMQSPIRP</u></b> Hepatic leukemia factor is a transcriptionally controlled transcription factor. Binds to DNA sites required for the transcription of alpha 1-antitrypsin, apolipoprotein CIII, transthyretin genes and HNF1-alpha. May be essential for development of the liver, kidney and intestine.
<b>CAC1B (2) <u>SYVSSLTSQSHPLRRV</u></b> Voltage-sensitive calcium channels (VSCC) mediate the entry of calcium ions into excitable cells and are also involved in a variety of calcium-dependent processes, including muscle contraction, hormone or neurotransmitter release, gene expression, cell motility, cell division and cell death. The isoform alpha-1B gives rise to N-type calcium currents.
<b>SYT16 (2) <u>EQKPKFSRSLTHGED</u></b> May be involved in the trafficking and exocytosis of secretory vesicles in non-neuronal tissues. Is Ca <sup>2+</sup> -independent.
<b>CBPZ (2) <u>PGQHELMEPEVKLIGN</u></b> Cleaves substrates with C-terminal arginine residues. Probably modulates the Wnt signaling pathway
<b>MAST2 (2) <u>LSPREQGKTQPPSAPR</u></b> Appears to link the dystrophin/utrophin network with microtubule filaments via the syntrophins. Phosphorylation of DMD or UTRN may modulate their affinities for associated proteins.
<b>NPAT (2) <u>ETTVPFPEESIVPAAK</u></b> Required for progression through the G1 and S phases of the cell cycle and for S phase entry.
<b>STAT4 (2) <u>VPSVFIPISTIRSDST</u></b> Carries out a dual function: signal transduction and activation of transcription. Involved in IL12 signaling.
<b>TJP1 (2) <u>GRAWPLPSSSRPQRSP</u></b> May be involved in transducing a signal required for tight junction assembly and stabilization. Plays a role in the regulation of cell migration
<b>TSYL2 (2) <u>RWPTETPSRPYGFQSG</u></b> Part of the CASK/TBR1/TSPYL2 transcriptional complex that modulates gene expression in response to neuronal synaptic activity. May inhibit cell proliferation
<b>NUP214 (1) <u>LVPERETLFNTLANNR</u></b> May serve as a docking site in the receptor-mediated import of substrates across the nuclear pore complex
<b>CEP97 (1) <u>LIPEHSSPVQDAQISQ</u></b> Acts as a key negative regulator of ciliogenesis in collaboration with CCP110 by capping the mother centriole thereby preventing cilia formation. Required for recruitment of CCP110 to the centrosome

**Table 5: Summary of positively filtered binding peptides (source: UniProt).** The sequencing counts are in brackets and the corresponding peptide sequence in bold; the motif-like residues are underlined. The five highlighted peptides were confirmed by ELISA assay and sequencing, the remaining targets were not confirmed after sequencing (see below).

The sequencing results together with the outcome of the clone phage ELISA for the aforementioned targets, confirmed five positive clones, highlighted in Table 5. A phage clone is considered as a positive binder if the absorbance ratio at 450 nm between the protein and the negative control is higher than 2 (Figure 34). The absorbance is measured at this wavelength because the TMB (3,3',5,5'-tetramethylbenzidine) soluble substrate that detects Horseradish Peroxidase (HRP) in presence of sulfuric acid has an absorbance maximum at 450 nm.

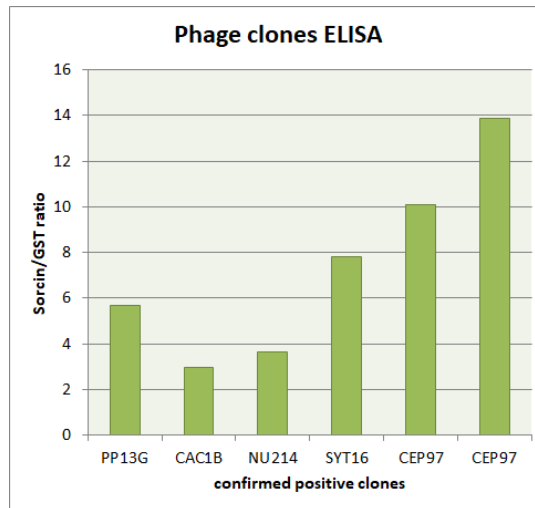


**Figure 34: Phage clones ELISA.** Target peptides confirmed after sequencing, (CEP97 was checked in duplicate). Only the clones with positive signal (ratio>2) were sequenced.

For the other clones from chosen set (CBL, STAT4, ZNF622, CBPZ, MAST2, NPAT, TJP1, TSYL2, HLF), no results are available, as the presence of constructs was not confirmed by sequencing (data not shown).

Intrinsically disordered regions of the proteins are not necessarily highly conserved; however, in case they are conserved, they probably have to be relevant for some biological interaction. To this end we checked for sequence conservation using PepTools in metazoan and Ensembl in placental mammalian and Consurf with no constraint. Ensembl multiple sequence alignment has also been represented with WebLogo (Figure 35); then Peptools overall 16-mer sequence conservation was associated to a score (0=conserved; 1=not conserved): here we established a threshold of 0.5 (Appendix 3). Ensembl and Consurf alignment was performed on the 5 confirmed targets, while Peptool alignment was performed on the complete peptides dataset (Appendix 3).

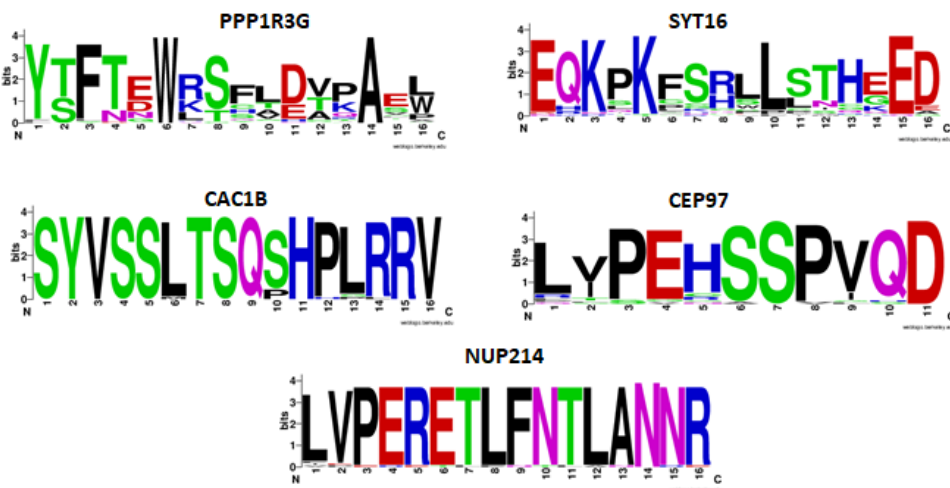


**Figure 35: WebLogo analysis on peptides sequence alignment.** Multiple sequence alignment was performed with Ensembl on the phage clones ELISA-validated targets. As shown, in placental mammalian subgroup, the five sequences appear to be rather conserved, except for PPP1R3G and SYT16.

Although PPP1R3G and SYT16 appear not to be as conserved as the other three targets, it is worth noticing that hydrophobic residues appear to be more

conserved than the others in PPP1R3G, as in SYT16 acidic residues and leucine.

Taken together, the filters of the pipeline allowed us to pick 5 out of 60 peptide targets for further *in vitro* binding validation; these targets are: PPP1R3G, CEP97, SYT16, CACN1B, NUP214.

### **3.12 Mutagenesis of putative crucial residues involved in Sorcin-targets interaction and binding affinity analysis through SPR and MicroScale Thermophoresis (MST) experiments**

To probe key binding residues of the motifs, a mutagenic analysis of the binding peptides was performed (See materials and methods). Due to some technical difficulties and phage cross-contamination, the analysis was only finalized for the CEP97 peptide. The mutations were designed based on Sorcin preferred binding motif ( $\Phi\Phi xP$  and  $D/E\Phi$ ). In case of CEP97, this led to the mutation of an “IPE” triplet at the beginning of the sequence, to “AAA”. The phage ELISA assay of the mutant CEP97 confirmed that the “IPE” stretch is crucial for Sorcin binding (Figure 36).

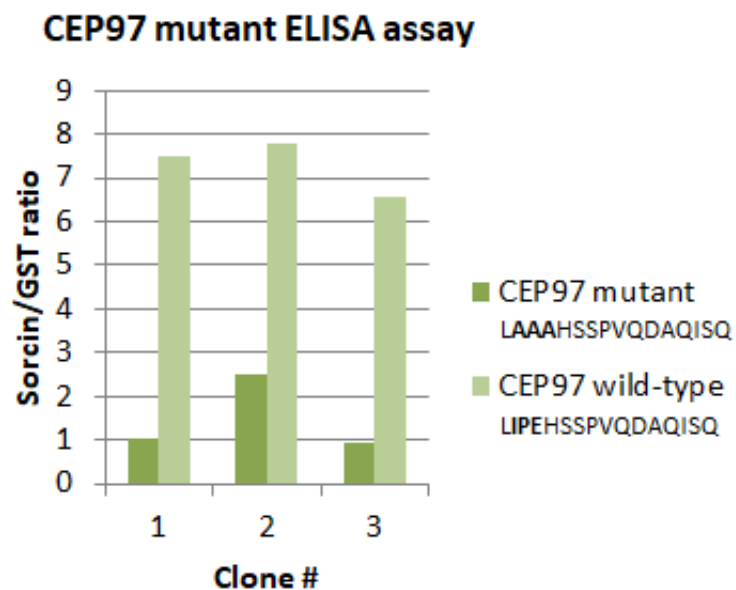


**Figure 36: Phage ELISA assay validation on mutated peptide (LAAHSSPVQDAQISQ) and wild type peptide (LPEHSSPVQDAQISQ).** In all of the three mutated clones the binding is disrupted, suggesting that the “IPE” stretch is crucial for Sorcin binding.

The five peptides were chosen *in vitro* for affinity determinations through MST: PPP1R3G, SYT16, CAC1B, CEP97, NUP214. The affinity measurements were performed in the presence of calcium (100  $\mu$ M CaCl<sub>2</sub>). Figure 37 shows examples of MST fitted traces with their K<sub>D</sub> values summarized in the table. Regarding NUP214, no fit was possible thus no K<sub>D</sub> is available.

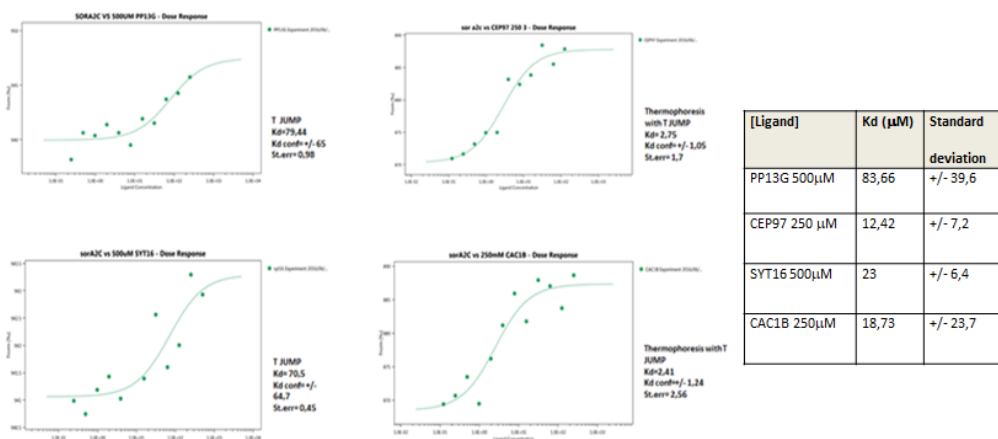


**Figure 37: *In vitro* Sorcin-peptides binding experiments using MST.** The four traces represent single MST experiments between Sorcin and PPP1R3G, CEP97, SYT16, CAC1B; no binding event was detected for NUP214. PPP1R3G and SYT16 traces were fitted with a T jump model, while CEP97 and CAC1B were fitted with a thermophoresis plus T jump model. In the table the  $K_D$  values calculated on three experiments are reported, with the corresponding standard deviation values.

The MST analysis showed a reasonable affinity for four out of five targets, even though the standard deviations are rather high and the quality of the fitting rather poor. Indeed the best fitting model should be the thermophoretic one, that takes into account the behaviour of the complex after the IR-laser is activated and molecules flow induced. On the contrary, the T jump and thermophoretic plus T jump models take into account the temperature jump induced by the IR-laser, thus the changes detected might be due to transient environmental changes around the fluorophore. Since the MST results were not sufficient as a validation of binding affinity for the selected peptides, SPR experiments were performed immobilizing Sorcin on the chip (as the ligand) and using the five peptides as analytes, using the HBS buffer supplemented with 500 $\mu\text{M}$   $\text{CaCl}_2$ , in a traditional SPR experiment setup.

The fitting and affinity analysis was possible only for CEP97, that binds to Sorcin with a  $K_D=104\mu\text{M}$  (Figure 38).

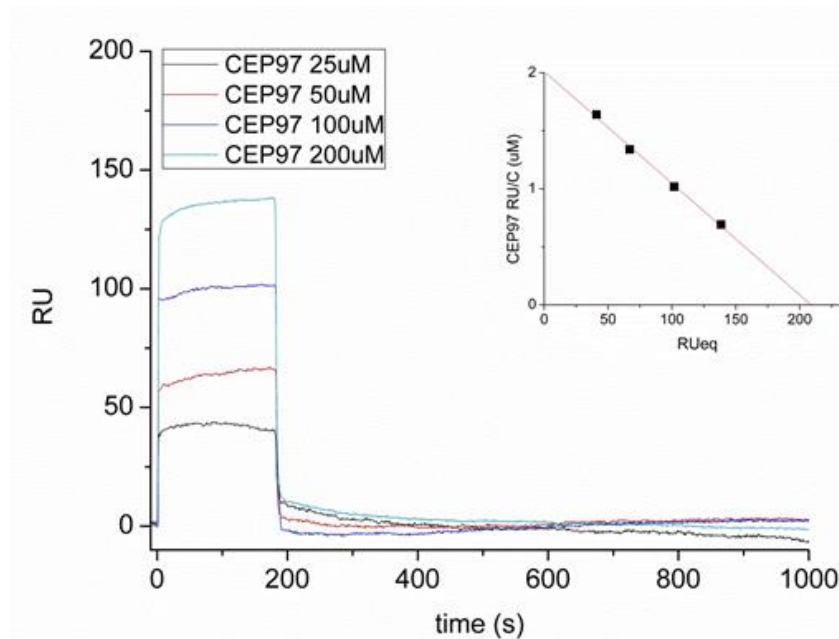


**Figure 38: SPR experiments and linear fitting for CEP97-Sorcin binding.** Traditional SPR experiment was performed with 1:2 increasing concentrations of the analyte in presence of 500 $\mu$ M CaCl<sub>2</sub>. The Scatchard plot is in the inset; linear fitting analysis give a  $K_D=104 \mu$ M.

In conclusion, through ProP-PD selection, further bioinformatics filtering analysis and subsequent *in vitro* binding validation, it has been possible to identify a novel Sorcin binding partner, CEP97. The low binding affinity is consistent with the ability of disordered binding regions to undertake transient interactions, crucial for biological processes regulation.

CEP97 is a negative regulator of ciliogenesis that acts in collaboration with CCP110 for the prevention of cilia formation; this interaction might open intriguing perspectives on Sorcin role during cell division (Lalioi VS et al. 2014).

Nevertheless additional information about binding characterization is necessary, as the binding affinity validation on the whole protein and/or co-Immunoprecipitation experiments in cells.

### 3.13 Selective calcium-dependent interactions between Sorcin and targets

The interactions between Sorcin and PDCD6 (programmed cell death protein 6) (formerly called Alg-2) a member of the PEF protein family, endowed with Sorcin N-terminal consensus binding motifs was tested by both SPR and colocalization experiments. PDCD6 has a role in the mechanisms of apoptosis onset, and was shown to interact with N-terminal peptide of annexin 11 in the presence of 50  $\mu\text{M}$   $\text{Ca}^{2+}$ , with a higher affinity than Sorcin (Sato H et al. 2002). PDCD6 has 36% identity with respect to Sorcin, displays similar structure and displays residues as Trp95 Arg125 and Met71, conserved also in Sorcin, which allow its interaction with Alix (Suzuki H et al. 2008) and potentially with the Sorcin N-terminal domain. Moreover, PDCD6 displays an N-terminal domain similar to that of Sorcin, and containing  $\Phi/\text{Gly}/\text{Met}-\Phi/\text{Gly}/\text{Met}-\text{x}-\text{P}$  sequences identified as Sorcin-interacting motifs.

SPR experiments show that both the whole Sorcin and SCBD are able to interact with PDCD6 in the presence of calcium, with a  $K_D = 3.5 \mu\text{M}$  (Figure 39 A1-A2). In the presence of EDTA, SCBD interacts with PDCD6 with a  $K_D = 5 \mu\text{M}$  whereas the calcium-free Sorcin interacts with PDCD6 with an even lower affinity ( $K_D = 12 \mu\text{M}$  Figure 39 B1-B2). Both association and dissociation are faster in the presence of calcium than in the presence of EDTA. The N-terminus has therefore an inhibitory activity in Sorcin-PDCD6 interaction at low calcium concentrations. Additionally, both Sorcin and SCBD interact with the N-terminal domain of PDCD6, with  $K_D = 5 \mu\text{M}$  for Sorcin and  $K_D = 6 \mu\text{M}$  for SCBD (Figure 39 C1-C2). Partial colocalization



between Sorcin and PDCD6 takes place in perinuclear regions of differentiated 3T3-L1 adipocytes and in the midbody of 3T3-L1 preadipocytes (Figure 39b). Sorcin also colocalizes with annexin 7 and annexin 11, which possess N-terminal domains containing  $\Phi$ /Gly/Met- $\Phi$ /Gly/Met-x-P sequences, in the midbody of 3T3-L1 preadipocytes (Figure 39b).

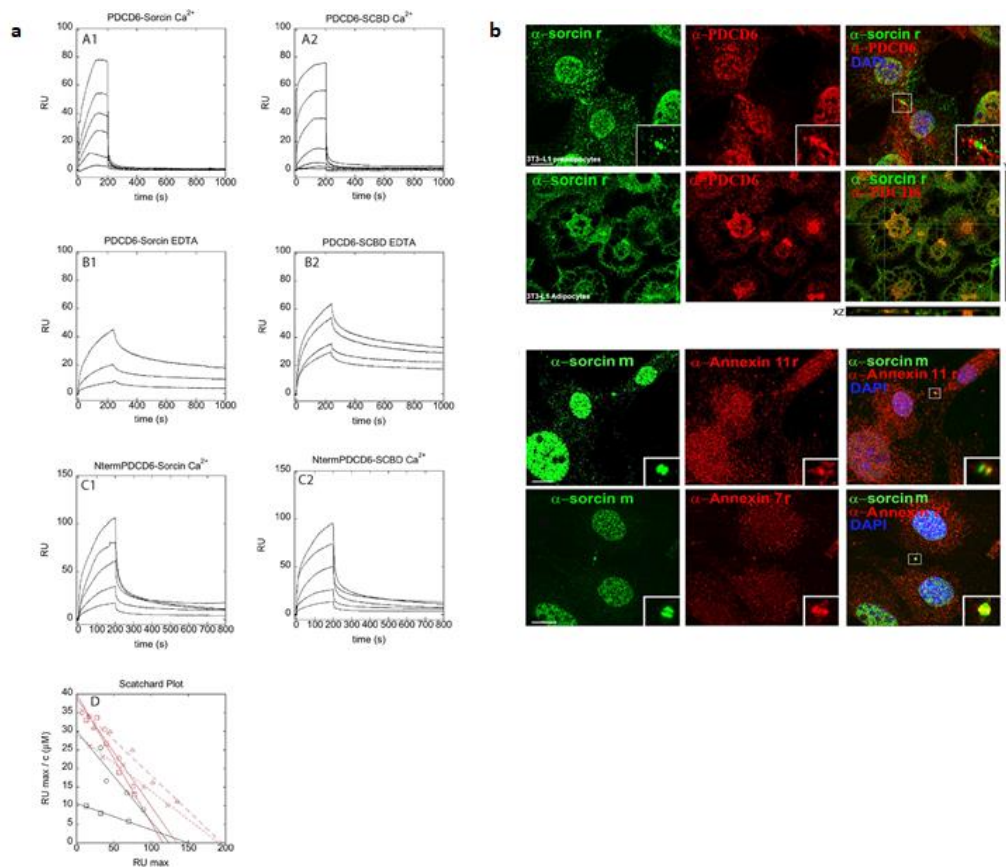


**Figure 39: Interaction of Sorcin with full-length PDCD6 and N-terminus of PDCD6, and colocalization of Sorcin with PDCD6 and annexins 7 and 11.** (a) A1-A2. Sensorgrams showing the interaction between PDCD6, immobilized on a COOH5 chip and different concentrations of Sorcin (left panel; from bottom to top: 200 nM, 400 nM, 800 nM, 1.5  $\mu$ M, 3  $\mu$ M, 6  $\mu$ M), and SCBD (right panel; from bottom to top: 50 nM, 100 nM, 200 nM, 500 nM, 1  $\mu$ M, 2.5  $\mu$ M, 5  $\mu$ M), in the presence of 100  $\mu$ M calcium. B1-B2. Sensorgrams showing the interaction between PDCD6, immobilized on a COOH5 chip and different concentrations of Sorcin (left panel: from bottom to top: 1.3  $\mu$ M, 4  $\mu$ M, 12  $\mu$ M), and SCBD (right panel: from bottom to top: 1.25  $\mu$ M, 2.5  $\mu$ M, 5  $\mu$ M, 10  $\mu$ M), in the presence of 1 mM EDTA. C1-C2. Sensorgrams showing the interaction between the N-terminal domain of PDCD6, immobilized on a COOH5 chip and different concentrations of Sorcin (left panel; from bottom

to top: 750 nM, 1.5  $\mu$ M, 3  $\mu$ M, 6  $\mu$ M, 12  $\mu$ M), and SCBD (right panel; from bottom to top: 750 nM, 1.5  $\mu$ M, 3  $\mu$ M, 6  $\mu$ M, 12  $\mu$ M), in the presence of 100  $\mu$ M calcium. D. Scatchard plots of the experiments in the panels from A to C, and linear fittings. Red squares: PDCD6-Sorcin interaction in the presence of 100  $\mu$ M calcium; red circles: PDCD6-SCBD interaction in the presence of 100  $\mu$ M calcium; black squares: PDCD6-Sorcin interaction in the presence of 1 mM EDTA; black circles: PDCD6-SCBD interaction in the presence of 1 mM EDTA; red triangles: N-terminal domain of PDCD6-Sorcin interaction in the presence of 100  $\mu$ M calcium; red crosses: N-terminal domain of PDCD6-SCBD interaction in the presence of 100  $\mu$ M calcium.

(b) (top) Experiments showing co-localization between Sorcin (rabbit  $\alpha$ -Sorcin, green) and PDCD6 (mouse  $\alpha$ -PDCD6, red), in 3T3-L1 preadipocytes in cytokinesis (top panel) and differentiated 3T3-L1 adipocytes (bottom panel) in X and Z axes. Bars: 10  $\mu$ m. Note the colocalization in the midbody of 3T3-L1 preadipocytes and in the perinuclear region of adipocytes.

(bottom) Experiments showing co-localization between Sorcin (mouse  $\alpha$ -Sorcin, green) and annexin11 (top panel: rabbit  $\alpha$ -annexin11, red), or annexin7 (bottom panel: rabbit  $\alpha$ -annexin7, red), in 3T3-L1 preadipocytes in cytokinesis. Bars: 10  $\mu$ m. Note the colocalization in the midbody (arrows and insets).

## Supplementary material

**Appendix 1: Results of next-generation sequencing.** The table summarizes the protein name (UniProt), the selected peptide sequence and the counts. Peptides with highest counts are highlighted.

Protein Name	Peptide	NGS count
<b>Protein phosphatase 1 regulatory subunit 3G (PPP1R3G)</b>	<b>YTFTEWRSFLDVPAEL</b>	<b>255</b>
<b>Zinc finger protein 622 (ZNF622)</b>	<b>LEFADFYDFRSSYPDH</b>	<b>14</b>
<b>E3 ubiquitin-protein ligase CBL (CBL)</b>	<b>PRLDLLPQRVCVPSSA</b>	<b>4</b>
<b>Hepatic leukemia factor (HLF)</b>	<b>HPGIPSPNCMQSPIRP</b>	<b>4</b>
Oxysterol-binding protein-related protein 9 (OSBPL9)	SSEDEFYDADEFHQSG	2
RAD51-associated protein 1 (RAD51AP1)	TMNKSPHISNCSVASD	2
Ankyrin repeat domain-containing protein 6 (ANKRD6)	LSSSDCTGSRLRNVKV	2
Protein FAM92B (FAM92B)	LQSLASQGTLQVQLSR	2
Glucocorticoid-induced transcript 1 protein (GLCCI1)	MPLSNISVPKSSVSRV	2
Vang-like protein 2 (VANGL2)	SSRKHRDRRDRHRSKS	2
cAMP-specific 3',5'-cyclic phosphodiesterase 4A (PDE4A)	MLNRELTHLSEMSRSG	2

Tubby-related protein 4 (TULP4)	QPCSSATLNRLTVPRY	2
Chromodomain-helicase-DNA-binding protein 9 (CHD9)	SHPQGNYSNSKLSPVH	2
Transducin-like enhancer protein 2 (TLE2)	LAAKPAPSTDSVALRS	2
UPF0602 protein C4orf47 (C4orf47)	RLLKGAPFKLNLHPRD	2
cAMP-specific 3',5'-cyclic phosphodiesterase 4D (PDE4D)	MLNRELTHLSEMSRSG	2
Translational activator GCN1 (GCN1L1)	QILQILTVQAQLRASP	2
Metabotropic glutamate receptor 4 (GRM4)	ALATKQTYVITYTNHAI	2
Signal transducer and activator of transcription 4 (STAT4)	VPSVFIPISTIRSDST	2
Carboxypeptidase Z (CBPZ)	PGQHELMEPEVKLIGN	2
Ubiquitin carboxyl-terminal hydrolase 48 (USP48)	MLVYRLQTQEKPNNTTV	2
Zinc finger and SCAN domain-containing protein 5C (ZSCAN5C)	MAANCTSSWSLGESCN	2
cAMP-specific 3',5'-cyclic phosphodiesterase 4B (PDE4B)	MLNRELTHLSEMSRSG	2
Hormonally up-regulated neu tumor-associated kinase (HUNK)	RTPRIVKKPEPHQGP	2
Nuclear pore-associated protein 1 (NPAP1)	SDSSFILGNPATPAPV	2
Plakophilin-4 (PKP4)	YSPEQTSLHESEGLG	2
Tight junction-associated protein 1 (TJAP1)	GRAWPLPSSSRPQRSP	2
Rho GTPase-activating protein 20 (ARHGAP20)	ALQKRPTTRDSPSASV	2
Histidine-rich glycoprotein (HRG)	HKHPLKPDNQFPQSV	2
Glycylpeptide N-tetradecanoyltransferase 2 (NMT2)	MTLQRTMKLYRLPDVT	2

Polypeptide N-acetylgalactosaminyltransferase 16 (GALNT16)	SEQLREDRTIPLIVTG	2
Genetic suppressor element 1 (GSE1)	KPVQHPLHPVPTPHHT	2
Putative centaurin-gamma-like family member 11P (CTGLF11P)	STTSPKLNLPSPHAN	2
Rho GTPase-activating protein 33 (ARHGAP33)	MVARSTDSLDPGEGS	2
Serine/threonine-protein kinase SIK2 (SIK2)	SVSTLPASVHPQLSPR	2
Meckel syndrome type 1 protein (MKS1)	EARESLPQDLVSPSGT	2
Histone-lysine N-methyltransferase 2C (KMT2C)	LQMNETTANRSPVRD	2
Putative testis-specific Y-encoded-like protein 3 (TSPY26P)	RWPTETPSRPYGFQSG	2
Lipopolysaccharide-responsive and beige-like anchor protein (LRBA)	RSSNAKLPSVPTVDSV	2
Voltage-dependent N-type calcium channel subunit alpha-1B (CACNA1B)	SYVSSLTSQSHPLRRV	2
Coiled-coil alpha-helical rod protein 1 (CCHCR1)	APTWLSDIPLVQPPGH	2
Protein transport protein Sec24A (SEC24A)	GNTSLTTNHQYVSSGY	2
Arf-GAP with GTPase, ANK repeat and PH domain-containing protein 11 (AGAP11)	STTSPKLNLPSPHAN	2
Synaptotagmin-16 (SYT16)	EQKPKFSRSLTHGED	2
Microtubule-associated serine/threonine-protein kinase 2 (MAST2)	LSPREQGKTQPPSAPR	2
Zinc finger and SCAN domain-containing protein 5A (ZSCAN5A)	MAANCTSSWSLGESCN	2

Coagulation factor V (F5)	HTVNPNMKEDGILGPI	2
Glioma tumor suppressor candidate region gene 1 protein (GLTSCR1)	YVSSSRSLGLPIAASS	2
Chitinase-3-like protein 2 (CHI3L2)	GPYPLVQAVKRSLSL	2
Protein NPAT (NPAT)	ETTVPFPEESIVPAAK	2
Guanine nucleotide-binding protein-like 3-like protein (GNL3L)	SNSMVDVCSVDRRSVL	2
Cell division cycle 5-like protein (CDC5L)	TPRSGTTPKPVINSTP	2
GTPase Era, mitochondrial (ERAL1)	THCPSPAVKDPNTQSV	2
Putative uncharacterized protein ENSP00000382790 ()	MIATVPLRHSIRDRKP	2
Putative uncharacterized protein NEXN-AS1 (NEXN-AS1)	EGSAPTPLTEGSLPTV	2
Testis-specific chromodomain protein Y 1 (CDY1B)	HTSVPRVKGGQRNITD	2
Testis-specific chromodomain protein Y 2 (CDY2B)	HTSVPRVKGGQRNITD	2
Retinal homeobox protein Rx (RAX)	VSSMKLQDSPLLSFSR	1
Cyclin-D-binding Myb-like transcription factor 1 (DMTF1)	NPTLLENKSGSGVPNS	1
Voltage-dependent calcium channel gamma-8 subunit (CACNG8)	SGGSGPSAILRLPSYR	1

**Appendix 2: GO TERM biological function (PepTool and DAVID).** List of the GO TERM functions of the selected dataset. Here are reported the functions in the ranges of p-values reported in brackets; the underlined entries match with known Sorcin biological function.

### PepTools:

(P value from 0,0000406 to 0,01)

cyclic nucleotide catabolic process	carbohydrate derivative catabolic process
cAMP catabolic process	organophosphate catabolic process
ribonucleotide catabolic process	neutrophil migration
cAMP metabolic process	neutrophil chemotaxis
purine ribonucleotide catabolic process	<u>regulation of cardiac muscle contraction</u>
<u>regulation of relaxation of cardiac muscle</u>	regulation of interleukin-2 production
<u>regulation of relaxation of muscle</u>	positive regulation of JNK cascade
cellular response to epinephrine stimulus	Hemostasis
<u>regulation of cardiac muscle cell contraction</u>	<u>regulation of calcium ion transmembrane transport</u>
<u>negative regulation of relaxation of cardiac muscle</u>	Blood coagulation
<u>negative regulation of relaxation of muscle</u>	<u>cellular response to drug</u>
purine nucleotide catabolic process	<u>regulation of calcium ion transmembrane transporter activity</u>
cyclic nucleotide metabolic process	granulocyte chemotaxis
response to epinephrine stimulus	positive regulation of stress-activated MAPK cascade
regulation of actin filament-based movement	positive regulation of stress-activated protein kinase signaling cascade
purine-containing compound catabolic process	granulocyte migration
nucleotide catabolic process	positive regulation of interferon-gamma production
cellular response to monoamine stimulus	<u>regulation of striated muscle contraction</u>
cellular response to catecholamine stimulus	neurotransmitter secretion
nucleoside phosphate catabolic process	
response to monoamine stimulus	
response to catecholamine stimulus	
regulation of ARF GTPase activity	
protein export from nucleus	
positive regulation of interleukin-2 production	

## DAVID:

(P VALUE FROM 0,000000695 TO 0,0012)

negative regulation of relaxation of cardiac muscle

negative regulation of relaxation of muscle

cAMP catabolic process

cyclic nucleotide catabolic process

ribonucleotide catabolic process

purine ribonucleotide catabolic process

regulation of relaxation of cardiac muscle

cAMP metabolic process

regulation of relaxation of muscle

cellular response to epinephrine stimulus

regulation of cardiac muscle cell contraction

response to epinephrine stimulus

purine nucleotide catabolic process

cyclic nucleotide metabolic process

regulation of actin filament-based movement

purine-containing compound catabolic process

nucleotide catabolic process

cellular response to monoamine stimulus

cellular response to catecholamine stimulus

nucleoside phosphate catabolic process

response to monoamine stimulus

response to catecholamine stimulus

regulation of ARF GTPase activity

positive regulation of interleukin-2 production

carbohydrate derivative catabolic process

organophosphate catabolic process

neutrophil migration

regulation of interleukin-2 production

neutrophil chemotaxis

positive regulation of JNK cascade

regulation of cardiac muscle contraction

Hemostasis

regulation of calcium ion transmembrane transport

Blood coagulation

cellular response to drug

regulation of calcium ion transmembrane transporter activity

granulocyte chemotaxis

positive regulation of stress-activated MAPK cascade

positive regulation of stress-activated protein kinase signaling cascade

granulocyte migration

positive regulation of interferon-gamma production

regulation of striated muscle contraction

regulation of ion transmembrane transporter activity

neurotransmitter secretion

regulation of transmembrane transporter activity

Ribosome biogenesis

regulation of cation channel activity

regulation of actin filament-based process

regulation of heart contraction

regulation of transporter activity

**Appendix 3: Ensembl (placental mammalian), PepTool (metazoan) sequence alignment, ConSurf representation of Ensembl sequence alignment.** A: Ensembl the residues conserved throughout the alignment are highlighted in a square vs. Homo sapiens sequence (in red), while in yellow are highlighted the original residues from the original peptide sequence. B: Peptool gives a value from 0=conserved to 1=not conserved; the applied threshold is 0.5. C: Consurf MSA representation gives information on conservation, buried/exposed, functionally/structurally relevant residues.

### A: Ensembl

#### PP13G (YTFTEWRSFLDVP AEL)

ENSLACP00000016420_Lcha/1-231	YTFNNWLSFIDTPARY
ENSXETP00000064016_Xtro/1-224	YSFNDWLSHLDCPATA
ENSLAFP00000020731_Lafr/1-282	YTFTEWRSFLDVP AEL
ENSDNOP00000018831_Dnov/1-356	YTFTEWRSFLDVP AEL
ENSSTOP00000016173_Itri/1-324	YTFTEWRTFLDVP AEL
ENSRNOP00000064180_Rnor/1-347	YTFTEWRTFLDVP AEL
ENSMUSP000000122712_Mmus/1-347	YTFTEWRTFLDVP AEL
ENSOGAP00000020989_Ogar/1-342	YTFTEWRSFLDVP AEL
ENSMMUP00000025235_Mmul/1-283	YTFTEWRSFLDVP AEL
ENSNLEP00000022740_Nleu/1-358	YTFTEWRSFLDVP AEL

ENSGGOP00000025034\_Ggor/1-358 YTFTEWRSFLDVP AEL  
 ENSP00000393832\_Hsap/1-358 YTFTEWRSFLDVP AEL  
 ENSPTRP00000060169\_Ptro/1-358 YTFTEWRSFLDVP AEL  
 ENSCSAP00000018620\_Csab/1-354 YTFTEWRSFLDVP AEL  
 ENSCJAP00000039772\_Cjac/1-287 YTFTEWRSFLDVP AEL  
 ENSAMEP00000018108\_Amel/1-249 YTFTEWRSFLDVP AEL  
 ENSMLUP00000020255\_Mluc/1-314 YTFTEWRSFLDVP AEL  
 ENSSSCP00000001065\_Sscr/1-353 YTFTEWRSFLDVP AEL  
 ENSBTAP000000055612\_Btau/1-344 YTFTEWRSFLDVP AEL  
 ENSONIP00000026205\_Onil/1-268 YTFNEWLSHVDAQAVP  
 ENSONIP00000026204\_Onil/1-232 YTFNDWLSHMDAQAVP  
 ENSPFOP00000024310\_Pfor/1-207 LTYNDWLSYVDAQAVP  
 ENSLOCP00000014321\_Locu/1-236 YTFNDWLSFVDAQAVA  
 ENSAMXP00000026840\_Amex/1-253 YTLDEWQSYVDARAE P  
 ENSDARP000000132511\_Drer/1-249 YTFNDWLSFVDAQAI P  
 ENSDARP000000118761\_Drer/1-285 YSFTNWKSCSETKAYW  
 ENSAMXP00000002759\_Amex/1-288 YSFTNWKSCSETKANW  
 ENSTRUP000000034907\_Trub/1-250 YSFTDWKSCSETKASW  
 ENSTNIP00000000313\_Tnig/1-288 FSFTGWKSCTEAKATW  
 ENSONIP00000026130\_Onil/1-267 YSFTGWKSCAEAKASW  
 ENSXMAP00000019665\_Xmac/1-270 YSFTEWKGS AETKASW  
 ENSPFOP00000007964\_Pfor/1-342 YSFTEWKSSAETKASW  
 ENSGMOP00000015353\_Gmor/1-244 YSFTEWKSH TETKASW  
 ENSONIP00000025510\_Onil/1-243 YSFTNWRTH TINTAASW  
 ENSPFOP00000001814\_Pfor/1-276 YSFTNWR TQTHTSALW  
 ENSXMAP00000020215\_Xmac/1-262 YSFTNWR TQTHTTALW  
 ENSTRUP00000001837\_Trub/1-183 YSFTSWH TRTETTASW  
 ENSAMXP000000026506\_Amex/1-290 YSFTDWKSSAESKACW  
 ENSDARP000000129035\_Drer/1-297 YSFTDWRSSADCRAGW  
 ENSLOCP000000022460\_Locu/1-268 YSFTGWKSSADTKACW

**NU214 (LVPERETLFNTLANNR)**

ENSPTRP00000036762\_Ptro/1-1459 LVPERETLFNTLANNR  
 ENSDORP00000003407\_Dord/1-2078 LVPERETLFNTLANNR  
 ENSPANP00000018828\_Panu/1-2065 LVPERETLFNTLANNR  
 ENSETEP00000008306\_Etel/1-2026 LVPERETLFNTLANNR  
 ENSP00000352400\_Hsap/1-2090 LVPERETLFNTLANNR  
 ENSCPOP00000002829\_Cpor/1-2076 LVPERETLFNTLANNR  
 ENSTTRP00000003698\_Ttru/1-2060 FVPERETLFNTLANNR  
 ENSTBEP00000004467\_Tbel/1-2048 LVPERETLFNTLANNR  
 ENSMLUP00000004455\_Mluc/1-2066 LVPERETLFNTLANNR  
 ENSRNOP00000033579\_Rnor/1-1790 VPERETLFNTLANNRE  
 ENSOGAP00000015017\_Ogar/1-1664 LVPERETLFNTLANNR  
 ENSLAFP00000000676\_Lafr/1-1539 LVPERETLFNTLANNR  
 ENSECAP00000020305\_Ecab/1-2001 LVPERETLFNTLANNR  
 ENSSARP00000002707\_Sara/1-1913 LE PERETLFNTLANNR  
 ENSDNOP00000013137\_Dnov/1-2100 LVPERETLFNTLANNR  
 ENSNLEP00000015422\_Nleu/1-2090 LVPERETLFNTLANNR  
 ENSCSAP00000010932\_Csab/1-2090 LVPERETLFNTLANNR  
 ENSAMEP00000017256\_Amel/1-2085 LVPERETLFNTLANNR  
 ENSCHOP00000000346\_Chof/1-1818 LVPERETLFNTLANNR  
 ENSOCUP00000000870\_Ocun/1-2094 LVPERETLFNTLANNR  
 ENSBTAP000000029190\_Btau/1-2074 LVPERETLFNTLANNR  
 ENSOPRP00000006059\_Opri/1-2046 LVPERETLFNTLANNR



ENSTSY00000012096\_Tsyr/1-2067 LVPERETLFNTLANNR  
 ENSOARP00000007571\_Oari/1-2084 LVPERETLFNTLANNR  
 ENSPVAP00000004008\_Pvam/1-2090 LVPERETLFNTLANNR  
 ENSSTOP00000010451\_Itri/1-2089 LVPERETLFNTLANNR  
 ENSCJAP00000015766\_Cjac/1-2091 LVPERETLFNTLANNR  
 ENSPPYP00000022085\_Pabe/1-2047 LVPERETLFNTLANNR  
 ENSGGOP00000016757\_Ggor/1-2069 LVPERETLFNTLANNR  
 ENSEEUP00000000411\_Eeur/1-2063 LVPERETLFNTLANNR  
 ENSMPUP00000012511\_Mpfu/1-2030 LVPERETLFNTLANNR  
 ENSMMPUP00000028616\_Mmul/1-2095 LVPERETLFNTLANNR  
 ENSPCAP00000008977\_Pcap/1-2086 LVPERETLFNTLANNR  
 ENSCAFP00000029512\_Cfam/1-2087 LVPERETLFNTLANNR  
 ENSMUSP00000066492\_Mmus/1-2085 LVPERETLFNTLANNR  
 ENSSSCP00000006118\_Sscr/1-2081 LVPERETLFNTLANNR

**CA1B(SYVSSLTSQSHPLRRV)**

ENSTTRP00000013136\_Ttru/1-2178 SYVSSLTSQSHPLRRV  
 ENSFCAP00000001128\_Fcat/1-2234 SYVSSLTSQSHPLRRV  
 ENSDORP00000010890\_Dord/1-2202 SYVSSLTSQPHPLRRV  
 ENSBTAP00000045932\_Btau/1-2331 SYVSSLTSQSHPLRRV  
 ENSCSAP00000012914\_Csab/1-2342 SYVSSLTSQSHPLRRV  
 ENSPANP00000017445\_Panu/1-2321 SYVSSLTSQSHPLRRV  
 ENSCPOP00000004005\_Cpor/1-2320 SYVSSLTSQSHPLRRV  
 ENSGGOP00000004729\_Ggor/1-2207 SYVSSLTSQSHPLRRV  
 ENSECAP00000010392\_Ecab/1-2226 SYVSSLTSQSHPLRRV  
 ENSOGAP00000014671\_Ogar/1-2336 SYVSSLTSQSHPLRRV  
 ENSSTOP00000004189\_Itri/1-2342 SYVSSLTSQSHPLRRV  
 ENSLAFP00000029481\_Lafr/1-2356 SYVSSMTSQPHPLRRV  
 ENSPTRP00000037005\_Ptro/1-1888 SYVSSLTSQSHPLRRV  
 ENSOANP00000018803\_Oana/1-2339 SYVSSLTSQPHHGLRV  
 ENSRNOP00000006162\_Rnor/1-2349 SYVSSLTSQSHPLRRV  
 ENSOARP00000000384\_Oari/1-1489 SYVSSLTSQSHPLRRV  
 ENSEEUP00000005237\_Eeur/1-2206 SYVSSLTSQSHPLRRV  
 ENSMMPUP00000040300\_Mmul/1-2241 SYVSSLTSQSHPLRRV  
 ENSPPYP00000022242\_Pabe/1-2119 SYVSSLTSQSHPLRRV  
 ENSMICP00000015302\_Mmur/1-2241 SYVSSLTSQSHPLRRV  
 ENSMUSP00000037416\_Mmus/1-2327 SYVSSLTSQSHPLRRV  
 ENSPVAP00000011230\_Pvam/1-2300 SYVSSLTSQPHPLRRV  
 ENSOPRP00000006610\_Opri/1-2230 SYVSSLTSQSHPLRRV  
 ENSCJAP00000024932\_Cjac/1-2345 SYVSSLTSQSHPLRRV  
 ENSCAFP00000028638\_Cfam/1-2334 SYVSSLTSQSHPLRRV  
 ENSMPUP00000015171\_Mpfu/1-1971 SYVSSLTSQSHPLRRV  
 ENSP00000360423\_Hsap/1-2339 SYVSSLTSQSHPLRRV

**CEP97 (LIPEHSPVQDAQISQ)**

ENSMMPUP00000008609\_Mmul/1-865 LIPEHSPVQD  
 ENSSARP00000007832\_Sara/1-861 LVPEHSSPVQD  
 ENSOARP00000019969\_Oari/1-858 FVPEHSSPIQD  
 ENSCSAP00000002556\_Csab/1-806 LIPEHSSPVQD  
 ENSGGOP00000025605\_Ggor/1-889 LIPEHSSPVQD  
 ENSOPRP00000003934\_Opri/1-859 PVPERASPVQD  
 ENSSTOP00000001559\_Itri/1-858 LVPEHSSPVQD  
 ENSMLUP00000010896\_Mluc/1-832 --PEHSSPLQD

ENSP00000342510\_Hsap/1-865 LIPEHSSPVQD  
 ENSCJAP0000000842\_Cjac/1-887 LIPEHSSPVQD  
 ENSPANP00000015263\_Panu/1-865 LIPEHSSPVQD  
 ENSFCAP0000003065\_Fcat/1-860 LVPEHSSPVQD  
 ENSCPOP00000019666\_Cpor/1-832 LVPEHSSPVQD  
 ENSOCUP0000009829\_Ocun/1-859 LVPEHSSPVQD  
 ENSDORP0000007874\_Dord/1-736 LSPEHSSPVQD  
 ENSCAFP00000014136\_Cfam/1-852 LVPEHSSPVQD  
 ENSNLEP0000004001\_Nleu/1-860 LIPEHSSPVQD  
 ENSLAFP00000013030\_Lafr/1-857 LVPEHSSPVQD  
 ENSOTEP0000002560\_Etel/1-854 QVSGHSSPVHD  
 ENSAMEP0000003933\_Amel/1-860 LVPEHSSPVQD  
 ENSTBEP0000005566\_Tbel/1-829 ----GSSVISD  
 ENSDNOP00000017282\_Dnov/1-861 LLSERSSPVQD  
 ENSRNOP0000002191\_Rnor/1-845 RTPHCSSPVQD  
 ENSPCAP0000004030\_Pcap/1-858 LVPVHSSPVQD  
 ENSSSCP00000012730\_Sscr/1-491 LVPEHSSPVQD  
 ENSOGAP0000009065\_Ogar/1-887 LIPEHSSPIQD  
 ENSPPYP00000015191\_Pabe/1-865 LIPEHSSPVQD  
 ENSMUSP00000023270\_Mmus/1-856 RTPHCSSPGQD  
 ENSBTAP00000017907\_Btau/1-858 LVPEHSSPIQD  
 ENSECAP00000019751\_Ecab/1-860 LVPEHSSPVQD  
 ENSPTRP00000051190\_Ptro/1-891 LIPEHSSPVQD  
 ENSMPUP00000011668\_Mpfu/1-857 LVPEHSSPVQD

**SYT16(EQKPKFSRLLTHGED)**

ENSFCAP0000007180\_Fcat/1-645 EQKSKFSHLLSTHEED  
 ENSNLEP00000017035\_Nleu/1-645 EQKPKFSRLLTHGED  
 ENSAMEP0000004497\_Amel/1-471 EQKSKYSHLLSTHEED  
 ENSMUP00000011488\_Mmul/1-645 EQKPKFSRLLTHGED  
 ENSRNOP00000073667\_Rnor/1-644 EQKTKCKHFLCTHQED  
 ENSMLUP00000015913\_Mluc/1-647 EQKPKVCHLLSTGEED  
 ENSETEP0000007584\_Etel/1-624 EQKPKFSRVLANQEED  
 ENSP00000478637\_Hsap/1-645 EQKPKFSRSLLTHGED  
 ENSCHOP00000011846\_Chof/1-497 EKKPKFSHLLSNYEED  
 ENSEEUP00000011316\_Eeur/1-635 DQKPKFSYLPSNHEED  
 ENSOARP00000022721\_Oari/1-643 EHKPKFPHCLSTHKED  
 ENSECAP00000022075\_Ecab/1-648 EQKPKFSCLLSIHEED  
 ENSDNOP00000014970\_Dnov/1-648 EQKPKFSHLLSNHEEE  
 ENSVPAP0000002217\_Vpac/1-531 EQKRKPSHWLPTHKED  
 ENSDORP00000015237\_Dord/1-622 NQKPKCSRLLSSHEED  
 ENSGGOP00000015716\_Ggor/1-645 EQKPKFSRLLTHGED  
 ENSMUSP000000106081\_Mmus/1-549 EQKIKCKRLLCTHQED  
 ENSCAFP00000039622\_Cfam/1-629 EQKSKFSRLLSTCEED  
 ENSOGAP00000014961\_Ogar/1-471 EQKPKLGSELIHCQA  
 ENSPTRP00000010890\_Ptro/1-645 EQKPKFSRLLTHGED  
 ENSSARP0000009906\_Sara/1-544 ERKPKFNQ-FSAHEED  
 ENSCJAP00000051609\_Cjac/1-645 EQKPKFSRLLSMHEED  
 ENSVPAP00000015109\_Pvam/1-625 EQNPKFCRLLSTGRED  
 ENSSSCP0000005479\_Sscr/1-471 EQKPKARRWLSTHKED  
 ENSOCUP00000014494\_Ocun/1-649 ERKQKFFHHLPSNREED  
 ENSLAFP00000016475\_Lafr/1-631 EQKLFKFSCLLSSQEEE  
 ENSPPYP0000006689\_Pabe/1-561 EQKPKFSRLLTHGED  
 ENSSTOP0000003494\_Itri/1-644 EQKPKCGRLLPTHEED

ENSMPUP00000006496\_Mpfu/1-645 EQKSKLSHLLSTHEEE  
 ENSCSAP00000010169\_Csab/1-650 EQKPKFSRLLLLTHGED  
 ENSOPRP00000004346\_Opri/1-618 EQRPFTSSNFLSTHEEG  
 ENSMICP00000010429\_Mmur/1-637 EQKLFKFSRLLSTCEED  
 ENSPANP00000017068\_Panu/1-585 EQKPKFSRLLLLTHGED  
 ENSTSYPP0000000756\_Tsyr/1-580 EQKQKFSRLLSTHKED  
 ENSTTRP00000013264\_Ttru/1-624 EHKPKPSRWLSTHEEA  
 ENSBTAP00000025211\_Btau/1-641 EHKPKPSHCLSTHKED

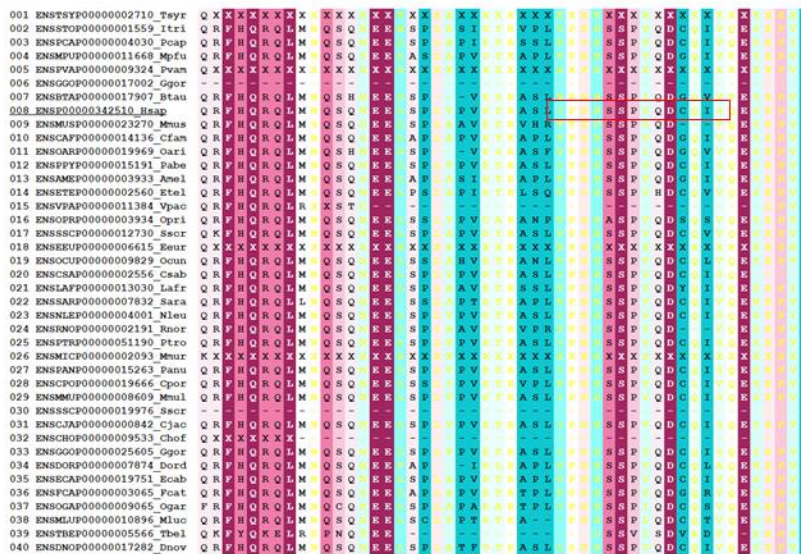
## B: Peptool

Protein name	Peptide sequence	PepTool value of conservation
Protein phosphatase 1 regulatory subunit 3G ( <b>PPP1R3G</b> )	YTFTEWRSFLDVPAEL	0.22
Zinc finger protein 622 ( <b>ZNF622</b> )	LEFADFYDFRSSYPDH	0.23
Rho GTPase-activating protein 33 ( <b>ARHGAP33</b> )	MVARSTDSLDPGEGS	0.3 (A.D)
RAD51-associated protein 1 ( <b>RAD51AP1</b> )	TMNKSPHISNCSVSD	0.31 (HCS)
Oxysterol-binding protein-related protein 9 ( <b>OSBPL9</b> )	SSEDEFYDADEFHQSG	0.34 (S.D)
Chromodomain-helicase-DNA-binding protein 9 ( <b>CHD9</b> )	SHPQGNYSNSKLSPVH	0.35 (Q.S)
Glucocorticoid-induced transcript 1 protein ( <b>GLCCI1</b> )	MPLSNISVPKSSVSRV	0.37
Spermatogenesis-associated protein 31A4 ( <b>SPATA31A4</b> )	LTSILPENFPVSPELR	0.42
Spermatogenesis-associated protein 31A7 ( <b>SPATA31A7</b> )	LTSILPENFPVSPELR	0.42
Ankyrin repeat domain-containing protein 6 ( <b>ANKRD6</b> )	LSSSDCTGSRLRNKV	0.44 (R)
Glycylpeptide N-tetradecanoyltransferase 2 ( <b>NMT2</b> )	MTLQRTMKLYRLPDVT	0.45
Spermatogenesis-associated protein 31A6 ( <b>SPATA31A6</b> )	LTSILPENFPVSPELR	0.45
Spermatogenesis-associated protein 31A2 ( <b>SPATA31A2</b> )	LTSILPENFPVSPELR	0.45

Spermatogenesis-associated protein 31A3 ( <b>SPATA31A3</b> )	LTSILPENFPVSPELR	0.45
Spermatogenesis-associated protein 31A5 ( <b>SPATA31A5</b> )	LTSILPENFPVSPELR	0.45
Spermatogenesis-associated protein 31A1 ( <b>SPATA31A1</b> )	LTSILPENFPVSPELR	0.45

### C: Consurf

#### CEP97 (LIPEHSSPVQDAQISQ)



#### Legend:

The conservation scale:



Variable                      Average                      Conserved

- e** - An exposed residue according to the neural-network algorithm.
- b** - A buried residue according to the neural-network algorithm.
- f** - A predicted functional residue (highly conserved and exposed).
- s** - A predicted structural residue (highly conserved and buried).
- X** - Insufficient data - the calculation for this site was performed on less than 10% of the sequences.







## CAC1B (SYVSSLTSQSHPLRRV)

2291                      2301  
**SSRTSYVSSL TSQSHPLRRV**  
 eeeeebebbb eeeeebeeee  
 ffffs sss ff f ff

### Legend:

The conservation scale:

1	2	3	4	5	6	7	8	9
Variable	Average			Conserved				

**e** - An exposed residue according to the neural-network algorithm.

**b** - A buried residue according to the neural-network algorithm.

**f** - A predicted functional residue (highly conserved and exposed).

**s** - A predicted structural residue (highly conserved and buried).

**X** - Insufficient data - the calculation for this site was performed on less than 10% of the sequences.

## NUP214 (LVPERETLFNTLANNR)

841                                      851                                      861  
**E Q K K K Q R H L L V P E R E T L F N T L A N N R**  
 eeeeeeeeebe beeeeeebbeb beeb e  
 f f                                      f f f f f s                                      s f f

The conservation scale:

1	2	3	4	5	6	7	8	9
Variable	Average			Conserved				

**e** - An exposed residue according to the neural-network algorithm.

**b** - A buried residue according to the neural-network algorithm.

**f** - A predicted functional residue (highly conserved and exposed).

**s** - A predicted structural residue (highly conserved and buried).

**X** - Insufficient data - the calculation for this site was performed on less than 10% of the sequences.

## **4. Discussion**



Sorcin is a cellular sensor for calcium, able to manage the intracellular concentration of the cation, while regulating other proteins (RyRs, SERCA, NCX) and helping to maintain calcium load in intracellular stores.

The ion binding provokes a consistent rearrangement in the SCBD, leading to the exposure of two hydrophobic binding pockets between EF1 and EF3, the EF hand motifs involved in ion coordination. These pockets, once accessible to the solvent, can be engaged in the interaction with different targets, including the N-terminal portion of the protein itself. Indeed the binding affinity of the whole protein towards PDCD6 (ALG-2) decreases in presence of EDTA.

Furthermore, Sorcin is able to bind directly to chemotherapeutic drugs as doxorubicin, vinblastine, paclitaxel, cisplatin and retinoic acid. Particularly, it is able to bind doxorubicin using two binding sites ( $K_{D1}$  nM range;  $K_{D2}$  low  $\mu$ M range), both in presence and absence of calcium. One of these two binding sites has been enlightened in the X-ray crystal structure: specifically, doxorubicin can bind between EF4 and EF5, the EF hand motifs involved in the homodimerization of the protein, and the other putative site results to be close to the D-helix.

Sorcin acts as a buffer for doxorubicin, hampering its intake in the nucleus of cancer cells, where doxorubicin acts by intercalating DNA and exerting topological constrain that blocks replication (Yang F et al., 2014). Indeed Sorcin changes localization upon doxorubicin treatment, acquiring a diffuse pattern in the cell. On the other hand upon retinoic acid treatment in APL cell line Sorcin migrates towards the insoluble portion of the cell, ER and nucleus mainly.

As a matter of fact different types of cancer cells, expressing diverse basal level of Sorcin protein, can be more or less sensitive to drug treatment. Hence, cells expressing high level of Sorcin resulted to be more resistant towards doxorubicin rather than cells expressing less Sorcin.

Sorcin-direct silencing in cancer cells with high levels of the protein, as H1299, results in an increase of cell death rate and cell growth arrest, an increase of doxorubicin intake in the nucleus and, as a late response, to the cleavage of PARP, that leads to the activation of apoptosis.

Additionally, Sorcin resides in the same amplicon of *ABCB1* gene (*MDR1*), located in 7q21.1 chromosomal portion. MDR1 is known to be involved in extrusion of xenobiotics from the cells, and overexpressed in cancer cell lines with a chemoresistant phenotype. It has been demonstrated that Sorcin silencing reduces MDR1 protein level and increases drug efflux from the cell.

However the mechanism that relates MDR1 and Sorcin in MDR phenotype arising remains still not fully understood. Possibly other genes in the amplicon (see Chapter 1.3.1, Figure 9) might collaborate to the resistance process, since many of them resulted to be over expressed or silenced whether assuming oncosuppressor functions, as lncRNA TP53TG1 (Diaz-Lagares et al., 2016). Indeed, the amplification of chromosome 7q21 region in neuroblastoma cancer cell lines (Flahaut et al., 2006), as well as the increased copy number of 7q21.12 region (including *ABCB1* gene) in lung cancer cells (Kitada and Yamasaki, 2007) and in leukemia cells (Kadioglu and Efferth, 2016) corresponds to drug resistance, suggesting the possible participation of other genes in the development of MDR phenotype.

Genomic instability and chromosomal rearrangements often affect cancer cells, resulting in genomic amplification, frequently translated in an increased copy number of *ABCB1* gene that can lead to the activation of MDR1 (Chen et al., 2002; Duesberg et al., 2007; Katoh et al., 2005; Kim et al., 2015; Mickley et al., 1997; Pang et al., 2005). Those rearrangements may either occur in upstream regions far from *ABCB1* promoter or may affect genomic alteration along 7q chromosomal arm that can associate with *ABCB1* activation (Chen et al., 2002; Knutsen et al., 1998).

Genomic investigations on *ABCB1* amplicon have been made, in order to understand whether the surrounding genes might have some role in the development of MDR phenotype or if they were amplified or suppressed in resistance-induced cancer cell lines. *ABCB1* gene expression can be increased up to 1092 fold in lung cancer cell with acquired paclitaxel resistance, showing a surprising discrepancy between the gene copy number and the expression level. Along with *ABCB1* gene expression enhancement, within the same amplicon (7q21.12), there is a concomitant amplification of *RUNDC3B* and *ADAM22* with an increased fold change of 38.5 and 27.7 respectively (Yabuki et al., 2007).

Taxane induced-resistant ovarian cancer cell lines showed a regional activation on chromosome 7q21.11-13 of about 22 co-expressed genes over an area of 8Mb, surrounding *ABCB1* gene. These genes include *SRI* (Sorcin), *MGC4175* (*TMEM243*), *DMTF1*, *CROT*, *ABCB1*, *ABCB4*, *ADAM22*, *RUNDC3B*, *DBF4* and the regional activation was driven by gene copy number alterations (Wang et al., 2006). Another research on taxane-resistant breast cancer cell lines reported gains in gene copy number on chromosome 7, specifically concerning ABC transporters (*ABCB1*, *ABCB4*), *SRI*, *DMTF1*,

*SLC25A40* and *CROT*, all belonging to the *ABCB1* amplicon (Hansen et al., 2016). Furthermore, a whole-genome characterization study on chemoresistant ovarian cancer cells reported an intergenic deletion between *ABCB1* and *SLC25A40* genes, that results in the creation of a fused transcript, with no evidence of this event in drug-sensitive samples. Additional transcriptome investigations showed the increase of *ABCB1*-*SLC25A40* fused transcript in resistant samples and the decrease of *SLC25A40* in sensitive specimen (Patch et al., 2015).

However, the genomic rearrangements and the high copy number cannot explain by themselves the unbelievably high fold increase in gene expression, suggesting that other mechanisms as such transcriptional enhancement, mRNA stabilization, post-transcriptional regulation and epigenetic modifications may contribute to these altered expressions. Interestingly also non-coding RNAs as miRNAs and long non-coding RNAs (lncRNA) may exert post-transcriptional regulatory functions in cancer cells, giving rise to metastatic or drug-resistant phenotypes. Indeed in the *ABCB1* amplicon a lncRNA (*TP53TG1*) resides, reported to be down-regulated in A549 cisplatin resistant lung cancer cells (Yang et al., 2013). On the other hand, deletions in the *ABCB1* locus in breast cancer patients determine a 2-8 times decreased expression of these MDR-related genes; patients with these deletions have a better response to neoadjuvant chemotherapy (Litviakov et al., 2016).

Overall, experimental evidences report an amplification of chromosome 7q21.12 region that can contribute with different extent to multidrug resistant phenotype development, as reviewed by Genovese and collaborators (Genovese et al. 2017, see pag 166).

Although Sorcin acts as a cellular sensor able to interact and regulate diverse binding partners, once activated by calcium binding, its network of interaction has still to be unraveled.

Combinatorial and Proteomic peptide phage display selection performed on Sorcin enabled us to better understand the preferred binding motifs and possibly disclose novel molecular partners.

Combinatorial peptide phage display revealed a binding preference to two short motifs one hydrophobic and one hydrophobic/acidic, in line with the structural evidence of the N terminal peptide binding to the D-helix and with the motifs enrichment found in the ProP-PD selection.

Proteomic peptide library was designed on intrinsically disordered regions of the human proteome, which are poorly complex in terms of structure and aminoacidic sequence, mainly composed by acidic and hydrophobic residues.

This low complexity enables these regions to be involved in transient, but biologically relevant, protein-protein interactions especially through short linear motifs (SLiMs), 3 to 10 aminoacidic stretches that take part in the binding event.

These transient interactions are generally difficult to characterize, even though the phage display selection process combined with a bioinformatics pipeline and *in vitro* binding assays eventually helped to find a novel binding partner of Sorcin.

CEP97, validated as an interactor of Sorcin, is a centriolar protein that recruits CCP110 collaborating to the negative control of ciliogenesis at the mother centriol. Lalioti VS and collaborators reported in 2014 the change in

Sorcin localization throughout the cell cycle. This may suggest a possible transient interaction between Sorcin and CEP97 at the end of cytokinesis translated in a negative regulation of microtubules formation.

To broaden our current knowledge about Sorcin activation, molecular mechanism of MDR phenotype regulation and network of transient interactions, further investigations are essential to address these topics in order to gain information about this multifaceted oncoprotein.

## **5. Conclusion and future perspectives**

Sorcina acts as a regulator of different processes in cells, ranging from cytokinesis, to relaxation of cardiomyocytes after excitation-contraction, and to MDR phenotype in cancer cells. Sorcina is able to bind and regulate different molecular partners, and can be regulated by them. As a matter of fact Sorcina can interact with kinases (Lalioi VS et al. 2014), ion channels, pumps and exchangers (RyRs, SERCA, NCX), other calcium sensors (PDCD6), and can bind small molecules, as chemotherapeutic drugs.

In this work we aimed to shed light on:

- calcium induced activation of Sorcina, by structural and functional studies,
- the molecular mechanism by which Sorcina regulates the resistance towards chemotherapeutic drugs in cancer cells,
- the SLiMs-based network of interactions in presence of calcium.

Despite the achievements in the characterization of the protein, the processes where it is involved and its network of interaction, the complete landscape of Sorcina function(s) has still not completely unveiled.

For these reasons, we aim to extend our knowledge on:

- i) the characterization of the transient and biologically relevant interactions of the whole proteins of the peptides selected by ProP-PD with Sorcina by SPR, protein co-ImmunoPrecipitation (co-IP) and/or confocal microscopy,
- ii) the binding sites where those protein-protein interactions take place, by X-ray crystallography/NMR or mutagenesis investigation;



- iii) the position of the second doxorubicin-binding site of Sorcin, probably at the D-helix, by X-ray crystallography, followed by the *in vitro* binding assays with mutants, in order to characterize the highest affinity and the lowest affinity sites;
- iv) the mechanism of ABCB1-Sorcin amplicon activation during MDR and characterization of specific transcriptional factors through Chromatin Immunoprecipitation (Ch-IP);
- v) the significance of Sorcin migration to insoluble fractions upon retinoic acid treatment in APL cells, beside the functional characterization of the role of Sorcin in APL models differentiation upon retinoic acid treatment

Overall, in the extended mosaic and complexity of biological processes, either physiological or pathological, Sorcin results to be an intriguing and fascinating sensor protein that takes part in important processes in cells. Sorcin is an important protein for cell survival and, for the aforementioned reasons, can be considered as an oncoprotein, and a marker of MDR and of poor prognosis in tumors. Sorcin may therefore represent a potential target for cancer therapy purposes: a further future goal of our research may be the discovery of molecules able to impair Sorcin interactions with its molecular targets involved in tumorigenesis and in the establishment of the MDR phenotype.

## **6. Materials and methods**

## 6.1 Cell cultures and western blots

H1299, Calu-1, A459 human lung carcinoma, HeLa human cervix adenocarcinoma, MDA-MB-468 and MDA-MB-231 breast adenocarcinoma cell lines were cultured in DMEM medium (Invitrogen-GIBCO) with 10% FBS (v/v) and 5% Penicillin/Streptomycin (v/v) at 37°C in a balanced air humidified incubator with 5% CO<sub>2</sub>, while NB4 human Acute Promyelocytic Leukemia (APL) cell lines were cultured in RPMI 1640 with 10% FBS (v/v) and 5% Penicillin/Streptomycin (v/v) in the same growth condition.

The cells were lysed in a 2% SDS lysis buffer (25 mM Tris-HCl at pH 7.5, 100 mM NaCl, 3 mM EDTA, 7% glycerol) with: NaF 1000X, NaVO<sub>3</sub> 100X, Na<sub>4</sub>PO<sub>7</sub> 20X, Aprotinin 1000X, Leupeptin 1000X, PMSF 100X protease and phosphatase inhibitors as final concentrations in order to get a lysate that includes all the proteins of the cell. Then for the nucleus/cytosol fractionation purpose the cells were first lysed in a 1% NP-40 lysis buffer (50 mM Tris-HCl pH 8, 150 mM NaCl) and subsequently in the abovementioned SDS lysis buffer.

Extracts of SDS lysed cells were sonicated for 10 s and centrifuged at 12000 rpm for 10 min to remove cell debris. Lysates were quantified in proteins content with Pierce<sup>TM</sup> BCA protein assay kit (Thermo Scientific) according to manufacturer's instructions.

13% acrylamide-bisacrylamide SDS gel electrophoresis (SDS-PAGE) were run for Sorcin, and 7% SDS-PAGE were run for PARP and MDR1. Proteins lysate content was checked by S-Ponceau staining. Western blotting analysis was performed with the following antibodies: rabbit polyclonal anti-human Sorcin (home-made), mouse monoclonal anti-PARP (Cell Signalling #9532),

mouse monoclonal anti-MDR1 (SantaCruz Biotechnologies, sc-13131) mouse monoclonal anti-tubulin (Sigma-Aldrich cat. T5168) and mouse monoclonal anti- $\beta$  actin (SantaCruz Biotechnologies, sc-81178). Goat secondary anti-mouse and anti-rabbit antibodies conjugated to horseradish peroxidase were used (BioRad cat. 170-6515, 170-6516). Immunostained bands were detected by chemiluminescence (Chemidoc, BioRad), and the intensity quantified with the tool of the Chemidoc software.

Mouse 3T3-L1 preadipocytes (ATCCR CL-173TM, American Type Culture Collection) and 3T3-L1 adipocytes were grown on plastic dishes or 10-mm glass coverslips using Dulbecco's modified Eagle's medium supplemented with 10% calf serum, 4 mM glutamine, 50 mg/l streptomycin, 100 IU/l penicillin and non-essential amino acids at 37 °C in a humidified CO<sub>2</sub> incubator. 3T3-L1 preadipocytes were differentiated into adipocytes as described by Tafuri, adding 7.5  $\mu$ M troglitazone in the medium on days 3 and 4 of differentiation (Tafuri SR et al. 1996).

The mouse  $\alpha$ -Sorcin (33–800) was from Zymed, the rabbit  $\alpha$  -Sorcin was homemade, the rabbit  $\alpha$ -annexin 11 (NB100–78588) was from Novus Biologicals, the rabbit  $\alpha$ -annexin 7 (ABIN65268) and the mouse  $\alpha$ -PDCD6 (H00010016-M01) were from Abnova.

## **6.2 Retinoic Acid, Doxorubicin treatment and silencing for Sorcin**

NB4 cell line were treated in a time course experiment for 24, 48, 72, 96 hours with 1.0  $\mu$ M Retinoic Acid (RA) final concentration used in clinical treatment of APL patients, in order to evaluate the differentiation, Sorcin relocalization and expression.

We performed a dose-response curve (0.1  $\mu$ M, 0.3  $\mu$ M, 0.6  $\mu$ M, 1.0  $\mu$ M); 0.6  $\mu$ M doxorubicin is the dose resulting in the best evaluation of time-dependent accumulation, and is compatible with doxorubicin plasma concentration 15'-2h after treatment of many different types of cancer (Kontny et al. 2013). 0.6  $\mu$ M doxorubicin concentration was used for most experiments. H1299 cells were transfected with a solution composed by Optimem medium (Invitrogen-GIBCO), Lipofectamine RNAimax (Invitrogen cat.13778-030) and a final concentration of 500 pM siRNA for Sorcin (CDS3 and 3'UTR) (IDT sequence to CDS3-exon3: GAUAGAUGCUGAUGAAUUGCAGAGA; sequence to 3'UTR-exon8: AGCUGUACACUUUCAAGUAAGAUCT), according to manufacturer's instructions. CDS3 siRNA silences both Sorcin isoforms (Landriscina et al. 2010). After 48 hours of transfection, the medium was replaced with fresh DMEM (Invitrogen-GIBCO) containing 0.6  $\mu$ M doxorubicin. To evaluate doxorubicin incorporation, cells were treated with the drug in time-course experiments (30 minutes to 3 hours incubation for cytofluorimetry, 3 hours and 5 hours for confocal microscopy). The analysis of biological effects of Sorcin silencing was performed 24 hours and 48 hours after treatment.

### **6.3 Doxorubicin uptake (confocal microscopy and FACS)**

The uptake of doxorubicin was evaluated through confocal microscopy and FACS (Fluorescent-associated Cell Sorting) thanks to the autofluorescence of the molecule (excitation wavelength 470 nm; emission wavelength 585 nm). To avoid cells drug saturation the analysis was performed between 30 minutes and 5 hours incubation.

For confocal microscopy, the medium was removed from the H1299 cell line, then washed with PBS. The cells were fixed in 2% paraformaldehyde for 10 minutes, washed in PBS and incubated 7 minutes in TO-PRO-3 (Invitrogen, cat. T3605), dilution 1:3000. To avoid fluorophore quenching, samples were covered with Vectashield<sup>R</sup> Mounting Medium (Vector Laboratories, cat. H-1000). Confocal images of slides were acquired at a Leica laser scanning microscope TCS-SP2.

In order to have a quantitative readout on doxorubicin incorporation we performed flow cytometry with CyAn ADP and Summit 4.3 software. The cells were dislodged with trypsin 0.05% (Invitrogen-GIBCO), the emission of doxorubicin was evaluated at 573 nm, and cells were gated as shown in the results. Data were analyzed with FCS4 express software.

#### **6.4 Sytox blue assay and cell counts**

To evaluate cell death we performed assays with Sytox Blue Dead Cell Stain, for flow cytometry (Invitrogen, Molecular Probes, cat. MP34857). According to the manufacturer's instructions, 200000 cells (H1299) were sampled each condition and incubated 15 minutes at room temperature with Sytox blue 1:1000 dilution. The samples were acquired at CyAn ADP by using Summit 4.3 software. The fluorescence excitation of nucleic acids of dead cells was measured with 405nm violet laser light. Data were analyzed with FCS4 express software.

Lung, breast cancer cell lines and HeLa cells were treated 48 hours with 0.6  $\mu$ M doxorubicin and the rate of Sytox blue incorporation was evaluated as aforementioned.

Although this assay is very reliable, we evaluated the effect of Sorcin silencing on cell death and the differentiation effect of retinoic acid with the traditional method of cell counts. The cells were dislodged diluted 1:1 with Trypan blue dye and counted in triplicates in a burker cell counting chamber.

### **6.5 Sorcin localization, confocal microscopy**

In order to dissect the relocalization of Sorcin upon 72 hours retinoic acid treatment in NB4 and upon 1 hour treatment with 0.6  $\mu$ M doxorubicin, the cell lines were processed as aforementioned for confocal microscopy purpose. After paraformaldehyde fixation, cells were incubated 30 minutes with a 1:200 dilution of primary antibody against Sorcin and, after PBS 1X washing steps, 30 minutes with Alexa Fluor 488 (Molecular Probes, Thermo Fisher)-conjugated secondary antibody against rabbit was used at a 1:500 dilution. A Leica laser scanning microscope TCS-SP2 device was used and images were acquired with Leica confocal software.

For immunofluorescence staining, mouse 3T3-L1 cells were plated and grown on 10 mm glass coverslips, fixed with 2% paraformaldehyde for 20 minutes, permeabilized with 0.2% Triton X-100 for 10 minutes and incubated in 50 mM glycine for 30 min more. Primary antibody dissolved in 1% bovine serum albumin was added and allowed to incubate overnight at 4 °C. Primary antibody was removed, wells washed and secondary AlexaFluor 488, 594 or 647 was added and incubated for 1 h at room temperature. Conventional immunofluorescence and confocal microscopy were performed using confocal LSM710 vertical and Axiovert135M microscope (Zeiss).

### **6.6 Rhodamine 123 incorporation**

To ascertain whether Sorcin silencing affects MDR1 functionality in pumping out the drugs from the cell, we performed a rhodamine 123

accumulation assay. This dye is extruded outside the cells by MDR1/MDR4 pumps. First the cells were silenced for 48 hours, as mentioned, then a time course accumulation assay was performed. We considered 250000 cells each time point (30 minutes, 1 hour, 2 hours) and the assay was carried out incubating the samples at 37°C in RPMI 1640 medium without and with 1 µM rhodamine 123.

After incubation the samples were pelleted and washed twice in ice cold PBS1X. Then they were analyzed at CyAn ADP by using Summit 4.3 software. The results were evaluated with FCS4 express software.

### **6.7 Differentiation and morphology**

To verify the differentiation of NB4 cells upon treatment the cells were washed from media and spotted on slides with Shandon Cytospin 4 (Thermo electron, Waltham, MA, USA) at 200 rpm for 5 minutes. Then the slides were embedded in a solution of Giemsa dye for 5 minutes, rinsed in PBS and finally embedded in a 1:20 dilution of the first used Wright-Giemsa solution for 13 minutes. The excess of dye was washed out with water and the slides were observed by optical microscopy.

### **6.8 Human Sorcin wild-type, SCBD and A2C mutant recombinant protein cloning, mutagenesis and purification.**

The cDNA of human Sorcin (I.M.A.G.E. Consortium clone 4281626) was amplified by PCR using primers containing restriction enzyme sequences recognized by NcoI and HindIII

SH\_NcoI\_For: 5'-GGGAAACCATGGCGTACCCGGGGCAT-3'



SH\_HindIII\_Rev: 5'-

GGGAAAGGGAAGCTTTTAAACGGTCATGACACAC-3'

The PCR product was then ligated in pET23d vector (Novagen, Madison, WI, USA) digested with the same enzymes. The pET23d-human wt-Sorcina thus obtained was transformed in *E. coli* BL21(DE3) cells for expression purpose.

The gene encoding Sorcin was also cloned into the pGEX-4t1 plasmid in order to have the GST-tagged protein.

The Sorcin A2C mutagenesis was performed on Sorcin gene cloned in pET23d plasmid, which resulted in an untagged protein. The A2C mutation was introduced to facilitate labelling on the N-terminal exposed Cys with Cy5 maleimide dye for MST experiment purpose. The mutagenesis was carried out using the following oligonucleotides:

SorA2C\_For: 5'-

GAAGGAGATATACCATGTGCTACCCGGGGCATCCTGG-3'

SorA2C\_Rev: 5'-

CCAGGATGCCCCGGGTAGCACATGGTATATCTCCTTC-3'

Human Sorcin calcium-binding domain (SCBD) was obtained from the pET23d vector with the insertion of a NcoI site in the suitable position to produce the truncated version of the protein, using the following oligonucleotides:

SorHSCBD\_NcoI\_For: 5'-

CGTTTCCCGGACAAACCATGGATCCGCTGTATGGTTACTTTGC-3'

SorHSCBD\_NcoI\_Rev: 5'-

GCAAAGTAACCATAACAGCGGATCCATGGTTTGTCCGGGAAACGC-  
3'

The sequences of the mutated vectors were verified by the Sanger dideoxynucleotide technique.

Wt-Sorcin, GST-tagged Sorcin, the Sorcin calcium binding domain (HSBD) and Sorcin A2C mutant were expressed in *E. coli* BL21(DE3) cells, and purified according to Meyers et al. (1995).

### **6.9 Surface Plasmon Resonance (SPR) experiments**

SPR experiments with chemotherapeutic agents were performed with a SensiQ Pioneer apparatus. Wild type human Sorcin was immobilized via amine coupling onto a COOH5 sensorchip, previously chemically activated by 100µl injection of a 1:1 mixture of N-ethyl-N'-3-(diethylaminopropyl)carbodiimide (200 mM) and N-hydroxysuccinimide (50 mM). Immobilizations were carried out in 20 mM sodium acetate at pH 4.5; the remaining groups were blocked by injecting 100 µl of 1 M ethanolamine hydrochloride at pH 9.5.

The amount of immobilized Sorcin was detected by mass concentration-dependent changes in the refractive index on the sensorchip surface, and corresponded to about 5000 resonance units (RU).

Samples of analytes (doxorubicin, cisplatin, vinblastine, paclitaxel and retinoic acid) were dissolved in 100% DMSO at a concentration of 10 mM, and subsequently diluted in sterile HEPES 20 mM pH 7.4, NaCl 150 mM, 500 µM CaCl<sub>2</sub> (or EDTA) 0.005% surfactant P-20 to yield 2% DMSO final

concentration (HSP-2%D buffer) and final drug concentration: 200  $\mu\text{M}$  or 20  $\mu\text{M}$  (for OneStep RA experiment). Further dilutions and all the experiments were carried out at 25°C in degassed HSP-2%D buffer.

For FastStep experiments, the analytes were automatically diluted in HSP-2%D and injected by 7 serial doubling steps (step contact time = 30 s, nominal flow rate = 100  $\mu\text{l}/\text{min}$ ). At the following time points: 1) 0-30 s; 2) 31-60 s; 3) 61-90 s; 4) 91-120 s; 5) 121-150 s; 6) 151-180 s; 7) 181-198 s, analyte concentrations were: 1) 1.25  $\mu\text{M}$ ; 2) 2.5  $\mu\text{M}$ ; 3) 5  $\mu\text{M}$ ; 4) 10  $\mu\text{M}$ ; 5) 20  $\mu\text{M}$ ; 6) 40  $\mu\text{M}$ ; 7) 80  $\mu\text{M}$ . For OneStep experiments, Taylor dispersions were exploited to generate analyte concentration gradients that provide high-resolution dose response in single injections. Full analyte titrations were recorded in HSPC-2%D over 4 orders of magnitude in concentration, up to 80  $\mu\text{M}$ .

In both FastStep and OneStep experiments, the increase in RU relative to baseline indicates complex formation between the immobilized Sorcin ligand and the analytes. The plateau region represents the steady-state phase of the interaction. The decrease in RU after 198 s in FastStep experiments, or after 350 s in OneStep experiments, indicates analyte dissociation from the immobilized Sorcin after HSP-2%D buffer injection. As a negative control, sensorchips were treated as described above in the absence of immobilized Sorcin. Values of the plateau signal at steady-state ( $R_{eq}$ ) and full fittings with 1, 2 and 3 sites were calculated from kinetic evaluation of the sensorgrams using the Qdat 4.0 program.

Surface Plasmon Resonance (SPR) experiments with PDCD6 and its N-terminus were carried out using a SensiQ Pioneer system. The sensor chip

(COOH5) was activated chemically by a 35  $\mu$ l injection of a 1:1 mixture of N-ethyl-N'-(3-(diethylaminopropyl)carbodiimide (200 mM) and N-hydroxysuccinimide (50 mM) at a flow rate of 5  $\mu$ l/min. Ligands, i.e. PDCD6 and the N-terminal domain of PDCD6 (KMAAYSYPGPGAGPGAAGAALP; a lysine residue has been added to the sequence to ensure peptide immobilization principally via the N-terminus), were immobilized on activated sensor chips via amine coupling. The immobilizations were carried out in 20 mM sodium acetate at pH 4.5; the remaining groups were blocked by injecting 1 M ethanolamine hydrochloride (35  $\mu$ l).

Proteins interacting with the ligands (in 10 mM HEPES pH 7.4, 150 mM NaCl + 0.005% surfactant P20) were injected on the sensor chip at a constant flow (30  $\mu$ l/min). The same procedure was set using the buffer with CaCl<sub>2</sub> at 100  $\mu$ M concentration, or with 1 mM EDTA. The increase in RU relative to baseline indicates complex formation; the plateau region represents the steady-state phase of the interaction, whereas the decrease in RU represents dissociation of Sorcin or SCBD from immobilized ligands after injection of buffer. Regeneration procedures are based on two long (2000 s and 500 s) injections of buffer, separated by a brief (5 s) injection of 10 mM NaOH. The sensorgrams were analysed using the SensiQ Qdat program.

In Sorcin-CEP97 SPR experiment Sorcin was immobilized as abovementioned, CEP97 peptide was dissolved in HEPES 20 mM pH 7.4, NaCl 150 mM, 500  $\mu$ M CaCl<sub>2</sub> to a final concentration of 1 mM. Then a traditional SPR experiment was performed using 4 serial dilution (1:2) from 25-200  $\mu$ M analyte final concentrations. The sensorgrams were analysed using the SensiQ Qdat program.

## 6.10 Fluorescence titrations

Static fluorescence measurements were performed at 25°C with a Horiba Fluoromax-4 spectrofluorometer using 1-cm path-length quartz cuvettes (slit width: 5 nm in excitation and emission). Fluorescence measurements were performed on Sorcin and SCBD, a shorter construct missing the first 32 residues, at two different concentrations: 30 nM and 37 nM, in Tris-HCl 10 mM pH 7.5 and EDTA (0.5 μM) or MgCl<sub>2</sub> (1 mM or 5 mM). The excitation wavelength was set at 280 nm and emission spectra were collected in the 300–400 nm range. Triplicate samples were measured; each figure represents the average of three experiments. Maximum emission occurs at 340 nm for SCBD and 338 nm for Sorcin. Upon doxorubicin addition, fluorescence quenching was observed to a maximum extent of about 60% in saturating condition. For each sample fluorescence was measured after 3 minutes of incubation.

Since doxorubicin absorbs light at 280 nm, fluorescence measurements are affected by the inner-filter effect. The following formula was employed for correction:  $F_{cor} = F_{obs} 10^{[(A_{ex})/2]}$ , where  $F_{cor}$  and  $F_{obs}$  are the corrected and observed fluorescence intensities, respectively, whereas  $A_{ex}$  is the absorbance of each concentration of ligand at 280 nm [IFE-correction]. The effect is negligible at the concentrations of doxorubicin used (5-3000 nM). Data were fitted with the software Qtiplot assuming two independent binding sites. The equation used for data fitting is the weighted sum of two independent binding events:  $K * ((k+c+x) - \sqrt{(k+c+x)^2 - 4*c*x}) / (2*c) + H * ((h+c+x) - \sqrt{(h+c+x)^2 - 4*c*x}) / (2*c)$ , where  $c$  is protein concentration,  $k$  and  $h$  are the two binding constants,  $K$  and  $H$  are the fraction of signal due to each binding event.

## **6.11 Crystallization, data collection and structure solution and refinement of Apo, calcium-bound and doxorubicin-bound Sorcin**

### **6.11.1 Apo and calcium-bound Sorcin X-Ray crystal structure**

Recombinant proteins (human Sorcin, SCBD and PDCD6) were expressed in pET vectors (Novagen) in *E. coli* BL21(DE3) cells, purified according to published procedures (Meyers MB et al. 1995) and dialysed in 20 mM Tris-HCl, at pH 7.5. Automated crystallization screening and by-hand optimization were carried out at 298 K by the hanging-drop vapor diffusion method. Since Sorcin precipitates when it is saturated with calcium, we performed the starting crystallization trials with commercial screens adding 5 mM CaCl<sub>2</sub> in the reservoir before mixing the crystallization drops. ApoSor resulted to be rather prone to crystallization even in the presence of calcium; therefore, in order to discriminate between apoSor and CaSor crystals we performed all the crystallization trials in double, with and without calcium. The apoSor crystallization trials were performed using a protein sample concentrated to about 10 mg/ml. Aliquots (1 µl) of the protein sample were mixed with an equal amount of reservoir solution containing 20-22% (w/v) polyethylene glycol 4000, 0.3-0.5 M ammonium sulfate. Crystals grew in 2 weeks and reached dimensions of 0.1 mm × 0.2 mm × 0.3 mm.

Crystals of CaSor were obtained by mixing 1 µl of protein solution, concentrated to about 15 mg/ml, using a reservoir solution containing: 20-25% (w/v) polyethylene glycol 3350, 0.5 M lithium sulfate, 0.1 M Tris-HCl at pH = 8.5 and 5 mM CaCl<sub>2</sub>. For data collection, apoSor and CaSor were cryo-protected in a solution containing 80% (v/v) of mother liquor and 20% (v/v) polyethylene glycol 200. The crystals were mounted in nylon loops and

flash frozen by quick submersion into liquid nitrogen and transported to the synchrotron-radiation source. Single-wavelength data sets ( $\lambda = 1 \text{ \AA}$ ) were collected from crystals of apoSor and CaSor at the 5.2 R beamline of the Synchrotron Radiation Source ELETTRA (Trieste, Italy), using a Pilatus 2 M detector at a temperature of 100 K. The data sets were processed with XDS45 and scaled with XSCALE (Kabsch W 2010). Crystal parameters and data collection statistics for the measured crystals are listed in Table 1.

The structure of apoSor was determined by molecular replacement with the program MOLREP (Vagin and Teplyakov, 1997) (CCP4 suite) using the structure of the calcium-free human Sorcin (PDB entry 1JUO) (Xie X et al., 2001) as search model.

The case of CaSor was more complex: first we solved the structure of SCBD (Sorcin Calcium Binding Domain) with calcium (Ca-SCBD, data not shown), using the structure of the calcium-free human Sorcin; then we used SCBD monomer to solve CaSor. Ca-SCBD crystallized in orthorhombic space group and the Matthews coefficient calculation indicated a dimeric asymmetric unit. The first attempts to solve the phase problem for Ca-SCBD using the whole apo-Sorcin dimer were unsuccessful, suggesting a wide conformational variation. Based on previous published results we expected that the variation regarded mainly the EF1–2–3 subdomain. For this reason we performed the rotational and translational searches with a truncated apo-dimer including E-F-G-H helices (EF4–5 plus part of EF3), finding a partial solution. We fixed this solution and repeated the search using the rest of the apo-model (helices A, B, C, D). Refinements were performed using the maximum-likelihood method with the program REFMAC (Murshudov et al., 1997) and model building with the program Coot (Emsley P, Cowtan K., 2004). The quality of

the models was assessed using the program PROCHECK (Laskowski et al.,1993). The structure of apoSor was refined to 2.1 Å resolution. The final model contains 168 residues (residues 30–198), 73 water molecules, 5 sulfate ions. The structure of CaSor was refined to 1.65 Å resolution. The final model contains 172 residues (residues 26–198), a six residues long peptide, 124 water molecules, 1 sulfate ion, 3 Ca<sup>2+</sup> ions with full occupancy and 3 PEG molecules for each monomer.

The coordinates for apoSor have been deposited in the Research Collaboratory for Structural Bioinformatics (RCSB) PDB with accession code 4UPG. The coordinates for CaSor have been deposited in the RCSB PDB with accession code 4USL.

### **6.11.2 Doxorubicin-bound Sorcin X-Ray crystal structure**

Crystallization experiments were performed with both human Sorcin and SCBD. Automated crystallization screening and by-hand optimization were carried out at 298 K by vapor diffusion method.

At first soaking technique was attempted but, while doxorubicin is deep red, the crystals stayed uncolored; then we moved to co-crystallization. Since Sorcin precipitates in presence of doxorubicin excess, trials were set up by adding the ligand to the crystallization drop (0.4 µl of 0.5 mM protein + 0.4 µl of reservoir + 0.1 µl of 30 mM doxorubicin) to a ligand/protein ratio of about 15. Colored crystals, from light pink to red, grew in many conditions but most of them resulted in poor diffraction. The best dataset collected was at 3.7Å resolution, from a SCBD crystal grew in 0.2 M MgCl<sub>2</sub>, 0.1 M Tris-HCl pH 7, 2.5 M NaCl. The crystals were cryoprotected by adding 40% w/v glucose to the mother liquor.



A single wavelength (0.9677  $\lambda$ ) dataset was collected at ESRF at 100 K on the ID30-A3 MASSIF3 beamline equipped with a Eiger-X-4M detector and processed with XDS (Kabsch W 2010). Crystal parameters and data collection statistics are reported in Table 6 (below).

PDB code	5MRA
Space group	P2 <sub>1</sub> 2 <sub>1</sub> 2 <sub>1</sub>
Cell parameters (Å)	a = 92.36, b = 104.98, c = 113.42
Asymmetric unit, residues	Tetramer, 166 per monomer
N° of bound ions	10 Mg <sup>++</sup>
<i>Data reduction</i>	
Resolution range (Å)	48.31–3.74 (3.96–3.74)
Unique reflections	11800 (1845)
Completeness (%)	99.0% (97.2%)
Redundancy	6.53 (6.47)
R <sub>merge</sub> (%)	10.2 (113.3)
CC(1/2)	99.9 (64.7)
I/ $\sigma$ (I)	11.81 (1.45)
<i>Data refinement</i>	
Resolution range (Å)	48.31–3.74 (3.83–3.74)
R <sub>cryst</sub> (%)	19.6 (35)
R <sub>free</sub> (%)	28.5 (37)
rms (angles) (°)	1.324
rms (bonds) (Å)	0.01
Wilson B-factor (Å <sup>2</sup> )	162.2
Residues in core regions of the Ramachandran plot (%)	90
Residues in allowed regions of the Ramachandran plot (%)	10

Values in parentheses are for the highest-resolution shell

**Table 6:** Crystal parameters, data collection statistics and refinement statistics

The structure was determined by molecular replacement with the program MOLREP (Vagin, Teplyakov 1997) (CCP4 suite) using the structure of the calcium-free human Sorcin (PDB entry 4UPG) as search model. Refinement was performed using the maximum-likelihood method with the program

REFMAC (Murshudov et al. 1997) and model building with the program Coot (Emsley, Cowtan 2004).

Fluorescence emission spectra of SCBD-doxorubicin crystals were collected at ESRF ID29S at 100K and excitation wavelength 473 nm. The experimental setup is described in more detail in a paper by Royant et al. (Royant et al. 2007).

### **6.12 Combinatorial Phage display**

We used a phage library displaying 16mer randomized peptides (diversity  $4 \times 10^{10}$ ) on the p8 protein flanked by spacer linkers at the N- and C- termini (SSSG- and GGGSGG, respectively).

The library is similar to the previously established C-terminal library (Tonikian R. et al. 2008), but displaying internal, instead of C-terminal, peptide stretches. Phage selections were performed in 5 rounds, following the detailed protocols by Huang and Sidhu (2011). To assess a potential calcium dependence of the interactions selections were performed in parallel using either 1 mM EDTA or 1 mM CaCl<sub>2</sub> during the incubation of the phage library with the bait protein as well as in all washing steps. Such an approach has previously been successfully used for the identification of calcium-dependent interactions for the calcium-binding protein S100B52. Clonal analysis and sequencing was performed as previously described below.

### **6.13 Proteomic peptide Phage display selection**

The selection process was an adaptation of methods by Huang and Sidhu (2011). The buffers were sterile filtered to minimize contaminations. TBS

(50mM Tris-HCl pH 7.5; 150mM NaCl) was used during the selections, and was supplemented with 1 mM CaCl<sub>2</sub>, except during protein immobilization when it was supplemented with 1 mM EDTA to avoid protein precipitation. Before the first day of selection 15 µg of Sorcin was coated in duplicate on a 96-well Maxisorp plate beside the negative control (GST), in a total volume of 100 µl of TBS 1 mM EDTA, to avoid Sorcin precipitation. The incubation of the proteins proceeded at 4<sup>0</sup>C over-night. The immobilization is unspecific and based on hydrophobic interaction. The plate with coated protein was blocked with 200 µl of blocking buffer (TBS, 1 mM CaCl<sub>2</sub>, 0.5% BSA) for 1 hour at 4<sup>0</sup>C on a shaking table.

Meanwhile the naïve peptide phage library was prepared. As it is stored in 25% glycerol, the first step was to precipitate it and resuspend it in appropriate buffer. 10 µl of phage library was diluted with 500 µl TBS. The phages were precipitated using 20% PEG8000 (w/v)/400 mM NaCl solution, 10 min incubation on ice and centrifugation for 10 minutes at 13000 rpm. The supernatant was aspirated and the pellet resuspended in TBS. The resuspended phage library was added to the GST-coated well for negative pre-selection for 1 hour at 4<sup>0</sup>C. Prior to addition of the phage library, the wells were washed four times with TBS, 1mM CaCl<sub>2</sub>, 0.05% Tween20 (TBST buffer). The wells coated with target protein were similarly washed before the phage library was moved from the pre-selection wells to target wells. Binding was allowed for 2 hours at 4<sup>0</sup>C.

Each day of selection, three 10 ml *E. coli* Omnimax cultures in 2TY (10 g Tryptone, 10 g Yeast extract and 5 g NaCl) medium were started from a stock culture. One was supplemented with 10 µg/ml tetracyclin to be used for elution of the actively growing phage, and the two other supplemented with

30 µg/ml kanamycin or 100 µg/ml carbenicillin served as controls for pre-infection of the cells with M13K07 helper phage or from the M13 phage. Once the Omnimax cells reached the log phase, they were used to elute bound phages from the bait protein. Unbound phages were removed from the wells, the wells were washed 4 times with TBST buffer and bound phages were eluted using *E. coli* Omnimax log phase culture; the elution proceeded 30 minutes at 37<sup>0</sup>C shaking after which the bacteria were infected with M13K07 helper phage for 45 minutes at 37<sup>0</sup>C. In the meantime, 2TY medium supplemented with kanamycin, carbenicillin and 0.3 mM IPTG was prepared. The hyperinfected bacteria were transferred from the wells to the media and were grown over-night at 37<sup>0</sup>C shaking.

To monitor the progress of the selection, serial dilutions of with *E. coli* infected with out-phages and in-phages were spotted carbenicillin containing agar plates. Out-phages are the phage eluted with *E. coli* log phase cell culture, the in-phages were from the resuspended naïve phage library.

The following day, the bacteria were pelleted by centrifugation (5000 rpm, 10 minutes). The phage containing supernatants were transferred to new falcon tubes containing 20% PEG8000 solution. The phages were precipitated on ice for 15 minutes and then pelleted for 15 minutes at 9000 rpm. The phage pellets were resuspended in TBST. The selection process was repeated for five days. In parallel, selections were performed in absence of calcium (i.e. by using a TBS buffer supplemented with 1 mM EDTA).

#### **6.14 Pooled phage ELISA assay**

In order to analyze the progress of the selection, a pooled phage ELISA assay was performed.

The bait protein and the negative control protein were immobilized in a 96-well Maxisorp plate (15 µg of protein beside 15 µg of GST as negative control). The wells were blocked with BSA (TBS, 1mM CaCl<sub>2</sub>, 0.5% BSA), phage pools from each selection day were added to protein and to control wells and incubated for 30 minutes at room temperature.

The wells were washed four times with TBST buffer, and the bound phage detected by incubation with 1:5000 dilution of M13 antibody-HRP conjugate solution and incubated for 30 minutes at room temperature. When the incubation time was over, wells were washed four times with TBST and one time with TBS. The bound antibody was detected adding peroxidase substrate to each well. The reaction was allowed to proceed for a maximum time of 10 minutes until the solution color turned blue. The reaction was stopped by the addition of 0.6 M H<sub>2</sub>SO<sub>4</sub>. The solution color turned yellow and the absorbance was read at 450 nm using a plate-reader spectrophotometer. The absorbance ratio between the wells coated with Sorcin and GST was calculated. A signal-to-background ratio higher than two suggested that the phage pools were getting enriched for specific Sorcin-binding clones. The pooled phage ELISA results suggested a saturation of binding clones the fourth day of selection.

### **6.15 Clonal phage ELISA and sequencing of binding clones**

To obtain single colonies of phage infected binding clones, a log phase cell culture of *E. coli* Omnimax was infected with the out-phage of the 4<sup>th</sup> day of selection for 30 minutes 37<sup>0</sup>C. A dilution series of infected cells was performed and the 6<sup>th</sup> dilution was plated on carbenicillin agar plate in and grown over night.

A 96-well plate was prepared with 350  $\mu$ l/well of 2TY medium, carbenicillin and M13K07 helper phages. Single phage infected phage colonies were picked to each well and the plate was then incubated over-night at 37<sup>0</sup>C shaking. The next day, the bacteria were pelleted by centrifugation (3500 rpm for 20 minutes). The phage containing supernatant was used for clonal phage ELISA assay as described in the previous section. The DNA of confirmed binding clones was then amplified by PCR reaction using primers annealing to regions flanking the peptide coding sequence. The success of the PCR reactions was confirmed through 1% agarose gel electrophoresis. The PCR products underwent a clean-up reaction with Shrimp Alkaline Phosphatase (SAP) to remove 5'- and 3'-phosphate groups from DNA and with Exonuclease 1 (EXO1). The concentration of PCR products was estimated through a new 1% agarose gel using a MassRuler<sup>TM</sup> DNA ladder. The samples were then sent for sequencing. Enriched binding phage pools were further analyzed through NGS.

#### **6.16 Data set analysis**

NGS generated information on a set of potential binding peptides. The dataset contained both specific binding clones and potentially non-specific clones. The first step was to focus on the more enriched peptides (i.e. with higher sequencing counts) and then to investigate if they contained a shared binding motif. In addition, the biological function of the host proteins harboring the identified ligands was analyzed. The data set analysis was carried out according to the following pipeline:

- a list of NGS high-count peptides was chosen for further analysis;

- among the unchosen peptides, sequences with a motif similar to Pro flanked by aromatic hydrophobic residues ( $\phi$ ) and/or aromatic hydrophobic residues flanked by acidic residues (D, E) e.g:  $\phi\phi xP$ ; E/D $\phi$  (from combinatorial phage display selection) were included in the list of targets;
- Sorcin-related biological function (GO TERM) list was generated;
- evolutionary sequence conservation of chosen peptides was verified using the Ensembl (<http://www.ensembl.org/index.html>) alignment tool among placental mammalian subgroup, and Peptools (<http://slim.ucd.ie/peptools/index.php>) among metazoan, and ConSurf server (<http://consurf.tau.ac.il/2016/>) without constraints; the Ensemble generated multiple sequence alignment was analyzed with WebLogo (<http://weblogo.berkeley.edu/logo.cgi>);
- subcellular and tissue localization were evaluated using the Compartments database (<http://compartments.jensenlab.org/Search>) (Binder et al. 2014), PaxDb (<http://pax-db.org/>), and Human Protein Atlas (<http://www.proteinatlas.org/>).
- network analysis was performed using Cytoscape (<http://www.cytoscape.org/>) on the novel dataset together with information obtained from Biogrid (<http://thebiogrid.org/>) and IntAct (<http://www.ebi.ac.uk/intact/>).

The Cytoscape network was generated using information of Biogrid and IntAct databases. The list of reported interactions for each peptide of NGS dataset were downloaded as text files. These files were used to build networks using Cytoscape. The networks of every target and Sorcin were

merged in a single network, then used to extract a network consisting of Sorcin first neighbour of the first neighbour interactions.

### **6.17 Phage clones analysis**

Binding was validated for selected phage clones through clonal phage ELISA. Oligonucleotide sequences were designed encoding the desired peptide sequences and flanked by annealing sites to the phagemid encoding the pVIII coat protein. Following the protocol developed by Kunkel (1985), designed oligos were phosphorylated using T4 PNK kinase, annealed to the phagemid ssDNA template, the second DNA strand synthesis was performed over-night at 20<sup>0</sup>C using T4 ligase and T7 polymerase.

The newly generated dsDNA was chemically transform into *E. coli* Omnimax cells. Finally as mentioned in the previous section, GST-tagged Sorcin and the negative control GST were immobilized on a 96 well plate and single colonies from transformation were picked in to a 1.2 ml well plate together with M13 M13K07 helper phage and carbenicillin in order to generate phage displaying desired peptides.

### **6.18 Phage clones mutants**

In order to find crucial residues involved in the interaction between Sorcin and selected targets (see below) mutants were designed where the chosen residues were replaced with alanine residues.

Mutagenic oligos were designed for PPP1R3G, CAC1B, NUP214, SYT16, CEP97. In the following list the bold letters of the peptide sequences represent designed mutated residues, whereas in the oligonucleotide sequences the bold-capital letters represent the mutated nucleotides.



PPP1R3G (YTFTEWRSFLDVPAE)

ctggctatacctttaccg**CGGC**gcgtagctttctggatgtgccggcgga

PPP1R3G (YTFTEWRSFLDVPAEL)

cgaatggcgtagctttctgg**CgGcG**cgcggaactgggtggag

CAC1B (SYVSSLTSQSHPLRRV)

cctgaccagccagagccat**GcgGC**gcgctcgtgtgggtggagg

SYT16 (EQKPKFSRSLTHGED)

catctggcgaacagaaa**GcgaaaCG**agccgtagcctgctgac

NUP214 (LVPERETLFLNLANNR)

ctcttcatctggcctgg**CgGcggCG**cgtgaaaccctgttaac

CEP97 (LIPEHSSPVQDAQISQ)

ctcttcatctggcctg**GCGGcggCG**catagcagcccgtgcag

The mutagenesis was performed on template ssDNA prepared for each phage clone. An *E. coli* CJ236 cell culture was grown in 2TY medium and chloramphenicol to reach the log phase. It was then infected for 30 minutes with the distinct phage clones. The infected cells were plated on carbenicillin agar plates to obtain single colonies. The following day single colonies were picked into 2TY medium supplemented with M13KO7 helper phages, carbenicillin and chloramphenicol and grown for 2 hours at 37<sup>0</sup> C shaking. Kanamycin was added to select bacteria co-infected with helper phages and the cultures were grown for 6 hours. Finally the cultures were transferred into 30ml of 2TY medium with carbenicillin, kenamycin and uridine then grown for 20 hours at 37<sup>0</sup> C. The day after the cells were centrifuged for 10 minutes at 1500 rpm at 4<sup>0</sup> C, the supernatant transferred to a new falcon tube containing 7,5 ml of PEG8000 0,4M NaCl and incubated for 5 minutes at

room temperature, to precipitate phages. Then the phages were pelleted by centrifugation, supernatant was decanted and the phage pellet resuspended in 0,5ml PBS. Single-stranded DNA from M13 phage was isolated using QIAGEN® Plasmid Kits according to manufacturer's instructions.

The mutants were generated according to Kunkel protocol described in phage clones paragraph (Kunkel, 1985). The binding of generated mutants was validated through phage ELISA assay.

### **6.19 Sorcin A2C cysteine labeling with Cy5 and MiscoScale Thermophoresis (MST)**

The purified Sorcin A2C mutant was diluted into the labeling reaction buffer (150 mM sodium bicarbonate pH 8.5) to make a 2 $\mu$ M protein solution. The labeling reaction was carried out adding 2 $\mu$ l of Cy5 (0,8mM) to 50  $\mu$ l of diluted protein; the reaction proceeded overnight at 4<sup>0</sup> C.

The excess of dye was removed using a desalting column step using Zeba™ Spin Desalting Columns (Thermo Scientific). The labeling buffer was exchanged with 20mM Hepes pH 7.5 through an overnight dialysis. Finally the concentration of the protein and the degree of labeling (DOL) was determined spectrophotometrically according to the following formulas:  $[P] = (A_{280} * A_{650}) / \epsilon_{\text{protein}}$ ;  $DOL = (A_{650} / \epsilon_{\text{dye}}) / [P]$ .

MST experiments were performed at Monolith NT.automated (Nanotemper Technologies).

MST is a fluorescence-based technique used to measure molecular interactions and kinetics. Thermophoresis is the motion of molecules in temperature field; it is very sensitive to changes in size, charge, solvation

shell and conformation of a molecule, indeed when an interaction occurs all these molecular properties can change allowing the quantification of binding events (Jerabek-Willemsen et al 2011; Jerabek-Willemsen et al. 2014). The temperature gradient is induced by an infrared laser, and the direct movement of molecules through the temperature gradient is detected thanks to a fluorescent label or intrinsic tryptophan fluorescence, if present, on ligands or target. Serial dilution of unlabeled molecule is performed and a constant concentration of labeled molecule is added to each dilution, so that every capillary has a different concentration of ligand against a constant concentration of target. The main advantage of MST is that the interaction is measured in solution and does not require a large consumption of sample. The signal consist of different subsequent processes that can be separated by their timescale and infrared laser source, and each of these individual phases contains information about the affinity and mechanism of binding (Jerabek-Willemsen et al. 2014). These phases are: Temperature Jump (T jump), thermophoresis, steady state, inverse temperature jump and back diffusion (Figure 40).

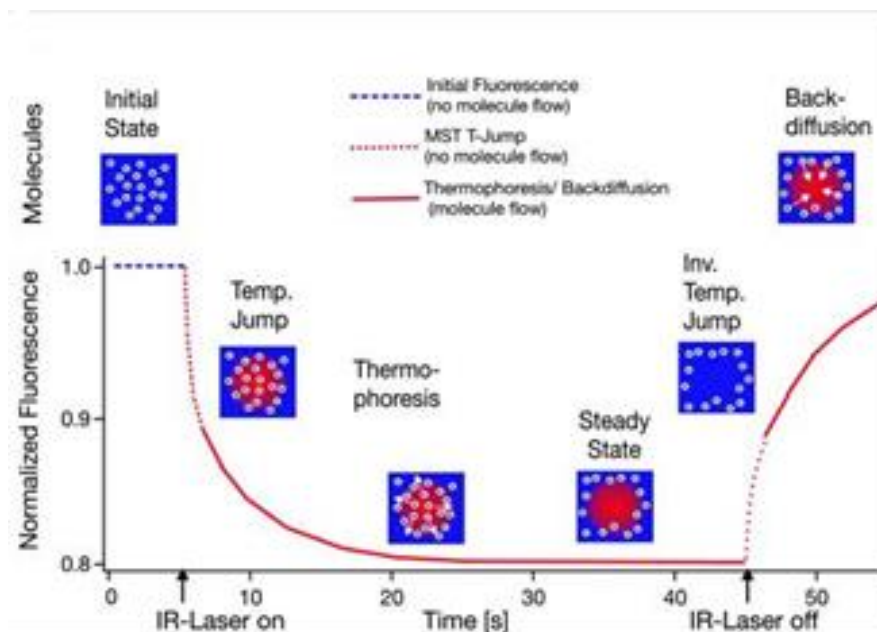


**Figure 40: A typical MST signal for a single capillary.** Here is shown the molecules behavior into the temperature field upon infrared laser excitation (Jerabek-Willemsen et al 2011).

To avoid protein precipitation or stickiness to capillary walls, premium coated capillaries were used and 0,05% of pluronic reagent was added to protein buffer (10 mM Hepes pH 7.5, 150mM NaCl, 100  $\mu$ M  $\text{CaCl}_2$ ). The experiments were carried out at a constant protein concentration (0.25  $\mu$ M) and 1:1 dilution series of the peptide, starting from a maximum concentration of 500  $\mu$ M (PPP1R3G, SYT16), 250  $\mu$ M (CAC1B, CEP97) or 1000  $\mu$ M (NUP214). Synthetic peptides were ordered and dissolved in milliQ water. The PPP1R3G peptide was dissolved in water with and the pH adjusted using 1mM NaOH to increase its solubility.

## References

- Ambudkar SV, Dey S, Hrycyna CA, Ramachandra M, Pastan I, Gottesman MM. (1999) “Biochemical, cellular, and pharmacological aspects of the multidrug transporter.” *Annu Rev Pharmacol Toxicol.*; 39:361-98.
- Andersson A, Forsén S, Thulin E, Vogel HJ (1983) “Cadmium-113 nuclear magnetic resonance studies of proteolytic fragments of calmodulin: assignment of strong and weak cation binding Sites” *Biochemistry* 22:2309– 2313
- Anthony DF, Beattie J, Paul A, Currie S (2007) “Interaction of calcium/calmodulin-dependent protein kinase II $\delta$ C with sorcin indirectly modulates ryanodine receptor function in cardiac myocytes” *J. Mol. Cell. Cardiol.* 43:492–503
- Bates, R.C.; Mercurio, A.M. (2005) “The epithelial-mesenchymal transition (EMT) and colorectal cancer progression.” *Cancer Biol. Ther.* 4, 365–370.
- Berridge MJ (2003) “Cardiac calcium signaling” *Biochem Soc Trans* 31(Pt 5):930-3
- Berridge MJ (2011) “Calcium signaling and Alzheimer’s disease” *Neurochem Res* 36(7):1149-56
- Bers DM, Despa S (2006) “Cardiac myocytes Ca<sup>2+</sup> and Na<sup>+</sup> regulation in normal and failing hearts” *J Pharmacol Sci* 100(5):315-22
- Binder JX et al. (2014) “COMPARTMENTS: unification and visualization of protein subcellular localization evidence.” *Database (Oxford)*;bau012.
- Blikstad C, Ivarsson Y. (2015) “High-throughput methods for identification of protein-protein interactions involving short linear motifs.” *Cell Commun Signal.*;13:38.
- Bonte D, Lindvall C, Liu H, Dykema K, Furge K, Weinreich M. (2008) “Cdc7-Dbf4 kinase overexpression in multiple cancers and tumor cell lines is correlated with p53 inactivation.” *Neoplasia.*;10(9):920-31.

- Borst P (2012) “Cancer drug pan-resistance: pumps, cancer stem cells, quiescence, epithelial to mesenchymal transition, blocked cell death pathways, persists or what?” *Open Biol.*;2(5):120066.
- Borst P, Elferink RO (2002) “Mammalian ABC transporters in health and disease.” *Annu Rev Biochem.* 71:537-92.
- Borst P, Schinkel AH (2013) “P-glycoprotein ABCB1: a major player in drug handling by mammals.” *J Clin Invest.*;123(10):4131-3.
- Buschow SI, van Balkom BW, Aalberts M, Heck AJ, Wauben M, Stoorvogel W (2010) “MHC class II-associated proteins in B-cell exosomes and potential functional implications for exosome biogenesis” *Immunol. Cell Biol.* 88: 851–856.
- Byler S, Goldgar S, Heerboth S, Leary M, Housman G, Moulton K, Sarkar S. (2014) “Genetic and epigenetic aspects of breast cancer progression and therapy.” *Anticancer Res.* ;34(3):1071-7.
- Byler S, Sarkar S. (2014) “Do epigenetic drug treatments hold the key to killing cancer progenitor cells?” *Epigenomics.* ;6(2):161-5.
- Carafoli E (2003) “Historical review: mitochondria and calcium: ups and downs of an unusual relationship” *Trends Biochem. Sci* 28:175–181
- Chaffer, C.; Brueckmann, I.; Scheel, C.; Kaestli, A.; Wiggins, P.; Rodrigues, L.; Brooks, M.; Reinhardt, F.; Su, Y.; Polyak, K.; et al. (2011) “Normal and neoplastic nonstem cells can spontaneously convert to a stem-like state.” *Proc. Natl. Acad. Sci. USA* 108, 7950–7955.
- Chaffer, C.; Weinberg, R. “A perspective on Cancer Cell Metastasis.” (2011) *Science* 331, 1559–1564.
- Chang G, Roth CB. (2001) “Structure of MsbA from *E. coli*: a homolog of the multidrug resistance ATP binding cassette (ABC) transporters.” *Science.* 7;293(5536):1793-800.
- Changenet-Barret P, Gustavsson T, Markovitsi D, Manet I, Monti S. (2013) “Unravelling molecular mechanisms in the fluorescence spectra of doxorubicin in aqueous solution by femtosecond fluorescence spectroscopy.” *Phys Chem Chem Phys.* ;15(8):2937-44.

- Chao CC, Ma CM, Lin-Chao S (1991) “Co-amplification and over-expression of two *mdr* genes in a multidrug-resistant human colon carcinoma cell line.” *FEBS Lett.*; 291(2):214-8.
- Chen G.K., Lacayo N.J., Duran G.E., Wang Y., Bangs C.D, Rea S., Kovacs M, Cherry A.M, Brown J.M. and Sikic B.I (2002) “Preferential expression of a mutant allele of the amplified MDR1 (ABCB1) gene in drug-resistant variants of a human sarcoma” *Genes, chromosomes & cancer* 34,372-383
- Choi CH (2005) “ABC transporters as multidrug resistance mechanisms and the development of chemosensitizers for their reversal.” *Cancer Cell Int.* 4;5:30.
- Clemen, C.S.; Herr, C.; Hovelmeyer, N.; Noegel, A.A. (2003) “The lack of annexin A7 affects functions of primary astrocytes.” *Exp. Cell Res.* 291, 406–414.
- Colotti G, Poser E, Fiorillo A, Genovese I, Chiarini V, Ilari A (2014) “Sorcin, a calcium binding protein involved in the multidrug resistance mechanisms in cancer cells” *Molecules* 19(9):13976-89
- Colotti G, Zamparelli C, Verzili D, Mella M, Loughrey CM, Smith GL, Chiancone E (2006) “The W105G and W99G sorcin mutants demonstrate the role of the D helix in the Ca (2+)-dependent interaction with annexin VII and the cardiac ryanodine receptor” *Biochemistry* 45:12519–29
- Collis LP, Meyers MB, Zhang J, Phoon CK, Sobie EA, Coetzee WA, Fishman GI. (2007) “Expression of a sorcin missense mutation in the heart modulates excitation-contraction coupling.” *FASEB J.*;21(2):475-87.
- Coombs CC, Tavakkoli M, Tallman MS. (2015) “Acute promyelocytic leukemia: where did we start, where are we now, and the future.” *Blood Cancer J.* ;5:e304.
- Crouch TH, Klee CB (1980) “Positive cooperative binding of calcium to bovine brain calmodulin. *Biochemistry*” 19:3692–3698
- Davey NE, Seo MH, Yadav VK, Jeon J, Nim S, Krystkowiak I, Blikstad C, Dong D, Markova N, Kim PM, Ivarsson Y. (2017) “Discovery of short linear motif-mediated interactions through phage

display of intrinsically disordered regions of the human proteome.” *FEBS J.* ;284(3):485-498.

- Degos L, Wang ZY (2001) “All trans retinoic acid in acute promyelocytic leukemia.” *Oncogene.*;20(49):7140-5.
- Del Prete D, Checler F, Chami M (2014) “Ryanodine receptors: Physiological function and deregulation in Alzheimer disease.” *Mol. Neurodegener.* 9, 21
- Deng, L.; Su, T.; Leng, A.; Zhang, X.; Xu, M.; Yan, L.; Gu, H.; Zhang, G. (2010) “Upregulation of soluble resistance-related calcium-binding protein (sorcin) in gastric cancer.” *Med. Oncol.* 27, 1102–1108.
- Diaz-Lagares A, Crujeiras AB, Lopez-Serra P, Soler M, Setien F, Goyal A, Sandoval J, Hashimoto Y, Martinez-Cardús A, Gomez A, Heyn H, Moutinho C, Espada J, Vidal A, Paúles M, Galán M, Sala N, Akiyama Y, Martínez-Iniesta M, Farré L, Villanueva A, Gross M, Diederichs S, Guil S, Esteller M. (2016) “Epigenetic inactivation of the p53-induced long noncoding RNA TP53 target 1 in human cancer.” *Proc Natl Acad Sci U S A.*;113(47):E7535-E7544.
- Duesberg P., Li R., Sachs R., Fabarius A, Upender M.B. and Hehlmann R. (2007) “Cancer drug resistance: the central role of the karyotype” *Drug resistance updates : reviews and commentaries in antimicrobial and anticancer chemotherapy* 10(1-2),51-58.
- Duester G (2009) “Keeping an eye on retinoic acid signaling during eye development.” *Chem Biol Interact.* ;178(1-3):178-81.
- Emsley P, Cowtan K. (2004) “Coot: model-building tools for molecular graphics.” *Acta Crystallogr D*; 60: 2126–2132.
- Flahaut M, Mühlethaler-Mottet A, Martinet D, Fattet S, Bourlout KB, Auderset K, Meier R, Schmutz NB, Delattre O, Joseph JM, Gross N. (2006) “Molecular cytogenetic characterization of doxorubicin-resistant neuroblastoma cell lines: evidence that acquired multidrug resistance results from a unique large amplification of the 7q21 region.” *Genes Chromosomes Cancer.*;45(5):495-508.



- Fornari FA, Randolph JK, Yalowich JC, Ritke MK, Gewirtz DA. (1994) "Interference by doxorubicin with DNA unwinding in MCF-7 breast tumor cells." *Mol Pharmacol.*;45(4):649-56.
- Fowler MR, Colotti G, Chiancone E, Higuchi Y, Seidler T, Smith GL(2009) "Complex modulation of L-type Ca<sup>2+</sup> current inactivation by sorcin in isolated rabbit cardiomyocytes" *Pflugers Arch.* 457:1049–1060.
- Fowler MR, Colotti G, Chiancone E, Smith GL, Fearon IM (2008) "Sorcin modulates cardiac L-type Ca<sup>2+</sup> current by functional interaction with the alpha1C subunit in rabbits" *Exp. Physiol.* 93:1233–1238
- Franceschini S, Ilari A, Verzili D, Zamparelli C, Antaramian A, Rueda A, Valdivia HH, Chiancone E, Colotti G (2008) "Molecular basis for the impaired function of the natural F112L sorcin mutant: X-ray crystal structure, calcium affinity, and interaction with annexin VII and the ryanodine receptor" *FASEB J.* 22:295–306
- Frank KF, Bölck B, Ding Z, Krause D, Hattebuhr N, Malik A, Brixius K, Hajjar RJ, Schrader J, Schwinger RH (2005) "Overexpression of sorcin enhances cardiac contractility in vivo and in vitro." *J Mol Cell Cardiol.*;38(4):607-15.
- Frederick CA, Williams LD, Ughetto G, van der Marel GA, van Boom JH, Rich A, Wang AH (1990) "Structural comparison of anticancer drug-DNA complexes: adriamycin and daunomycin." *Biochemistry.*;29(10):2538-49.
- French PJ, Swagemakers SM, Nagel JH, Kouwenhoven MC, Brouwer E, van der Spek P, Luider TM, Kros JM, van den Bent MJ, Sillevius Smitt PA. (2005) "Gene expression profiles associated with treatment response in oligodendrogliomas." *Cancer Res.* 65(24):11335-44.
- Gao Y, Li W, Liu X, Gao F, Zhao X. (2015) "Reversing effect and mechanism of soluble resistance-related calcium-binding protein on multidrug resistance in human lung cancer A549/DDP cells." *Mol med reP*; 11: 2118–2124.

- Gonzales PA, Pisitkun T, Hoffert JD, Tchapyjnikov D, Star RA, Kleta R, Wang NS, Knepper MA (2009) “Large-scale proteomics and phosphoproteomics of urinary exosomes” *J. Am. Soc. Nephrol.* 20:363–379
- Gottesman MM, Fojo T, Bates SE (2002) “Multidrug resistance in cancer: role of ATP-dependent transporters.” *Nat Rev Cancer.*;2(1):48-58.
- Gracy, K.N.; Clarke, C.L.; Meyers, M.B.; Pickel, V.M. (1999) “N-methyl-D-aspartate receptor 1 in the caudate-putamen nucleus: Ultrastructural localization and co-expression with sorcin, a 22,000 mol. wt calcium binding protein.” *Neuroscience* 90, 107–117.
- Hamada, H.; Okochi, E.; Oh-hara, T.; Tsuruo, T. (1988) “Purification of the Mr 22,000 calcium-binding protein (sorcin) associated with multidrug resistance and its detection with monoclonal antibodies.” *Cancer Res.* 48, 3173–3178.
- Hansen C, Tarabykina S, la Cour JM, Lollike K, Berchtold MW (2003) “The PEF family proteins sorcin and grancalcin interact in vivo and in vitro” *FEBS Lett.* 545:151–154
- Hansen S.N., Ehlers N.S., Zhu S., Thomsen M.B., Nielsen R.L., Liu D., Wang G., Hou Y., Zhang X., Xu X., Bolund L., Yang H., Wang J., Moreira J., Ditzel H.J., Brunner N., Schrohl A.S., Stenvang J. and Gupta R. (2016) “The stepwise evolution of the exome during acquisition of docetaxel resistance in breast cancer cells” *BMC genomics* 17,442.
- He, Q.; Zhang, G.; Hou, D.; Leng, A.; Xu, M.; Peng, J.; Liu, T. (2011) “Overexpression of sorcin results in multidrug resistance in gastric cancer cells with up-regulation of P-gp.” *Oncol. Rep.* 25,237–243.
- Hilgendorf C, Ahlin G, Seithel A, Artursson P, Ungell AL, Karlsson J (2007) “Expression of thirty-six drug transporter genes in human intestine, liver, kidney, and organotypic cell lines.” *Drug Metab Dispos.* ;35(8):1333-40.
- Holland LZ. (2007) “Developmental biology: a chordate with a difference.” *Nature.* ;447(7141):153-5.

- Holohan C, Van Schaeybroeck S, Longley DB, Johnston PG (2013) "Cancer drug resistance: an evolving paradigm." *Nat Rev Cancer.* ;13(10):714-26.
- Housman G, Byler S, Heerboth S, Lapinska K, Longacre M, Snyder N, Sarkar S. (2014) "Drug resistance in cancer: an overview. *Cancers*" (Basel). ;6(3):1769-92.
- Hu, Y.; Cheng, X.; Li, S.; Zhou, Y.; Wang, J.; Cheng, T.; Yang, M.; Xiong, D. (2013) "Inhibition of sorcin reverses multidrug resistance of K562/A02 cells and MCF-7/A02 cells via regulating apoptosis-related proteins." *Cancer Chemother. Pharmacol.* 72, 789–798.
- Hu, Y.; Li, S.; Yang, M.; Yan, C.; Fan, D.; Zhou, Y.; Zhang, Y.; Yague, E.; Xiong, D. (2014) "Sorcin silencing inhibits epithelial-to-mesenchymal transition and suppresses breast cancer metastasis in vivo." *Breast Cancer Res. Treat.* 143, 287–299.
- Huang H and Sidhu SS (2011) "Studying binding specificities of peptide recognition modules by high-throughput phage display selections." *Methods Mol Biol.*;781:87-97.
- Ilari A, Johnson KA, Nastopoulos V, Verzili D, Zamparelli C, Colotti G, Tsernoglou D, Chiancone E (2002) "The crystal structure of the sorcin calcium binding domain provides a model of Ca<sup>2+</sup>-dependent processes in the full-length protein" *J Mol Biol* 317(3):447-58
- Ivarsson Y, Arnold R, McLaughlin M, Nim S, Joshi R, Ray D, Liu B, Teyra J, Pawson T, Moffat J, Li SS, Sidhu SS, Kim PM. (2014) "Large-scale interaction profiling of PDZ domains through proteomic peptide-phage display using human and viral phage peptidomes." *Proc Natl Acad Sci U S A.* ;111(7):2542-7.
- Januchowski R, Wojtowicz K, Sujka-Kordowska P, Andrzejewska M, Zabel M. (2013) "MDR gene expression analysis of six drug-resistant ovarian cancer cell lines." *Biomed Res Int.*;2013:241763.
- Jerabek-Willemsen M et al. (2011) "Molecular interaction studies using Microscale Thermophoresis" *Assay and drug development technologies*; 9(4):342-353.

- Jerabek-Willemsen M et al. (2014) “MicroScale Thermophoresis: Interaction analysis and beyond” *Journal of molecular structure*;1077: 101-113.
- Jia, J., Tarabykina, S., Hansen, C., Berchtold, M. & Cygler, M. (2001) “Structure of apoptosis-linked protein ALG-2: insights into Ca<sup>2+</sup>-induced changes in penta-EF-hand proteins.” *Structure* 9, 267–75.
- Juergens, R.; Wrangle, J.; Vendetti, F.; Murphy, S.C.; Zhao, M.; Coleman, B.; Sebree, R.; Rodgers, K.; Hooker, C.M.; Franco, N.; et al. (2011) “Combination epigenetic therapy has efficacy in patients with refractory advanced non-small cell lung cancer.” *Cancer Discov.* 1, 598–607.
- Kabsch, W. (2010) “Xds.” *Acta Crystallographica Section D-Biological Crystallography* 66, 125–132.
- Kadioglu O, Efferth T (2016) “Peptide aptamer identified by molecular docking targeting translationally controlled tumor protein in leukemia cells.” *Invest New Drugs.*;34(4):515-21.
- Kantharidis P, El-Osta A, deSilva M, Wall DM, Hu XF, Slater A, Nadalin G, Parkin JD, Zalcberg JR. (1997) “Altered methylation of the human MDR1 promoter is associated with acquired multidrug resistance.” *Clin Cancer Res.* ;3(11):2025-32.
- Katoh H., Shibata T., Kokubu A., Ojima H., Loukopoulos P., Kanai Y., Kosuge T., Fukayama M., Kondo T, Sakamoto M., Hosoda F., Ohki M., Imoto I., Inazawa J. and Hirohashi S. (2005) “Genetic profile of hepatocellular carcinoma revealed by array-based comparative genomic hybridization: identification of genetic indicators to predict patient outcome” *Journal of hepatology* 43,863-874.
- Kaufman RJ, Malhotra JD (2014) “Calcium trafficking integrates endoplasmic reticulum function with mitochondria bioenergetics” *Biochimica et Biophysica Acta* 1843:2233-2239
- Kawakami, M.; Nakamura, T.; Okamura, N.; Komoto, C.; Markova, S.; Kobayashi, H.; Hashimoto, N.; Okumura, K.; Sakaeda, T. (2007) “Knock-down of sorcin induces up-regulation of MDR1 in HeLa cells.” *Biol. Pharm. Bull.* 30, 1065–1073.
- Kawasaki H, Kretsinger RH (1995) “Calcium-binding proteins 1: EF-hands. *Protein Profile*” 2:297–490

- Kim I.W., Han N., Kim M.G., Kim T. and Oh J.M, (2015) “Copy number variability analysis of pharmacogenes in patients with lymphoma, leukemia, hepatocellular, and lung carcinoma using The Cancer Genome Atlas data” *Pharmacogenetics and genomics* 25,1-7.
- Kitada K, Yamasaki T. (2007) “The MDR1/ABCB1 regional amplification in large inverted repeats with asymmetric sequences and microhomologies at the junction sites.” *Cancer Genet Cytogenet.*;178(2):120-7.
- Knutsen T., Mickley L.A., Ried T., Green E.D., du Manoir S., Schrock E., Macville M., Ning Y., Robey R., Polymeropoulos M., Torres R. and Fojo T. (1998) “Cytogenetic and molecular characterization of random chromosomal rearrangements activating the drug resistance gene, MDR1/P-glycoprotein, in drug-selected cell lines and patients with drug refractory ALL” *Genes, chromosomes & cancer* 23,44-54.
- Kontny NE, Wurthwein G, Joachim B, Boddy AV, Krischke M, Fuhr U et al. (2013) “Population pharmacokinetics of doxorubicin: establishment of a NONMEM model for adults and children older than 3 years.” *Cancer chemother pharmacol*; 71: 749–763.
- Kunkel TA (1985) “Rapid and efficient site-specific mutagenesis without phenotypic selection” *PNAS*;82:488-492.
- Kwon NS, Kim DS, Yun HY. (2017) “Leucine-rich glioma inactivated 3: integrative analyses support its prognostic role in glioma.” *Onco Targets Ther.* ;10:2721-2728.
- Lai RC, Chen TS, Lim SK (2011) “Mesenchymal stem cell exosome: A novel stem cell-based therapy for cardiovascular disease” *Regen. Med.* 6:481–492.
- Lalioti VS, Ilari A, O'Connell DJ, Poser E, Sandoval IV, Colotti G (2014) “Sorcin links calcium signaling to vesicle trafficking, regulates Polo-like kinase 1 and is necessary for mitosis” *PLoS One.* 9(1):e85438
- Landriscina M, Laudiero G, Maddalena F, Amoroso MR, Piscazzi A, Cozzolino F, Monti M, Garbi C, Fersini A, Pucci P, et al. (2010) “Mitochondrial chaperone Trap1 and the calcium binding protein

Sorcin interact and protect cells against apoptosis induced by antitublastic agents” *Cancer Res.* 70:6577–6586

- Laskowski, R. A., Moss, D. S. & Thornton, J. M. (1993) “Main-Chain Bond Lengths and Bond Angles in Protein Structures.” *Journal of Molecular Biology* 231, 1049–1067.
- Lee WP (1996) “Purification, cDNA cloning, and expression of human sorcin in vincristine-resistant HOB1 lymphoma cell lines.” *Arch Biochem Biophys.* ;325(2):217-26.
- Lin LM, Li BX, Xiao JB, Lin DH, Yang BF. (2005) “Synergistic effect of all-trans-retinoic acid and arsenic trioxide on growth inhibition and apoptosis in human hepatoma, breast cancer, and lung cancer cells in vitro.” *World J Gastroenterol.* ;11(36):5633-7.
- Litviakov N.V., Cherdyntseva N.V., Tsyganov M.M., Slonimskaya E.M., Ibragimova M.K., Kazantseva P.V., Kzhyskowska J. and Choinzonov E.L. (2016) “Deletions of multidrug resistance gene loci in breast cancer leads to the down-regulation of its expression and predict tumor response to neoadjuvant chemotherapy” *Oncotarget* 7, 7829-7841.
- Liu, X.; Chen, L.; Feng, B.; Liu, G. “Reversing effect of sorcin in the drug resistance of human nasopharyngeal carcinoma.” (2014) *Anat. Rec.* 297, 215–221.
- Lokuta AJ, Meyers MB, Sander PR, Fishman GI, Valdivia HH (1997) “Modulation of cardiac ryanodine receptors by sorcin” *J. Biol. Chem* 272:25333–25338
- Lomovskaya N, Otten SL, Doi-Katayama Y, Fonstein L, Liu XC, Takatsu T, Inventi-Solari A, Filippini S, Torti F, Colombo AL, Hutchinson CR (1999) “Doxorubicin overproduction in *Streptomyces peucetius*: cloning and characterization of the *dnrU* ketoreductase and *dnrV* genes and the *doxA* cytochrome P-450 hydroxylase gene.” *J Bacteriol.* ;181(1):305-18.
- Longley DB, Johnston PG (2005) “Molecular mechanisms of drug resistance.” *J Pathol.*;205(2):275-92.
- Maddalena F, Laudiero G, Piscazzi A, Secondo A, Scorziello A, Lombardi V, Matassa DS, Fersini A, Neri V, Esposito F et al. (2011)

- “Sorcin induces a drug-resistant phenotype in human colorectal cancer by modulating Ca<sup>2+</sup> homeostasis” *Cancer Res.* 71:7659–7669
- Maddalena F, Sisinni L, Lettini G, Condelli V, Matassa DS, Piscazzi A, Amoroso MR, La Torre G, Esposito F, Landriscina M (2013) “Resistance to paclitaxel in breast carcinoma cells requires a quality control of mitochondrial antiapoptotic proteins by TRAP1” *Mol Oncol* 7(5):895-906
  - Maki M, Kitaura Y, Satoh H, Ohkouchi S, Shibata H (2002) “Structures, functions and molecular evolution of the penta-EF-hand Ca<sup>2+</sup>-binding proteins” *Biochim. Biophys. Acta* 1600:51–60
  - Marvin DA, Symmons MF, Straus SK. (2014) “Structure and assembly of filamentous bacteriophages.” *Prog Biophys Mol Biol.*;114(2):80-122.
  - Matsumoto T, Hisamatsu Y, Ohkusa T, Inoue N, Sato T, Suzuki S, Ikeda Y, Matsuzaki M (2005) “Sorcin interacts with sarcoplasmic reticulum Ca<sup>2+</sup>-ATPase and modulates excitation-contraction coupling in the heart” *Basic Res. Cardiol.* 100:250–262.
  - Meador WE, Means AR, Quioco FA (1992) “Target enzyme recognition by calmodulin: 2.4 A structure of a calmodulin-peptide complex” *Science* 257:1251–1255.
  - Meador WE, Means AR, Quioco FA (1993) “Modulation of calmodulin plasticity in molecular recognition on the basis of x-ray structures” *Science* 262:1718–1721
  - Mella M, Colotti G, Zamparelli C, Verzili D, Ilari A, Chiancone E (2003) “Information transfer in the penta-EF-hand protein sorcin does not operate via the canonical structural/functional pairing. A study with site-specific mutants” *J Biol Chem* 278:24921–8
  - Meyers MB, Pickel VM, Sheu SS, Sharma VK, Scotto KW, Fishman GI (1995) “Association of sorcin with the cardiac ryanodine receptor” *J Biol Chem* 270:26411–26418
  - Meyers MB, Biedler JL. (1981) “Increased synthesis of a low molecular weight protein in vincristine-resistant cells. *Biochem Biophys Res Commun.* 99(1):228-35.
  - Mickley L.A., Spengler B.A., Knutsen T.A., Biedler J.L. and Fojo T., (1997) “Gene rearrangement: a novel mechanism for

MDR-1 gene activation” *The Journal of clinical investigation* 99,1947-1957.

- Momparler RL, Karon M, Siegel SE, Avila F. (1976) “Effect of adriamycin on DNA, RNA, and protein synthesis in cell-free systems and intact cells.” *Cancer Res.*;36(8):2891-5.
- Murshudov GN, Vagin AA, Dodson EJ. (1997) “Refinement of macromolecular structures by the maximum-likelihood method.” *Acta Crystallogr D*; 53: 240–255.
- Němcová-Fürstová V, Kopperová D, Balušíková K, Ehrlichová M, Brynychová V, Václavíková R, Daniel P, Souček P, Kovář J. (2016) “Characterization of acquired paclitaxel resistance of breast cancer cells and involvement of ABC transporters.” *Toxicol Appl Pharmacol.* 2016;310:215-228.
- Noordeen, NA, Meur G, Rutter GA, Leclerc I 2012) “Glucose-induced nuclear shuttling of ChREBP is mediated by sorcin and Ca<sup>2+</sup> ions in pancreatic β-cells.” *Diabetes*, 61, 574–585.
- Pack-Chung, E.; Meyers, M.B.; Pettingell, W.P.; Moir, R.D.; Brownawell, A.M.; Cheng, I.; Tanzi, R.E.; Kim, T.W. (2000) “Presenilin 2 interacts with sorcin, a modulator of the ryanodine receptor.” *J. Biol. Chem.* 275, 14440–14445.
- Padar, S.; van Breemen, C.; Thomas, D.W.; Uchizono, J.A.; Livesey, J.C.; Rahimian, R. (2004) “Differential regulation of calcium homeostasis in adenocarcinoma cell line A549 and its Taxol-resistant subclone.” *Br. J. Pharmacol.* 142, 305–316.
- Pang B, Wijdeven RH, van der Zanden SY, Qiao X, Blomen V, Hoogstraat M, Lips EH, Janssen L, Wessels L, Brummelkamp TR, Neefjes J. (2015) “Genome-Wide Identification and Characterization of Novel Factors Conferring Resistance to Topoisomerase II Poisons in Cancer.” *Cancer Res.*;75(19):4176-87.
- Pang B, Qiao X, Janssen L, Velds A, Groothuis T, Kerkhoven R, Nieuwland M, Ovaa H, Rottenberg S, van Tellingen O, Janssen J, Huijgens P, Zwart W, Neefjes J. (2013) “Drug-induced histone eviction from open chromatin contributes to the chemotherapeutic effects of doxorubicin.” *Nat Commun.*;4:1908.



- Pang E., Hu Y., Chan K.Y., Lai P.B, Squire J.A., Macgregor P.F., Beheshti B., Albert M., Leung T.W. and Wong N., (2005) “Karyotypic imbalances and differential gene expressions in the acquired doxorubicin resistance of hepatocellular carcinoma cells” *Laboratory investigation; a journal of technical methods and pathology* 85,664-674.
- Parekh, H.K.; Deng, H.B.; Choudhary, K.; Houser, S.R.; Simpkins, H. (2002) “Overexpression of sorcin, a calcium-binding protein, induces a low level of paclitaxel resistance in human ovarian and breast cancer cells.” *Biochem. Pharmacol.* 63, 1149–1158.
- Partha SK, Ravulapalli R, Allingham JS, Campbell RL, Davies PL (2014) “Crystal structure of calpain-3 penta-EF-hand (PEF) domain - a homodimerized PEF family member with calcium bound at the fifth EF-hand.” *FEBS J.*;281(14):3138-49
- Patch A.M., Christie E.L., Etemadmoghadam D., Garsed D.W., George J., Fereday S., Nones K., Cowin P., Alsop K., Bailey P.J., Kassahn K.S., Newell F., Quinn M.C., Kazakoff S., Quek K., Wilhelm-Benartzi C. et al. Bowtell D.D., (2015) “Whole-genome characterization of chemoresistant ovarian cancer” *Nature* 521,489-494.
- Pettit, F. K., Bare, E., Tsai, A. & Bowie, J. U. (2007)“HotPatch: a statistical approach to finding biologically relevant features on protein surfaces.” *J Mol Biol* 369, 863–79.
- Pigram WJ, Fuller W, Hamilton LD (1972) “Stereochemistry of intercalation: interaction of daunomycin with DNA.” *Nat New Biol.*;235(53):17-9.
- Pisitkun T, Shen RF, Knepper MA (2004) “Identification and proteomic profiling of exosomes in human urine” *Proc. Natl. Acad. Sci. USA* 101:13368–13373.
- Pomeroy S.L, Tamayo P, Gaasenbeek M, Sturla L.M, Angelo M, McLaughlin M.E, Kim J.Y, Goumnerova L.C, Black P.M, Lau C, et al. (2002) “Prediction of central nervous system embryonal tumour outcome based on gene expression.” *Nature* 415, 436–442.
- Poston CN, Duong E, Cao Y, Bazemore-Walker CR (2011) “Proteomic analysis of lipid raft-enriched membranes isolated from internal organelles” *Biochem Biophys Res Comm* 415(2):355-60

- Qi, J.; Liu, N.; Zhou, Y.; Tan, Y.; Cheng, Y.; Yang, C.; Zhu, Z.; Xiong, D. Overexpression of sorcin in multidrug resistant human leukemia cells and its role in regulating cell apoptosis. *Biochem. Biophys. Res. Commun.* 2006, 349, 303–309.
- Qu, Y.; Yang, Y.; Liu, B.; Xiao, W. (2010) “Comparative proteomic profiling identified sorcin being associated with gemcitabine resistance in non-small cell lung cancer.” *Med. Oncol.* 27,1303–1308.
- Rosenthal EA, Ranchalis J, Crosslin DR, Burt A, Brunzell JD, Motulsky AG, Nickerson DA; NHLBI GO Exome Sequencing Project, Wijsman EM, Jarvik GP. (2013) “Joint linkage and association analysis with exome sequence data implicates SLC25A40 in hypertriglyceridemia.” *Am J Hum Genet.*;93(6):1035-45.
- Rossi, S, ed. (2013). *Australian Medicines Handbook* (2013 ed.). Adelaide: The Australian Medicines Handbook Unit Trust. **ISBN 978-0-9805790-9-3**
- Royant A, Carpentier P, Ohana J, McGeehan J, Paetzold B, Noirclerc-Savoye M et al. (2007) “Advances in spectroscopic methods for biological crystals. 1. Fluorescence lifetime measurements.” *J Appl Crystallogr*; 40: 1105–1112.
- Salzer U, Hinterdorfer P, Hunger U, Borken C, Prohaska R(2002) “Ca<sup>++</sup>-dependent vesicle release from erythrocytes involves stomatin-specific lipid rafts, synexin (annexin VII), and sorcin” *Blood* 99:2569–2577
- Sarkar, S.; Horn, G.; Moulton, K.; Oza, A.; Byler, S.; Kokolus, S.; Longacre, M. (2013) “Cancer development, progression and therapy: An epigenetic overview.” *Int. J. Mol. Sci.* 14, 21087–21113.
- Satoh, H., Shibata, H., Nakano, Y., Kitaura, Y. & Maki, M. (2002) “ALG-2 interacts with the amino-terminal domain of annexin XI in a Ca<sup>(2+)</sup> -dependent manner.” *Biochem Biophys Res Commun* 291, 1166–72.
- Sauna, Z.; Ambudkar, S. (2001) “Characterization of the catalytic cycle of ATP hydrolysis by human P-glycoprotein. The two ATP hydrolysis events in a single catalytic cycle are kinetically similar but affect different functional outcomes.” *J. Biol. Chem.* 276, 11653–11661.

- Seidler T, Miller SL, Loughrey CM, Kania A, Burow A, Kettlewell S, Teucher N, Wagner S, Kogler H, Meyers M.B et al. (2003) “Effects of adenovirus-mediated sorcin overexpression on excitation-contraction coupling in isolated rabbit cardiomyocytes” *Circ. Res.* 93:132–139.
- Shai R, Shi T, Kremen TJ, Horvath S, Liao LM, Cloughesy TF, Mischel PS, Nelson SF. (2003) “Gene expression profiling identifies molecular subtypes of gliomas.” *Oncogene.* 22(31):4918-23.
- Shang Y, Cai X, Fan D (2013) “Roles of epithelial-mesenchymal transition in cancer drug resistance.” *Curr Cancer Drug Targets.*13(9):915-29.
- Singh A, Settleman J (2010) “EMT, cancer stem cells and drug resistance: an emerging axis of evil in the war on cancer.” *Oncogene;* 29(34):4741-51.
- Stausman, R.; Morikawa, T.; Shee, K.; Barzily-Rokni, M.; Qian, Z.R.; Du, J.; Davis, A.; Mongare, M.M.; Gould, J.; Frederick, D.T.; et al. (2012) “Tumor micro-environment elicits innate resistance to RAF inhibitors through HGF secretion.” *Nature* 487, 500–504.
- Su M, Alonso S, Jones JW, Yu J, Kane MA, Jones RJ, Ghiaur G (2015) “All-Trans Retinoic Acid Activity in Acute Myeloid Leukemia: Role of Cytochrome P450 Enzyme Expression by the Microenvironment.” *PLoS One.* 10(6):e0127790.
- Suarez J, McDonough PM, Scott BT, Suarez-Ramirez A, Wang H, Fricovsky ES, Dillmann WH (2013) “Sorcin modulates mitochondrial Ca<sup>2+</sup> handling and reduces apoptosis in neonatal rat cardiac myocytes” *Am. J. Physiol. Cell Physiol.* 304:C248–256
- Sun L, Hui A.M, Su Q, Vortmeyer A, Kotliarov Y, Pastorino S, Passaniti A, Menon J, Walling J, Bailey R, et al. (2006) “Neuronal and glioma-derived stem cell factor induces angiogenesis within the brain.” *Cancer Cell* 9, 287–300.
- Sundell GN, Ivarsson Y. (2014) “Interaction analysis through proteomic phage display.” *Biomed Res Int.*;2014:176172.

- Suzuki H, Kawasaki M, Inuzuka T, Okumura M, Kakiuchi T, Shibata H et al. (2008) “Structural basis for Ca<sup>2+</sup>-dependent formation of ALG-2/Alix peptide complex: Ca<sup>2+</sup>/EF3-driven arginine switch mechanism.” *Structure*, 16: 1562–1573.
- Tacar O, Sriamornsak P, Dass CR. (2013) “Doxorubicin: an update on anticancer molecular action, toxicity and novel drug delivery systems.” *J Pharm Pharmacol.* ;65(2):157-70.
- Tafuri, S.R. (1996) “Troglitazone enhances differentiation, basal glucose uptake, and Glut1 protein levels in 3T3-L1 adipocytes.” *Endocrinology* 137, 4706–12.
- Takeda, T.; Asahi, M.; Yamaguchi, O.; Hikoso, S.; Nakayama, H.; Kusakari, Y.; Kawai, M.; Hongo, K.; Higuchi, Y.; Kashiwase, K.; et al. (2005) “Presenilin 2 regulates the systolic function of heart by modulating Ca<sup>2+</sup> signaling.” *FASEB J.* 19, 2069–2071.
- Tan, Y.; Li, G.; Zhao, C.; Wang, J.; Zhao, H.; Xue, Y.; Han, M.; Yang, C. (2003) “Expression of sorcin predicts poor outcome in acute myeloid leukemia.” *Leuk. Res.* 27, 125–131.
- Tonikian R. et al. (2008) “A specificity map for the PDZ domain family.” *Plos Biology* 6, 2043–2059.
- Vagin A, Teplyakov A. (1997) “MOLREP: an automated program for molecular replacement.” *J Appl Crystallogr*; 30: 1022–1025.
- Van der Blik AM, Meyers MB, Biedler JL, Hes E, Borst P (1986) “A 22-kd protein (sorcin/V19) encoded by an amplified gene in multidrug-resistant cells, is homologous to the calcium-binding light chain of calpain” *EMBO J.* 5:3201–3208
- Van der Blik AM, Baas F, Van der Velde-Koerts T, Biedler JL, Meyers MB, Ozols RF, Hamilton TC, Joenje H, Borst P. (1988) “Genes amplified and overexpressed in human multidrug-resistant cell lines.” *Cancer Res.* 48(21):5927-32.
- Van der Blik AM, Baas F, Ten Houte de Lange T, Kooiman PM, Van der Velde-Koerts T, Borst P. (1987) “The human mdr3 gene encodes a novel P-glycoprotein homologue and gives rise to alternatively spliced mRNAs in liver.” *EMBO J.* ;6(11):3325-31.

- Vance JE (2014) “MAM (mitochondria-associated membranes) in mammalian cells: lipids and beyond” *Biochimica et Biophysica Acta* 1841(4):595-609
- Varrin AE, Prasad AA, Scholz RP, Ramer MD, Duncker BP (2005) “A mutation in Dbf4 motif M impairs interactions with DNA replication factors and confers increased resistance to genotoxic agents.” *Mol Cell Biol.*;25(17):7494-504.
- Venkatesh K, Srikanth L, Vengamma B, Chandrasekhar C, Sanjeevkumar A, Mouleshwara Prasad BC, Sarma PV. (2013) “In vitro differentiation of cultured human CD34+ cells into astrocytes.” *Neurol India.*;61(4):383-8.
- Wang SL, Tam MF, Ho YS, Pai SH, Kao MC (1995) “Isolation and molecular cloning of human sorcin a calcium-binding protein in vincristine-resistant HOB1 lymphoma cells.” *Biochim Biophys Acta.* ,1260(3):285-93.
- Wang Y.C., Juric D., Francisco B., Yu R.X, Duran G.E., Chen G.K., Chen X. and Sikic B.I. (2006) “Regional activation of chromosomal arm 7q with and without gene amplification in taxane-selected human ovarian cancer cell lines” *Genes, chromosomes & cancer* 45,365-374.
- Werner, C.J.; Heyny-von Haussen, R.; Mall, G.; Wolf, S. (2008) “Proteome analysis of human substantia nigra in Parkinson’s disease.” *Proteome Sci.* 6, 8.
- Woods, W.S.; Boettcher, J.M.; Zhou, D.H.; Kloepper, K.D.; Hartman, K.L.; Lador, D.T.; Qi, Z.;Rienstra, C.M.; George, J.M. (2007) “Conformation-specific binding of alpha-synuclein to novel protein partners detected by phage display and NMR spectroscopy.” *J. Biol. Chem.* 282, 34555–34567.
- Xie X, Dwyer MD, Swenson L, Parker MH, Botfield MC (2001) “Crystal structure of calcium-free human sorcin: a member of the penta-EF-hand protein family” *Protein Sci* 10:2419-2425
- Xie H.; Chang, M.; Hu, X.; Wang, D.; Tian, M.; Li, G.; Jiang, H.; Wang, Y.; Dong, Z.; Zhang, Y.; et al. (2011) “Proteomics analysis of MPP+-induced apoptosis in SH-SY5Y cells.” *Neurol. Sci.* 32, 221–228.

- Xu P, Jiang YF, Wang JH. (2015) “shRNA-mediated silencing of sorcin increases drug chemosensitivity in myeloma KM3/DDP and U266/ADM cell lines.” *Int J Clin Exp Pathol.* ;8(3):2300-10.
- Yabuki N., Sakata K., Yamasaki T., Terashima H., Mio T., Miyazaki Y., Fujii T. and Kitada K, (2007) “Gene amplification and expression in lung cancer cells with acquired paclitaxel resistance” *Cancer genetics and cytogenetics* 173,1-9.
- Yamagishi, N.; Nakao, R.; Kondo, R.; Nishitsuji, M.; Saito, Y.; Kuga, T.; Hatayama, T.; Nakayama, Y. (2014) “Increased expression of sorcin is associated with multidrug resistance in leukemia cells via up-regulation of MDR1 expression through cAMP response element-binding protein.” *Biochem. Biophys. Res. Commun.* 448, 430–436.
- Yang F, Teves SS, Kemp CJ, Henikoff S. (2014) “Doxorubicin, DNA torsion, and chromatin dynamics.” *Biochim Biophys Acta.*;1845(1):84-9.
- Yang Y., Li H., Hou S., Hu B., Liu J. and Wang J. (2013) “The noncoding RNA expression profile and the effect of lncRNA AK126698 on cisplatin resistance in non-small-cell lung cancer cell” *PloS one* 8,e65309.
- Yang, Y.X.; Chen, Z.C.; Zhang, G.Y.; Yi, H.; Xiao, Z.Q. (2008) “A subcellular proteomic investigation into vincristine-resistant gastric cancer cell line.” *J. Cell Biochem.* 104, 1010–1021.
- Yokota T, Kouno J, Adachi K, Takahashi H, Teramoto A, Matsumoto K, Sugisaki Y, Onda M, Tsunoda T (2006) “Identification of histological markers for malignant glioma by genome-wide expression analysis: Dynein, alpha-PIX and sorcin.” *Acta Neuropathol.*, 111, 29–38.
- Zamparelli C, Macquaide N, Colotti G, Verzili D, Seidler T, Smith GL, Chiancone E (2010) “Activation of the cardiac Na<sup>+</sup>-Ca<sup>2+</sup> exchanger by sorcin via the interaction of the respective Ca<sup>2+</sup>-binding domains” *J. Mol. Cell. Cardiol.* 49:132–141
- Zamparelli C, Ilari A, Verzili D, Giangiacomo L, Colotti G, Pascarella S, Chiancone E (2000) “Structure-function relationship in sorcin, a member of penta EF-hand family. Interaction of sorcin fragments with the ryanodine receptor and an Escherichia Coli model system” *Biochemistry* 39(4):658-66

- Zamparelli C, Ilari A, Verzili D, Vecchini P, Chiancone E (1997) “Calcium- and pH-linked oligomerization of sorcin causing translocation from cytosol to membrane” FEBS lett 409(1):1-6
- Zhou, Y.; Xu, Y.; Tan, Y.; Qi, J.; Xiao, Y.; Yang, C.; Zhu, Z.; Xiong, D. (2006) “Sorcin, an important gene associated with multidrug-resistance in human leukemia cells.” Leuk. Res. 30, 469–476.

## **Acknowledgments**

Eventually I want to state my gratitude to all the people that helped me during these intense three years; from my PhD student colleagues to Prof. Francesco Fazi and his group (Silvia, Teresa, Ernestina and Claudia) and of course Prof. Ylva Ivarsson and her group beside all the lab members of Chemistry department of the BMC of Uppsala University, for the support and the kind suggestions.

A special thanks also to Dr. Gianni Colotti, Dr. Andrea Ilari and Dr. Annarita Fiorillo for allowing me to grow up as a scientist and as a person during these years.



## List of published papers

- **“Not only P-glycoprotein: amplification of the ABCB1-containing chromosome region 7q21 confers multidrug resistance upon cancer cells by coordinated overexpression of an assortment of resistance-related proteins.”** Ilaria Genovese, Andrea Ilari, Yehuda G. Assaraf, Francesco Fazi, Gianni Colotti, *Drug Resistance Updates* (Oct 2017) **32**:23-46.
- **“Binding of chemotherapeutic agents to Sorcin impairs cell death and increases drug resistance in cancer cells”** Ilaria Genovese; Andrea Ilari; Annarita Fiorillo; Silvia Masciarelli; Francesco Fazi; Gianni Colotti. *Cell Death and Disease* (Jul 2017) **8(7)**:e2950
- **“Structural basis of Sorcin-mediated calcium-dependent signal transduction.”** Andrea Ilari, Annarita Fiorillo, Elena Poser, Vasiliki Lalioti, Gustav N Sundell, Ylva Ivarsson, Ilaria Genovese, Gianni Colotti. *Scientific Report* (Nov 2015) **18**, 5-16828.

### Published papers on PhD side projects:

- **“Polyamine-trypanothione pathway: an update.”** Ilari Andrea, Fiorillo Annarita, Genovese Ilaria, Colotti Gianni. *Future Med Chem.* (Jan 2017) **9(1)**:61-77.
- **“Surface Plasmon Resonance: A Useful Strategy for the Identification of Small Molecule Argonaute 2 Protein Binders.”** Poser Elena, Genovese Ilaria, Masciarelli Silvia, Bellissimo Teresa, Fazi Fazi, Colotti Gianni. *Methods Mol Biol.* (Jan 2017) **1517**:223-237.
- **“Small Molecules Targeting the miRNA-Binding Domain of Argonaute 2: From Computer-Aided Molecular Design to RNA Immunoprecipitation.”** Bellissimo Teresa, Masciarelli Silvia, Poser Elena, Genovese Ilaria, Del Rio Alberto, Colotti Gianni, Fazi Francesco. *Methods Mol Biol.* (Jan 2017) **1517**:211-221.
- **“Short peptides from leucyl-tRNA synthetase rescue disease-causing mitochondrial tRNA point mutations.”** Perli E, Fiorillo A, Giordano C, Pisano A, Montanari A, Grazioli P, Campese AF, Di Micco P, Tuppen HA, Genovese I, Poser E, Preziuso C, Taylor RW, Morea V, Colotti G, d'Amati G. *Hum Mol Genet.* (Mar 2016) **25(5)**:903-15



## Not only P-glycoprotein: Amplification of the *ABCB1*-containing chromosome region 7q21 confers multidrug resistance upon cancer cells by coordinated overexpression of an assortment of resistance-related proteins

Ilaria Genovese<sup>a,1</sup>, Andrea Ilari<sup>b,1</sup>, Yehuda G. Assaraf<sup>c,1</sup>, Francesco Fazi<sup>d,\*</sup>, Gianni Colotti<sup>b,\*</sup>

<sup>a</sup> Dept. Biochemical Sciences, Sapienza University, P.le A. Moro 5, 00185 Rome, Italy

<sup>b</sup> Institute of Molecular Biology and Pathology, Italian National Research Council (IBPM-CNR), c/o Dept. Biochemical Sciences, Sapienza University, P.le A. Moro 5, 00185 Rome, Italy

<sup>c</sup> The Fred Wyszowski Cancer Research Lab, Faculty of Biology, Technion-Israel Institute of Technology, Haifa, Israel

<sup>d</sup> Dept. Anatomical, Histological, Forensic & Orthopedic Sciences, Section of Histology and Medical Embryology, Sapienza University, Via A. Scarpa 14-16, 00161 Rome, Italy

### ARTICLE INFO

#### Keywords:

ABC transporters  
P-glycoprotein (P-gp)  
Cancer  
Chemotherapeutic drugs  
Multidrug resistance  
7q21 amplicon  
Sorcin

### ABSTRACT

The development of drug resistance continues to be a dominant hindrance toward curative cancer treatment. Overexpression of a wide-spectrum of ATP-dependent efflux pumps, and in particular of *ABCB1* (P-glycoprotein or MDR1) is a well-known resistance mechanism for a plethora of cancer chemotherapeutics including for example taxanes, anthracyclines, *Vinca* alkaloids, and epipodophyllotoxins, demonstrated by a large array of published papers, both in tumor cell lines and in a variety of tumors, including various solid tumors and hematological malignancies. Upon repeated or even single dose treatment of cultured tumor cells or tumors *in vivo* with anti-tumor agents such as paclitaxel and doxorubicin, increased *ABCB1* copy number has been demonstrated, resulting from chromosomal amplification events at 7q11.2-21 locus, leading to marked P-glycoprotein overexpression, and multidrug resistance (MDR). Clearly however, additional mechanisms such as single nucleotide polymorphisms (SNPs) and epigenetic modifications have shown a role in the overexpression of *ABCB1* and of other MDR efflux pumps. However, notwithstanding the design of 4 generations of *ABCB1* inhibitors and the wealth of information on the biochemistry and substrate specificity of ABC transporters, translation of this vast knowledge from the bench to the bedside has proven to be unexpectedly difficult.

Many studies show that upon repeated treatment schedules of cell cultures or tumors with taxanes and anthracyclines as well as other chemotherapeutic drugs, amplification, and/or overexpression of a series of genes genomically surrounding the *ABCB1* locus, is observed. Consequently, altered levels of other proteins may contribute to the establishment of the MDR phenotype, and lead to poor clinical outcome. Thus, the genes contained in this *ABCB1* amplicon including *ABCB4*, *SRI*, *DBF4*, *TMEM243*, and *RUNDC3B* are overexpressed in many cancers, and especially in MDR tumors, while *TP53TG1* and *DMTF1* are *bona fide* tumor suppressors. This review describes the role of these genes in cancer and especially in the acquisition of MDR, elucidates possible connections in transcriptional regulation (co-amplification/repression) of genes belonging to the same *ABCB1* amplicon region, and delineates their novel emerging contributions to tumor biology and possible strategies to overcome cancer MDR.

### Introduction

The development of drug resistance limits the effectiveness of chemotherapeutic drug treatment in cancer, with over 90% treatment failure rate in metastatic tumors. Many mechanisms, either intrinsic or acquired, operate to confer drug resistance (Goler-Baron and Assaraf,

2011; Gonen and Assaraf, 2012; Gottesman, 2002; Holohan et al., 2013; Housman et al., 2014; Ifergan et al., 2005; Longley et al., 2006; Wijdeven et al., 2016; Zhitomirsky and Assaraf, 2016). Poor drug solubility and toxicity to normal tissues limit the doses of chemotherapeutic drugs that can be administered to cancer patients, while pharmacokinetic effects, i.e. absorption, distribution, metabolism and

\* Corresponding authors.

E-mail addresses: [francesco.fazi@uniroma1.it](mailto:francesco.fazi@uniroma1.it) (F. Fazi), [gianni.colotti@uniroma1.it](mailto:gianni.colotti@uniroma1.it) (G. Colotti).

<sup>1</sup> All authors equally contributed.

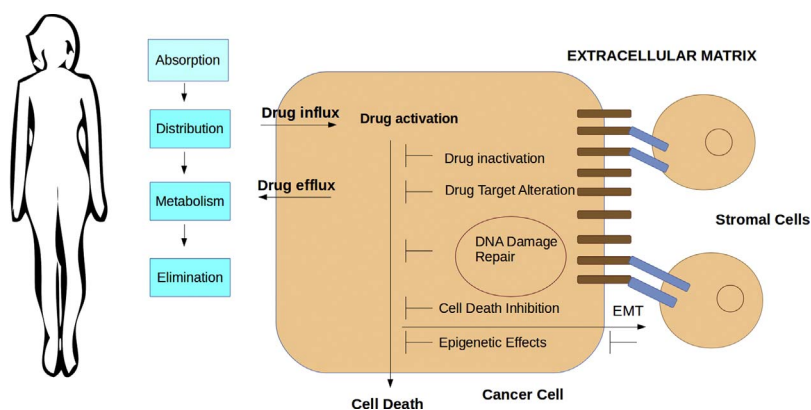


**Fig. 1.** Mechanisms that confer drug resistance upon human cancer cells. Left: pharmacokinetic factors, i.e. drug absorption, distribution, metabolism and elimination (ADME), limit the effective concentration of the drug that reach the cancer. Center and right: Drug influx and efflux limit the amount of drug that enters the tumor cell; multiple documented mechanisms, such as drug inactivation, drug target alteration, drug compartmentalization, enhanced DNA damage repair, cell cycle/checkpoint alterations, apoptosis inhibition and epigenetic alterations limit tumor cell death; epithelial-to-mesenchymal transition and metastasis are also possible escape routes of tumor cells (Alizadeh et al., 2015; Gonen and Assaraf, 2012; Holohan et al., 2013; Housman et al., 2014; Wijdeven et al., 2016; Zhitomirsky and Assaraf, 2016).

elimination, limit the actual amount of drug that reaches the tumor. Furthermore, at the level of the tumor, several established mechanisms confer resistance to one or more chemotherapeutic agents including impaired drug uptake due to decreased expression and/or loss of drug influx transporters, enhanced drug efflux, alterations in plasma membrane lipid composition, inhibition of apoptosis, enhanced DNA damage repair, cell cycle and/or checkpoint alterations, drug compartmentalization away from the drug target, increased drug metabolism and inactivation, drug target alteration, and epithelial-mesenchymal (EMT) transition (Bram et al., 2009; Debatin and Kramer, 2004; Fojo and Bates, 2003; Goler-Baron et al., 2012; Gonen and Assaraf, 2012; Holohan et al., 2013; Housman et al., 2014; Ifergan et al., 2005; Lowe et al., 2004; Maier et al., 2005; Raz et al., 2014; Stark et al., 2011; Zhitomirsky and Assaraf, 2016) (Fig. 1). Some of these mechanisms confer resistance to single agents, thus allowing possible effective treatment with alternative chemotherapeutic drugs, while other confers resistance to multiple, structurally unrelated chemotherapeutic drugs (i.e. multidrug resistance, MDR), thereby rendering the tumor refractory to drug treatment, hence markedly decreasing cure rates. Moreover, tumor heterogeneity is an important determinant in the development of drug resistance (Alizadeh et al., 2015; Andor et al., 2016; Lawrence et al., 2013; Swanton, 2012): both genetic and non-genetic mechanisms contribute to the generation of different subpopulations of cancer cells within individual tumors, and clonal selection upon treatment can account for positive selection of drug-resistant tumor populations. In particular, the presence of cancer stem cells (CSCs) in the tumor is a critical factor for the acquisition of chemoresistance. CSCs constitute a minor subpopulation of cells intrinsically resistant to chemotherapeutic drugs, due to epigenetic mechanisms that determine increased expression of anti-apoptotic proteins and of ATP-binding cassette (ABC) transporters, which mediate multidrug efflux, and their inherent quiescence (Al-Hajj et al., 2004; Dean, 2009; Feuerhake et al., 2000; Lerner and Harrison, 1990; Peters et al., 1998; Shibue and Weinberg, 2017; Zhou et al., 2001). Since the drug treatment affects only the sensitive population, the drug-resistant cell subpopulation survives and eventually spreads, making the cancer treatment ineffective.

### MDR efflux pumps of the ABC superfamily of transporters

Among the mechanisms of drug resistance, the predominant one in cancer cells and possibly the most studied one is the drug efflux by proteins of a large superfamily of ATP-dependent efflux pumps, i.e. the ATP-binding cassette (ABC) transporters (Li et al., 2016b). This superfamily is composed of 48 genes and 3 pseudogenes (HUGO Gene Nomenclature Committee, <http://www.genenames.org/cgi-bin/genefamilies/set/417>), belonging to 7 subfamilies (ABCA through ABCG), mostly ATP-dependent transporters of metabolites, xenobiotics and signaling molecules through cell membranes against their concentration gradients (Dean, 2005; Fletcher et al., 2010; Fletcher et al., 2016). ABC transporters belong to one

of the largest and more diffused superfamily, with representatives in all phyla, from prokaryotes to humans (Wilkens, 2015). ABC transporters can be grouped into exporters (which export lipids, sterols, drugs, and a large variety of primary and secondary metabolites) and importers (which take up a large variety of nutrients, biosynthetic precursors, trace metals and vitamins); bacteria use both ABC importers and exporters, while all eukaryotic ABC pumps are exporters, except for ABCA4 (Quazi et al., 2012).

### Structural organization of ABC transporters

Canonically, ABC transporters are organized in four domains, i.e. two nucleotide-binding well conserved domains (NBD) or subunits and two transmembrane domains (TBD) or subunits, that can be more heterogeneous (Fig. 2). Prokaryotic ABC transporters are often assembled from separate protein subunits, composed of two NBDs and two TMDs, either identical (homodimeric) or different (heterodimeric); most importers have additional substrate-binding domains or proteins, which bind the substrate in the periplasm (Gram-negative bacteria) or external space (Gram-positive bacteria and Archaea) and deliver it to the TMDs. Eukaryotic exporters are composed of one rather large polypeptide containing two NBDs and two TMDs (e.g., ABCB1), or consist of two polypeptides, each of which contains an NBD and a TMD as in the prokaryotic exporters (Biemans-Oldehinkel et al., 2006; ter Beek et al., 2014).

The NBDs are ABC components, i.e. ATPase domains that bind and hydrolyze ATP, about 200-amino acid long, with two subdomains, a RecA-like domain and a  $\alpha$ -helical domain (Fig. 2A). NBDs are characterized by the presence of the following motifs: 1) An A-loop, with a conserved aromatic residue (often a tyrosine), that serves to position the ATP by stacking with the adenine ring; 2) the P-loop or Walker A motif (GXXGXGK(S/T)), a phosphate-binding loop with a highly conserved lysine residue, whose backbone amide nitrogens and the  $\epsilon$ -amino group form a network of interactions with  $\beta$ - and  $\gamma$ -phosphates of ATP; 3) the Walker B motif ( $\phi\phi\phi\phi\phi\phi\phi\phi$ DE, where  $\phi$  is a hydrophobic amino acid) which coordinates the magnesium ion via the conserved aspartate residue, while the second acidic residue at the end (usually a glutamate residue) is the general base that polarizes the attacking water molecule (Oldham and Chen, 2011); 4) the D-loop (consensus motif: SALD); 5) the H-loop (or switch region), with a highly conserved histidine that interacts with the conserved aspartate from the D-loop, the glutamate residue of the Walker B motif and with the  $\gamma$ -phosphate of the ATP, and helps positioning of the attacking water, of the general base and of the magnesium ion; 6) the Q-loop, containing eight residues with a conserved N-terminal glutamine, located at the interface between the RecA-like subdomain and the  $\alpha$ -helical subdomain, in contact with the TMDs; the glutamine residue can move in and out of the active site during the ATP hydrolysis cycle, forming the active site upon Mg-ATP binding and disrupting upon ATP hydrolysis; 7) the ABC signature motif (or C motif, LSGGQ) is located at the  $\alpha$ -helical subdomain, a characteristic feature of the ABC superfamily, not present in other P-loop

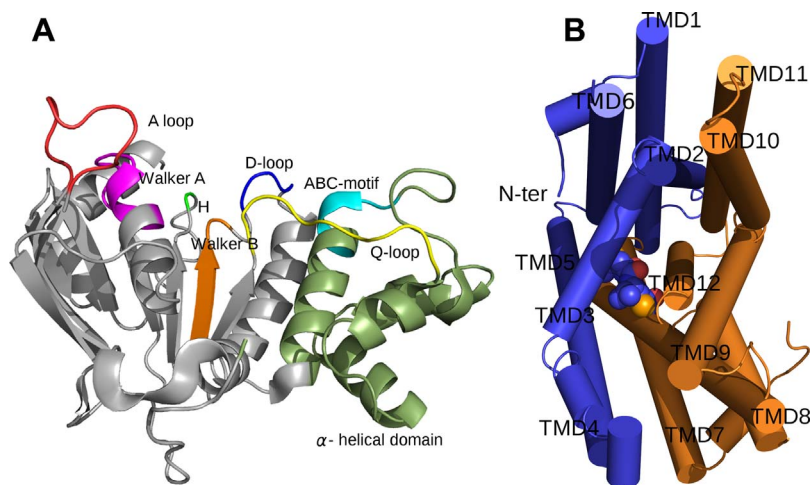


**Fig. 2.** Structure of a Nucleotide Binding Domain (NBD) and a Transmembrane Domain (TMD) of *ABCB1* (PDB code: 4M2T). A: Structure of NBD: domains and highly conserved sequence motifs are color-coded: Green,  $\alpha$ -helical domain; Gray, regulatory C-terminal domain; Red, A-loop; Magenta, Walker A; Orange, Walker B; Blue, D-loop; Green, H-loop; Cyan, ABC motif; Yellow, Q-loop. B: Structure of *ABCB1* TMD dimer, view along the two-fold symmetry axis from the inward side (the NBD domain is not represented): the two TMDs of an ABC transporter are colored in blue and orange.  $\alpha$ -helices are numbered TMD1–12. (For interpretation of the references to colour in this figure legend, the reader is referred to the web version of this article.)

NTPases such as the F1-ATPase (Hanekop et al., 2006; Li et al., 2016b; Smith et al., 2002; ter Beek et al., 2014; Verdon et al., 2003).

Two ATP binding sites are formed by the two NBDs of each ABC transporters; however, it is yet unclear whether or not the hydrolysis of two ATP molecules is needed for each transport cycle. In the bacterial maltose transporter MalEFGK<sub>2</sub> two functional ATP sites are needed, while only one functional ATP site is needed in the histidine transporter HisP<sub>2</sub>MQJ, and some ATP transporters have only a single ATPase site, while the second one is degenerated (Davidson and Sharma, 1997; Jones and George, 2013; Nikaido and Ames, 1999; Procko et al., 2009). The two NBDs can assume a closed conformation if tightly packed together, or an open conformation if more distant. ATP hydrolysis can take place only in the closed conformation; the release of ADP and phosphate destabilizes the NBD dimer, the RecA-like and  $\alpha$ -helical domains move apart, the NBD dimer dissociates, and the movement can be transmitted to the TMDs.

TMDs are more heterogeneous. In ABC exporters, however, TMDs have a common structural fold, based on the presence of a six transmembrane helix-based core (Fig. 2B), which considerably stretches out into the cytosol, where a short coupling helix protrudes from the TMD and fits in a groove of NBD between the RecA-like and  $\alpha$ -helical domains, containing the Q-loop, allowing the transduction of the ATP-dependent movement of NBD to TMD (Dawson and Locher, 2006; Hollenstein et al., 2007). The transmembrane helices of the two TMDs usually form a pore that can either be accessible from the cytoplasm (inward facing) or from outside the cell (outward facing) (Figs. 2 and 3): according to the alternating-access model, alternation between these conformations occurs during the catalytic cycle, to allow substrate binding and its transport across the membrane, against its chemical gradient (Ward et al., 2007).

Several catalytic mechanisms have been proposed for ABC transporters (Higgins and Linton, 2004; Jones and George, 2014; Linton and Higgins, 2007; Sauna et al., 2007; Senior et al., 1995). For eukaryotic ABC exporters, the catalytic cycle has the following steps: substrate binding to the inward face of TMDs, binding of two ATP molecules to NBDs, dimerization of the NBDs, conformational change of TMDs from inward facing to outward facing, ATP hydrolysis, release of substrate from the outward face of TMDs and of ADP and phosphate from NBDs and NBD dissociation (Wilkins, 2015). However, it is likely that not all ATP transporters function based on the very same mechanisms (Locher, 2016): lipid transporters as PglK and ABCA1 have been proposed to have only outwardly-facing conformations, and possibly a lateral access mechanism (Perez et al., 2015; Qian et al., 2017). The substrate-binding site is rather poorly defined in ABC exporters, and multiple and flexible sites can be present, therefore making them multidrug transporters and generating overlapping exporting function among them.

### *ABCB1* transporters and MDR

Enhanced efflux of chemotherapeutic drugs by at least 15 ABC exporters has been shown to mediate MDR in cancer cells (Fletcher et al., 2016; Li et al., 2016b; Szakacs et al., 2006). The most important human ABC transporter involved in drug disposition and in MDR is *ABCB1* (also known as MDR1, P-glycoprotein, P-gp), while an important role is recognized also for ABCG2 (Breast cancer resistance protein, BCRP) and for ABCC1 (Multidrug Resistance Protein 1, MRP1), ABC exporters with broad substrate and inhibitor specificity, and wide tissue and cellular distribution, especially in physiological epithelial/endothelial barriers, partially overlapping with those of *ABCB1* (Fletcher et al., 2016; Mao and Unadkat, 2015; Natarajan et al., 2012; Zhang et al., 2015).

### *ABCB1* (MDR1, P-glycoprotein, P-gp)

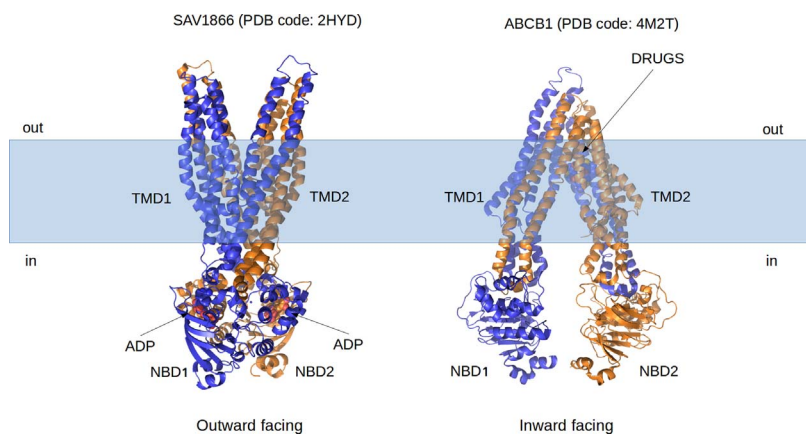
*ABCB1* has been discovered more than 40 years ago (Juliano and Ling, 1976). In humans, the *ABCB1* and *ABCB4* genes, originating from an endoduplication event, are located adjacent to each other on the long arm of chromosome 7 (7q21) and encode two similar proteins (78% identity) (Callen et al., 1987; Chin et al., 1989). In rodents, a further duplication gave rise to the genes *ABCB1a* and *ABCB1b*, with largely overlapping substrate specificities.

### *ABCB1* structure and function

*ABCB1* is expressed at low levels in most human and rodent tissues, while high expression levels are present in the apical surface of epithelial cells, such as intestine, liver bile ductule, kidney proximal tubules, pancreatic ductules, adrenal gland, placenta, testis (blood-testis barrier) and brain capillaries (blood-brain barrier), oriented towards the lumen or the blood (Chin et al., 1989; Cordon-Cardo et al., 1990; Cordon-Cardo et al., 1989; Fojo et al., 1987; Schinkel, 1999; Thiebaut et al., 1987).

To characterize the function of *ABCB1*, knockout mice were generated harboring a disruption of the *ABCB1a* gene, the *ABCB1b* gene, or both the *ABCB1a* and *ABCB1b* genes together (Schinkel et al., 1997; Schinkel et al., 1994). These three mouse strains were healthy and fertile, with no abnormalities in anatomy, lifespan and in many other parameters, with respect to wild type mice under normal conditions; however, they displayed drastic pharmacokinetic differences upon administration of drugs, with marked reduction of the intestinal, hepatobiliary and urinary excretion of drugs (Schinkel et al., 1997; Schinkel et al., 1994; Smit et al., 1998; Sparreboom et al., 1997; van Asperen et al., 1996; van Asperen et al., 1999). Altered pharmacokinetics and increased accumulation of paclitaxel, doxorubicin and vinblastine, i.e. some of the most important chemotherapeutic drugs, administered





against a number of cancers, was demonstrated in these mice (Sparreboom et al., 1997; van Asperen et al., 1996; van Asperen et al., 1999). In addition, ivermectin, loperamide, doxorubicin, digoxin, vinblastine, paclitaxel, erythromycin and many other drugs, which in wild type mice (and in humans) do not accumulate in the brain and are not neurotoxic, penetrate the blood-brain barrier and have serious neurotoxic effects in the CNS of *ABCB1*(-/-) mice (Schinkel et al., 1994; Schinkel et al., 1996; Schinkel et al., 1995; Schuetz et al., 1998; van Asperen et al., 1997).

Thus, both localization and characterization indicate an important role of *ABCB1* in the protection of the brain, the testis and of the fetus from toxic xenobiotics. *ABCB1* is responsible for the extrusion of xenobiotics and metabolites into the gut lumen, into the bile and urine, thus reducing their absorption, toxicity and bioavailability and hence making a major contribution to their ADME (absorption, distribution, metabolism and excretion). *ABCB1* possibly plays a role in the transport of endogenous molecules and metabolites (such as phospholipids, glycolipids, platelet-activating factors, amyloid  $\beta$ -peptides, and cytokines) and in exporting hormones such as aldosterone and progesterone, from the adrenal gland and the uterine epithelium (Sharom, 2008, 2011; Silva et al., 2015).

Several crystal structures of eukaryotic *ABCB1* proteins from mouse, *Cyanidioschyzon merolae* and *Caenorhabditis elegans* have been reported (Aller et al., 2009; Esser et al., 2017; Jin et al., 2012; Kodan et al., 2014; Li et al., 2014; Szcwzyk et al., 2015; Verhalen et al., 2017; Ward et al., 2013; Wen et al., 2013), and showed that the overall structure of *ABCB1* is similar to that of other ABC transporters (Fig. 3). Since *ABCB1* is expressed as one gene product containing both halves, similar but not identical, its structure is intrinsically asymmetric (Wen et al., 2013). Structures of mouse *ABCB1a* (87% identical to human *ABCB1*) in the apo-form, of mutant forms and in the presence of rationally designed ligands yielded insight on the “polyspecificity” of *ABCB1* in substrate interactions, on mechanism of ligand entry and on atomistic models of ATP-coupled transport (Fig. 4). All structures belong to a wide range of inward-facing conformations, with highly flexible TMDs and various distances between the two NBDs, which can determine opening and closing motion of the ABC exporter and thereby a number of possible binding sites due to the exposure of several flexible hydrophobic surfaces in the vicinity of the membrane (Esser et al., 2017; Szcwzyk et al., 2015; Verhalen et al., 2017; Ward et al., 2013). A recent work by McHaurab and colleagues used double electron–electron resonance and molecular dynamics simulations to model *ABCB1* in the outward-facing conformation and to model energy-dependent movement and substrate efflux (Fig. 4). In this model, most *ABCB1* molecules in the cell are inward-facing, with dissociated and fully ATP-bound NBDs (Fig. 4, step 1), ready to bind the substrate with its high-affinity substrate pocket exposed to the cytoplasmic leaflet of the membrane (Fig. 4, step 2); drug extrusion requires a two-stage hydrolysis (Fig. 4, steps 3 and 4), and substrate release outside the cell by outwardly-facing *ABCB1*, a

conformation with lower affinity for the substrate (Verhalen et al., 2017).

#### *ABCB1* expression in cancers and MDR

In various cancer cell lines of distinct tissue lineage, *ABCB1* expression increases upon repeated drug treatment cycles with various chemotherapeutic drugs, rendering them MDR (Juliano and Ling, 1976; Ueda et al., 1987a; Assaraf et al., 1989a, 1989b). In addition, many early studies showed high overexpression of *ABCB1* in colon, kidney, ovary, adrenocortical and hepatocellular tumors (Bourhis et al., 1989; Fojo et al., 1987; Goldstein et al., 1989; Pirkner et al., 1989). Direct association between *ABCB1* expression levels, drug resistance and poor prognosis have been found in acute myelogenous leukemia (AML) (Broxterman et al., 1999; Dorr et al., 2001; Grogan et al., 1993; Han et al., 2000; Leith et al., 1999; Michieli et al., 1999; van der Kolk et al., 2000; Zhou et al., 1995), breast cancer (Burger et al., 2003; Dexter

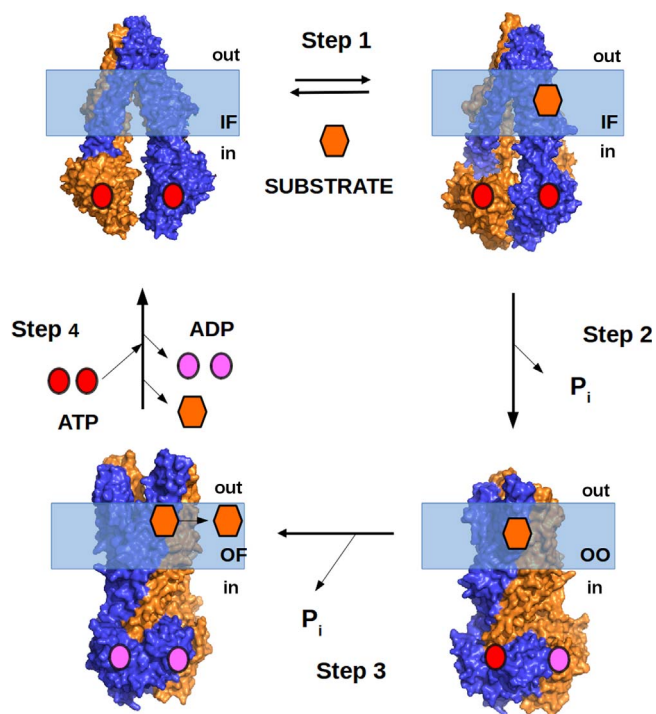


Fig. 4. Mechanism of action of *ABCB1*. Top-left: inward-facing (IF), ATP-bound *ABCB1* with non-dimerized NBDs; top-right: upon substrate binding, NBDs dimerize; bottom-right: hydrolysis of the first ATP occurs, and a doubly occluded (OO) transition state is formed; bottom-left: after hydrolysis of the second ATP, an outward-facing (OF) transition state is formed, and release of the substrate outside the cell occurs (Verhalen et al., 2017).

et al., 1998; Kao et al., 2001; Nooter et al., 1997; Sun et al., 2000; Trock et al., 1997; Vecchio et al., 1997), osteosarcoma (Chan et al., 1997), bladder cancer (Clifford et al., 1996; Nakagawa et al., 1997; Park et al., 1994; Tada et al., 2002), ovarian cancer (van der Zee et al., 1995), central nervous system (Abe et al., 1998; Perri et al., 2001) and other tumors and diseases.

In the Guidance Compliance Regulatory Information for the evaluation of drug interactions (<https://www.fda.gov/downloads/Drugs/GuidanceComplianceRegulatoryInformation/Guidances/ucm292362.pdf>), the US Food and Drug Administration (FDA) recommends that all investigational drugs should be evaluated *in vitro* to determine whether or not they are transport substrates of *ABCB1* (P-glycoprotein) or *ABCG2* (BCRP); the International Transporter Consortium recommends *in vitro* analysis of interaction with *ABCB1* as a major bottleneck for filing a new drug application (International Transporter et al., 2010).

#### *ABCB1 mutations and polymorphism*

In the last years, a number of mutations and polymorphisms in the human *ABCB1* gene have been described, although sometimes with conflicting results (Schwab et al., 2003; Wolking et al., 2015). The NCBI dbSNP single nucleotide polymorphisms database currently (September 11th, 2017) lists 24289 nucleotide variants, including 1563 coding sequence variants (639 missense and 924 synonymous variants). Among the identified single nucleotide polymorphisms (SNPs), the dbSNP database counts only 1 pathogenic SNP, i.e. c.554G > T, yielding the G185V mutation (Choi et al., 1988; Safa et al., 1990). In addition, at least 14 SNPs, occurring only at low allele frequencies of <0.01, are reported to be associated with alterations in *ABCB1* functions (Wolf et al., 2011), concerning pharmacokinetics, treatment response and drug-related toxicity; the analysis of the literature show that no conclusive results are available (Wolking et al., 2015).

#### *Epigenetic regulation of ABCB1 expression in drug response*

Deregulation of epigenetic programs, in terms of DNA methylation and post-transcriptional regulation of histone proteins, cooperates with genetic alterations towards the establishment and progression of cancer as well as the development of the classical MDR phenotype mediated by *ABCB1* (Baker et al., 2005; Chen et al., 2005; Scotto, 2003). The binding of specific transcription factors to their DNA-response elements located in 'distal' and 'proximal' promoter regions of the *ABCB1* gene (Ueda et al., 1987b), and the methylation/demethylation status of this genomic locus, determine the repression or transactivation of *ABCB1* expression, associated with survival and treatment response (Arrigoni et al., 2016; Dejeux et al., 2010; Mencialha et al., 2013; Reed et al., 2010). In AML for example, an inverse correlation between methylation and *ABCB1* expression in clinical samples has been described; the hypomethylated status of *ABCB1* promoter region was proposed as a necessary condition for *ABCB1* gene overexpression and for the establishment of P-glycoprotein-mediated MDR in AML patients (Nakayama et al., 1998). In bladder cancer as well, the degree of methylation in the *ABCB1* promoter region appears to be closely associated with *ABCB1* gene expression and the emergence of the MDR phenotype (Tada et al., 2000). In breast cancer, the acquisition of drug resistance appears to be related to the methylation of the *ABCB1* downstream promoter accompanied by a regional genomic amplification of a locus in chromosome 7 containing the *ABCB1* gene and its *ABCB4* neighbor gene (Reed et al., 2008).

Recently, also the histone methylation and acetylation, occurring on lysine residues within histone tails, are emerging as relevant players for the epigenetic regulation of *ABCB1* gene expression and chemotherapy drug response (Henrique et al., 2013). Huo et al., evidenced that transcriptional activation of *ABCB1* gene expression is accompanied by increased methylation on lysine 4 of histone H3 (H3K4), and that the histone methyltransferase MLL1 is involved in this regulation. In this

respect, knockdown of MLL1 decreased the constitutive expression of *ABCB1*, increased cellular retention of *ABCB1* substrates, and sensitized cancer cells to chemotherapeutic agents (Huo et al., 2010). An induction of H3K4 methylation within the coding regions of the *ABCB1* gene was also evidenced after treatment with the histone deacetylase (HDAC) inhibitor Trichostatin A (TSA), resulting in upregulation of *ABCB1* (Baker et al., 2005; Jin and Scotto, 1998). Interestingly, it was also shown that TSA treatment induced an increase in *ABCB1* expression in drug-sensitive small cell lung carcinoma (SCLC) cells, but strongly decreased its expression in drug-resistant cells through a transcriptional mechanism, independently from promoter methylation (El-Khoury et al., 2007). Moreover, in colon and pancreatic cancer cell lines, it was demonstrated that the increase in *ABCB1* mRNA expression observed after TSA treatment is not associated with an active P-gp protein expression, suggesting that well tolerated HDAC inhibitors may represent a potential therapeutic avenue to potentiate the effects of anti-tumor drugs that are P-glycoprotein substrates (Balaguer et al., 2012). In T-cell leukemia, the transcriptional control of *ABCB1* expression is achieved by two molecular mechanisms: when densely methylated, *ABCB1* is transcriptionally silent via a mechanism that is TSA independent. TSA induced significant acetylation of histones H3 and H4 but did not activate transcription, whereas 5-azacytidine, inducing DNA demethylation, lead to partial relief of transcriptional repression. *ABCB1* expression was significantly increased following the combination of 5-azacytidine and TSA treatments suggesting that, upon demethylation, activation of *ABCB1* is mediated by HDAC (El-Osta et al., 2002). Of note, the use of depsipeptide, an HDAC inhibitor, in combination with retinoic acid (RA) treatment, in Acute Promyelocytic Leukemia (APL) cells, prior to doxorubicin treatment, prevents doxorubicin-induced apoptosis in NB4 APL cells, by inducing the *ABCB1* gene and *ABCB1* expression, partially through CCAAT box-associated histone acetylation (Tabe et al., 2006). On the contrary, combined treatment of depsipeptide and RA following doxorubicin treatment, lead to enhanced doxorubicin-induced apoptosis. These results underline the critical importance of modulation of *ABCB1* expression by the use of epigenetics modulating drugs, and indicate that this is a critical point to take into consideration for the future design of clinical trials that combine epigenetics modulators and chemotherapeutic agents.

#### *Post-transcriptional regulation of ABCB1 expression by microRNAs in drug response*

miRNAs are small ( $\approx 22$  nucleotides long) noncoding RNAs which are evolutionary conserved and play a key role in the regulation of gene expression; miRNAs are significantly deregulated in cancer, and each cancer phenotype is defined and characterized by a unique miRNA signature, highlighting miRNAs as relevant molecules for cancer diagnostics and possible therapeutic interventions (Blandino et al., 2014). miRNAs can act by targeting a spectrum of distinct players, involved in the establishment of cancer MDR (Zhang and Wang, 2017). Of note, since many drugs need the expression of specific genes to exert their antineoplastic activity, miRNAs which affect the post-transcriptional regulation of pharmacogenomics-related genes, such as those responsible for drug metabolism or transport as well as those directly targeted by the drugs, are also emerging as potent regulators of drug efficacy (Rukov and Shomron, 2011). Several miRNAs are involved in different regulatory pathways that confer chemoresistance to cancer cells, as the ID4-miR-9\*-SOX2-ABCC3/ABCC6 pathway which imparts stemness potential and chemoresistance in glioma cells (Jeon et al., 2011), and the miR27b-CCNG1-p53-miR-508-5p axis which regulates MDR in gastric cancer (Shang et al., 2016).

The identification of the expression levels of miRNAs targeting genes involved in the binding or in the transport of chemotherapeutic drugs may be extremely useful to identify the possible acquisition of drug resistance during cancer treatment (Yamamoto et al., 2011). For example, Pan et al. found that miR-328, which targets the *ABCG2* gene,

encoding for a MDR efflux transporter of the ABC superfamily, may affect the transport of the anticancer drug mitoxantrone (MX) across the plasma membrane and the sensitivity of MCF-7 breast cancer cells to this anthracycline drug (Pan et al., 2009). Also miR-345 and miR-7, targeting ABCB1 gene, which encodes for the human multidrug resistance-associated protein 1 (MRP1), were associated with acquired resistance of MCF-7 breast cancer cells to cisplatin (Pogribny et al., 2010).

Moreover, different miRNAs were described with a functional role in the regulation of the expression and activity of *ABCB1*, the founding member of the ABC superfamily of multidrug efflux transporters that is a dominant pump responsible for MDR (Garofalo and Croce, 2013; Li et al., 2016b; Livney and Assaraf, 2013; Wijdeven et al., 2016). As described above, the plasma membrane overexpression of *ABCB1* in cancer cells leads to an increased drug efflux and impairs the achievement of an intracellular cytotoxic drug concentration. Of note, various miRNAs targeting this ABC superfamily member were described to be involved in the regulation of drug efflux activity of this transporter as well as in drug response (Geretto et al., 2017; Lopes-Rodrigues et al., 2014). It has been shown that 3'-UTR variants of *ABCB1* with shortened length may be synthesized during the acquisition of drug resistance and this may lead to the loss of miRNA binding sites and hence alleviating this miRNA-based repression of *ABCB1* expression (Bruhn et al., 2016). However, altered levels of miRNAs affecting *ABCB1* expression were also recently described. For example, in human intestinal epithelial cells miR-145 negatively regulates the expression and function of *ABCB1* through direct interaction with its mRNA 3'-UTR (Ikemura et al., 2013), while in ovarian cancer the development of cisplatin resistance was related to the up-regulation of miR-130a, resulting in *ABCB1*-mediated MDR (Li et al., 2015; Yang et al., 2012). By targeting *ABCB1*, miR-873 and miR-595 also contribute to the regulation of drug resistance and the activity of cisplatin in inhibiting tumor growth in ovarian cancer (Tian et al., 2016; Wu et al., 2016). Interestingly, miR-27a and miR-451 induce the activation of *ABCB1* expression and their modulation with antagonirs enhances the sensitivity of ovarian cancer cells via enhanced intracellular accumulation of doxorubicin (Zhu et al., 2008). In contrast, in colorectal cancer, restoration of miR-451 decreases *ABCB1* expression and results in sensitization to irinotecan (Bitarte et al., 2011); whereas, up-regulation of miR-27a in hepatocellular carcinoma cells decreased the *ABCB1* expression via FZD7/ $\beta$ -catenin signaling pathway, enhancing the sensitivity of these cells to 5-fluorouracil resulting in 5-fluorouracil-induced apoptosis (Chen et al., 2013b). Moreover, in breast cancer cells as well, miR-451 was reported to mediate down-regulation of *ABCB1* gene expression, resulting in increased sensitivity of tMCF-7 breast cancer cells to doxorubicin (Kovalchuk et al., 2008). In hepatocellular carcinoma cells, a novel role for miR-491-3p was identified resulting in *ABCB1*-mediated MDR, suggesting the potential application of miR-491-3p as a therapeutic strategy for repression of P-glycoprotein-dependent MDR tumors (Zhao et al., 2017). In gastric cancer, the overexpression of miR-508-5p, targeting the 3'-UTR of *ABCB1*, was sufficient to reverse MDR in cancer cells to multiple chemotherapeutic drugs, both *in vitro* and *in vivo*, and, interestingly, miR-508-5p might act as a prognostic factor for overall survival in this tumor (Shang et al., 2014). In neuroblastoma cells, it was shown that epigenetic silencing of miR-137 in doxorubicin-resistant cells contributes to overexpression of the constitutive androstane receptor (CAR) and, in turn, *ABCB1*, and that treatment with the 5-azacytidine, a methylation inhibitor, increased miR-137 expression and sensitized doxorubicin-resistant neuroblastoma cells to this anthracycline (Takwi et al., 2014). Moreover, the hyper-methylation of the promoter region of miR-129-5p is recently gaining relevance in the development of drug resistance in gastric cancer cells and this miRNA, by targeting MDR-related ABC transporters as *ABCB1*, was proposed as a potential therapeutic target to enhance drug sensitivity of gastric cancers (Wu et al., 2014). In gastric cancer, it was also evidenced that miR-129 was able to reverse cisplatin-resistance through repression of

*ABCB1* gene expression and activation of the caspase-mediated intrinsic apoptotic pathway (Lu et al., 2017). Of note, the nanoparticles-mediated co-delivery of miR-129-5p and doxorubicin significantly increased miR-129-5p expression in doxorubicin-resistant MCF-7 breast cancer cells, which effectively overcame MDR achieving a 100-fold increase in *ABCB1* gene expression, thereby increasing intracellular drug accumulation and cytotoxicity in this tumor cell line model (Yi et al., 2016). This synergistic therapeutic option was also recently reported for miR-375 in hepatocellular carcinoma (Fan et al., 2017). Moreover, in breast cancer it was further reported that the overexpression of miR-298 as well results in down-regulation of *ABCB1* gene expression, increasing nuclear accumulation of doxorubicin and cytotoxicity in doxorubicin-resistant cells (Bao et al., 2012). In mouse leukemia cells it was reported that the restored expression of miR-381 or miR-495 in doxorubicin-resistant K562 cells correlates with a decreased *ABCB1* gene expression and with an increased drug uptake by these cells (Xu et al., 2013). More recently, in the same cellular system, restoration of miR-9 expression was also able to reverse cancer cell drug resistance *in vitro* and sensitized tumors to chemotherapy *in vivo* by targeted repression of *ABCB1* gene expression (Li et al., 2017). In addition, in gallbladder cancer, miR-218-5p enhanced sensitivity of gemcitabine by abolishing PRKCE-induced up-regulation of *ABCB1* (Wang et al., 2017). Table 1 shows miRNAs acting on *ABCB1* in MDR (vs. non-MDR) tumors.

#### Transport substrates of *ABCB1*

*ABCB1* is able to bind and extrude out of cells a plethora of chemically, structurally and pharmaceutically distinct compounds including drugs used as anti-cancer chemotherapeutics, inflammation, immunosuppression, infection, allergy, hypertension, and arrhythmia (Table 2); more than one thousand compounds have been described as *ABCB1* substrates (Didziapetris et al., 2003). The high flexibility, fuzziness and complexity of drug substrate binding sites of *ABCB1* (Esser et al., 2017; Szewczyk et al., 2015; Verhalen et al., 2017; Ward et al., 2013) explain the wide number of drug classes of these *ABCB1* substrates, which include small molecules, as cations, amino acids and carbohydrates, larger molecules, as chemotherapeutic drugs, ionophores, fluorescent dyes and steroids and larger molecules such as peptides, polysaccharides and proteins (Borgnia et al., 1996; Didziapetris et al., 2003; Eytan et al., 1994; Sharom, 2011; Silva et al., 2015; Zhou, 2008). Many of these substrates are relatively hydrophobic and weakly amphipathic, typically contain aromatic rings and a positively charged nitrogen, and often their binding occurs with  $K_D$  values of 10  $\mu$ M–1 mM (Morrissey et al., 2012). This substrate “poly-specificity” is crucial for *ABCB1* to exert its role as a xenobiotics efflux pump, able to protect cells from a high number of cytotoxicants. In addition, substrates binding to *ABCB1* partially overlap to those bound by other ABC transporters, such as ABCB1, ABCB2 and ABCG2, and by cytochrome P450 3A enzymes, in particular CYP3A4: a coordinate interplay between these proteins can operate to protect cells as a barrier in the bioavailability of drugs, especially when orally administered (Casorbi, 2006; Cummins et al., 2002; Kim et al., 1999).

#### *ABCB1* transport inhibitors

The induction of *ABCB1* upon exposure to cancer chemotherapeutics is an important cause of MDR; conversely, inhibition of *ABCB1* transport is one of the most studied clinical strategies to counteract MDR, with the aim to interfere with chemotherapeutic drug efflux, thereby increasing their accumulation and hence their cytotoxic effect in cancer cells. Mechanistically, *ABCB1* inhibitors may exert their activity by binding and blocking the substrate binding site of the transporter, either in competitive, non-competitive or allosteric fashion, by interfering with ATP hydrolysis, by binding the transporter in site independent of the drug binding site which allosterically alters the intact structure and function of *ABCB1*, or by altering the integrity and functionality of cell

**Table 1**  
miRNA acting on *ABCB1* in MDR (vs. non-MDR) cancers.

miRNA	Direct expression	<i>ABCB1</i> target	Effect on		Cancer
			expression	drug resistance	
miR-9	↓	<i>ABCB1</i>	↑	↑ Adriamycin	MDR chronic myelogenous leukemia vs. non-MDR
miR-27a	↑	?	↑	↑ Doxorubicin, vinblastine	MDR ovarian cancer vs. non-MDR
miR-129	↓	FZD7/β-catenin	↑	↑ 5-fluorouracil	MDR hepatocellular carcinoma vs. non-MDR
miR-129-5p	↓	<i>ABCB1</i>	↑	↑ Cisplatin	MDR gastric cancer vs. non-MDR
	↓	<i>ABCB1</i>	↑	↑ Vincristine, 5-fluorouracil, cisplatin	MDR gastric cancer vs. non-MDR
	↓	<i>ABCB1</i> , CDK6	↑	↑ Doxorubicin	MDR breast cancer vs. non-MDR
miR-130a	↓	<i>ABCB1</i>	↑	↑ Cisplatin	MDR ovarian cancer vs. non-MDR
miR-137	↓	CAR	↑	↑ Doxorubicin	MDR neuroblastoma vs. non-MDR
miR-145	↓	<i>ABCB1</i>	↑		Intestinal epithelial cells vs. ischemia-reperfusion cells
miR-218-5p	↓	PRKCE	↑	↑ Gemcitabine	Gallbladder cancer vs. non cancer
miR-298	↓	<i>ABCB1</i>	↑	↑ Doxorubicin	MDR breast cancer vs. non-MDR
miR-375	↓	<i>ABCB1</i> , AEG1, YAP1, ATG7	↑	↑ Doxorubicin	MDR hepatocellular carcinoma vs. non-MDR
miR-381	↓	<i>ABCB1</i>	↑	↑ Doxorubicin	MDR chronic myelogenous leukemia vs. non-MDR
miR-451	↑	?	↑	↑ Doxorubicin	MDR ovarian cancer vs. non-MDR
	↓	COX2/Wnt	↑	↑ Irinotecan	MDR colonspheres vs. non-MDR
	↓	<i>ABCB1</i>	↑	↑ Doxorubicin	MDR breast cancer vs. non-MDR
miR-491-3p	↓	<i>ABCB1</i> , Sp3	↑	↑ Doxorubicin, vinblastine	MDR hepatocellular carcinoma vs. non-MDR
miR-495	↓	<i>ABCB1</i>	↑	↑ Doxorubicin	MDR chronic myelogenous leukemia vs. non-MDR
miR-508-5p	↓	<i>ABCB1</i> , ZNRD1	↑	↑ Adriamycin, Vincristine, 5-fluorouracil, cisplatin	MDR gastric cancer vs. non-MDR
miR-595	↓	<i>ABCB1</i>	↑	↑ Cisplatin	MDR ovarian cancer vs. non-MDR
miR-873	↓	<i>ABCB1</i>	↑	↑ Cisplatin	MDR ovarian cancer vs. non-MDR

**Table 2**  
Classes of *ABCB1* substrates.  
Data from: Didziapetris et al. (2003), Sharom (2011), Silva et al. (2015), Zhou (2008).

Classes of <i>ABCB1</i> substrates	
Substrate class	Examples
Anti-arrhythmics	Digoxin, quinidine, verapamil.
Antibiotics (antimicrobial drugs)	Clarithromycin, doxycycline, erythromycin, gramicidin A, grepafloxacin, itraconazole, ketoconazole, levofloxacin, rifampicin, sparfloxacin, tetracycline, valinomycin.
Anticancer chemotherapeutic drugs	Alkylating agents: chlorambucil, cisplatin Antibiotics: actinomycines (actinomycin D), anthracyclines (daunorubicin, doxorubicin), mitoxantrone, mytomicin C. Antimetabolites: cytarabine, 5-fluorouracil, hydroxyurea, methotrexate. Camptothecins: irinotecan, topotecan. Epidermal growth factor receptor inhibitors: erlotinib, gefitinib Epidodophyllotoxins: etoposide, teniposide Taxanes: docetaxel, paclitaxel. Tyrosine kinase inhibitors: imatinib, nilotinib Vinca alkaloids: vinblastine, vincristine Others: bisantrene, tamoxifen.
Anticonvulsants and anti-epileptics	Carbamazepine, phenobarbital, phenytoin, topiramate.
Antidepressants	Amitriptyline, doxepin, nortriptyline.
Anti-diarrheal drugs	Loperamide (opioid), octreotide
Antiemetics	Domperidone, ondansetron.
Antigout drugs	Colchicine
Antihelmintics	Ivermectin
Antihistamine	Fexofenadine, terfenadine.
Anti-HIV	Amprenavir, indinavir, nelfinavir, ritonavir, saquinavir.
Antihypertensives	Celiprolol, debrisoquine, losartan, prazosin, reserpine, talinolol.
Calcium channel blockers	Azidopine, diltiazem, nifedipine, nifedipine, verapamil.
Calmodulin antagonists	trans-flupentixol, trifluoperazine.
Cardiac glycosides	Digitoxin, digoxin.
Cyclic peptides	Beauvericin, valspodar (PSC-833).
Fluorescent dyes	Calcein AM, Hoechst 33342, Rhodamine 123.
Histamine H <sub>2</sub> -receptor antagonists	Cimetidine, ranitidine
Hypocholesterolizing drugs	Lovastatin, simvastatin
Immunosuppressive agents	Cyclosporin A, sirolimus, tacrolimus, valspodar (PSC-833)
Linear peptides	ALLN (Acetyl-leucyl-leucyl-norleucine), leupeptin, pepstatin A
Neuromuscular blocking agents	Vecuronium
Natural products	Curcumin, Flavonoids.
Neuroleptics	Chlorpromazine, phenothiazine
Pesticides	Endosulfan, methylparathion, paraquat.
Steroid hormones	Aldosterone, corticosterone, cortisol, dexamethasone, estradiol, methylprednisolone.
Others	Amino acids, bilirubin, carbohydrates, cations, polysaccharides



**Table 3**Classes of *ABCB1* inhibitors.Data from [Palmeira et al. \(2012a\)](#), [Silva et al. \(2015\)](#).

Classes of <i>ABCB1</i> inhibitors	
Inhibitor class	Examples
<b>First generation</b>	
Analgesics	Meperidine, pentazocine
Anesthetic drugs	Benzyl alcohol, chloroform, diethyl ether, propofol
Antibiotics	Azithromycin, bafilomycin, brefeldin A, cefoperazone, ceftriaxone, clarithromycin, erythromycin, nigericin, salinomycin, valinomycin
Anticancer drugs	Antiandrogen; bicalutamide, mitotane Estrogen receptor antagonists: tamoxifen Farnesyl transferase inhibitors: lonafarnib, tipifarnib Tyrosine kinase inhibitors: erlotinib, gefitinib, lapatinib
Antifungal drugs	Aureobasidin A, dihydrotychantonol A, econazole, itraconazole, ketoconazole
Antihistaminic drugs	Astemizole, azelastine, benzquinamide, terfenadine, tesmilifene
Anti-inflammatory drugs	Zomepirac, indomethacin, SC236, curcumin, ibuprofen, NS-398
Antidepressants	Amoxapine, loxapine, sertraline, paroxetine, fluoxetine
Antiprotozoal drugs	Hycanthone, metronidazole, monensin, quinine
Antiviral drugs	Concanamycin A, nelfinavir, ritonavir, saquinavir
Anxiolytics	Midazolam
Cardiac drugs	Antiarrhythmics: amiodarone, propafenone, quinidine Calcium channel blockers: amiodarone, bepridil, deverapamil, diltiazem, emopamil, felodipine, isradipine, lomerizine, mibefradil, nicardipine, nifedipine, nifedipine, nimodipine, nitrendipine, propafenone, quinidine, tetrandrine, verapamil. Antiplatelet drug: dipyridamole Antihypertensives: carvedilol, doxazosin, prazosin, reserpine.
CNS stimulators	Amoxapine, caffeine, cotinine, loxapine, nicotine, pentoxifylline, sertraline
CNS depressants	Chlorpromazine, trans-flupentixol, haloperidol, perospirone, perphenazine, prochlorpromazine, trifluoperazine
Cholesterol-lowering drugs	Atorvastatin,
Immunosuppressant drugs	Cyclosporin A, tacrolimus, sirolimus
Phosphodiesterase inhibitors	Vardenafil
Steroid hormones	Cortisol, medroxyprogesterone, methylprednisolone, mifepristone, progesterone, SB4723, SB4769, tirilazad, U-74389F
Others	Bromocriptine, disulfiram, methadone, tetrabenazine
<b>Second generation</b>	
	BIBW22BS, biricodar (VX 710), CGP 42700, cinchonine, dexverapamil, dextniguldipine, dofequidar (MS-209), hydro-cinchonine, KR-30031, MM36, PAK-104P, quinine homodimer Q2, RO44-5912, S9788, SB-RA-31012 (tRA96023), stipiamide homodimer, timcodar (VX-853), toremifene, valsopodar (PSC 833), WK-X-34
<b>Third generation</b>	
	Annamycin, CBT-1, DP7, elacridar (GF120918), laniquidar (R101933), mitotane, ontogen (OC144093), PGP-4008, tariquidar (XR9576), zosuquidar (LY335979),
<b>Fourth generation</b>	
Natural products	Alkaloids: ellipticine, pervilleine F Cannabinoids: cannabidiol Coumarins: cnidiadin, conferone, DCK, praeruptorin A, rivulobirin A Diterpenes: euphodendroidin D, jolkinol B, pepluanin A, portlanquinol Flavonoids: baicalein heptamethoxyflavone, nobiletin, quercetin, sinensetin, tangeretin Ginsenosides: 20S-ginsenoside Lignans: nirtetralin, schisandrin A, silibinin Polyenes: pentadeca-(8,13)-dien-11-yn-2-one Sesquiterpenes: dihydro- $\beta$ -agarofuransesquiterpenes Taccalonolides: taccalonolides A Triterpenes: oleanolic acid, siphonolol A, siphonolone E, uvaol
Peptidomimetics	Peptide 15, reversin 121, reversin 205, XR9051
Surfactants and Lipids	Cremophor EL, Nonidet P40 Pluronic P85, poly(ethylene glycol)-300 (PEG-300), Tween-20, Triton X-100,
Dual ligands	Dual inhibitors of <i>ABCB1</i> and tumor cell growth (e.g.: aminated thioxanthones)

membrane lipids, or by altering plasma membrane fluidity ([Drori et al., 1995](#); [Shapiro and Ling, 1997](#); [Silva et al., 2015](#); [Varma et al., 2003](#)).

Classification into four generations of *ABCB1* inhibitors according to their potency, selectivity and drug–drug interaction potential ([Palmeira et al., 2012a](#)), rather than to their chronology of discovery and characterization, is useful ([Table 3](#)). The first generation of *ABCB1* transport inhibitors comprises classical inhibitors such as the founding member verapamil as well as cyclosporine A and all compounds which were previously described as having other therapeutic applications. The first identified *ABCB1* transport inhibitor has been the calcium channel blocker verapamil, able to increase the intracellular accumulation of chemotherapeutic drugs as doxorubicin, vincristine and vinblastine by competing with these drugs ([Miller et al., 1991](#); [Tsuruo et al., 1981](#)). Verapamil, as many other of first-generation *ABCB1* substrate, and presumably acts by competing for efflux with other *ABCB1* substrates ([Varma et al., 2003](#); [Yusa and Tsuruo, 1989](#)). Verapamil sensitizes cancer cells to several anticancer drugs, such as doxorubicin, increasing

their cytotoxic activity ([Futscher et al., 1996](#)); many clinical studies on the use of verapamil, alone and in combination regimens, against various cancers and other diseases have been carried out, and some are still ongoing (<https://clinicaltrials.gov/>). A number of “already-in-clinical-use” *ABCB1* inhibitors have been discovered, belonging to several classes, such as calcium channels blockers (e.g., verapamil), anti-malarial drugs (e.g., quinine), immunosuppressants (e.g., cyclosporine A), anesthetics (e.g., chloroform), antibiotics (e.g., erythromycin, and ceftriaxone), antifungal drugs (e.g., ketoconazole), antivirals (e.g., nelfinavir, and saquinavir), CNS stimulators or anti-depressants (e.g., caffeine, nicotine, and chlorpromazine), as well as steroids (e.g., cortisol, and progesterone). In addition, some *ABCB1* transport inhibitors are themselves anticancer drugs, such as tamoxifen, and tyrosine kinase inhibitors as erlotinib and lapatinib ([Table 3](#)) ([Palmeira et al., 2012a](#); [Sharom, 2011](#); [Silva et al., 2015](#); [Zhou, 2008](#)). Often, the clinical use of these *ABCB1* inhibitors is hampered by their intrinsic toxicity, because high concentrations of these drugs are needed to inhibit *ABCB1* efflux

activity, given their low affinity for *ABCB1*. Further, since many first-generation *ABCB1* inhibitors are also substrates of other transporters and/or enzymes, pharmacokinetic interactions are complex and sometimes unpredictable (Ambudkar et al., 1999).

Second-generation *ABCB1* transport inhibitors were designed from compounds with another recognized activity, but which were subjected to structural modifications in order to decrease their principal therapeutic activity and to enhance *ABCB1* inhibitory activity, in order to achieve decreased toxicity and higher potency (Kathawala et al., 2015; Palmeira et al., 2012a; Silva et al., 2015). These compounds include derivatives of anticancer, cardiovascular and immunosuppressive agents (Table 2). For example, valsopodar (PSC-833) is a non-immunosuppressive derivative of cyclosporine A; although it is 5- to 20-fold more potent than its parent compound, and also exhibited promising pre-clinical results, its administration in combination with anticancer drugs inhibits the metabolism and extrusion of such cytotoxic agents, thus leading to unacceptable toxicity which requires chemotherapy dose reduction (Advani et al., 2001; Advani et al., 2005; Bates et al., 2001; Bauer et al., 2005; Chico et al., 2001). In addition, many of these compounds inhibit cytochrome P450 enzymes, resulting in unpredictable pharmacokinetic interactions.

Third-generation *ABCB1* inhibitors (Table 3) were developed by using quantitative structure-activity relationships (QSAR) and combinatorial chemistry, which specifically and potently inhibit the ABC exporter at nanomolar concentrations, without affecting cytochrome P450 enzymes (Coley, 2010; Dantzig et al., 2001; Palmeira et al., 2012a; Silva et al., 2015). Often these compounds inhibit *ABCB1* based on a non-competitive mechanism; the most promising ones are possibly tariquidar, elacridar and zosuquidar (Akhtar et al., 2011; Dantzig et al., 2001; Fox and Bates, 2007; Hyafil et al., 1993; Weidner et al., 2016). Zosuquidar, a difluoro-cyclopropyl dibenzosuberane derivative, is very potent, is effective at nanomolar concentrations and has no interaction with cytochrome P450 and with other drug efflux pumps (Bihorel et al., 2007; Dantzig et al., 2001; Dantzig et al., 1999; Green et al., 2001; Kemper et al., 2004). However, third-generation *ABCB1* inhibitors have encountered unexpected toxicity problems, and clinical trials have yielded modest results (Pusztai et al., 2005; Ruff et al., 2009); for example, a phase III trial for the treatment of AML and myelodysplastic syndrome (MDS) using zosuquidar did not meet its primary endpoint (Cripe et al., 2010).

Fourth-generation *ABCB1* inhibitors (Table 3) include various classes of compounds, i.e. natural compounds, surfactants and lipids, peptides and molecules with dual activity (Palmeira et al., 2012a). Hundreds of natural compounds, obtained from several natural sources, and belonging to many chemical families, such as alkaloids, flavonoids, coumarins, resins, saponins and terpenoids (Dewanjee et al., 2017), have been described thus far as acting on ABC transporters, thereby offering potential for semi-synthetic modification to produce new scaffolds which could serve as valuable tools to evade the systemic toxicities shown by synthetic counterparts. However, reports in the literature are sometimes contradictory: for example quercetin has been reported to have opposite effects on *ABCB1* and MDR (Critchfield et al., 1994; Phang et al., 1993; Rodgers and Grant, 1998) perhaps also due to its inhibition of Cytochrome P-450 enzymes.

Surfactants have complex relationship with *ABCB1*-dependent drug efflux and MDR; they alter membrane fluidity, perturbing lipid bilayers, and drug-membrane partitioning; they also interact with *ABCB1*, inflict modifications in secondary and tertiary enzyme structure, inhibit ABC transporter activity and increase cellular drug accumulation (Regev et al., 2007; Sharom, 2014; Shieh et al., 2011; Shukla et al., 2017).

Some peptides, such as reversins, are able to potently inhibit *ABCB1* in a non-competitive manner (Arnaud et al., 2010); they have been recently used as conjugate copolymers with anthracyclines to overcome MDR (Koziołova et al., 2016; Sivak et al., 2017).

Dual ligands, able to simultaneously modulate *ABCB1* and other enzymes, have been recently described. Apart from their ability to

inhibit other ABC transporters shown by several inhibitors, dual ligands include aminated thioxanthenes, targeting *ABCB1* and DNA-intercalating, and verapamil-like compounds, targeting *ABCB1* and NO synthase (Colabufo et al., 2011; Namanja-Magliano et al., 2017; Palmeira et al., 2012b).

#### Other strategies to overcome *ABCB1*-dependent MDR

Collateral sensitivity (CS) is the ability of compounds to selectively kill MDR cells over parental cells from which they were derived (Pluchino et al., 2012). CS agents are MDR-selective compounds that can act with different mechanisms; one of such mechanisms is apoptosis via reactive oxygen species (ROS) overproduction following futile ATP hydrolysis cycles in cells with high-*ABCB1* levels, induced by iron-chelating compounds such as Dp44mT or N-(2-hydroxy acetophenone) glycinate (Ganguly et al., 2010; Jansson et al., 2010); Dp44mT also acts by hijacking lysosomal *ABCB1* (Jansson et al., 2015; Seebacher et al., 2016). Other CS-inducing drugs exploit increased sensitivity to bioenergy states: treatment with 2-deoxy-D-glucose, a hexokinase II inhibitor, induces apoptosis in MDR cells, that rely on glycolysis for ATP generation due to the Warburg effect resulting from hypoxia in tumor microenvironment (Bell et al., 1998; Kaplan et al., 1991).

Another strategy to overcome MDR in *ABCB1*-overexpressing cells is the use of nanoparticle delivery of anticancer drugs. Nanoparticles that are taken up by the cell via endocytosis often bypass and evade the ABC transporters responsible for efflux of cytotoxic drugs once released into the cytoplasm (Bar-Zeev et al., 2016; Bar-Zeev et al., 2017; Cerqueira et al., 2015; Fracasso et al., 2016; Huang et al., 2011; Livney and Assaraf, 2013; Shapira et al., 2011; Song et al., 2010; Yuan et al., 2016).

#### Drug inducers of *ABCB1* expression

Cells exposed to a P-glycoprotein cytotoxic drug substrate either upon stepwise selection or single dose exposure, frequently display the MDR phenotype often due to high overexpression of *ABCB1* levels, frequently due to gene amplification or increased transcription (Assaraf and Borgnia, 1994; Assaraf et al., 1989a, 1989b; Borgnia et al., 1996; Fojo et al., 1985; Roninson, 1992; Roninson et al., 1986; Scotto et al., 1986; Shen et al., 1986).

Many molecules (Table 4), and in particular many chemotherapeutic drugs, induce *ABCB1* overexpression via multiple mechanisms, involving genomic amplification, upregulation of transcription, mRNA splicing, transport and stability. Constitutive *ABCB1* transcription mostly depends on a few elements, i.e. two GC-rich regions (GC-boxes), located from -110 to -103 and from -56 to -45 bases upstream of the major +1 start site in the human *ABCB1* promoter, the CCAAT box (Y-box), the p53 element and possibly the AP-1 and T-cell factor elements (see above, for a review see (Silva et al., 2015)). In addition, stress-induced upregulation of *ABCB1* expression occurs, depending on ROS, heat shock, inflammation and ionizing radiations, acting via a wealth of transcription factors, such as phosphoinositide 3-kinase (PI3K)/Akt, extracellular signal-regulated kinases (ERKs; or mitogen-activated protein kinases, MAPKs), c-Jun NH2-terminal protein kinase (JNK), protein kinase C (PKC) and nuclear factor-κB (NF-κB), cyclic adenosine monophosphate responsive element (CRE) and heat-shock factor (HSF), acting on several pathways in a very complex manner (Callaghan et al., 2008; Chin et al., 1990; Krishnamurthy et al., 2012; Labialle et al., 2002; Miyazaki et al., 1992; Nwaozuzu et al., 2003; Scotto, 2003; Scotto and Egan, 1998; Silva et al., 2015; Vilaboa et al., 2000; Wong et al., 2010; Zhou and Kuo, 1997).

*ABCB1* can be induced by several stimuli, acting on these regulatory elements, directly or indirectly. Apart from the stress conditions abovementioned, many molecules are able to induce *ABCB1* overexpression. Table 4 reports a list of *ABCB1* inducers, the mode they have been described to act through, and the level of induction observed upon cell treatment: these compounds are rather heterogeneous in

**Table 4**  
Drugs inducing ABCB1 expression.

Drugs inducing ABCB1 expression	
Inducer	Action
Abacavir	1.5-fold ABCB1 induction upon 15 $\mu$ M treatment for 72 h in hCMEC/D3 cells (Chan et al., 2013)
N-Acetoxy-2-acetylaminofluorene	3.2-fold ABCB1 expression increase upon 40 $\mu$ M treatment for 8 h in HepG2 cells (Kuo et al., 2002)
2-Acetyl-aminofluorene	7.5-fold ABCB1 induction upon 100 $\mu$ M treatment for 24 h in rat hepatoma cells (Deng et al., 2001)
Actinomycin D	2.5-fold ABCB1 mRNA induction upon 400 ng/mL treatment for 72 h in human T lymphoblastoid CCRF-CEM cells (Gekeler et al., 1988)
Aflatoxin B1	ABCB1 mRNA induction upon 3 mg/kg i.p. treatment for 48 h in Fischer rats (Burt and Thorgeirsson, 1988)
Ambrisentan	2.3-fold ABCB1 expression upon 50 $\mu$ M treatment for 96 h in LS180 cells (Weiss et al., 2013)
Amiodarone	2.4-fold ABCB1 induction upon 10 $\mu$ M treatment for 72 h in LS180 cells (Schuetz et al., 1996)
Amrenavir	3.5-fold ABCB1 induction upon 10 $\mu$ M treatment for 72 h in LS180 cells (Perloff et al., 2000)
Arsenite	3-fold ABCB1 induction upon 250 nM treatment for 24 h in TRL1215 cells (Liu et al., 2001)
Artemisinin	13.5-fold ABCB1 mRNA induction upon 10 $\mu$ M treatment for 6 h in Caco-2 cells (Riganti et al., 2009b)
Asiatic acid	2.6-fold ABCB1 induction upon 25 $\mu$ M treatment for 48 h in LS180 cells (Abuznait et al., 2011b)
Atazanavir	2.5-fold ABCB1 induction upon 10 $\mu$ M treatment for 72 h in hCMEC/D3 cells (Zastre et al., 2009)
Atorvastatin	4-fold ABCB1 mRNA induction upon 10 $\mu$ M treatment for 72 h in T84 cells (Haslam et al., 2008a)
Avermectin	2.6-fold ABCB1 induction upon 0.5 $\mu$ M treatment for 12 h in Drosophila S2 cells (Luo et al., 2013)
Beclomethasone	2.1-fold ABCB1 expression increase upon 50 $\mu$ M treatment for 72 h in Caco-2 cells (Crowe and Tan, 2012)
Benzopyrene	Increased ABCB1 expression upon 50 $\mu$ M treatment for 72 h in Caco-2 cell (Sugihara et al., 2007)
Bethametasone	4-fold ABCB1 induction upon 0.4 $\mu$ M treatment for 24 h in placenta cells (Manceau et al., 2012)
Bilirubin	18-fold ABCB1 mRNA induction upon 100 $\mu$ M treatment for 24 h in T84 cells (Naruhashi et al., 2011)
Bosentan	3.7-fold ABCB1 induction upon 50 $\mu$ M treatment for 96 h in LS180 cells (Weiss et al., 2013)
Bromocriptine	10-fold ABCB1 induction upon 100 $\mu$ M treatment for 24 h in rat Reuber H35 cells (Furuya et al., 1997)
Budesonide	1.6-fold ABCB1 induction upon 50 $\mu$ M treatment for 72 h in Caco-2 cells (Maier et al., 2007)
Cadmium	3.7-fold ABCB1 induction upon 10 $\mu$ M treatment for 72 h in Caco-2 cells (Thevenod et al., 2000)
Caffeine	Increased ABCB1 expression upon 5–100 $\mu$ M treatment for 48 h in LS180 cells (Abuznait et al., 2011a)
Capsaicin	2-fold ABCB1 induction upon 50 $\mu$ M treatment for 72 h in Caco-2 cells (Han et al., 2006)
Carbamazepine	7.6-fold ABCB1 induction upon 50 $\mu$ M treatment for 72 h in human blood lymphocytes (Owen et al., 2006)
Catechine	2.3-fold ABCB1 induction upon 10 $\mu$ M treatment for 4 weeks in Caco-2 cells (Lohner et al., 2007)
Celiprolol	3.2-fold ABCB1 induction upon 100 $\mu$ M treatment for 72 h in Caco-2 cells (Anderle et al., 1998)
Cembratriene	3-fold ABCB1 induction upon 25 $\mu$ M treatment for 48 h in LS180 cells (Abuznait et al., 2011b)
Cholate	1.8-fold ABCB1 mRNA induction upon 100 $\mu$ M treatment for 24 h in T84 cells (Naruhashi et al., 2011)
Chrysin	2.8-fold ABCB1 induction upon 10 $\mu$ M treatment for 4 weeks in Caco-2 cells (Lohner et al., 2007)
Ciclesonide	1.7-fold ABCB1 induction upon 50 $\mu$ M treatment for 72 h in Caco-2 cells (Crowe and Tan, 2012)
Cisplatin	2.7-fold ABCB1 expression upon 3 mg/kg treatment for 96 h in liver and kidney of Sprague-Dawley rats (Demeule et al., 1999)
Clotrimazole	4.1-fold ABCB1 induction upon 10 $\mu$ M treatment for 72 h in LS180 cells (Schuetz et al., 1996)
Colchicine	1.8-fold ABCB1 induction upon 100 $\mu$ M treatment for 24 h in Caco-2 cells (Silva et al., 2014)
Colupulones	1.3-fold ABCB1 induction upon 1 $\mu$ M treatment for 48 h in LS180 cells (Bharate et al., 2015)
Cyanidin	2.7-fold ABCB1 induction upon 10 $\mu$ M treatment for 4 weeks in Caco-2 cells (Lohner et al., 2007)
Cycloheximide	27-fold ABCB1 mRNA induction upon 10 $\mu$ M treatment for 24 h in RC3 cells (Gant et al., 1992)
Cyclosporine A	2-fold ABCB1 mRNA induction upon 5 $\mu$ g/mL treatment for 48 h in LS180 cells (Herzog et al., 1993)
Cytarabine	1.3-fold ABCB1 induction upon 0.5 $\mu$ M treatment for 24 h in HL60 leukemia cells (Prenekert et al., 2009)
Dadzein	1.7-fold ABCB1 induction upon 10 $\mu$ M treatment for 4 weeks in Caco-2 cells (Lohner et al., 2007)
Daunorubicin	3-fold ABCB1 induction upon 1.5 $\mu$ g/mL treatment for 4 h in CEM/A7R cells (Hu et al., 1995)
Daurunavir	1.7-fold ABCB1 induction upon 10 $\mu$ M treatment for 72 h in hCMEC/D3 cells (Chan et al., 2013)
Depsideptide	6.3-fold ABCB1 mRNA induction upon 5 ng/mL treatment for 72 h in 108 renal carcinoma cells (Robey et al., 2006)
Dexamethasone	2.9- and 1.9-fold ABCB1 expression upon 50 mg/kg/7day treatment for 96 h in intestine and liver, respectively, of Wistar rats (Kageyama et al., 2006)
Digoxin	92-fold ABCB1 mRNA induction upon 1 $\mu$ M treatment for 72 h in T84 cells (Haslam et al., 2008b)
1,25-Dihydroxyvitamin D3	5.9-fold ABCB1 induction upon 2.5 $\mu$ g/kg/day treatment for 8 days in fxr(-/-) mice kidney (Chow et al., 2011)
Diltiazem	4-fold ABCB1 mRNA induction upon 10 $\mu$ g/mL treatment for 48 h in LS180 cells (Herzog et al., 1993)
Docetaxel	Increased ABCB1 expression upon 10 $\mu$ M treatment for 48 h in LS180 cells (Harmsen et al., 2010)
Doxorubicin	Increased ABCB1 and ABCB1 mRNA expression upon 3 $\mu$ M treatments in MCF-7 cells (Mealey et al., 2002)
Doxycycline	8-fold increased ABCB1 expression upon 100 $\mu$ g/mL treatment for 12 weeks in MCF-7 cells (Mealey et al., 2002)
Efavirenz	8-fold increased ABCB1 expression upon 10 $\mu$ M treatment for 72 h in hCMEC/D3 cells (Chan et al., 2013)
Epigallocatechin-3-gallate	2.2-fold ABCB1 induction upon 10 $\mu$ M treatment for 4 weeks in Caco-2 cells (Lohner et al., 2007)
Epirubicin	3-fold ABCB1 induction upon 1.5 $\mu$ g/mL treatment for 8 h in CEM/A7R cells (Hu et al., 1995)
Eriodictyol	2.1-fold ABCB1 induction upon 10 $\mu$ M treatment for 4 weeks in Caco-2 cells (Lohner et al., 2007)
Erlotinib	2.9-fold ABCB1 induction upon 10 $\mu$ M treatment for 48 h in LS180V cells (Harmsen et al., 2013)
Erythromycin	3.3-fold ABCB1 induction upon 15 mg/kg treatment for 7 days in Rhesus monkey livers (Gant et al., 1995)
$\beta$ -Estradiol	4-fold ABCB1 mRNA induction upon 50 $\mu$ M treatment for 48 h in LS180 cells (Abuznait et al., 2011a)
Ethinylestradiol	1.6-fold ABCB1 induction upon 0.5 pM treatment for 48 h in Caco-2 cells (Arias et al., 2014)
Fascaplysin	7-fold ABCB1 induction upon 1 $\mu$ M treatment for 48 h in LS180 cells (Manda et al., 2016)
Flavone	3-fold ABCB1 induction upon 10 $\mu$ M treatment for 4 weeks in Caco-2 cells (Lohner et al., 2007)
5-Fluorouracil	4.5-fold ABCB1 induction upon 2 $\mu$ g/mL treatment for 72 h in CEM/A7R cells (Hu et al., 1999)
Fluticasone	+87% ABCB1 induction upon 50 $\mu$ M treatment for 72 h in Caco-2 cells (Crowe and Tan, 2012)
Gefinitib	3-fold ABCB1 induction upon 10 $\mu$ M treatment for 48 h in LS180V cells (Harmsen et al., 2013)
Genistein	2-fold ABCB1 induction upon 10 $\mu$ M treatment for 4 weeks in Caco-2 cells (Lohner et al., 2007)
Hyperforin	3-fold ABCB1 induction upon 150 nM treatment for 48 h in LS180 cells (Abuznait et al., 2011a)
Hypericin	7-fold ABCB1 induction upon 3 $\mu$ M treatment for 72 h in LS180V cells (Perloff et al., 2001)
Idarubicin	4-fold ABCB1 induction upon 0.1 $\mu$ g/mL treatment for 24 h in CEM/A7R cells (Hu et al., 1999)
Indinavir	1.6-fold ABCB1 induction upon 10 $\mu$ M treatment for 72 h in LS180V cells (Perloff et al., 2000)
Insulin	+89% ABCB1 induction upon 10 U/kg/day treatment for 5 weeks in Sprague-Dawley rats (Liu et al., 2008)
Ivermectin	2-fold ABCB1 induction upon 10 $\mu$ M treatment for 72 h in JWZ murine hepatic cells (Menez et al., 2012)
Lopinavir	2.3-fold ABCB1 induction upon 10 $\mu$ M treatment for 72 h in hCMEC/D3 cells (Chan et al., 2013)

(continued on next page)

Table 4 (continued)

Drugs inducing ABCB1 expression	
Inducer	Action
Mangiferin	2.4-fold ABCB1 induction upon 200 $\mu$ M treatment for 72 h in HK2 cells (Chieli et al., 2010)
Methylprednisolone	+ 50% ABCB1 induction upon 50 $\mu$ M treatment for 72 h in Caco-2 cells (Crowe and Tan, 2012)
Midazolam	5.9-fold ABCB1 induction upon 10 $\mu$ M treatment for 72 h in LS180 cells (Schuetz et al., 1996)
Mitoxantrone	30/100-fold ABCB1 mRNA induction upon 1 $\mu$ g/mL treatment for 8 h in NIH 3T3 cells (Schrenk et al., 1996)
Morphine	2-fold ABCB1 induction upon 20 mg/kg/day treatment for 5 days in Sprague-Dawley rat brains (Aquilante et al., 2000)
Myricetin	2.5-fold ABCB1 induction upon 10 $\mu$ M treatment for 4 weeks in Caco-2 cells (Lohner et al., 2007)
Naringenin	1.8-fold ABCB1 induction upon 10 $\mu$ M treatment for 4 weeks in Caco-2 cells (Lohner et al., 2007)
Nelfinavir	3.5-fold ABCB1 induction upon 10 $\mu$ M treatment for 72 h in LS180V cells (Perloff et al., 2000)
Nevirapine	1.6-fold ABCB1 induction upon 15 $\mu$ M treatment for 72 h in hCMEC/D3 cells (Chan et al., 2013)
Nicardipine	6-fold ABCB1 mRNA induction upon 10 $\mu$ M treatment for 48 h in LS180 cells (Herzog et al., 1993)
Nifedipine	4-fold ABCB1 mRNA induction upon 5 $\mu$ g/mL treatment for 48 h in LS180 cells (Herzog et al., 1993)
Nilotinib	3.6-fold ABCB1 induction upon 10 $\mu$ M treatment for 48 h in LS180V cells (Harmsen et al., 2013)
Oleocanthal	2.3-fold ABCB1 induction upon 25 $\mu$ M treatment for 48 h in LS180 cells (Abuznait et al., 2011b)
Ouabain	3.4-fold ABCB1 mRNA induction upon 1 $\mu$ M treatment for 24 h in HT29 cells (Riganti et al., 2009a)
Oxycodone	4-fold ABCB1 induction upon 5 mg/kg/day treatment for 8 days in Sprague-Dawley rat livers (Hassan et al., 2007)
Paclitaxel	Increased ABCB1 expression upon 10 $\mu$ M treatment for 48 h in LS180 cells (Harmsen et al., 2010)
Parthenolide	6-fold ABCB1 mRNA induction upon 10 $\mu$ M treatment for 6 h in HT29 cells (Riganti et al., 2009b)
Phenobarbital	14-fold ABCB1 induction upon 1 mM treatment for 72 h in LS180 cells (Schuetz et al., 1996)
Phenothiazine	6.5-fold ABCB1 expression upon 50 mg/kg/day treatment for 72 h in bile canalicular membrane vesicles of Wistar rats (Watanabe et al., 1995)
Phenytoin	ABCB1 induction upon 50 mg/kg/day treatment for 21 days in Sprague-Dawley rat brains (Wen et al., 2008)
Piperine	2-fold ABCB1 expression upon 100 $\mu$ M treatment for 72 h in Caco-2 cells (Han et al., 2008)
Pregnenolone-16 $\alpha$ - carbonitrile	+ 53% ABCB1 expression upon 5 $\mu$ M treatment for 6 h in brain capillaries from CB6F1 rats (Bauer et al., 2006)
Propranolol	4-fold ABCB1 induction upon 200 $\mu$ M treatment for 24 h in LS180 cells (Collett et al., 2004)
Quercetin	2.5-fold ABCB1 induction upon 10 $\mu$ M treatment for 4 weeks in Caco-2 cells (Lohner et al., 2007)
Rapamycin	4.9-fold ABCB1 induction upon 10 $\mu$ M treatment for 72 h in LS180 cells (Schuetz et al., 1996)
Reserpine	29-fold ABCB1 induction upon 10 $\mu$ M treatment for 72 h in LS180 cells (Schuetz et al., 1996)
Retinoic acid	20-fold ABCB1 mRNA induction upon 5 $\mu$ M treatment for 72 h in SK-N-SH cells (Bates et al., 1989)
Rifampicin	16-fold ABCB1 induction upon 10 $\mu$ M treatment for 72 h in LS180 cells (Schuetz et al., 1996)
Ritonavir	4.2-fold ABCB1 induction upon 10 $\mu$ M treatment for 72 h in LS180V cells (Perloff et al., 2000)
Saquinavir	2.4-fold ABCB1 induction upon 10 $\mu$ M treatment for 72 h in LS180V cells (Perloff et al., 2000)
Sildenafil	2.1-fold ABCB1 induction upon 5 $\mu$ M treatment for 96 h in LS180 cells (Weiss et al., 2013)
Tacrolimus	3.2-fold ABCB1 induction upon 10 $\mu$ M treatment for 72 h in LS180 cells (Schuetz et al., 1996)
Tadalafil	3.3-fold ABCB1 induction upon 20 $\mu$ M treatment for 96 h in LS180 cells (Weiss et al., 2013)
Tamoxifen	6-fold ABCB1 induction upon 50 mg/kg/day treatment for 7 days in Rhesus monkey livers (Gant et al., 1995)
Taxifolin	1.8-fold ABCB1 induction upon 10 $\mu$ M treatment for 4 weeks in Caco-2 cells (Lohner et al., 2007)
$\gamma$ -Tocotrienol	2.4-fold ABCB1 induction upon 25 $\mu$ M treatment for 48 h in LS180 cells (Abuznait et al., 2011b)
Trichostatin A	20-fold ABCB1 mRNA induction upon 100 ng/mL treatment for 24 h in SW620 cells (Jin and Scotto, 1998)
Verapamil	3-fold ABCB1 induction upon 10 $\mu$ M treatment for 72 h in Caco-2 cells (Anderle et al., 1998)
Vinblastine	7.5-fold ABCB1 induction upon 0.011 $\mu$ M treatment for 72h in Caco-2 cells (Anderle et al., 1998)
Vincristine	ABCB1 induction upon 0.1 $\mu$ M treatment for 48 h in LS180 cells (Harmsen et al., 2010)

nature, structure and origin. ABCB1 inducers include many drugs (among which several chemotherapeutic drugs and tyrosine kinase inhibitors, usually also ABCB1 substrates), natural compounds and marine compounds, and phosphodiesterase-5 inhibitors.

### The ABCB1 amplicon

#### MDR and the genes in the human ABCB1 amplicon

The human ABCB1 (*MDR1*) gene resides in chromosome 7q21.1 region (Callen et al., 1987); its ability to confer MDR when over-expressed or amplified (Callen et al., 1987; Fojo et al., 1987; Schoenlein, 1993; Scotto et al., 1986; Van der Bliek et al., 1986b) and the increase in ABCB1 expression upon chemotherapeutic drug treatment (Abolhoda et al., 1999; Atalay et al., 2006; Brugger et al., 2002; Chin et al., 1990; Gekeler et al., 1988; Hu et al., 1995; Liu et al., 2002; Park et al., 1994; Schneider et al., 1993) have been largely reported throughout the years.

The amplification of chromosome 7q21 region in neuroblastoma cancer cell lines (Flahaut et al., 2006), as well as the increased copy number of 7q21.12 region (including ABCB1 gene) in lung cancer cells (Kitada and Yamasaki, 2007) and in leukemia cells (Kadioglu and Efferth, 2016) correspond to drug resistance, suggesting the possible participation of other genes in the development of the MDR phenotype.

Genomic instability and chromosomal rearrangements often affect

cancer cells, resulting in genomic amplification, frequently translated in an increased copy number of the ABCB1 gene that leads to a marked transactivation of ABCB1 gene overexpression (Chen et al., 2002; Duesberg et al., 2007; Katoh et al., 2005; Kim et al., 2015; Mickley et al., 1997; Pang et al., 2005). These genomic rearrangements may either occur in upstream regions far from the ABCB1 promoter or may affect genomic alterations along the 7q chromosomal arm that can correlate with ABCB1 activation (Chen et al., 2002; Knutsen et al., 1998).

Genomic investigations focusing on the ABCB1 amplicon have been undertaken in order to understand whether or not the surrounding genes might have some role in the development of the MDR phenotype or if they were co-amplified or suppressed in resistance-induced cancer cell lines. ABCB1 gene expression can be increased up to 1000-fold in lung cancer cells with acquired paclitaxel resistance, showing a surprising discrepancy between the gene copy number and the expression level. Along with ABCB1 gene expression enhancement, within the same amplicon (7q21.12), there is a concomitant co-amplification of *RPIB9* (*RUNDC3B*) and *ADAM22* with an increased fold change of 38.5 and 27.7, respectively (Yabuki et al., 2007).

Taxane-induced MDR ovarian cancer cell lines showed a regional activation on chromosome 7q21.11-13 of about 22 co-expressed genes over an area of 8Mb, surrounding the ABCB1 gene. These genes include *SRI* (Sorcin), *MGC4175* (*TMEM243*), *DMTF1*, *CROT*, *ABCB1*, *ABCB4*, *ADAM22*, *RUNDC3B*, *DBF4* and the regional activation was driven by



gene copy number gains (Wang et al., 2006). Another study on taxane-resistant breast cancer cell lines reported gains in gene copy number on chromosome 7, specifically concerning ABC transporters (*ABCB1*, *ABCB4*), *SRI*, *DMTF1*, *SLC25A40* and *CROT*, all belonging to the *ABCB1* amplicon (Hansen et al., 2016). Furthermore, a whole-genome characterization study on chemoresistant ovarian cancer cells reported an intergenic deletion between *ABCB1* and *SLC25A40* genes and that results in the creation of a fused transcript, with no evidence of this event in drug-sensitive tumor samples. Additional transcriptome investigations showed the increase of *ABCB1*-*SLC25A40* fused transcript in chemoresistant human ovarian cancer samples and the decrease of *SLC25A40* in drug sensitive specimens (Patch et al., 2015).

However, the genomic rearrangements and the high copy number cannot explain by themselves the unexpected high level increase in gene expression, suggesting that other mechanisms as such transcriptional upregulation, mRNA stabilization, post-transcriptional regulation and epigenetic modifications may contribute to this enhanced gene expression. Interestingly, non-coding RNAs as miRNAs and long non-coding RNAs (lncRNA) may exert post-transcriptional regulatory functions in cancer cells, giving rise to metastatic or drug-resistant phenotypes. Indeed in the *ABCB1* amplicon a lncRNA (*TP53TG1*) resides, reported to be down-regulated in A549 cisplatin-resistant lung cancer cells (Yang et al., 2013). On the other hand, deletions in the *ABCB1* genes locus in breast cancer patients determine a 2–8-fold decreased expression of these MDR locus-related genes; cancer patients harboring these deletions display a better response to neoadjuvant chemotherapy (Litviakov et al., 2016).

Overall, many published studies report that a genomic amplification of chromosome 7q21.12 region, where *ABCB1* and related genes reside (Fig. 5), occurs in MDR tumors, and that amplification and/or overexpression of these genes contributes to the MDR phenotype (Bonte et al., 2008; Chao et al., 1991; Cheng et al., 2013; Finalet Ferreira et al., 2014; Flahaut et al., 2006; Hansen et al., 2016; Januchowski et al., 2017; Kadioglu and Efferth, 2016; Kitada and Yamasaki, 2007; Lee et al., 2017; Litviakov et al., 2016; Patch et al., 2015; Sasi et al., 2017; Torigoe et al., 1995; Van der Bliek et al., 1988; Van der Bliek et al., 1986a; Van der Bliek et al., 1986b; Yabuki et al., 2007). The core of the amplicon is formed by the genes *Sorcin* (*SRI*), *ADAM22*, *DBF4*, *SLC25A40*, *RUNDC3B* (*RPIP9*), *ABCB1*, *ABCB4*, *CROT*, *TP53TG1* lncRNA, *TMEM243* (*MGC4175*) and *DMTF1* (*DMP1*) (Fig. 5). All of these genes have been found to be associated with tumorigenesis and MDR; very important contributions to the MDR phenotype are due in particular to the overexpression of *DBF4* and *Sorcin*, which are considered as important markers of poor prognosis and drivers of MDR in several types of cancers, acting on different mechanisms with respect to *ABCB1*. Selective inhibitors of *Sorcin* expression and of *CDC7-DBF4* activity have been recently developed, and are considered good potential anti-tumor candidates (see below).

### *ABCB1* amplicon genes: regulation, cancer and MDR

#### *Sorcin* (*SRI*)

*Sorcin* was originally isolated by Meyers and Biedler in 1981 as a soluble, low molecular weight protein in hamster lung cancer cell line resistant to vincristine, and this feature was used to give *sorcin* the name of *Sorcin* (SOLuble Resistance-related Calcium binding protein)

(Meyers and Biedler, 1981). *Sorcin* belongs to the penta EF-hand (PEF) protein family; as other members of this family, upon calcium binding, *Sorcin* undergoes a conformational change, leading to the exposure of hydrophobic surfaces that enable the interaction with membranes and other binding partners (Ilari et al., 2015). Among them, *Sorcin* binds and controls proteins involved in the regulation of intracellular calcium concentration as Ryanodine Receptors (RyRs), Sarco/endoplasmic reticulum  $\text{Ca}^{2+}$ -ATPase (SERCA pumps) and  $\text{Na}^{+}/\text{Ca}^{2+}$  exchanger (NCX), leading to the termination of contraction and the onset of relaxation (Colotti et al., 2014; Franceschini et al., 2008; Zamparelli et al., 2010). *Sorcin* is phosphorylated by several kinases involved in cell cycle progression or calcium homeostasis, regulating calcium load in storage organelles and vesicle trafficking (Lalioti et al., 2014).

*Sorcin* is overexpressed in many cancers of distinct tissue origin, especially those displaying the *ABCB1*-dependent MDR phenotype. The *Sorcin* gene resides in the same amplicon of *ABCB1* and was identified as a resistance-related gene because its genomic locus is co-amplified along with *ABCB1* in cancer cells displaying the MDR phenotype (Van der Bliek et al., 1986a). Although for many years *Sorcin* overexpression was thought to be an accidental by-product of this genomic co-amplification process (Van der Bliek et al., 1988), a large body of published studies considered *Sorcin* both as a marker and a cause of MDR. *Sorcin* is found overexpressed in many human tumors including lymphoma, leukemia, gastric cancer, lung cancer, adenocarcinoma, breast cancer, nasopharyngeal cancer and ovarian cancer, particularly in malignancies with the *ABCB1*-dependent MDR phenotype (Deng et al., 2010; Gao et al., 2015; Padar et al., 2004; Qi et al., 2006; Qu et al., 2010; Sun et al., 2017; Tan et al., 2003; Yamagishi et al., 2014; Yang et al., 2008; Zhou et al., 2006).

Many studies have dissected the role of *Sorcin* in MDR cancer types, indicating its role as an oncoprotein. In doxorubicin-resistant K562/A02 leukemia cell lines, *Sorcin* was found consistently up-regulated compared to the drug-sensitive parental cell line, and the overexpression in the resistant line conferred MDR (Hu et al., 2013; Qi et al., 2006; Sun et al., 2017; Yamagishi et al., 2014; Zhou et al., 2006). *Sorcin* expression levels in leukemia patients generally correlate with low-response to chemotherapies and poor prognosis. Moreover, *Sorcin* overexpression by gene transfection resulted in increased drug resistance to a variety of chemotherapeutic agents, including doxorubicin, etoposide, homoharringtonine and vincristine in K562 cells; and conferred drug resistance to vincristine, adriamycin, paclitaxel and 5-fluorouracil in SGC7901 cells, ovarian and breast cancer, thereby confirming the ability of *Sorcin* overexpression to enhance drug resistance. Consistently, inhibition of *Sorcin* expression by RNA interference techniques led to reversal of MDR in many tumor cell lines, as MDR K562/A02 and *Sorcin*-transfected K562, MCF-7/A02, HeLa, colorectal cancer and CNE2/DDPls (Colotti et al., 2014; Dabaghi et al., 2016; Gao et al., 2015; Gong et al., 2014; Hamada et al., 1988; He et al., 2011; Hu et al., 2013; Hu et al., 2014; Kawakami et al., 2007; Liu et al., 2014; Maddalena et al., 2011; Parekh et al., 2002; Sun et al., 2017; Zhou et al., 2006).

Additionally, a recent study showed that directed siRNA-*Sorcin* silencing decreased *ABCB1* protein levels in a H1299 lung cancer cell line, with a consequent increase in rhodamine123 efflux out of the cells, confirming a direct relationship between *Sorcin* and regulation of *ABCB1* transport activity in MDR cells. Besides, *Sorcin* is able to bind

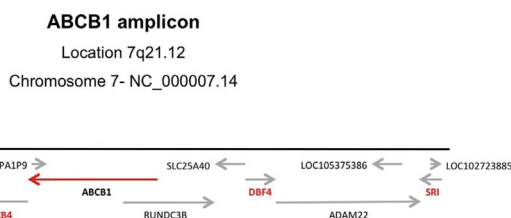
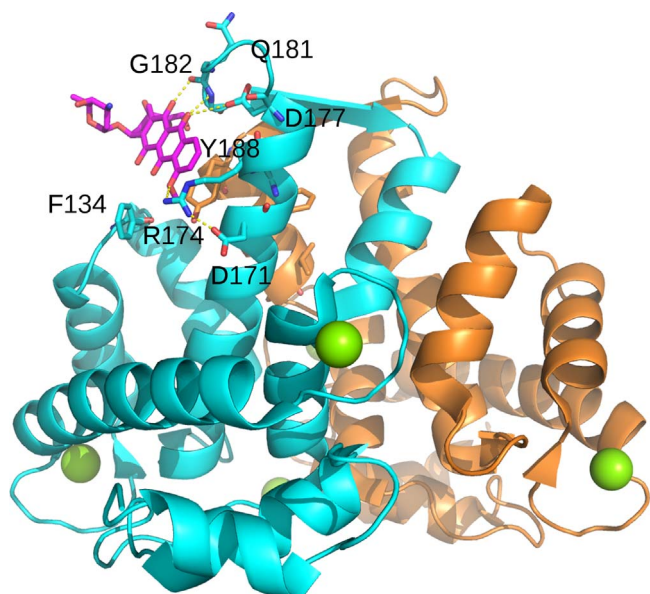


Fig. 5. The *ABCB1* amplicon. Genes in the 7q21.12 region are shown.



**Fig. 6.** Structure of Sorcin in complex with doxorubicin. The two monomers of Sorcin are indicated in cyan and orange, and doxorubicin in magenta sticks. The residues involved in doxorubicin binding are indicated and represented as sticks; calcium ions are represented as green spheres (Genovese et al., 2017). (For interpretation of the references to colour in this figure legend, the reader is referred to the web version of this article.)

directly doxorubicin, paclitaxel, vinblastine and cisplatin, acting as a protein drug sink thus hampering nuclear uptake of doxorubicin, thus allowing cell survival (Genovese et al., 2017). Sorcin is highly expressed and is able to bind doxorubicin with high affinity on the EF5-hand (Fig. 6), which does not bind calcium and is involved in homodimer formation (Genovese et al., 2017).

Furthermore, Sorcin silencing inhibits the epithelial-to-mesenchymal (EMT) transition in the human breast cancer MDA-MB-213 cell line, possibly via E-cadherin and VEGF expression, and reduces breast cancer metastasis, while Sorcin overexpression increases migration and invasion *in vitro* (Hu et al., 2014). Sorcin expression levels are significantly up-regulated in hepatocellular carcinoma (HCC) tumors compared with matched adjacent non-tumor liver tissues and normal liver tissues, and expression levels correlate with HCC metastasis. HCC patients with high Sorcin expression had both shorter survival and higher recurrence than those with low Sorcin expression. Sorcin expression is therefore an independent and significant risk factor for survival and recurrence of HCC patients. Sorcin can promote HCC and colorectal cancer cell proliferation, migration, and invasion *in vitro*, and facilitate cancer growth, metastasis and EMT, by activating extracellular signal-regulated kinase (ERK) and/or PI3K/Akt signaling pathways (Lei et al., 2017; Tong et al., 2015).

Several groups are currently studying the role of Sorcin in the development of MDR in cancer cells, disclosing intriguing findings. Yamagishi and collaborators found that Sorcin expression correlates with *ABCB1* up-regulation, indeed Sorcin induced *ABCB1* expression through a cAMP response element (CRE) located within  $-716$  and  $-709$  bp in the *ABCB1* gene. Consistently, they found that up-regulation of Sorcin induces *ABCB1* expression through the inducible activation of CREB (cAMP response element-binding protein) pathway increasing the phosphorylation of CREB1 and its binding to the CRE binding site in the *ABCB1* promoter (Yamagishi et al., 2014).

A shorter isoform (18 kDa) of Sorcin, identified to be located in mitochondria, is the aim of the quality control system operated by ER-associated TRAP1. The latter protein is up-regulated in several human tumors and can modulate apoptosis; indeed, transfection experiments of a TRAP1 deletion mutant in TRAP1-silenced cells increased the expression of mitochondrial sorcin and protected cells from apoptosis

upon treatment with ER stress agents and paclitaxel (Maddalena et al., 2013), suggesting a putative post-transcriptional regulation of sorcin expression. Sorcin, loading calcium in ER and mitochondria, participates in the prevention of ER stress and unfolded protein response, and increases cell escape from apoptosis (Lalioti et al., 2014; Maddalena et al., 2011; Maddalena et al., 2013), shifting the equilibrium between cell life and death towards proliferation in MDR cancer cells over-expressing Sorcin.

For these reasons, Sorcin is an interesting oncoprotein and MDR marker, able to bind several chemotherapeutic drugs, whose over-expression results in the MDR phenotype. Sorcin expression is directly linked to *ABCB1* up-regulation, and is itself involved in regulation of the *ABCB1*-dependent MDR phenotype. The modulation of Sorcin expression and activity (Li et al., 2016a; Sun et al., 2017) is emerging as a possible strategy for overcoming tumorigenesis, cancer-related EMT and MDR.

#### ADAM22

ADAM22 is a non-catalytic metalloprotease involved in both regulation of cell adhesion and spreading and inhibition of cell proliferation. It acts as a neuronal receptor for LGI1 and as a ligand with the integrin  $\alpha v \beta 3$  and also with integrin dimers containing  $\alpha 6$  or  $\alpha 9$  in the brain (D'Abaco et al., 2006), thus regulating synaptic transmission (Fukata et al., 2006; Liu et al., 2009). In ovarian cell lines and in two different human breast cancer cell lines, MCF-7 and MDA-MB-231, exposure to docetaxel induced resistance to the drug, accompanied by overexpression of ADAM22 and many other proteins of the *ABCB1* amplicon (Hansen et al., 2016; Wang et al., 2006). Microarray analysis uncovered that ADAM22 is overexpressed in doxorubicin-resistant osteosarcoma cell lines (Ma et al., 2017). ADAM22 is a target of SRC1, steroid co-activator protein 1; in this respect, SRC1 overexpression enhances ADAM22 expression in endocrine-sensitive MCF-7 breast cancer cells. An enrichment of SRC1 was found at the ADAM22 promoter through chromatin immunoprecipitation (ChIP) experiments in endocrine-resistant breast cancer but not in the sensitive one, suggesting the ability of this protein to promote tumor progression. SRC1-dependent ADAM22 expression in response to tamoxifen has been observed; ADAM22 is considered a prognostic and therapeutic drug target in the treatment of endocrine-resistant breast cancer. Further, ADAM22 gene methylation is associated with malignant transformation of ovarian endometriosis (Bolger and Young, 2013; McCartan et al., 2012; Ren et al., 2014).

#### DBF4

DBF4 is a positive regulatory subunit of the CDC7 kinase that plays a central role in DNA replication and cell proliferation, being essential for the progression through the S phase. Indeed, the DBF4-CDC7 complex phosphorylates the Mcm2 helicase at Ser40 and Ser53, thereby allowing the initiation of eukaryotic DNA replication. CDC7 levels appear to be constant throughout the cell cycle, whereas DBF4 levels have a burst in late G1 phase and decrease at the end of mitosis (Cheng et al., 2013; Pasero et al., 1999; Weinreich and Stillman, 1999). CDC7-DBF4 is essential for the initiation of DNA replication; during the G1 phase CDC7-DBF4 is down-regulated by RAD53-dependent phosphorylation of DBF4, which allows origin licensing and prevents premature replication initiation (Zegerman and Diffley, 2010), while in the S phase, the intra-S-phase checkpoint is activated by CDC7-DBF4, by removing the inhibitory activity of Mcm4 (Sheu and Stillman, 2010).

DBF4 has three motifs, N, M and C, which regulate its interaction with various binding partners. The N motif is located at the N-terminus of the protein and is believed to interact with ORC and RAD53, a kinase required for check-point mediated cell cycle arrest (Duncker et al., 2002). The C and N motifs are involved in the response towards genotoxic agents, while less is known about the M motif (Fung et al., 2002), even though it seems to have a role in cell proliferation, since it mediates the interaction with Mcm2 (Varrin et al., 2005).

Both CDC7 and DBF4 are overexpressed in many cancer cell lines and primary tumors; tumor cell lines with increased CDC7 protein levels also have increased DBF4, whose gene can be present in extra copies in some tumors (Bonte et al., 2008; Cheng et al., 2013). Overexpression of CDC7-DBF4 has been reported in many human tumors, including ovarian cancer, colorectal cancer, melanoma, diffuse large B-cell lymphoma, oral squamous cell carcinoma and breast cancer, and is correlated with poor prognosis and advanced grade tumor grade (Bonte et al., 2008; Chen et al., 2013a; Cheng et al., 2013; Choschzick et al., 2010; Clarke et al., 2009; Hou et al., 2012; Kulkarni et al., 2009; Nambiar et al., 2007). A high correlation between loss of p53 function and up-regulation of DBF4 and CDC7 is observed in primary breast cancer, suggesting that the increased amount of CDC7-DBF4 is presumably a common driver mutation for this malignancy (Bonte et al., 2008). Higher DBF4-expressing melanomas were associated with lower relapse-free survival, and higher proliferation (Nambiar et al., 2007). High expression of CDC7-DBF4 correlates with poor prognosis in patients with large B-cell lymphoma (Hou et al., 2012), and is a marker of resistance to DNA-damaging compounds in oral carcinoma (Cheng et al., 2013), and a marker of chemoresistance to cisplatin, mitomycin C, taxol, hydroxyurea and etoposide in lung adenocarcinoma and bladder cancer (Sasi et al., 2017). 6-fold overexpression of DBF4 was recently found in docetaxel-resistant prostate cancer cells with respect to docetaxel-sensitive cells (Lee et al., 2017), and overexpression of DBF4 was acquired during progression towards docetaxel resistance in taxane-treated breast cancer cells (Hansen et al., 2016).

MIR29a regulates BPDE-induced DNA damage response (and determines increased cell lethality) through repression of CDC7-DBF4 kinase expression in lung cancer cells, while overexpression of CDC7-DBF4 determines resistance to BPDE (Barkley and Santocanale, 2013). Further, CDC7-DBF4 is highly expressed in colorectal cancer and is considered a potential therapeutic target in cancers with high p53 expression and an independent prognostic biomarker in colorectal cancer enabling to select patients for adjuvant anti-CDC7-DBF4 treatment (Melling et al., 2015). Since the CDC7-DBF4 kinase is considered a novel and promising cancer target, inhibitors of the CDC7-DBF4 kinase have been recently developed, and are considered good potential anti-tumor candidates: in particular, the benzofuroprymidinone XL413 is a selective inhibitor, able to arrest cell cycle and inhibit tumor growth in a Colo-2015 xenograft model (Koltun et al., 2012); pyridinyl-pyrrole derivative compounds (such as PHA-767491) have antitumor activity on glioblastoma, pancreatic cancer, breast cancer and other tumors (Erbayraktar et al., 2016; Montagnoli et al., 2008; Natoni et al., 2011; Sasi et al., 2017).

#### SLC25A40

SLC25A40 belongs to the solute carrier 25 (SLC25) nuclear-encoded protein family residing on mitochondrial membranes, and in some cases in other organelle membranes, and protects mitochondria from oxidative stress (Palmieri, 2013). These proteins are widely expressed in eukaryotic cells and they possess conserved structural features as, a tripartite structure, six hydrophobic transmembrane  $\alpha$ -helices and a 3-fold repeated signature motif. Members of this family can vary by the nature and size of the transported substrates, for the modes of transport and driving force (Palmieri, 2013).

SLC25A40 mRNA and SLC25A40 protein are highly expressed in brain and central nervous system (Haitina et al., 2006). Valach and coworkers reported a relationship between SLC25A40 overexpression and tumorigenesis, and they found it to be also activated in cancer-associated fibroblasts (Valach et al., 2012).

SLC25A40 was reported to be overexpressed in drug-resistant cancer cell (Hansen et al., 2016), and an *ABCBI*-SLC25A40 fused transcript product was observed in resistant ovarian cancer cells (Patch et al., 2015); its precise role in MDR has not been fully elucidated yet.

#### RUNDC3B (RPIP9)

RUNDC3B (RUN domain-containing protein 3B) function has not been determined yet, but it is known to contain a RUN domain used to interact with RAP2 (explaining the alternative name RAP2 binding-protein 9, RPIP9), a RAS-protein involved in the MAPK cascade. RUNDC3B also contains a binding site for MAPK signaling pathway intermediates, being in the middle between RAP2 and MAPK pathway, thus it is likely to be involved in the RAS-like GTPase signaling pathway (Burmeister et al., 2017; Finalet Ferreiro et al., 2014).

Both RUNDC3B isoforms are highly expressed in brain tissue; RUNDC3B is activated in tumorigenic breast cancer cell lines and in the breast cancer primary tumor (Raguz et al., 2005).

*RUNDC3B* is in the same amplicon of *ABCBI* and is transcribed from the complementary DNA strand of the *ABCBI* gene (Fig. 5); it may interfere with alternative regulation of *ABCBI* promoter regulation. Treatment with histone deacetylases inhibitors (iHDACs) of colon and pancreatic carcinomas results in an increased expression of *ABCBI* and *RUNDC3B* mRNAs (Balaguer et al., 2012). In addition, both *ABCBI* and *RUNDC3B* overexpression was found in breast cancer cells compared to normal tissues, with a correlation between this overexpression and poor prognosis in breast cancer (Raguz et al., 2005).

Integrative genomic studies report an increased expression of *RUNDC3B* in paclitaxel-resistant ovarian cancer cells (Januchowski et al., 2017) and a correlation between tumor growth advantage and chemoresistance in hepatosplenic T-cell lymphoma where a gain of chromosome 7q arm corresponds to an up-regulation of *RUNDC3B* (Finalet Ferreiro et al., 2014).

#### *ABCBA* (*PGY3*, *MDR3*)

*ABCBA*, a member of ABC transporters, is encoded by the *ABCBA* (*MDR3*) gene, and is an ATP-dependent phospholipid efflux translocator and a positive regulator of biliary lipid secretion, acting as a phospholipid flippase which translocates phosphatidylcholine (PC) from liver hepatocytes into bile, thus being essential for bile formation. It can also influence the composition of lipids of the plasma membrane, recruiting PC, phosphatidylethanolamine (PE) and sphingomyelin (SM) towards non-raft membrane domain or contributing to cholesterol and SM-enrichment in raft membranes in hepatocytes (Morita and Terada, 2014). *ABCBA* cooperates with ATP8B1 to protect hepatocytes from the detergent activity of bile salts (Groen et al., 2011).

*ABCBA* and *ABCBI* belong to ABC transporters superfamily, and are encoded by fused genes, arising from an endoduplication event, and often co-amplified because of their genomic proximity (about 500 Kb); they share 80% nucleotide sequence identity, and 77% identity and 82% similarity in the amino acidic sequence (Callen et al., 1987; Torigoe et al., 1995; Van der Bliet et al., 1987; Van der Bliet et al., 1988).

*ABCBA* is well expressed in the liver; its substrates are PC and some hydrophobic drugs, while in MDR cells *ABCBA* is particularly selective for paclitaxel and vinblastine (Gottesman et al., 2002; Thomas and Coley, 2003). *ABCBA* is co-amplified with *ABCBI* in several MDR cancer cell lines. In doxorubicin-resistant colon cancer cell lines, its mRNA is up-regulated up to 40-fold compared to parental cell lines, and this amplification is possibly due to the concomitant amplification of the *ABCBI* gene (Chao et al., 1991). A dose-dependent increase in *ABCBI* and *ABCBA* levels is observed in doxorubicin-, paclitaxel- and vincristine-resistant cancer cell lines upon drug selection; further, in some of these tumor cell lines, up-regulation of *ABCBA* was higher than that of *ABCBI*, suggesting a compensatory mechanism in drug resistance when *ABCBI* is not overexpressed, and an active role for *ABCBA* in MDR, driven preferentially towards doxorubicin and paclitaxel (Januchowski et al., 2017; Januchowski et al., 2014a; Januchowski et al., 2014b).

The increased mRNA and protein levels of *ABCBA* along with those of *ABCBI* in acquired paclitaxel-resistant breast cancer cells highlights a role of *ABCBA* in taxane resistance, since it was shown that directed siRNA silencing towards *ABCBI* did not restore the complete paclitaxel



sensitivity in these cancer cell lines co-overexpressing both *ABCB1* and *ABCB4* (Nemcova-Furstova et al., 2016). This matter is still conflicting, as while *ABCB4* silencing in paclitaxel-resistant ovarian cancer cells does not fully restore drug sensitivity, *ABCB1* silencing completely reverses MDR (Duan et al., 2004a). However, it seems that transcriptional regulation of *ABCB4* gene expression relies mostly on *ABCB1* co-amplification; nevertheless, *ABCB4* has a role in drug resistance, preferentially in taxanes, hence complementing the protective role of *ABCB1* against various MDR type anticancer drugs

#### CROT

Carnitine *O*-octanoyltransferase is a peroxisomal protein that plays a role in lipid metabolism and fatty-acid beta-oxidation. DNA copy increase and increased expression of CROT, together with that of other proteins of the 7q21.11-13 chromosomal region, was observed upon progressive administration of paclitaxel and docetaxel to 18 ovarian cancer cell lines (Wang et al., 2006), and of docetaxel to the MCF-7 breast cancer cell line (Hansen et al., 2016). MiR-33 co-downregulates the expression of ABC transporters and CROT (Fernandez-Hernando et al., 2011).

#### *TP53TG1* lncRNA

*TP53TG1* is a p53-induced lncRNA, which is activated upon DNA damage and acts as a tumor suppressor, contributing to p53 response to DNA damage (Diaz-Lagares et al., 2016). It was reported to bind YBX1 DNA/RNA binding protein, preventing its nuclear localization and subsequent activation of oncogenes (Diaz-Lagares et al., 2016). The first evidence of its down-regulation came from microarray experiments performed on A549 cisplatin-resistant lung cancer cell lines (Yang et al., 2013). In colorectal cancer cells the *TP53TG1* promoter undergoes a hypermethylation that causes the release of the YBX1 protein and subsequent transcription of oncogenes, resulting in an MDR phenotype (Lizarbe et al., 2017). The same findings were reported by Diaz-Lagares and coworkers in other cancer cell lines (Diaz-Lagares et al., 2016).

Beside the epigenetic inactivation of *TP53TG1* transcription, its upregulation has been reported in T lymphocytes exposed to ionizing radiations, in colon cancer cells treated with bleomycin or cisplatin and in docetaxel-resistant breast cancer cells (Hansen et al., 2016; Kabacik et al., 2015; Takei et al., 1998). *TP53TG1* is the first lncRNA activated upon induction of double strand breaks (DSBs), confirming its activation upon cell stress and DNA damage (Kabacik et al., 2015). Additionally, overexpression of *TP53TG1* has been observed in glioma cells, compared to normal brain tissue. This up-regulation results in cell proliferation and migration, especially under glucose deprivation (Chen et al., 2017). Cellular *TP53TG1* lncRNA expression is up-regulated under stress conditions (and in docetaxel-resistant breast cancer cells), but its promoter can be epigenetically silenced in cancer cells leading to the development of MDR, suggesting a role in the development of intrinsic MDR.

#### *TMEM243* (MM-TRAG, or *MGC4175*)

*TMEM243* (MDR1- and mitochondrial taxol resistance-associated protein transmembrane protein 243) is a transmembrane protein that localizes at nuclei, mitochondria and cell membrane; it is expressed in all tissues with no reported differences between normal tissues and chemotherapy naïve cancer cells (Duan et al., 2004b), and is overexpressed in taxane-resistant ovarian cancer cells (Wang et al., 2006), a possible indication of a role in acquired MDR.

Microarray experiments reported an up-regulation in taxol- and doxorubicin-resistant cancer cell lines, compared to the non-treated cancer cells. Under these conditions, *TMEM243* is present as a single copy gene, and its overexpression is not due to genomic amplification or gene rearrangements (Duan et al., 2004b), suggesting a mechanism of acquired MDR. Furthermore its expression has been reported as associated with paclitaxel resistance in drug-resistant breast cancer cells (Dorman et al., 2016) and in doxorubicin-resistant osteosarcoma cell

lines, where microarray and qPCR experiments showed a 2-fold upregulation (Rajkumar and Yamuna, 2008).

#### *DMTF1* (*DMP1*)

*DMTF1* (Cyclin-D binding myb-like transcription factor 1) is a transcriptional activator of *CDN2A/ARF* locus in response to RAS-RAF signaling promoting cell growth arrest p53-mediated. It binds to ARF activating its transcription and stimulating p53 quenching with oncogenic signaling pathways (RAS, HER2neu, C-MYC, cyclin D), thus acting as an oncosuppressor (Frazier et al., 2012; Fry et al., 2016). *DMTF1* contains a cyclin D-binding domain, three central myb or myb-like domains, and two flanking acidic transactivation domains. The structure of the N-terminal, myb-like domain of *DMTF1* has been solved by NMR (PDB accession code: 2LLK). In *DMTF1*, myb-like domains are able to bind both DNA and proteins. *DMTF1* physically interacts with p53, preventing its ubiquitination by Mdm2, thus promoting nuclear localization of p53 (Frazier et al., 2012; Kendig et al., 2017). *DMTF1* is highly expressed in terminally differentiated cells and experimental evidence showed that in hematopoietic cell lines, its repression occurred by WT1, which is expressed only in hematopoietic progenitors, thereby leading to leukemia (Tschan et al., 2008). Furthermore *DMTF1* mRNA is decreased in AML cell lines compared to normal granulocytes and treatment with ATRA restored normal levels of the *DMTF1* transcript (Inoue and Fry, 2016).

Van Dekken and collaborators reported a high level of amplification of genes residing on the 7q chromosome region in adenocarcinoma of the gastroesophageal junction, including *DMTF1* (van Dekken et al., 2006). Acquisition of docetaxel resistance in breast cancer cells correlates with overexpression of *DMTF1*, together with that of other proteins of the *ABCB1* amplicon (Hansen et al., 2016). On the other hand, the human *DMTF1* gene appears to be deleted in 40% of human non-small-cell lung carcinoma (NSCLC), that generally have normal levels of ARF and p53 (Sugiyama et al., 2008); corroborating results reported that *DMTF1* deletion in breast cancer cell lines brings about features of tumor aggressiveness renders p53 inactive (Fry et al., 2017). In addition, *DMTF1* transcription is repressed upon anthracycline treatment, thus leading to NF-kappaB-dependent repression of the Arf-p53 pathway; both *DMTF1*(-/-) and *ARF*(-/-) cells are anthracycline-resistant (Taneja et al., 2007).

Other researchers reported that *DMTF1* deletion cooperates with KRAS signaling for the development of cancer *in vivo*, and confirmed that it acts as a primary regulator of lung carcinogenesis, being a regulator of ARF-p53 pathway (Mallakin et al., 2007).

It has been observed that this deletion brings a consequent loss of *DMTF1* and leads to tumorigenesis in a mouse model as well; it has been noted that *DMTF1*(+/-) mice, harboring a copy of the gene, still developed tumors, suggesting a *DMTF1* haploinsufficiency (Inoue et al., 2007). The hemizygous copy of *DMTF1* gene is found at high frequency in breast cancer cells (Maglic et al., 2015), undergoing a fine post-transcriptional regulation. Indeed its mRNA is alternatively spliced to three variants ( $\alpha, \beta, \gamma$ ) that can exert different functions (Inoue and Fry, 2016). *DMTF1 $\gamma$*  has an unknown function, but interestingly  $\alpha$  and  $\beta$  variants have two divergent functions; in breast cancer, the  $\alpha$  variant is p53-dependent and acts as a tumor suppressor, whereas the  $\beta$  variant is p53-independent and acts as an oncogene. Furthermore, *DMTF1*  $\beta/\alpha$  ratio increases with neoplastic transformation, and high  $\beta$  variant expression is associated with a shorter survival rate in cancer. *DMTF1 $\beta$*  was also found overexpressed in primary breast cancer, with a negative impact on patients survival, and it does not activate ARF, suggesting that the  $\beta$  variant may antagonize  $\alpha$ 's dependent ARF activation, leading to cell proliferation and tumorigenesis (Inoue and Fry, 2016). Alternative splicing of *DMTF1* transcript is a way for cancer cells to modulate survival and proliferation since it has been observed that 30% of breast cancer cells have higher amounts of  $\beta$  rather than  $\alpha$ , and that the  $\beta$  mRNA is 43–55% higher in breast cancer while the  $\beta$  protein is increased by 60% in tumors, suggesting a fine post-transcriptional



regulation (Maglic et al., 2015). The DMTF1 $\beta$  variant can be thus considered a cancer biomarker, and proteins that activate the *DMTF1* promoter or stabilize the DMTF1 $\alpha$  variant, lead to regression of tumor growth *in vitro* (Fry et al., 2017).

Another strategy of post-transcriptional regulation of the *DMTF1* gene is exerted by miR-155, an oncogenic microRNA. In bladder cancer tissues miR-155 reduces the expression of DMTF1, leading to cell cycle progression and enhancement of cancer cell growth (Peng et al., 2015).

DMTF1 expression regulation in cancer mainly relies on gene deletion, since it is generally considered as a haploinsufficient tumor suppressor, and also on post-transcriptional regulation that leads to its down-regulation, even though alternative splicing plays an intriguing role in the up-regulation of the oncogenic DMTF1 variant (Inoue and Fry, 2016).

### Future perspectives

The idea of *ABCB1* as a major player in MDR is now outdated, and 4 generations of *ABCB1* transport inhibitors have been unexpectedly and disappointingly ineffective in the clinic. Emerging contributions to MDR in tumors continue to increase, and resistance to chemotherapeutic drugs is now considered a complicated puzzle, with an ever-increasing number of pieces, involved in many different functions, with complex and intricate connections, acting at multiple regulatory levels. Even at the single level of *ABCB1* expression, the co-amplification and/or co-expression of genes of chromosome 7q21 residing on the same amplicon is emerging as a factor that contributes and modulates MDR.

The contribution of *TP53TG1 lncRNA*, *TMEM243*, *SLC25A40*, *RUNDC3B*, *ADAM22*, and in particular of *SRI*, *ABCB4*, *DMTF1* and *DBF4* is now acknowledged as an important determinant of MDR. Deciphering their functions could pave the way for the development of novel clinically relevant strategies for therapeutic interventions in cancer. In addition, gene-targeting and expression modulation strategies, e.g. by the use of epigenetic drugs, non-coding RNAs or natural products can represent possible options, both for the improvement of the knowledge of the molecular basis of MDR and for drug discovery. CDC7-DBF4 inhibitors are already available and are considered good potential anti-tumor drug candidates: PHA-767491 and XL413 are selective inhibitors, with good antitumor activity vs. several tumors, such as glioblastoma, pancreatic cancer, colon and breast cancer (Erbayraktar et al., 2016; Montagnoli et al., 2008; Natoni et al., 2011; Sasi et al., 2017). The use of combined administration of drugs targeting *ABCB1*, Sorcin and CDC7-DBF4 could prove a viable and more effective therapeutic strategy against MDR tumors.

### Conclusions

MDR continues to pose a dominant obstacle towards curative chemotherapy against various human cancers. ATP-driven efflux pumps, *ABCB1* in particular, are responsible for drug expulsion and have a significant role in conferring MDR upon various cancer cells, that develop cross-resistance to diverse anticancer drugs, resulting in the failure of chemotherapy in multiple malignancies (Ambudkar et al., 1999; Fletcher et al., 2016; Holohan et al., 2013; Li et al., 2016b; Sharom, 2011; Silva et al., 2015). Overexpression of *ABCB1* in tumors, particularly upon chemotherapeutic treatment, is possibly the major cause of treatment failure; notwithstanding the design of 4 generations of *ABCB1* transport inhibitors and the wealth of information on the biochemistry and substrate specificity of ABC transporters, translation of this knowledge from the bench to the bedside has proved to be unexpectedly difficult.

Many studies have shown that upon repeated treatment of cultured tumor cell lines with a plethora of anticancer drugs including for example taxenes, anthracyclines, *Vinca* alkaloids, epipodophyllotoxins and other chemotherapeutic drugs, amplification, and/or overexpression of a series of genes surrounding the genomic *ABCB1* locus is

observed; altered levels of these proteins may correlate with the establishment of the MDR phenotype, and lead to poor clinical outcome. Genes in the *ABCB1* amplicon (with the exception of the tumor suppressor *TP53TG1 lncRNA*) were generally up-regulated in many cancers, and especially in MDR tumors; all of these genes are directly involved in tumor growth and drug resistance and finely regulated in various modes, from canonical transcriptional upregulation to epigenetic and post-transcriptional control.

The genes in the *ABCB1* amplicon exert important roles for cell survival in cancer or MDR status, as p53-mediators of cell growth arrest (*TP53TG1* and *DMTF1*), cell cycle or cell proliferation regulators (*DBF4* and *ADAM22*), mediators of signaling pathways (*RUNDC3B*), mitochondrial transmembrane proteins (*SLC25A40* and *TMEM243*), ATP-driven pumps (*ABCB4*) or calcium and xenobiotic sensors (Sorcin). In particular, Sorcin is able to limit the cytotoxic activity of chemotherapeutic agents in tumor cells and to confer MDR via three known mechanisms: by direct binding to chemotherapeutic drugs as well as its overexpression on the one hand induces *ABCB1* overexpression and on the other hand activates pathways leading to EMT and metastasis.

In conclusion, the gain of knowledge about these genes and their role in cancer and chemoresistance can possibly pave the way towards the development of novel biomarkers as well as offer important information on tumorigenesis and MDR mechanisms. A possible strategy to overcome MDR in cancer could be by considering the targeting of these proteins, which are often co-overexpressed along with *ABCB1* in MDR tumors, and can be used as biomarkers of poor cancer patient outcome.

### Acknowledgements

Financial support: Italian Association for Cancer Research (AIRC) StG 4841; FILAS-RU-2014-1020; Sapienza University of Rome “Progetti di Ateneo” to F.F.; Ministry of Health RF-2010-2309790; MIUR PRIN20154JRJPP; CNR Nanomax “NADINE” “Nanotechnology-based Diagnostics In Neurological diseases and Experimental oncology”, CNCCS CNR, InterOmics Synlether CNR, PNR-CNR Aging Program 2012–2014 to G.C.

### References

- Abe, T., Mori, T., Wakabayashi, Y., Nakagawa, M., Cole, S.P., Koike, K., Kuwano, M., Hori, S., 1998. Expression of multidrug resistance protein gene in patients with glioma after chemotherapy. *J. Neurooncol.* 40, 11–18.
- Abolhoda, A., Wilson, A.E., Ross, H., Danenberg, P.V., Burt, M., Scotto, K.W., 1999. Rapid activation of MD R1 gene expression in human metastatic sarcoma after *in vivo* exposure to doxorubicin. *Clin. Cancer Res.* 5, 3352–3356.
- Abuznait, A.H., Patrick, S.G., Kaddoumi, A., 2011a. Exposure of LS-180 cells to drugs of diverse physicochemical and therapeutic properties up-regulates P-glycoprotein expression and activity. *J. Pharm. Pharm. Sci.* 14, 236–248.
- Abuznait, A.H., Qosa, H., O’Connell, N.D., Akbarian-Tefaghi, J., Sylvester, P.W., El Sayed, K.A., Kaddoumi, A., 2011b. Induction of expression and functional activity of P-glycoprotein efflux transporter by bioactive plant natural products. *Food Chem. Toxicol.* 49, 2765–2772.
- Advani, R., Fisher, G.A., Lum, B.L., Hausdorff, J., Halsey, J., Litchman, M., Sikic, B.I., 2001. A phase I trial of doxorubicin, paclitaxel, and valspodar (PSC 833), a modulator of multidrug resistance. *Clin. Cancer Res.* 7, 1221–1229.
- Advani, R., Lum, B.L., Fisher, G.A., Halsey, J., Chin, D.L., Jacobs, C.D., Sikic, B.I., 2005. A phase I trial of liposomal doxorubicin, paclitaxel and valspodar (PSC-833), an inhibitor of multidrug resistance. *Ann. Oncol.* 16, 1968–1973.
- Akhtar, N., Ahad, A., Khar, R.K., Jaggi, M., Aqil, M., Iqbal, Z., Ahmad, F.J., Talegaonkar, S., 2011. The emerging role of P-glycoprotein inhibitors in drug delivery: a patent review. *Expert Opin. Ther. Patents* 21, 561–576.
- Al-Hajji, M., Becker, M.W., Wicha, M., Weissman, I., Clarke, M.F., 2004. Therapeutic implications of cancer stem cells. *Curr. Opin. Genet. Dev.* 14, 43–47.
- Alizadeh, A.A., Aranda, V., Bardelli, A., Blanpain, C., Bock, C., Borowski, C., Caldas, C., Califano, A., Doherty, M., Elsner, M., Esteller, M., Fitzgerald, R., Korbil, J.O., Lichter, P., Mason, C.E., Navin, N., Pe’er, D., Polyak, K., Roberts, C.W., Siu, L., Snyder, A., Stower, H., Swanton, C., Verhaak, R.G., Zenklusen, J.C., Zuber, J., Zucman-Rossi, J., 2015. Toward understanding and exploiting tumor heterogeneity. *Nat. Med.* 21, 846–853.
- Aller, S.G., Yu, J., Ward, A., Weng, Y., Chittaboina, S., Zhuo, R., Harrell, P.M., Trinh, Y.T., Zhang, Q., Urbatsch, I.L., Chang, G., 2009. Structure of P-glycoprotein reveals a molecular basis for poly-specific drug binding. *Science* 323, 1718–1722.

- Ambudkar, S.V., Dey, S., Hrycyna, C.A., Ramachandra, M., Pastan, I., Gottesman, M.M., 1999. Biochemical, cellular, and pharmacological aspects of the multidrug transporter. *Annu. Rev. Pharmacol. Toxicol.* 39, 361–398.
- Anderle, P., Niederer, E., Rubas, W., Hilgendorf, C., Spahn-Langguth, H., Wunderli-Allenspach, H., Merkle, H.P., Langguth, P., 1998. P-Glycoprotein (P-gp) mediated efflux in Caco-2 cell monolayers: the influence of culturing conditions and drug exposure on P-gp expression levels. *J. Pharm. Sci.* 87, 757–762.
- Andor, N., Graham, T.A., Jansen, M., Xia, L.C., Aktipis, C.A., Petritsch, C., Ji, H.P., Maley, C.C., 2016. Pan-cancer analysis of the extent and consequences of intratumor heterogeneity. *Nat. Med.* 22, 105–113.
- Aquilante, C.L., Letrent, S.P., Pollack, G.M., Brouwer, K.L., 2000. Increased brain P-glycoprotein in morphine tolerant rats. *Life Sci.* 66, 147–PL51.
- Arias, A., Rigalli, J.P., Villanueva, S.S., Ruiz, M.L., Luquita, M.G., Perdomo, V.G., Vore, M., Catania, V.A., Mottino, A.D., 2014. Regulation of expression and activity of multidrug resistance proteins MRP2 and MDR1 by estrogenic compounds in Caco-2 cells. Role in prevention of xenobiotic-induced cytotoxicity. *Toxicology* 320, 46–55.
- Arnau, O., Koubeissi, A., Ettouati, L., Terreux, R., Alame, G., Grenot, C., Dumontet, C., Di Pietro, A., Paris, J., Falson, P., 2010. Potent and fully noncompetitive peptidomimetic inhibitor of multidrug resistance P-glycoprotein. *J. Med. Chem.* 53, 6720–6729.
- Arrigoni, E., Galimberti, S., Petrini, M., Danesi, R., Di Paolo, A., 2016. ATP-binding cassette transmembrane transporters and their epigenetic control in cancer: an overview. *Expert Opin. Drug Metab. Toxicol.* 12, 1419–1432.
- Assaraf, Y.G., Borgnia, M.J., 1994. Probing the interaction of the multidrug-resistance phenotype with the polypeptide ionophore gramicidin D via functional channel formation. *Eur. J. Biochem./FEBS* 222, 813–824.
- Assaraf, Y.G., Molina, A., Schimke, R.T., 1989a. Cross-resistance to the lipid-soluble antifolate trimetrexate in human carcinoma cells with the multidrug-resistant phenotype. *J. Natl. Cancer Inst.* 81, 290–294.
- Assaraf, Y.G., Molina, A., Schimke, R.T., 1989b. Sequential amplification of dihydrofolate reductase and multidrug resistance genes in Chinese hamster ovary cells selected for stepwise resistance to the lipid-soluble antifolate trimetrexate. *J. Biol. Chem.* 264, 18326–18334.
- Atalay, C., Deliloglu Gurhan, I., Irkkan, C., Gunduz, U., 2006. Multidrug resistance in locally advanced breast cancer. *Tumour Biol.* 27, 309–318.
- Baker, E.K., Johnstone, R.W., Zalberg, J.R., El-Osta, A., 2005. Epigenetic changes to the MD R1 locus in response to chemotherapeutic drugs. *Oncogene* 24, 8061–8075.
- Balaguer, T.M., Gomez-Martinez, A., Garcia-Morales, P., Lacueva, J., Calpena, R., Ververte, L.R., Riquelme, N.L., Martinez-Lacaci, I., Ferragut, J.A., Saceda, M., 2012. Dual regulation of P-glycoprotein expression by trichostatin A in cancer cell lines. *BMC Mol. Biol.* 13, 25.
- Bao, L., Hazari, S., Mehra, S., Kaushal, D., Moroz, K., Dash, S., 2012. Increased expression of P-glycoprotein and doxorubicin chemoresistance of metastatic breast cancer is regulated by miR-298. *Am. J. Pathol.* 180, 2490–2503.
- Bar-Zeev, M., Assaraf, Y.G., Livney, Y.D., 2016. beta-casein nanovehicles for oral delivery of chemotherapeutic Drug combinations overcoming P-glycoprotein-mediated multidrug resistance in human gastric cancer cells. *Oncotarget* 7, 23322–23334.
- Bar-Zeev, M., Livney, Y.D., Assaraf, Y.G., 2017. Targeted nanomedicine for cancer therapeutics: towards precision medicine overcoming drug resistance. *Drug Resist. Updates: Rev. Comment. Antimicrob. Anticancer Chemother.* 31, 15–30.
- Barkley, L.R., Santocanale, C., 2013. MicroRNA-29a regulates the benzo[a]pyrene dihydrodiol epoxide-induced DNA damage response through Cdc7 kinase in lung cancer cells. *Oncogenesis* 2, e57.
- Bates, S.E., Mickley, L.A., Chen, Y.N., Richert, N., Rudick, J., Biedler, J.L., Fojo, A.T., 1989. Expression of a drug resistance gene in human neuroblastoma cell lines: modulation by retinoic acid-induced differentiation. *Mol. Cell. Biol.* 9, 4337–4344.
- Bates, S., Kang, M., Meadows, B., Bakke, S., Choyke, P., Merino, M., Goldspiel, B., Chico, I., Smith, T., Chen, C., Robey, R., Bergan, R., Figg, W.D., Fojo, T., 2001. A Phase I study of infusional vinblastine in combination with the P-glycoprotein antagonist PSC 833 (valsopodar). *Cancer* 92, 1577–1590.
- Bauer, K.S., Karp, J.E., Garimella, T.S., Wu, S., Tan, M., Ross, D.D., 2005. A phase I and pharmacologic study of idarubicin, cytarabine, etoposide, and the multidrug resistance protein (MDR1/Pgp) inhibitor PSC-833 in patients with refractory leukemia. *Leuk. Res.* 29, 263–271.
- Bauer, B., Yang, X., Hartz, A.M., Olson, E.R., Zhao, R., Kalvass, J.C., Pollack, G.M., Miller, D.S., 2006. In vivo activation of human pregnane X receptor tightens the blood-brain barrier to methadone through P-glycoprotein up-regulation. *Mol. Pharmacol.* 70, 1212–1219.
- Bell, S.E., Quinn, D.M., Kellett, G.L., Warr, J.R., 1998. 2-Deoxy-D-glucose preferentially kills multidrug-resistant human KB carcinoma cell lines by apoptosis. *Br. J. Cancer* 78, 1464–1470.
- Bharate, J.B., Batarseh, Y.S., Wani, A., Sharma, S., Vishwakarma, R.A., Kaddoumi, A., Kumar, A., Bharate, S.B., 2015. Synthesis and P-glycoprotein induction activity of colupulone analogs. *Org. Biomol. Chem.* 13, 5488–5496.
- Biemans-Oldehinkel, E., Doeven, M.K., Poolman, B., 2006. ABC transporter architecture and regulatory roles of accessory domains. *FEBS Lett.* 580, 1023–1035.
- Bihorel, S., Camenisch, G., Lemaire, M., Scherrmann, J.M., 2007. Modulation of the brain distribution of imatinib and its metabolites in mice by valsopodar, zosuquidar and elacridar. *Pharm. Res.* 24, 1720–1728.
- Bitarte, N., Bandres, E., Boni, V., Zarate, R., Rodriguez, J., Gonzalez-Huarriz, M., Lopez, I., Javier Sola, J., Alonso, M.M., Fortes, P., Garcia-Foncillas, J., 2011. MicroRNA-451 is involved in the self-renewal, tumorigenicity, and chemoresistance of colorectal cancer stem cells. *Stem Cells* 29, 1661–1671.
- Blandino, G., Fazi, F., Donzelli, S., Kedmi, M., Sas-Chen, A., Muti, P., Strano, S., Yarden, Y., 2014. Tumor suppressor microRNAs: a novel non-coding alliance against cancer. *FEBS Lett.* 588, 2639–2652.
- Bolger, J.C., Young, L.S., 2013. ADAM22 as a prognostic and therapeutic drug target in the treatment of endocrine-resistant breast cancer. *Vitam. Horm.* 93, 307–321.
- Bonte, D., Lindvall, C., Liu, H., Dykema, K., Furge, K., Weinreich, M., 2008. Cdc7-Dbf4 kinase overexpression in multiple cancers and tumor cell lines is correlated with p53 inactivation. *Neoplasia* 10, 920–931.
- Borgnia, M.J., Eytan, G.D., Assaraf, Y.G., 1996. Competition of hydrophobic peptides, cytotoxic drugs, and chemosensitizers on a common P-glycoprotein pharmacophore as revealed by its ATPase activity. *J. Biol. Chem.* 271, 3163–3171.
- Bourhis, J., Goldstein, L.J., Riou, G., Pastan, I., Gottesman, M.M., Benard, J., 1989. Expression of a human multidrug resistance gene in ovarian carcinomas. *Cancer Res.* 49, 5062–5065.
- Bram, E.E., Stark, M., Raz, S., Assaraf, Y.G., 2009. Chemotherapeutic drug-induced ABCG2 promoter demethylation as a novel mechanism of acquired multidrug resistance. *Neoplasia* 11, 1359–1370.
- Broxterman, H.J., Sonneveld, P., Pieters, R., Lankelma, J., Eekman, C.A., Loonen, A.H., Schoester, M., Ossenkoppele, G.J., Lowenberg, B., Pinedo, H.M., Schuurhuis, G.J., 1999. Do P-glycoprotein and major vault protein (MVP/LRP) expression correlate with in vitro daunorubicin resistance in acute myeloid leukemia? *Leukemia* 13, 258–265.
- Brugger, D., Brischwein, K., Liu, C., Bader, P., Niethammer, D., Gekeler, V., Beck, J.F., 2002. Induction of drug resistance and protein kinase C genes in A2780 ovarian cancer cells after incubation with antineoplastic agents at sublethal concentrations. *Anticancer Res.* 22, 4229–4232.
- Bruhn, O., Drerup, K., Kaehler, M., Haenisch, S., Roder, C., Cascorbi, I., 2016. Length variants of the ABCB1 3'-UTR and loss of miRNA binding sites: possible consequences in regulation and pharmacotherapy resistance. *Pharmacogenomics* 17, 327–340.
- Burger, H., Foekens, J.A., Look, M.P., Meijer-van Gelder, M.E., Klijn, J.G., Wiemer, E.A., Stoter, G., Nooter, K., 2003. RNA expression of breast cancer resistance protein, lung resistance-related protein, multidrug resistance-associated proteins 1 and 2, and multidrug resistance gene 1 in breast cancer: correlation with chemotherapeutic response. *Clin. Cancer Res.* 9, 827–836.
- Burmeister, D.W., Smith, E.H., Cristel, R.T., McKay, S.D., Shi, H., Arthur, G.L., Davis, J.W., Taylor, K.H., 2017. The expression of RUNDC3 B is associated with promoter methylation in lymphoid malignancies. *Hematol. Oncol.* 35, 25–33.
- Burt, R.K., Thorgerisson, S.S., 1988. Coincidence of MDR-1 multidrug-resistance and cytochrome P-450 genes in rat liver by xenobiotics. *J. Natl. Cancer Inst.* 80, 1383–1386.
- Callaghan, R., Crowley, E., Potter, S., Kerr, I.D., 2008. P-glycoprotein: so many ways to turn it on. *J. Clin. Pharmacol.* 48, 365–378.
- Callen, D.F., Baker, E., Simmers, R.N., Seshadri, R., Roninson, I.B., 1987. Localization of the human multiple drug resistance gene, MD R1, to 7q21.1. *Hum. Genet.* 77, 142–144.
- Cascorbi, I., 2006. Role of pharmacogenetics of ATP-binding cassette transporters in the pharmacokinetics of drugs. *Pharmacol. Ther.* 112, 457–473.
- Cerqueira, B.B., Lasham, A., Shelling, A.N., Al-Kassar, R., 2015. Nanoparticle therapeutics: technologies and methods for overcoming cancer. *Eur. J. Pharm. Biopharm.* 97, 140–151.
- Chan, H.S., Grogan, T.M., Haddad, G., DeBoer, G., Ling, V., 1997. P-glycoprotein expression: critical determinant in the response to osteosarcoma chemotherapy. *J. Natl. Cancer Inst.* 89, 1706–1715.
- Chan, G.N., Patel, R., Cummins, C.L., Bendayan, R., 2013. Induction of P-glycoprotein by antiretroviral drugs in human brain microvessel endothelial cells. *Antimicrob. Agents Chemother.* 57, 4481–4488.
- Chao, C.C., Ma, C.M., Lin-Chao, S., 1991. Co-amplification and over-expression of two mdr genes in a multidrug-resistant human colon carcinoma cell line. *FEBS Lett.* 291, 214–218.
- Chen, G.K., Lacayo, N.J., Duran, G.E., Wang, Y., Bangs, C.D., Rea, S., Kovacs, M., Cherry, A.M., Brown, J.M., Sikić, B.I., 2002. Preferential expression of a mutant allele of the amplified MD R1 (ABCB1) gene in drug-resistant variants of a human sarcoma. *Genes Chromosomes Cancer* 34, 372–383.
- Chen, K.G., Wang, Y.C., Schaner, M.E., Francisco, B., Duran, G.E., Juric, D., Huff, L.M., Padilla-Nash, H., Ried, T., Fojo, T., Sikić, B.I., 2005. Genetic and epigenetic modeling of the origins of multidrug-resistant cells in a human sarcoma cell line. *Cancer Res.* 65, 9388–9397.
- Chen, H.J., Zhu, Z., Wang, X.L., Feng, Q.L., Wu, Q., Xu, Z.P., Wu, J., Yu, X.F., Qian, H.L., Lu, Q., 2013a. Expression of huCdc7 in colorectal cancer. *World J. Gastroenterol.* 19, 3130–3133.
- Chen, Z., Ma, T., Huang, C., Zhang, L., Lv, X., Xu, T., Hu, T., Li, J., 2013b. MiR-27a modulates the MD R1/P-glycoprotein expression by inhibiting FZD7/beta-catenin pathway in hepatocellular carcinoma cells. *Cell. Signal.* 25, 2693–2701.
- Chen, X., Gao, Y., Li, D., Cao, Y., Hao, B., 2017. LncRNA-TP53TG1 participated in the stress response under glucose deprivation in glioma. *J. Cell. Biochem.* <http://dx.doi.org/10.1002/jcb.26175>.
- Cheng, A.N., Jiang, S.S., Fan, C.C., Lo, Y.K., Kuo, C.Y., Chen, C.H., Liu, Y.L., Lee, C.C., Chen, W.S., Huang, T.S., Wang, T.Y., Lee, A.Y., 2013. Increased Cdc7 expression is a marker of oral squamous cell carcinoma and overexpression of Cdc7 contributes to the resistance to DNA-damaging agents. *Cancer Lett.* 337, 218–225.
- Chico, M.H., Kang, R., Bergan, J., Abraham, S., Bakke, B., Meadows, A., Rutt, R., Robey, P., Choyke, M., Merino, B., Goldspiel, T., Smith, S., Steinberg, W.D., Figg, T., Fojo, S., Bates Phase, 2001. Phase I study of infusional paclitaxel in combination with the P-glycoprotein antagonist PSC 833. *J. Clin. Oncol.* 19, 832–842.
- Chieli, E., Romiti, N., Rodeiro, I., Garrido, G., 2010. In vitro modulation of ABCB1/P-glycoprotein expression by polyphenols from *Mangifera indica*. *Chem. Biol. Interact.* 186, 287–294.
- Chin, J.E., Soffir, R., Noonan, K.E., Choi, K., Roninson, I.B., 1989. Structure and expression of the human MD R (P-glycoprotein) gene family. *Mol. Cell. Biol.* 9, 3808–3820.

- Chin, K.V., Tanaka, S., Darlington, G., Pastan, I., Gottesman, M.M., 1990. Heat shock and arsenite increase expression of the multidrug resistance (MDR1) gene in human renal carcinoma cells. *J. Biol. Chem.* 265, 221–226.
- Choi, K.H., Chen, C.J., Krieger, M., Roninson, I.B., 1988. An altered pattern of cross-resistance in multidrug-resistant human cells results from spontaneous mutations in the *mdr1* (P-glycoprotein) gene. *Cell* 53, 519–529.
- Choschzick, M., Lebeau, A., Marx, A.H., Tharun, L., Terracciano, L., Heilenkotter, U., Jaenicke, F., Bokemeyer, C., Simon, R., Sauter, G., Schwarz, J., 2010. Overexpression of cell division cycle 7 homolog is associated with gene amplification frequency in breast cancer. *Hum. Pathol.* 41, 358–365.
- Chow, E.C., Durk, M.R., Cummins, C.L., Pang, K.S., 2011. 1 $\alpha$ , 25-dihydroxyvitamin D3 up-regulates P-glycoprotein via the vitamin D receptor and not farnesoid X receptor in both *fxr*(-/-) and *fxr*(+/+) mice and increased renal and brain efflux of digoxin in mice in vivo. *J. Pharmacol. Exp. Ther.* 337, 846–859.
- Clarke, L.E., Fontaine, T.J., Hennessy, J., Bruggeman, R.D., Clarke, J.T., Mauger, D.T., Helm, K.F., 2009. Cdc7 expression in melanomas, Spitz tumors and melanocytic nevi. *J. Cutan. Pathol.* 36, 433–438.
- Clifford, S.C., Neal, D.E., Lunec, J., 1996. Alterations in expression of the multidrug resistance-associated protein (MRP) gene in high-grade transitional cell carcinoma of the bladder. *Br. J. Cancer* 73, 659–666.
- Colabufo, N.A., Contino, M., Berardi, F., Perrone, R., Panaro, M.A., Cianciulli, A., Mitolo, V., Azzariti, A., Quatrone, A., Paradiso, A., 2011. A new generation of MDR modulating agents with dual activity: p-gp inhibitor and iNOS inducer agents. *Toxicol. In Vitro* 25, 222–230.
- Coley, H.M., 2010. Overcoming multidrug resistance in cancer: clinical studies of p-glycoprotein inhibitors. *Methods Mol. Biol.* 596, 341–358.
- Collett, A., Taniaris-Hughes, J., Warhurst, G., 2004. Rapid induction of P-glycoprotein expression by high permeability compounds in colonic cells in vitro: a possible source of transporter mediated drug interactions? *Biochem. Pharmacol.* 68, 783–790.
- Colotti, G., Poser, E., Fiorillo, A., Genovese, I., Chiarini, V., Ilari, A., 2014. Sorcin, a calcium binding protein involved in the multidrug resistance mechanisms in cancer cells. *Molecules* 19, 13976–13989.
- Cordon-Cardo, C., O'Brien, J.P., Casals, D., Rittman-Grauer, L., Biedler, J.L., Melamed, M.R., Bertino, J.R., 1989. Multidrug-resistance gene (P-glycoprotein) is expressed by endothelial cells at blood-brain barrier sites. *Proc. Natl. Acad. Sci. U. S. A.* 86, 695–698.
- Cordon-Cardo, C., O'Brien, J.P., Boccia, J., Casals, D., Bertino, J.R., Melamed, M.R., 1990. Expression of the multidrug resistance gene product (P-glycoprotein) in human normal and tumor tissues. *J. Histochem. Cytochem.* 38, 1277–1287.
- Cripe, L.D., Uno, H., Paietta, E.M., Litzow, M.R., Ketterling, R.P., Bennett, J.M., Rowe, J.M., Lazarus, H.M., Luger, S., Tallman, M.S., 2010. Zosuquidar, a novel modulator of P-glycoprotein, does not improve the outcome of older patients with newly diagnosed acute myeloid leukemia: a randomized, placebo-controlled trial of the Eastern Cooperative Oncology Group 3999. *Blood* 116, 4077–4085.
- Critchfield, J.W., Welsh, C.J., Phang, J.M., Yeh, G.C., 1994. Modulation of adriamycin accumulation and efflux by flavonoids in HCT-15 colon cells. Activation of P-glycoprotein as a putative mechanism. *Biochem. Pharmacol.* 48, 1437–1445.
- Crowe, A., Tan, A.M., 2012. Oral and inhaled corticosteroids: differences in P-glycoprotein (ABCBI) mediated efflux. *Toxicol. Appl. Pharmacol.* 260, 294–302.
- Cummins, C.L., Jacobsen, W., Benet, L.Z., 2002. Unmasking the dynamic interplay between intestinal P-glycoprotein and CYP3A4. *J. Pharmacol. Exp. Ther.* 300, 1036–1045.
- D'Abaco, G.M., Ng, K., Paradiso, L., Godde, N.J., Kaye, A., Novak, U., 2006. ADAM22, expressed in normal brain but not in high-grade gliomas, inhibits cellular proliferation via the disintegrin domain. *Neurosurgery* 58, 179–186 (discussion 179–186).
- Dabaghi, M., Rahgozar, S., Moshtaghan, J., Moafi, A., Abedi, M., Pourabutaleb, E., 2016. Overexpression of SORCIN is a prognostic biomarker for multidrug-resistant pediatric acute lymphoblastic leukemia and correlates with upregulated MD R1/P-gp. *Genet. Test. Mol. Biomarkers* 20, 516–521.
- Dantzig, A.H., Shepard, R.L., Law, K.L., Tabas, L., Pratt, S., Gillespie, J.S., Binkley, S.N., Kuhfeld, M.T., Starling, J.J., Wrighton, S.A., 1999. Selectivity of the multidrug resistance modulator, LY335979, for P-glycoprotein and effect on cytochrome P-450 activities. *J. Pharmacol. Exp. Ther.* 290, 854–862.
- Dantzig, A.H., Law, K.L., Cao, J., Starling, J.J., 2001. Reversal of multidrug resistance by the P-glycoprotein modulator, LY335979, from the bench to the clinic. *Curr. Med. Chem.* 8, 39–50.
- Davidson, A.L., Sharma, S., 1997. Mutation of a single MalK subunit severely impairs maltose transport activity in *Escherichia coli*. *J. Bacteriol.* 179, 5458–5464.
- Dawson, R.J., Locher, K.P., 2006. Structure of a bacterial multidrug ABC transporter. *Nature* 443, 180–185.
- Dean, M., 2005. The genetics of ATP-binding cassette transporters. *Methods Enzymol.* 400, 409–429.
- Dean, M., 2009. ABC transporters, drug resistance, and cancer stem cells. *J. Mammary Gland Biol. Neoplasia* 14, 3–9.
- Debatin, K.M., Krammer, P.H., 2004. Death receptors in chemotherapy and cancer. *Oncogene* 23, 2950–2966.
- Dejeux, E., Ronneberg, J.A., Solvang, H., Bukholm, I., Geisler, S., Aas, T., Gut, I.G., Borresen-Dale, A.L., Lonning, P.E., Kristensen, V.N., Tost, J., 2010. DNA methylation profiling in doxorubicin treated primary locally advanced breast tumours identifies novel genes associated with survival and treatment response. *Mol. Cancer* 9, 68.
- Demeule, M., Bossard, M., Beliveau, R., 1999. Cisplatin induces renal expression of P-glycoprotein and canalicular multispecific organic anion transporter. *Am. J. Physiol.* 277, F832–840.
- Deng, L., Lin-Lee, Y.C., Claret, F.X., Kuo, M.T., 2001. 2-acetylaminofluorene up-regulates rat *mdr1b* expression through generating reactive oxygen species that activate NF-kappa B pathway. *J. Biol. Chem.* 276, 413–420.
- Deng, L., Su, T., Leng, A., Zhang, X., Xu, M., Yan, L., Gu, H., Zhang, G., 2010. Upregulation of soluble resistance-related calcium-binding protein (sorcin) in gastric cancer. *Med. Oncol.* 27, 1102–1108.
- Dewanjee, S., Dua, T.K., Bhattacharjee, N., Das, A., Gangopadhyay, M., Khanra, R., Joardar, S., Riaz, M., Feo, V., Zia-Ul-Haq, M., 2017. Natural products as alternative choices for P-Glycoprotein (P-gp) inhibition. *Molecules* 22.
- Dexter, D.W., Reddy, R.K., Geles, K.G., Bansal, S., Myint, M.A., Rogakto, A., Leighton, J.C., Goldstein, L.J., 1998. Quantitative reverse transcriptase-polymerase chain reaction measured expression of MD R1 and MRP in primary breast carcinoma. *Clin. Cancer Res.* 4, 1533–1542.
- Diaz-Lagares, A., Crujeiras, A.B., Lopez-Serra, P., Soler, M., Setien, F., Goyal, A., Sandoval, J., Hashimoto, Y., Martinez-Cardus, A., Gomez, A., Heyn, H., Moutinho, C., Espada, J., Vidal, A., Paules, M., Galan, M., Sala, N., Akiyama, Y., Martinez-Iniesta, M., Farre, L., Villanueva, A., Gross, M., Diederichs, S., Guil, S., Esteller, M., 2016. Epigenetic inactivation of the p53-induced long noncoding RNA TP53 target 1 in human cancer. *Proc. Natl. Acad. Sci. U. S. A.* 113, E7535–E7544.
- Didziapetris, R., Japertas, P., Avdeef, A., Petrauskas, A., 2003. Classification analysis of P-glycoprotein substrate specificity. *J. Drug Target.* 11, 391–406.
- Dorman, S.N., Baranova, K., Knoll, J.H., Urquhart, B.L., Mariani, G., Carcangiu, M.L., Rogan, P.K., 2016. Genomic signatures for paclitaxel and gemcitabine resistance in breast cancer derived by machine learning. *Mol. Oncol.* 10, 85–100.
- Dorr, R., Karanes, C., Spier, C., Grogan, T., Greer, J., Moore, J., Weinberger, B., Schiller, G., Pearce, T., Litchman, M., Dalton, W., Roe, D., List, A.F., 2001. Phase I/II study of the P-glycoprotein modulator PSC 833 in patients with acute myeloid leukemia. *J. Clin. Oncol.* 19, 1589–1599.
- Drori, S., Eytan, G.D., Assaraf, Y.G., 1995. Potentiation of anticancer-drug cytotoxicity by multidrug-resistance chemosensitizers involves alterations in membrane fluidity leading to increased membrane permeability. *Eur. J. Biochem./FEBS* 228, 1020–1029.
- Duan, Z., Brakora, K.A., Seiden, M.V., 2004a. Inhibition of ABCB1 (MDR1) and ABCB4 (MDR3) expression by small interfering RNA and reversal of paclitaxel resistance in human ovarian cancer cells. *Mol. Cancer Ther.* 3, 833–838.
- Duan, Z., Brakora, K.A., Seiden, M.V., 2004b. MM-TRAG (MGCA175), a novel intracellular mitochondrial protein, is associated with the taxol- and doxorubicin-resistant phenotype in human cancer cell lines. *Gene* 340, 53–59.
- Duesberg, P., Li, R., Sachs, R., Fabarius, A., Upender, M.B., Hehlmann, R., 2007. Cancer drug resistance: the central role of the karyotype. *Drug Resist. Updates* 10, 51–58.
- Duncker, B.P., Shimada, K., Tsai-Pflugfelder, M., Pasero, P., Gasser, S.M., 2002. An N-terminal domain of Dbf4p mediates interaction with both origin recognition complex (ORC) and Rad53p and can deregulate late origin firing. *Proc. Natl. Acad. Sci. U. S. A.* 99, 16087–16092.
- El-Khoury, V., Breuzard, G., Fourre, N., Dufer, J., 2007. The histone deacetylase inhibitor trichostatin A downregulates human MD R1 (ABCB1) gene expression by a transcription-dependent mechanism in a drug-resistant small cell lung carcinoma cell line model. *Br. J. Cancer* 97, 562–573.
- El-Osta, A., Kantharidis, P., Zalberg, J.R., Wolffe, A.P., 2002. Precipitous release of methyl-CpG binding protein 2 and histone deacetylase 1 from the methylated human multidrug resistance gene (MDR1) on activation. *Mol. Cell. Biol.* 22, 1844–1857.
- Erbayraktar, Z., Alural, B., Erbayraktar, R.S., Erkan, E.P., 2016. Cell division cycle 7-kinase inhibitor PHA-767491 hydrochloride suppresses glioblastoma growth and invasiveness. *Cancer Cell Int.* 16, 88.
- Esser, L., Zhou, F., Pluchino, K.M., Shiloach, J., Ma, J., Tang, W.K., Gutierrez, C., Zhang, A., Shukla, S., Madigan, J.P., Zhou, T., Kwong, P.D., Ambudkar, S.V., Gottesman, M.M., Xia, D., 2017. Structures of the multidrug transporter P-glycoprotein reveal asymmetric ATP binding and the mechanism of polyspecificity. *J. Biol. Chem.* 292, 446–461.
- Eytan, G.D., Borgnina, M.J., Regev, R., Assaraf, Y.G., 1994. Transport of polypeptide ionophores into proteoliposomes reconstituted with rat liver P-glycoprotein. *J. Biol. Chem.* 269, 26058–26065.
- Fan, Y.P., Liao, J.Z., Lu, Y.Q., Tian, D.A., Ye, F., Zhao, P.X., Xiang, G.Y., Tang, W.X., He, X.X., 2017. MiR-375 and doxorubicin Co-delivered by liposomes for combination therapy of hepatocellular carcinoma. *Mol. Ther. Nucl. Acids* 7, 181–189.
- Fernandez-Hernando, C., Suarez, Y., Rayner, K.J., Moore, K.J., 2011. MicroRNAs in lipid metabolism. *Curr. Opin. Lipidol.* 22, 86–92.
- Feuerhake, F., Sigg, W., Hofer, E.A., Dimpfl, T., Welsch, U., 2000. Immunohistochemical analysis of Bcl-2 and Bax expression in relation to cell turnover and epithelial differentiation markers in the non-lactating human mammary gland epithelium. *Cell Tissue Res.* 299, 47–58.
- Finalet Ferreira, J., Rouhgharabaei, L., Urbankova, H., van der Krogt, J.A., Michaux, L., Shetty, S., Krenacs, L., Tousseyn, T., De Paep, P., Uyttebroeck, A., Verhoef, G., Taghon, T., Vandenberghe, P., Cools, J., Wlodarska, I., 2014. Integrative genomic and transcriptomic analysis identified candidate genes implicated in the pathogenesis of hepatosplenic T-cell lymphoma. *PLoS One* 9, e102977.
- Flahaut, M., Muhlethaler-Mottet, A., Martinet, D., Fattet, S., Boulroud, K.B., Auderset, K., Meier, R., Schmutz, N.B., Delattre, O., Joseph, J.M., Gross, N., 2006. Molecular cytogenetic characterization of doxorubicin-resistant neuroblastoma cell lines: evidence that acquired multidrug resistance results from a unique large amplification of the 7q21 region. *Genes Chromosomes Cancer* 45, 495–508.
- Fletcher, J.I., Haber, M., Henderson, M.J., Norris, M.D., 2010. ABC transporters in cancer: more than just drug efflux pumps. *Nat. Rev. Cancer* 10, 147–156.
- Fletcher, J.I., Williams, R.T., Henderson, M.J., Norris, M.D., Haber, M., 2016. ABC transporters as mediators of drug resistance and contributors to cancer cell biology. *Drug Resist. Updates* 26, 1–9.
- Fojo, T., Bates, S., 2003. Strategies for reversing drug resistance. *Oncogene* 22, 7512–7523.
- Fojo, A.T., Whang-Peng, J., Gottesman, M.M., Pastan, I., 1985. Amplification of DNA



- sequences in human multidrug-resistant KB carcinoma cells. *Proc. Natl. Acad. Sci. U. S. A.* 82, 7661–7665.
- Fojo, A.T., Ueda, K., Slamon, D.J., Poplack, D.G., Gottesman, M.M., Pastan, I., 1987. Expression of a multidrug-resistance gene in human tumors and tissues. *Proc. Natl. Acad. Sci. U. S. A.* 84, 265–269.
- Fox, E., Bates, S.E., 2007. Tariquidar (XR9576): a P-glycoprotein drug efflux pump inhibitor. *Expert Rev. Anticancer Ther.* 7, 447–459.
- Fracasso, G., Falvo, E., Colotti, G., Fazi, F., Ingegneri, T., Amalfitano, A., Doglietto, G.B., Alfieri, S., Boffi, A., Morea, V., Conti, G., Tremante, E., Giacomini, P., Arcovito, A., Ceci, P., 2016. Selective delivery of doxorubicin by novel stimuli-sensitive nanoferritins overcomes tumor refractoriness. *J. Controlled Release* 239, 10–18.
- Franceschini, A., Ilari, D., Verzili, C., Zamparelli, A., Antaramian, A., Rueda, H.H., Valdivia, E., Chiancone, G., 2008. Molecular basis for the impaired function of the natural P112L sorcin mutant: x-ray crystal structure, calcium affinity, and interaction with annexin VII and the ryanodine receptor. *FASEB J.* 22, 295–306.
- Frazier, D.P., Kendig, R.D., Kai, F., Maglic, D., Sugiyama, T., Morgan, R.L., Fry, E.A., Lagedrost, S.J., Sui, G., Inoue, K., 2012. Dmp1 physically interacts with p53 and positively regulates p53's stability, nuclear localization, and function. *Cancer Res.* 72, 1740–1750.
- Fry, E.A., Taneja, P., Inoue, K., 2016. Clinical applications of mouse models for breast cancer engaging HER2/neu. *Integr. Cancer Sci. Ther.* 3, 593–603.
- Fry, E.A., Taneja, P., Inoue, K., 2017. Oncogenic and tumor-suppressive mouse models for breast cancer engaging HER2/neu. *Int. J. Cancer* 140, 495–503.
- Fukata, Y., Adesnik, H., Iwanaga, T., Bredt, D.S., Nicoll, R.A., Fukata, M., 2006. Epilepsy-related ligand/receptor complex LGI1 and ADAM22 regulate synaptic transmission. *Science* 313, 1792–1795.
- Fung, A.D., Ou, J., Bueler, S., Brown, G.W., 2002. A conserved domain of *Schizosaccharomyces pombe* dfp1(+) is uniquely required for chromosome stability following alkylation damage during S phase. *Mol. Cell. Biol.* 22, 4477–4490.
- Furuya, K.N., Thottassery, J.V., Schuetz, E.G., Sharif, M., Schuetz, J.D., 1997. Bromocriptine transcriptionally activates the multidrug resistance gene (*pgp2/mdr1b*) by a novel pathway. *J. Biol. Chem.* 272, 11518–11525.
- Futscher, B.W., Foley, N.E., Gleason-Guzman, M.C., Meltzer, P.S., Sullivan, D.M., Dalton, W.S., 1996. Verapamil suppresses the emergence of P-glycoprotein-mediated multidrug resistance. *Int. J. Cancer* 66, 520–525.
- Ganguly, A., Basu, S., Chakraborty, P., Chatterjee, S., Sarkar, A., Chatterjee, M., Choudhuri, S.K., 2010. Targeting mitochondrial cell death pathway to overcome drug resistance with a newly developed iron chelate. *PLoS One* 5, e11253.
- Gant, T.W., Silverman, J.A., Thorgeirsson, S.S., 1992. Regulation of P-glycoprotein gene expression in hepatocyte cultures and liver cell lines by a trans-acting transcriptional repressor. *Nucleic Acids Res.* 20, 2841–2846.
- Gant, T.W., O'Connor, C.K., Corbitt, R., Thorgeirsson, U., Thorgeirsson, S.S., 1995. In vivo induction of liver P-glycoprotein expression by xenobiotics in monkeys. *Toxicol. Appl. Pharmacol.* 133, 269–276.
- Gao, Y., Li, W., Liu, X., Gao, F., Zhao, X., 2015. Reversing effect and mechanism of soluble resistance-related calcium-binding protein on multidrug resistance in human lung cancer A549/DDP cells. *Mol. Med. Rep.* 11, 2118–2124.
- Garofalo, M., Croce, C.M., 2013. MicroRNAs as therapeutic targets in chemoresistance. *Drug Resist. Updates* 16, 47–59.
- Gekeler, G., Frese, H., Diddens, H., 1988. Expression of a P-glycoprotein gene is inducible in a multidrug-resistant human leukemia cell line. *Biochem. Biophys. Res. Commun.* 155, 754–760.
- Genovese, I., Fiorillo, A., Ilari, A., Masciarelli, S., Fazi, F., Colotti, G., 2017. Binding of doxorubicin to Sorcin impairs cell death and increases drug resistance in cancer cells. *Cell. Death. Dis.* 8, e2950.
- Geretto, M., Pulliero, A., Rosano, C., Zhabayeva, D., Bersimbaev, R., Izzotti, A., 2017. Resistance to cancer chemotherapeutic drugs is determined by pivotal microRNA regulators. *Am. J. Cancer Res.* 7, 1350–1371.
- Goldstein, L.J., Galski, H., Fojo, A., Willingham, M., Lai, S.L., Gazdar, A., Pirker, R., Green, A., Crist, W., Brodeur, G.M., et al., 1989. Expression of a multidrug resistance gene in human cancers. *J. Natl. Cancer Inst.* 81, 116–124.
- Goler-Baron, V., Assaraf, Y.G., 2011. Structure and function of ABCG2-rich extracellular vesicles mediating multidrug resistance. *PLoS One* 6, e16007.
- Goler-Baron, V., Sladkevich, I., Assaraf, Y.G., 2012. Inhibition of the PI3K-Akt signaling pathway disrupts ABCG2-rich extracellular vesicles and overcomes multidrug resistance in breast cancer cells. *Biochem. Pharmacol.* 83, 1340–1348.
- Gonen, N., Assaraf, Y.G., 2012. Antifolates in cancer therapy: structure, activity and mechanisms of drug resistance. *Drug Resist. Updates* 15, 183–210.
- Gong, Z., Sun, P., Chu, H., Zhu, H., Sun, D., Chen, J., 2014. Overexpression of sorcin in multidrug-resistant human breast cancer. *Oncol. Lett.* 8, 2393–2398.
- Gottesman, M.M., Fojo, T., Bates, S.E., 2002. Multidrug resistance in cancer: role of ATP-dependent transporters. *Nat. Rev. Cancer* 2, 48–58.
- Gottesman, M.M., 2002. Mechanisms of cancer drug resistance. *Annu. Rev. Med.* 53, 615–627.
- Green, L.J., Marder, P., Slapak, C.A., 2001. Modulation by LY335979 of P-glycoprotein function in multidrug-resistant cell lines and human natural killer cells. *Biochem. Pharmacol.* 61, 1393–1399.
- Groen, A., Romero, M.R., Kunne, C., Hoosdally, S.J., Dixon, P.H., Wooding, C., Williamson, C., Seppen, J., Van den Oever, K., Mok, K.S., Paulusma, C.C., Linton, K.J., Oude Elferink, R.P., 2011. Complementary functions of the flippase ATP8B1 and the floppase ABCB4 in maintaining canalicular membrane integrity. *Gastroenterology* 141, 1927–1937 (e1921–1924).
- Grogan, T.M., Spier, C.M., Salmon, S.E., Matzner, M., Rybski, J., Weinstein, R.S., Scheper, R.J., Dalton, W.S., 1993. P-glycoprotein expression in human plasma cell myeloma: correlation with prior chemotherapy. *Blood* 81, 490–495.
- Haitina, T., Lindblom, J., Renstrom, T., Fredriksson, R., 2006. Fourteen novel human members of mitochondrial solute carrier family 25 (SLC25) widely expressed in the central nervous system. *Genomics* 88, 779–790.
- Hamada, H., Okochi, E., Oh-hara, T., Tsuruo, T., 1988. Purification of the Mr 22,000 calcium-binding protein (sorcin) associated with multidrug resistance and its detection with monoclonal antibodies. *Cancer Res.* 48, 3173–3178.
- Han, K., Kahng, J., Kim, M., Lim, J., Kim, Y., Cho, B., Kim, H.K., Min, W.S., Kim, C.C., Lee, K.Y., Kim, B.K., Kang, C.S., 2000. Expression of functional markers in acute non-lymphoblastic leukemia. *Acta Haematol.* 104, 174–180.
- Han, Y., Tan, T.M., Lim, L.Y., 2006. Effects of capsaicin on P-gp function and expression in Caco-2 cells. *Biochem. Pharmacol.* 71, 1727–1734.
- Han, Y., Chin Tan, T.M., Lim, L.Y., 2008. In vitro and in vivo evaluation of the effects of piperine on P-gp function and expression. *Toxicol. Appl. Pharmacol.* 230, 283–289.
- Hanekop, N., Zaitseva, J., Jenewein, S., Holland, I.B., Schmitt, L., 2006. Molecular insights into the mechanism of ATP-hydrolysis by the NBD of the ABC-transporter HlyB. *FEBS Lett.* 580, 1036–1041.
- Hansen, S.N., Ehlers, N.S., Zhu, S., Thomsen, M.B., Nielsen, R.L., Liu, D., Wang, G., Hou, Y., Zhang, X., Xu, X., Bolund, L., Yang, H., Wang, J., Moreira, J., Ditzel, H.J., Brunner, N., Schrohl, A.S., Stenvang, J., Gupta, R., 2016. The stepwise evolution of the exome during acquisition of docetaxel resistance in breast cancer cells. *BMC genomics* 17, 442.
- Harmsen, S., Meijerman, I., Febus, C.L., Maas-Bakker, R.F., Beijnen, J.H., Schellens, J.H., 2010. PXR-mediated induction of P-glycoprotein by anticancer drugs in a human colon adenocarcinoma-derived cell line. *Cancer Chemother. Pharmacol.* 66, 765–771.
- Harmsen, S., Meijerman, I., Maas-Bakker, R.F., Beijnen, J.H., Schellens, J.H., 2013. PXR-mediated P-glycoprotein induction by small molecule tyrosine kinase inhibitors. *Eur. J. Pharm. Sci.* 48, 644–649.
- Haslam, S., Jones, K., Coleman, T., Simmons, N.L., 2008a. Induction of P-glycoprotein expression and function in human intestinal epithelial cells (T84). *Biochem. Pharmacol.* 76, 850–861.
- Haslam, S., Jones, K., Coleman, T., Simmons, N.L., 2008b. Rifampin and digoxin induction of MD R1 expression and function in human intestinal (T84) epithelial cells. *Br. J. Pharmacol.* 154, 246–255.
- Hassan, H.E., Myers, A.L., Lee, I.J., Coop, A., Eddington, N.D., 2007. Oxycodone induces overexpression of P-glycoprotein (ABCB1) and affects paclitaxel's tissue distribution in Sprague Dawley rats. *J. Pharm. Sci.* 96, 2494–2506.
- He, Q., Zhang, G., Hou, D., Leng, A., Xu, M., Peng, J., Liu, T., 2011. Overexpression of sorcin results in multidrug resistance in gastric cancer cells with up-regulation of P-gp. *Oncol. Rep.* 25, 237–243.
- Henrique, R., Oliveira, A.L., Costa, V.L., Baptista, T., Martins, A.T., Morais, A., Oliveira, J., Jeronimo, C., 2013. Epigenetic regulation of MD R1 gene through post-translational histone modifications in prostate cancer. *BMC Genom.* 14, 898.
- Herzog, C.E., Tsokos, M., Bates, S.E., Fojo, A.T., 1993. Increased mdr-1/P-glycoprotein expression after treatment of human colon carcinoma cells with P-glycoprotein antagonists. *J. Biol. Chem.* 268, 2946–2952.
- Higgins, C.F., Linton, K.J., 2004. The ATP switch model for ABC transporters. *Nat. Struct. Mol. Biol.* 11, 918–926.
- Hollenstein, K., Frei, D.C., Locher, K.P., 2007. Structure of an ABC transporter in complex with its binding protein. *Nature* 446, 213–216.
- Holohan, C., Van Schaeybroeck, S., Longley, D.B., Johnston, P.G., 2013. Cancer drug resistance: an evolving paradigm. *Nat. Rev. Cancer* 13, 714–726.
- Hou, Y., Wang, H.Q., Ba, Y., 2012. High expression of cell division cycle 7 protein correlates with poor prognosis in patients with diffuse large B-cell lymphoma. *Med. Oncol.* 29, 3498–3503.
- Housman, G., Byler, S., Heerboth, S., Lapinska, K., Longacre, M., Snyder, N., Sarkar, S., 2014. Drug resistance in cancer: an overview. *Cancers* 6, 1769–1792.
- Hu, F., Slater, A., Wall, D.M., Kantharidis, P., Parkin, J.D., Cowman, A., Zalberg, J.R., 1995. Rapid up-regulation of mdr1 expression by anthracyclines in a classical multidrug-resistant cell line. *Br. J. Cancer* 71, 931–936.
- Hu, F., Slater, A., Rischin, D., Kantharidis, P., Parkin, J.D., Zalberg, J., 1999. Induction of MD R1 gene expression by anthracycline analogues in a human drug resistant leukemia cell line. *Br. J. Cancer* 79, 831–837.
- Hu, Y., Cheng, X., Li, S., Zhou, Y., Wang, J., Cheng, T., Yang, M., Xiong, D., 2013. Inhibition of sorcin reverses multidrug resistance of K562/A02 cells and MCF-7/A02 cells via regulating apoptosis-related proteins. *Cancer Chemother. Pharmacol.* 72, 789–798.
- Hu, Y., Li, S., Yang, M., Yan, C., Fan, D., Zhou, Y., Zhang, Y., Yague, E., Xiong, D., 2014. Sorcin silencing inhibits epithelial-to-mesenchymal transition and suppresses breast cancer metastasis in vivo. *Breast Cancer Res. Treat.* 143, 287–299.
- Huang, P., Sun, S.P., Cheng, S.H., Lee, C.H., Wu, C.Y., Yang, C.S., Lo, L.W., Lai, Y.K., 2011. Enhanced chemotherapy of cancer using pH-sensitive mesoporous silica nanoparticles to antagonize P-glycoprotein-mediated drug resistance. *Mol. Cancer Ther.* 10, 761–769.
- Huo, H., Magro, P.G., Pietsch, E.C., Patel, B.B., Scotto, K.W., 2010. Histone methyltransferase MLL1 regulates MD R1 transcription and chemoresistance. *Cancer Res.* 70, 8726–8735.
- Hyafil, F., Vergely, C., Du Vignaud, P., Grand-Perret, T., 1993. In vitro and in vivo reversal of multidrug resistance by GF120918, an acridonecarboxamide derivative. *Cancer Res.* 53, 4595–4602.
- Ifergan, I., Scheffer, G.L., Assaraf, Y.G., 2005. Novel extracellular vesicles mediate an ABCG2-dependent anticancer drug sequestration and resistance. *Cancer Res.* 65, 10952–10958.
- Ikemura, K., Yamamoto, M., Miyazaki, S., Mizutani, H., Iwamoto, T., Okuda, M., 2013. MicroRNA-145 post-transcriptionally regulates the expression and function of P-glycoprotein in intestinal epithelial cells. *Mol. Pharmacol.* 83, 399–405.
- Ilari, A., Fiorillo, A., Poser, E., Lalioti, V.S., Sundell, G.N., Ivarsson, Y., Genovese, I., Colotti, G., 2015. Structural basis of Sorcin-mediated calcium-dependent signal

- transduction. *Sci. Rep.* 5, 16828.
- Inoue, K., Fry, E.A., 2016. Novel molecular markers for Breast cancer. *Biomark. Cancer* 8, 25–42.
- Inoue, K., Mallakin, A., Frazier, D.P., 2007. Dmp1 and tumor suppression. *Oncogene* 26, 4329–4335.
- International Transporter, C., Giacomini, K.M., Huang, S.M., Tweedie, D.J., Benet, L.Z., Brouwer, K.L., Chu, X., Dahlin, A., Evers, R., Fischer, V., Hillgren, K.M., Hoffmaster, K.A., Ishikawa, T., Keppler, D., Kim, R.B., Lee, C.A., Niemi, M., Polli, J.W., Sugiyama, Y., Swaan, P.W., Ware, J.A., Wright, S.H., Yee, S.W., Zamek-Gliszczynski, M.J., Zhang, L., 2010. Membrane transporters in drug development. *Nat. Rev. Drug Discov.* 9, 215–236.
- Jansson, P.J., Hawkins, C.L., Lovejoy, D.B., Richardson, D.R., 2010. The iron complex of Dp44mT is redox-active and induces hydroxyl radical formation: an EPR study. *J. Inorg. Biochem.* 104, 1224–1228.
- Jansson, P.J., Yamagishi, T., Arvind, A., Seebacher, N., Gutierrez, E., Stacy, A., Maleki, S., Sharp, D., Sahni, S., Richardson, D.R., 2015. Di-2-pyridylketone 4,4-dimethyl-3-thiosemicarbazone (Dp44mT) overcomes multidrug resistance by a novel mechanism involving the hijacking of lysosomal P-glycoprotein (Pgp). *J. Biol. Chem.* 290, 9588–9603.
- Januchowski, R., Wojtowicz, K., Andrzejewska, M., Zabel, M., 2014a. Expression of MDR1 and MDR3 gene products in paclitaxel-, doxorubicin- and vincristine-resistant cell lines. *Biomed. Pharmacother.* = *Biomed. Pharmacother.* 68, 111–117.
- Januchowski, R., Zawierucha, P., Rucinski, M., Andrzejewska, M., Wojtowicz, K., Nowicki, M., Zabel, M., 2014b. Drug transporter expression profiling in chemoresistant variants of the A2780 ovarian cancer cell line. *Biomed. Pharmacother.* = *Biomed. Pharmacother.* 68, 447–453.
- Januchowski, R., Sterzynska, K., Zawierucha, P., Rucinski, M., Swierczewska, M., Partyka, M., Bednarek-Rajewska, K., Brazert, M., Nowicki, M., Zabel, M., Klejewska, A., 2017. Microarray-based detection and expression analysis of new genes associated with drug resistance in ovarian cancer cell lines. *Oncotarget* 8, 49944–49958.
- Jeon, H.M., Sohn, Y.W., Oh, S.Y., Kim, S.H., Beck, S., Kim, S., Kim, H., 2011. ID4 imparts chemoresistance and cancer stemness to glioma cells by derepressing miR-9<sup>\*</sup>-mediated suppression of SOX2. *Cancer Res.* 71, 3410–3421.
- Jin, S., Scotto, K.W., 1998. Transcriptional regulation of the MDR1 gene by histone acetyltransferase and deacetylase is mediated by NF- $\kappa$ B. *Mol. Cell. Biol.* 18, 4377–4384.
- Jin, M.S., Oldham, M.L., Zhang, Q., Chen, J., 2012. Crystal structure of the multidrug transporter P-glycoprotein from *Caenorhabditis elegans*. *Nature* 490, 566–569.
- Jones, P.M., George, A.M., 2013. Mechanism of the ABC transporter ATPase domains: catalytic models and the biochemical and biophysical record. *Crit. Rev. Biochem. Mol. Biol.* 48, 39–50.
- Jones, P.M., George, A.M., 2014. A reciprocating twin-channel model for ABC transporters. *Q. Rev. Biophys.* 47, 189–220.
- Juliano, R.L., Ling, V., 1976. A surface glycoprotein modulating drug permeability in Chinese hamster ovary cell mutants. *Biochim. Biophys. Acta* 455, 152–162.
- Kabacik, S., Manning, G., Raffy, C., Bouffier, S., Badie, C., 2015. Time, dose and ataxia telangiectasia mutated (ATM) status dependency of coding and noncoding RNA expression after ionizing radiation exposure. *Radiat. Res.* 183, 325–337.
- Kadioglu, O., Efferth, T., 2016. Peptide aptamer identified by molecular docking targeting translationally controlled tumor protein in leukemia cells. *Invest. New Drugs* 34, 515–521.
- Kageyama, M., Fukushima, K., Togawa, T., Fujimoto, K., Taki, M., Nishimura, A., Ito, Y., Sugioka, N., Shibata, N., Takada, K., 2006. Relationship between excretion clearance of rhodamine 123 and P-glycoprotein (Pgp) expression induced by representative Pgp inducers. *Biol. Pharm. Bull.* 29, 779–784.
- Kao, C.H., Tsai, S.C., Liu, T.J., Ho, Y.J., Wang, J.J., Ho, S.T., ChangLai, S.P., 2001. P-Glycoprotein and multidrug resistance-related protein expressions in relation to technetium-99 m methoxyisobutylisonitrile scintimammography findings. *Cancer Res.* 61, 1412–1414.
- Kaplan, O., Jaroszewski, J.W., Clarke, R., Fairchild, C.R., Schoenlein, P., Goldenberg, S., Gottesman, M.M., Cohen, J.S., 1991. The multidrug resistance phenotype: 31P nuclear magnetic resonance characterization and 2-deoxyglucose toxicity. *Cancer Res.* 51, 1638–1644.
- Kathawala, R.J., Gupta, P., Ashby Jr., C.R., Chen, Z.S., 2015. The modulation of ABC transporter-mediated multidrug resistance in cancer: a review of the past decade. *Drug Resist. Updates* 18, 1–17.
- Katoh, T., Shibata, A., Kokubu, H., Ojima, P., Loukopoulos, Y., Kanai, T., Kosuge, M., Fukayama, T., Kondo, M., Sakamoto, F., Hosoda, M., Ohki, I., Imoto, J., Inazawa, S., 2005. Genetic profile of hepatocellular carcinoma revealed by array-based comparative genomic hybridization: identification of genetic indicators to predict patient outcome. *J. Hepatol.* 43, 863–874.
- Kawakami, M., Nakamura, T., Okamura, N., Komoto, C., Markova, S., Kobayashi, H., Hashimoto, N., Okumura, K., Sakaeda, T., 2007. Knock-down of sorcin induces up-regulation of MD R1 in HeLa cells. *Biol. Pharm. Bull.* 30, 1065–1073.
- Kemper, E.M., Cleypool, C., Boogerd, W., Beijnen, J.H., van Tellingen, O., 2004. The influence of the P-glycoprotein inhibitor zosuquidar trihydrochloride (LY335979) on the brain penetration of paclitaxel in mice. *Cancer Chemother. Pharmacol.* 53, 173–178.
- Kendig, R.D., Kai, F., Fry, E.A., Inoue, K., 2017. Stabilization of the p53-DNA complex by the nuclear protein dmp1alpha. *Cancer Invest.* 35, 301–312.
- Kim, R.B., Wandel, C., Leake, B., Cvetkovic, M., Fromm, M.F., Dempsey, P.J., Roden, M.M., Belas, F., Chaudhary, A.K., Roden, D.M., Wood, A.J., Wilkinson, G.R., 1999. Interrelationship between substrates and inhibitors of human CYP3A and P-glycoprotein. *Pharm. Res.* 16, 408–414.
- Kim, W., Han, N., Kim, M.G., Kim, T., Oh, J.M., 2015. Copy number variability analysis of pharmacogenes in patients with lymphoma, leukemia, hepatocellular, and lung carcinoma using The Cancer Genome Atlas data. *Pharmacogenet. Genomics* 25, 1–7.
- Kitada, K., Yamasaki, T., 2007. The MDR1/ABCB1 regional amplification in large inverted repeats with asymmetric sequences and microhomologies at the junction sites. *Cancer Genet. Cytogenet.* 178, 120–127.
- Knutsen, T., Mickley, L.A., Ried, T., Green, E.D., du Manoir, S., Schrock, E., Macville, M., Ning, Y., Robey, R., Polymeropoulos, M., Torres, R., Fojo, T., 1998. Cytogenetic and molecular characterization of random chromosomal rearrangements activating the drug resistance gene, MD R1/P-glycoprotein, in drug-selected cell lines and patients with drug refractory ALL. *Genes Chromosomes Cancer* 23, 44–54.
- Kodan, A., Yamaguchi, T., Nakatsu, T., Sakiyama, K., Hipolito, C.J., Fujioka, A., Hirokane, R., Ikeguchi, K., Watanabe, B., Hiratake, J., Kimura, Y., Suga, H., Ueda, K., Kato, H., 2014. Structural basis for gating mechanisms of a eukaryotic P-glycoprotein homolog. *Proc. Natl. Acad. Sci. U. S. A.* 111, 4049–4054.
- Koltun, E.S., Tshahko, A.L., Brown, D.S., Aay, N., Arcalas, A., Chan, V., Du, H., Engst, S., Ferguson, K., Franzini, M., Galan, A., Holst, C.R., Huang, P., Kane, B., Kim, M.H., Li, J., Markby, D., Mohan, M., Noson, K., Plonowski, A., Richards, S.J., Robertson, S., Shaw, K., Stott, G., Stout, T.J., Young, J., Yu, P., Zaharia, C.A., Zhang, W., Zhou, P., Nuss, J.M., Xu, W., Kearney, P.C., 2012. Discovery of XL413, a potent and selective CDC7 inhibitor. *Bioorg. Med. Chem. Lett.* 22, 3727–3731.
- Kovalchuk, O., Filkowski, J., Meservy, J., Ilnytsky, Y., Tryndyak, V.P., Chekhun, V.F., Pogribny, I.P., 2008. Involvement of microRNA-451 in resistance of the MCF-7 breast cancer cells to chemotherapeutic drug doxorubicin. *Mol. Cancer Ther.* 7, 2152–2159.
- Kozilova, E., Janouskova, O., Cuchalova, L., Hvezdova, Z., Hrabeta, J., Eckschlager, T., Sivak, L., Ulbrich, K., Etrych, T., Subr, V., 2016. Overcoming multidrug resistance in Dox-resistant neuroblastoma cell lines via treatment with HPMA copolymer conjugates containing anthracyclines and P-gp inhibitors. *J. Controlled Release* 233, 136–146.
- Krishnamurthy, K., Vadam, K., Kanagasabai, R., Druhan, L.J., Ilangovan, G., 2012. Heat shock factor-1 knockout induces multidrug resistance gene, MD R1b, and enhances P-glycoprotein (ABCB1)-based drug extrusion in the heart. *Proc. Natl. Acad. Sci. U. S. A.* 109, 9023–9028.
- Kulkarni, A.A., Kingsbury, S.R., Tudzarova, S., Hong, H.K., Laddo, M., Rashid, M., Rodriguez-Acebes, S., Prevost, A.T., Lederemann, J.A., Stoerber, K., Williams, G.H., 2009. Cdc7 kinase is a predictor of survival and a novel therapeutic target in epithelial ovarian carcinoma. *Clin. Cancer Res.* 15, 2417–2425.
- Kuo, M.T., Liu, Z., Wei, Y., Lin-Lee, Y.C., Tatabe, S., Mills, G.B., Unate, H., 2002. Induction of human MDR1 gene expression by 2-acetylaminofluorene is mediated by effectors of the phosphoinositide 3-kinase pathway that activate NF-kappaB signaling. *Oncogene* 21, 1945–1954.
- Labialle, S., Gayet, L., Marthinet, E., Rigal, D., Baggetto, L.G., 2002. Transcriptional regulators of the human multidrug resistance 1 gene: recent views. *Biochem. Pharmacol.* 64, 943–948.
- Lalioi, S., Ilari, A., O'Connell, D.J., Poser, E., Sandoval, I.V., Colotti, G., 2014. Sorcin links calcium signaling to vesicle trafficking, regulates Polo-like kinase 1 and is necessary for mitosis. *PLoS One* 9, e85438.
- Lawrence, M.S., Stojanov, P., Polak, P., Kryukov, G.V., Cibulskis, K., Sivachenko, A., Carter, S.L., Stewart, C., Mermel, C.H., Roberts, S.A., Kiezun, A., Hammerman, P.S., McKenna, A., Drier, Y., Zou, L., Ramos, A.H., Pugh, T.J., Stransky, N., Helman, E., Kim, J., Sougnez, C., Ambrogio, L., Nickerson, E., Shefler, E., Cortes, M.L., Auclair, D., Saksena, G., Voet, D., Noble, M., DiCara, D., Lin, P., Lichtenstein, L., Heiman, D.I., Fennell, T., Imielinski, M., Hernandez, B., Hodis, E., Baca, S., Dulak, A.M., Lohr, J., Landau, D.A., Wu, C.J., Melendez-Zajig, J., Hidalgo-Miranda, A., Koren, A., McCarroll, S.A., Mora, J., Crompton, B., Onofrio, R., Parkin, M., Winckler, W., Ardlie, K., Gabriel, S.B., Roberts, C.W.M., Biegel, J.A., Stegmaier, K., Bass, A.J., Garraway, L.A., Meyerson, M., Golub, T.R., Gordenin, D.A., Sunyaev, S., Lander, E.S., Getz, G., 2013. Mutational heterogeneity in cancer and the search for new cancer-associated genes. *Nature* 499, 214–218.
- Lee, S., Kim, K., Ho, J.N., Jin, H., Byun, S.S., Lee, E., 2017. Analysis of resistance-associated gene expression in docetaxel-resistant prostate cancer cells. *Oncol. Lett.* 14, 3011–3018.
- Lei, X., Liang, Y., Chen, J., Xiao, S., Lei, J., Li, J., Duanmu, J., Jiang, Q., Liu, D., Tang, C., Li, T., 2017. Sorcin predicts poor prognosis and promotes metastasis by facilitating epithelial-mesenchymal transition in hepatocellular carcinoma. *Sci. Rep.* 7, 10049.
- Leith, C.P., Kopecky, K.J., Chen, I.M., Eijddens, L., Slovak, M.L., McConnell, T.S., Head, D.R., Weick, J., Grever, M.R., Appelbaum, F.R., Willman, C.L., 1999. Frequency and clinical significance of the expression of the multidrug resistance proteins MD R1/P-glycoprotein, MRP1, and LRP in acute myeloid leukemia: a Southwest Oncology Group Study. *Blood* 94, 1086–1099.
- Lerner, C., Harrison, D.E., 1990. 5-Fluorouracil spares hemopoietic stem cells responsible for long-term repopulation. *Exp. Hematol.* 18, 114–118.
- Li, J., Jaimes, K.F., Aller, S.G., 2014. Refined structures of mouse P-glycoprotein. *Protein Sci.* 23, 34–46.
- Li, N., Yang, L., Wang, H., Yi, T., Jia, X., Chen, C., Xu, P., 2015. MiR-130a and miR-374a function as novel regulators of cisplatin resistance in human ovarian cancer A2780Cells. *PLoS One* 10, e0128886.
- Li, G.Y., Zhang, L., Liu, J.Z., Chen, S.G., Xiao, T.W., Liu, G.Z., Wang, J.X., Wang, L.X., Hou, M., 2016a. Marine drug Haishengsu increases chemosensitivity to conventional chemotherapy and improves quality of life in patients with acute leukemia. *Biomed. Pharmacother.* = *Biomed. Pharmacother.* 81, 160–165.
- Li, W., Zhang, H., Assaraf, Y.G., Zhao, K., Xu, X., Xie, J., Yang, D.H., Chen, Z.S., 2016b. Overcoming ABC transporter-mediated multidrug resistance: molecular mechanisms and novel therapeutic drug strategies. *Drug Resist. Updates* 27, 14–29.
- Li, Y., Zhao, L., Li, N., Miao, Y., Zhou, H., Jia, L., 2017. miR-9 regulates the multidrug resistance of chronic myelogenous leukemia by targeting ABCB1. *Oncol. Rep.* 37, 2193–2200.
- Linton, K.J., Higgins, C.F., 2007. Structure and function of ABC transporters: the ATP

- switch provides flexible control. *Pflügers Archiv: Eur. J. Physiol.* 453, 555–567.
- Litviakov, N.V., Cherdynseva, N.V., Tsyganov, M.M., Slonimskaya, E.M., Ibragimova, M.K., Kazantseva, P.V., Kzhyshkowska, J., Choinzonov, E.L., 2016. Deletions of multidrug resistance gene loci in breast cancer leads to the down-regulation of its expression and predict tumor response to neoadjuvant chemotherapy. *Oncotarget* 7, 7829–7841.
- Liu, J., Chen, H., Miller, D.S., Saavedra, J.E., Keefer, L.K., Johnson, D.R., Klaassen, C.D., Waalkes, M.P., 2001. Overexpression of glutathione S-transferase II and multidrug resistance transport proteins is associated with acquired tolerance to inorganic arsenic. *Mol. Pharmacol.* 60, 302–309.
- Liu, Z.L., Onda, K., Tanaka, S., Toma, T., Hirano, T., Oka, K., 2002. Induction of multidrug resistance in MOLT-4 cells by anticancer agents is closely related to increased expression of functional P-glycoprotein and MD R1 mRNA. *Cancer Chemother. Pharmacol.* 49, 391–397.
- Liu, H., Liu, X., Jia, L., Liu, Y., Yang, H., Wang, G., Xie, L., 2008. Insulin therapy restores impaired function and expression of P-glycoprotein in blood-brain barrier of experimental diabetes. *Biochem. Pharmacol.* 75, 1649–1658.
- Liu, H., Shim, A.H., He, X., 2009. Structural characterization of the ectodomain of a disintegrin and metalloproteinase-22 (ADAM22), a neural adhesion receptor instead of metalloproteinase: insights on ADAM function. *J. Biol. Chem.* 284, 29077–29086.
- Liu, X., Chen, L., Feng, B., Liu, G., 2014. Reversing effect of sorcin in the drug resistance of human nasopharyngeal carcinoma. *Anat. Rec.* 297, 215–221.
- Livney, Y.D., Assaraf, Y.G., 2013. Rationally designed nanovehicles to overcome cancer chemoresistance. *Adv. Drug Deliv. Rev.* 65, 1716–1730.
- Lizarbe, M.A., Calle-Espinosa, J., Fernandez-Lizarbe, E., Fernandez-Lizarbe, S., Robles, M.A., Olmo, N., Turnay, J., 2017. Colorectal cancer: from the genetic model to posttranscriptional regulation by noncoding RNAs. *BioMed Res. Int.* 2017, 7354260.
- Locher, K.P., 2016. Mechanistic diversity in ATP-binding cassette (ABC) transporters. *Nat. Struct. Mol. Biol.* 23, 487–493.
- Lohner, K., Schnabele, K., Daniel, H., Oesterle, D., Rechkemmer, G., Gottlicher, M., Wenzel, U., 2007. Flavonoids alter P-gp expression in intestinal epithelial cells in vitro and in vivo. *Mol. Nutr. Food Res.* 51, 293–300.
- Longley, D.B., Allen, W.L., Johnston, P.G., 2006. Drug resistance, predictive markers and pharmacogenomics in colorectal cancer. *Biochim. Biophys. Acta* 1766, 184–196.
- Lopes-Rodrigues, H., Seca, D., Sousa, E., Sousa, R.T., Lima, M.H., 2014. The network of P-glycoprotein and microRNAs interactions. *Int. J. Cancer* 135, 253–263.
- Lowe, S.W., Cepero, E., Evan, G., 2004. Intrinsic tumour suppression. *Nature* 432, 307–315.
- Lu, C., Shan, Z., Li, C., Yang, L., 2017. MiR-129 regulates cisplatin-resistance in human gastric cancer cells by targeting P-gp. *Biomed. Pharmacother.* = *Biomed. Pharmacother.* 86, 450–456.
- Luo, L., Sun, Y.J., Yang, L., Huang, S., Wu, Y.J., 2013. Avermectin induces P-glycoprotein expression in S2 cells via the calcium/calmodulin/NF-kappaB pathway. *Chem. Biol. Interact.* 203, 430–439.
- Ma, Xiao-Long, Zhu, Kun-Peng, Zhang, Chun-Lin, 2017. Identification of gene expression profiles associated with doxorubicin resistance in paired doxorubicin-resistant and doxorubicin-sensitive osteosarcoma cell lines. *Int. J. Clin. Exp. Pathol.* 10 (6), 6254–6267 [www.ijcep.com](http://www.ijcep.com) /ISSN:1936-2625/IJCEP0049959.
- Maddalena, F., Laudiero, G., Piscazzi, A., Secondo, A., Scorziello, A., Lombardi, V., Matassa, D.S., Fersini, A., Neri, V., Esposito, F., Landriscina, M., 2011. Sorcin induces a drug-resistant phenotype in human colorectal cancer by modulating Ca(2+) homeostasis. *Cancer Res.* 71, 7659–7669.
- Maddalena, F., Sisinni, L., Lettini, G., Condelli, V., Matassa, D.S., Piscazzi, A., Amoroso, M.R., La Torre, G., Esposito, F., Landriscina, M., 2013. Resistance to paclitaxel in breast carcinoma cells requires a quality control of mitochondrial antiapoptotic proteins by TRAP1. *Mol. Oncol.* 7, 895–906.
- Maglic, D., Stovall, D.B., Cline, J.M., Fry, E.A., Mallakin, A., Taneja, P., Caudell, D.L., Willingham, M.C., Sui, G., Inoue, K., 2015. DMP1beta, a splice isoform of the tumour suppressor DMP1 locus, induces proliferation and progression of breast cancer. *J. Pathol.* 236, 90–102.
- Maier, C., Dahlstroem, C., Haefliger, A., Plum, C., 2005. Identifying DNA methylation biomarkers of cancer drug response. *Am. J. Pharmacogenom.* 5, 223–232.
- Maier, A., Zimmermann, C., Beglinger, C., Drewe, J., Gutmann, H., 2007. Effects of budesonide on P-glycoprotein expression in intestinal cell lines. *Br. J. Pharmacol.* 150, 361–368.
- Mallakin, A., Sugiyama, T., Taneja, P., Matise, L.A., Frazier, D.P., Choudhary, M., Hawkins, G.A., D'Agostino Jr., R.B., Willingham, M.C., Inoue, K., 2007. Mutually exclusive inactivation of DMP1 and ARF/p53 in lung cancer. *Cancer Cell* 12, 381–394.
- Manceau, S., Giraud, C., Declèves, X., Scherrmann, J.M., Artiguesbelle, F., Goffinet, F., Chappuy, H., Vinot, C., Treluyer, J.M., 2012. ABC drug transporter and nuclear receptor expression in human cytotrophoblasts: influence of spontaneous syncytialization and induction by glucocorticoids. *Placenta* 33, 927–932.
- Manda, S., Sharma, S., Wani, A., Joshi, P., Kumar, V., Guru, S.K., Bharate, S.S., Bhusan, S., Vishwakarma, R.A., Kumar, A., Bharate, S.B., 2016. Discovery of a marine-derived bis-indole alkaloid faspalylin, as a new class of potent P-glycoprotein inducer and establishment of its structure-activity relationship. *Eur. J. Med. Chem.* 107, 1–11.
- Mao, Q., Unadkat, J.D., 2015. Role of the breast cancer resistance protein (BCRP/ABCG2) in drug transport—an update. *AAPS J.* 17, 65–82.
- McCartan, D., Bolger, J.C., Fagan, A., Byrne, C., Hao, Y., Qin, L., McLroy, M., Xu, J., Hill, A.D., Gaora, P.O., Young, L.S., 2012. Global characterization of the SRC-1 transcriptome identifies ADAM22 as an ER-independent mediator of endocrine-resistant breast cancer. *Cancer Res.* 72, 220–229.
- Mealey, K.L., Barhoumi, R., Burghardt, R.C., Safe, S., Kochevar, D.T., 2002. Doxycycline induces expression of P glycoprotein in MCF-7 breast carcinoma cells. *Antimicrob. Agents Chemother.* 46, 755–761.
- Melling, N., Muth, J., Simon, R., Bokemeyer, C., Terracciano, L., Sauter, G., Izbiicki, J.R., Marx, A.H., 2015. Cdc7 overexpression is an independent prognostic marker and a potential therapeutic target in colorectal cancer. *Diagn. Pathol.* 10, 125.
- Mencalha, A.L., Rodrigues, E.F., Abdelhay, E., Fernandez, T.S., 2013. Accurate monitoring of promoter gene methylation with high-resolution melting polymerase chain reaction using the ABCB1 gene as a model. *Genet. Mol. Res.: GMR* 12, 714–722.
- Menez, C., Mselli-Lakhal, L., Foucaud-Vignault, M., Balaguer, P., Alvinerie, M., Lespine, A., 2012. Ivermectin induces P-glycoprotein expression and function through mRNA stabilization in murine hepatocyte cell line. *Biochem. Pharmacol.* 83, 269–278.
- Meyers, M.B., Biedler, J.L., 1981. Increased synthesis of a low molecular weight protein in vincristine-resistant cells. *Biochem. Biophys. Res. Commun.* 99, 228–235.
- Michieli, M., Damiani, D., Ermacor, A., Masolini, P., Raspadori, D., Visani, G., Scheper, R.J., Baccarani, M., 1999. P-glycoprotein, lung resistance-related protein and multidrug resistance associated protein in de novo acute non-lymphocytic leukaemias: biological and clinical implications. *Br. J. Haematol.* 104, 328–335.
- Mickley, L.A., Spengler, B.A., Knutsen, T.A., Biedler, J.L., Fojo, T., 1997. Gene rearrangement: a novel mechanism for MDR-1 gene activation. *J. Clin. Invest.* 99, 1947–1957.
- Miller, T.P., Grogan, T.M., Dalton, W.S., Spier, C.M., Scheper, R.J., Salmon, S.E., 1991. P-glycoprotein expression in malignant lymphoma and reversal of clinical drug resistance with chemotherapy plus high-dose verapamil. *J. Clin. Oncol.* 9, 17–24.
- Miyazaki, M., Kohno, K., Uchiyama, T., Tanimura, H., Matsuo, K., Nasu, M., Kuwano, M., 1992. Activation of human multidrug resistance-1 gene promoter in response to heat shock stress. *Biochem. Biophys. Res. Commun.* 187, 677–684.
- Montagnoli, A., Valsasina, B., Croci, V., Menichincheri, M., Rainoldi, S., Marchesi, V., Tibolla, M., Tenca, P., Brotherton, D., Albanese, C., Patton, V., Alzani, R., Ciavolella, A., Sola, F., Molinari, A., Volpi, D., Avanzi, N., Fiorentini, F., Cattoni, M., Healy, S., Ballinari, D., Pesenti, E., Isacchi, A., Moll, J., Bensimon, A., Vanotti, E., Santocanale, C., 2008. A Cdc7 kinase inhibitor restricts initiation of DNA replication and has antitumor activity. *Nat. Chem. Biol.* 4, 357–365.
- Morita, S.Y., Terada, T., 2014. Molecular mechanisms for biliary phospholipid and drug efflux mediated by ABCB4 and bile salts. *BioMed Res. Int.* 2014, 954781.
- Morrissey, K.M., Wen, C.C., Johns, S.J., Zhang, L., Huang, S.M., Giacomini, K.M., 2012. The UCSF-FDA TransPortal: a public drug transporter database. *Clin. Pharmacol. Ther.* 92, 545–546.
- Nakagawa, M., Emoto, A., Nasu, N., Hanada, T., Kuwano, M., Cole, S.P., Nomura, Y., 1997. Clinical significance of multi-drug resistance associated protein and P-glycoprotein in patients with bladder cancer. *J. Urol.* 157, 1264–1265 (discussion 1264–1265).
- Nakayama, M., Wada, M., Harada, T., Nagayama, J., Kusaba, H., Ohshima, K., Kozuru, M., Komatsu, H., Ueda, R., Kuwano, M., 1998. Hypomethylation status of CpG sites at the promoter region and overexpression of the human MD R1 gene in acute myeloid leukemias. *Blood* 92, 4296–4307.
- Namanja-Magliano, H.A., Bohn, K., Agrawal, N., Willoughby, M.E., Hrycyna, C.A., Chmielewski, J., 2017. Dual inhibitors of the human blood-brain barrier drug efflux transporters P-glycoprotein and ABCG2 based on the antiviral azidothymidine. *Bioorg. Med. Chem.* 25, 5128–5132.
- Nambiar, S., Mirmohammadsadegh, A., Hassan, M., Mota, R., Marini, A., Alaoui, A., Tannapel, A., Hegemann, J.H., Hengge, U.R., 2007. Identification and functional characterization of ASK/Dbf4, a novel cell survival gene in cutaneous melanoma with prognostic relevance. *Carcinogenesis* 28, 2501–2510.
- Naruhashi, K., Kurahashi, Y., Fujita, Y., Kawakita, E., Yamasaki, Y., Hattori, K., Nishimura, A., Shibata, N., 2011. Comparison of the expression and function of ATP binding cassette transporters in Caco-2 and T84 cells on stimulation by selected endogenous compounds and xenobiotics. *Drug Metab. Pharmacokinet.* 26, 145–153.
- Natarajan, K., Xie, Y., Baer, M.R., Ross, D.D., 2012. Role of breast cancer resistance protein (BCRP/ABCG2) in cancer drug resistance. *Biochem. Pharmacol.* 83, 1084–1103.
- Natoni, A., Murillo, L.S., Kliszczak, A.E., Catherwood, M.A., Montagnoli, A., Samali, A., O'Dwyer, M., Santocanale, C., 2011. Mechanisms of action of a dual Cdc7/Cdk9 kinase inhibitor against quiescent and proliferating CLL cells. *Mol. Cancer Ther.* 10, 1624–1634.
- Nemcova-Furstova, D., Kopperova, K., Balusikova, M., Ehrlichova, V., Brynychova, R., Vaclavikova, P., Daniel, P., Soucek, J., 2016. Characterization of acquired paclitaxel resistance of breast cancer cells and involvement of ABC transporters. *Toxicol. Appl. Pharmacol.* 310, 215–228.
- Nikaido, K., Ames, G.F., 1999. One intact ATP-binding subunit is sufficient to support ATP hydrolysis and translocation in an ABC transporter, the histidine permease. *J. Biol. Chem.* 274, 26727–26735.
- Nooter, K., Brutel de la Riviere, G., Look, M.P., van Wingerden, K.E., Henzen-Logmans, S.C., Scheper, R.J., Flens, M.J., Klijn, J.G., Stoter, G., Foekens, J.A., 1997. The prognostic significance of expression of the multidrug resistance-associated protein (MRP) in primary breast cancer. *Br. J. Cancer* 76, 486–493.
- Nwaozuzu, O.M., Sellers, L.A., Barrand, M.A., 2003. Signalling pathways influencing basal and H(2)O(2)-induced P-glycoprotein expression in endothelial cells derived from the blood-brain barrier. *J. Neurochem.* 87, 1043–1051.
- Oldham, M.L., Chen, J., 2011. Snapshots of the maltose transporter during ATP hydrolysis. *Proc. Natl. Acad. Sci. U. S. A.* 108, 15152–15156.
- Owen, A., Goldring, C., Morgan, P., Park, B.K., Pirmohamed, M., 2006. Induction of P-glycoprotein in lymphocytes by carbamazepine and rifampicin: the role of nuclear hormone response elements. *Br. J. Clin. Pharmacol.* 62, 237–242.
- Padar, S., van Breemen, C., Thomas, D.W., Uchizono, J.A., Livesey, J.C., Rahimian, R., 2004. Differential regulation of calcium homeostasis in adenocarcinoma cell line A549 and its Taxol-resistant subclone. *Br. J. Pharmacol.* 142, 305–316.
- Palmeira, A., Sousa, E., Vasconcelos, M.H., Pinto, M.M., 2012a. Three decades of P-gp inhibitors: skimming through several generations and scaffolds. *Curr. Med. Chem.* 19,



- 1946–2025.
- Palmeira, A., Vasconcelos, M.H., Paiva, A., Fernandes, M.X., Pinto, M., Sousa, E., 2012b. Dual inhibitors of P-glycoprotein and tumor cell growth: (re)discovering thioxanthones. *Biochem. Pharmacol.* 83, 57–68.
- Palmieri, F., 2013. The mitochondrial transporter family SLC25: identification, properties and physiopathology. *Mol. Aspects Med.* 34, 465–484.
- Pan, Y.Z., Morris, M.E., Yu, A.M., 2009. MicroRNA-328 negatively regulates the expression of breast cancer resistance protein (BCRP/ABCG2) in human cancer cells. *Mol. Pharmacol.* 75, 1374–1379.
- Pang, E., Hu, Y., Chan, K.Y., Lai, P.B., Squire, J.A., Macgregor, P.F., Beheshti, B., Albert, M., Leung, T.W., Wong, N., 2005. Karyotypic imbalances and differential gene expressions in the acquired doxorubicin resistance of hepatocellular carcinoma cells. *Lab. Invest.* 85, 664–674.
- Parekh, H.K., Deng, H.B., Choudhary, K., Houser, S.R., Simpkins, H., 2002. Overexpression of sorcin, a calcium-binding protein, induces a low level of paclitaxel resistance in human ovarian and breast cancer cells. *Biochem. Pharmacol.* 63, 1149–1158.
- Park, J., Shinohara, N., Liebert, M., Noto, L., Flint, A., Grossman, H.B., 1994. P-glycoprotein expression in bladder cancer. *J. Urol.* 151, 43–46.
- Pasero, P., Duncker, B.P., Schwob, E., Gasser, S.M., 1999. A role for the Cdc7 kinase regulatory subunit Dbf4p in the formation of initiation-competent origins of replication. *Genes. Dev.* 13, 2159–2176.
- Patch, A.M., Christie, E.L., Etemadmoghadam, D., Garsed, D.W., George, J., Fereday, S., et al., 2015. Whole-genome characterization of chemoresistant ovarian cancer. *Nature* 521, 489–494.
- Peng, Y., Dong, W., Lin, T.X., Zhong, G.Z., Liao, B., Wang, B., Gu, P., Huang, L., Xie, Y., Lu, F.D., Chen, X., Xie, W.B., He, W., Wu, S.X., Huang, J., 2015. MicroRNA-155 promotes bladder cancer growth by repressing the tumor suppressor DMTF1. *Oncotarget* 6, 16043–16058.
- Perez, C., Gerber, S., Boilevin, J., Bucher, M., Darbre, T., Aebi, M., Raymond, J.L., Locher, K.P., 2015. Structure and mechanism of an active lipid-linked oligosaccharide flipase. *Nature* 524, 433–438.
- Perloff, M.D., von Moltke, L.L., Fahey, J.M., Daily, J.P., Greenblatt, D.J., 2000. Induction of P-glycoprotein expression by HIV protease inhibitors in cell culture. *AIDS* 14, 1287–1289.
- Perloff, M.D., von Moltke, L.L., Stormer, E., Shader, R.I., Greenblatt, D.J., 2001. Saint John's wort: an in vitro analysis of P-glycoprotein induction due to extended exposure. *Br. J. Pharmacol.* 134, 1601–1608.
- Perri, T., Fogel, M., Mor, S., Horev, G., Meller, I., Lovén, D., Issakov, J., Kollender, Y., Smirnov, A., Zaizov, R., Cohen, I.J., 2001. Effect of P-glycoprotein expression on outcome in the Ewing family of tumors. *Pediatr. Hematol. Oncol.* 18, 325–334.
- Peters, R., Leyvraz, S., Perey, L., 1998. Apoptotic regulation in primitive hematopoietic precursors. *Blood* 92, 2041–2052.
- Phang, J.M., Poore, C.M., Lopaczynska, J., Yeh, G.C., 1993. Flavonol-stimulated efflux of 7, 12-dimethylbenz(a)anthracene in multidrug-resistant breast cancer cells. *Cancer Res.* 53, 5977–5981.
- Pirker, R., Goldstein, L.J., Ludwig, H., Linkesch, W., Lechner, C., Gottesman, M.M., Pastan, I., 1989. Expression of a multidrug resistance gene in blast crisis of chronic myelogenous leukemia. *Cancer Commun.* 1, 141–144.
- Pluchino, K.M., Hall, M.D., Goldsborough, A.S., Callaghan, R., Gottesman, M.M., 2012. Collateral sensitivity as a strategy against cancer multidrug resistance. *Drug Resist. Updates* 15, 98–105.
- Pogribny, P., Filkowski, J.N., Tryndyak, V.P., Golubov, A., Shpileva, S.I., Kovalchuk, O., 2010. Alterations of microRNAs and their targets are associated with acquired resistance of MCF-7 breast cancer cells to cisplatin. *Int. J. Cancer* 127, 1785–1794.
- Prekert, M., Uggla, B., Tina, E., Tidefelt, U., Strid, H., 2009. Rapid induction of P-glycoprotein mRNA and protein expression by cytarabine in HL-60 cells. *Anticancer Res.* 29, 4071–4076.
- Procko, E., O'Mara, M.L., Bennett, W.F., Tieleman, D.P., Gaudet, R., 2009. The mechanism of ABC transporters: general lessons from structural and functional studies of an antigenic peptide transporter. *FASEB J.* 23, 1287–1302.
- Pusztai, L., Wagner, P., Ibrahim, N., Rivera, E., Theriault, R., Booser, D., Symmans, F.W., Wong, F., Blumenschein, G., Fleming, D.R., Rouzier, R., Boniface, G., Hortobagyi, G.N., 2005. Phase II study of tariquidar, a selective P-glycoprotein inhibitor, in patients with chemotherapy-resistant, advanced breast carcinoma. *Cancer* 104, 682–691.
- Qi, J., Liu, N., Zhou, Y., Tan, Y., Cheng, Y., Yang, C., Zhu, Z., Xiong, D., 2006. Overexpression of sorcin in multidrug resistant human leukemia cells and its role in regulating cell apoptosis. *Biochem. Biophys. Res. Commun.* 349, 303–309.
- Qian, H., Zhao, X., Cao, P., Lei, J., Yan, N., Gong, X., 2017. Structure of the human lipid exporter ABCA1. *Cell* 169, 1228–1239 (e1210).
- Qu, Y., Yang, Y., Liu, B., Xiao, W., 2010. Comparative proteomic profiling identified sorcin being associated with gemcitabine resistance in non-small cell lung cancer. *Med. Oncol.* 27, 1303–1308.
- Quazi, F., Lenevich, S., Molday, R.S., 2012. ABCA4 is an N-retinylidene-phosphatidylethanolamine and phosphatidylethanolamine importer. *Nat. Commun.* 3, 925.
- Raguz, S., De Bella, M.T., Slade, M.J., Higgins, C.F., Coombes, R.C., Yague, E., 2005. Expression of RPIIP9 (Rap2 interacting protein 9) is activated in breast carcinoma and correlates with a poor prognosis. *Int. J. Cancer* 117, 934–941.
- Rajkumar, T., Yamuna, M., 2008. Multiple pathways are involved in drug resistance to doxorubicin in an osteosarcoma cell line. *Anticancer Drugs* 19, 257–265.
- Raz, S., Sheban, D., Gonen, N., Stark, M., Berman, B., Assaraf, Y.G., 2014. Severe hypoxia induces complete antifolate resistance in carcinoma cells due to cell cycle arrest. *Cell. Death. Dis.* 5, e1067.
- Reed, K., Hembruff, S.L., Laberge, M.L., Villeneuve, D.J., Cote, G.B., Parisenti, A.M., 2008. Hypermethylation of the ABCB1 downstream gene promoter accompanies ABCB1 gene amplification and increased expression in docetaxel-resistant MCF-7 breast tumor cells. *Epigenetics* 3, 270–280.
- Reed, K., Hembruff, S.L., Sprowl, J.A., Parisenti, A.M., 2010. The temporal relationship between ABCB1 promoter hypomethylation, ABCB1 expression and acquisition of drug resistance. *Pharmacogenom.* J. 10, 489–504.
- Regev, R., Katzir, H., Yeheksely-Hayon, D., Eytan, G.D., 2007. Modulation of P-glycoprotein-mediated multidrug resistance by acceleration of passive drug permeation across the plasma membrane. *FEBS J.* 274, 6204–6214.
- Ren, F., Wang, D.B., Li, T., Chen, Y.H., Li, Y., 2014. Identification of differentially methylated genes in the malignant transformation of ovarian endometriosis. *J. Ovarian Res.* 7, 73.
- Riganti, C., Campia, I., Polimeni, M., Pescarmona, G., Ghigo, D., Bosia, A., 2009a. Digoxin and ouabain induce P-glycoprotein by activating calmodulin kinase II and hypoxia-inducible factor-1alpha in human colon cancer cells. *Toxicol. Appl. Pharmacol.* 240, 385–392.
- Riganti, C., Doublier, S., Viarisio, D., Miraglia, E., Pescarmona, G., Ghigo, D., Bosia, A., 2009b. Artemisinin induces doxorubicin resistance in human colon cancer cells via calcium-dependent activation of HIF-1alpha and P-glycoprotein overexpression. *Br. J. Pharmacol.* 156, 1054–1066.
- Robey, R.W., Zhan, Z., Piekarz, R.L., Kayastha, G.L., Fojo, T., Bates, S.E., 2006. Increased MD R1 expression in normal and malignant peripheral blood mononuclear cells obtained from patients receiving desipeptide (FR901228, FK228, NSC630176). *Clin. Cancer Res.* 12, 1547–1555.
- Rodgers, E.H., Grant, M.H., 1998. The effect of the flavonoids, quercetin, myricetin and epicatechin on the growth and enzyme activities of MCF7 human breast cancer cells. *Chem. Biol. Interact.* 116, 213–228.
- Roninson, B., Chin, J.E., Choi, K.G., Gros, P., Housman, D.E., Fojo, A., Shen, D.W., Gottesman, M.M., Pastan, I., 1986. Isolation of human mdr DNA sequences amplified in multidrug-resistant KB carcinoma cells. *Proc. Natl. Acad. Sci. U. S. A.* 83, 4538–4542.
- Roninson, B., 1992. From amplification to function: the case of the MD R1 gene. *Mutat. Res.* 276, 151–161.
- Ruff, P., Vorobiof, D.A., Jordaan, J.P., Demetriou, G.S., Moodley, S.D., Nosworthy, A.L., Werner, I.D., Raats, J., Burgess, L.J., 2009. A randomized, placebo-controlled, double-blind phase 2 study of docetaxel compared to docetaxel plus zosuquidar (LY335979) in women with metastatic or locally recurrent breast cancer who have received one prior chemotherapy regimen. *Cancer Chemother. Pharmacol.* 64, 763–768.
- Rukov, J.L., Shomron, N., 2011. MicroRNA pharmacogenomics: post-transcriptional regulation of drug response. *Trends Mol. Med.* 17, 412–423.
- Safa, A.R., Stern, R.K., Choi, K., Agresti, M., Tamai, I., Mehta, N.D., Roninson, I.B., 1990. Molecular basis of preferential resistance to colchicine in multidrug-resistant human cells conferred by Gly-185-Val-185 substitution in P-glycoprotein. *Proc. Natl. Acad. Sci. U. S. A.* 87, 7225–7229.
- Sasi, N.K., Bhutkar, A., Lanning, N.J., MacKeigan, J.P., Weinreich, M., 2017. DDK promotes tumor chemoresistance and survival via multiple pathways. *Neoplasia* 19, 439–450.
- Sauna, Z.E., Kim, I.W., Nandigama, K., Kopp, S., Chiba, P., Ambudkar, S.V., 2007. Catalytic cycle of ATP hydrolysis by P-glycoprotein: evidence for formation of the E.S reaction intermediate with ATP-gamma-S, a nonhydrolyzable analogue of ATP. *Biochemistry* 46, 13787–13799.
- Schinkel, A.H., Smit, J.J., van Tellingen, O., Beijnen, J.H., Wagenaar, E., van Deemter, L., Mol, C.A., van der Valk, M.A., Robanus-Maandag, E.C., te Riele, H.P., et al., 1994. Disruption of the mouse mdr1a P-glycoprotein gene leads to a deficiency in the blood-brain barrier and to increased sensitivity to drugs. *Cell* 77, 491–502.
- Schinkel, A.H., Wagenaar, E., van Deemter, L., Mol, C.A., Borst, P., 1995. Absence of the mdr1a P-glycoprotein in mice affects tissue distribution and pharmacokinetics of dexamethasone, digoxin, and cyclosporin A. *J. Clin. Invest.* 96, 1698–1705.
- Schinkel, A.H., Wagenaar, E., Mol, C.A., van Deemter, L., 1996. P-glycoprotein in the blood-brain barrier of mice influences the brain penetration and pharmacological activity of many drugs. *J. Clin. Invest.* 97, 2517–2524.
- Schinkel, A.H., Mayer, U., Wagenaar, E., Mol, C.A., van Deemter, L., Smit, J.J., van der Valk, M.A., Voordouw, A.C., Spits, H., van Tellingen, O., Zijlmans, J.M., Fibbe, W.E., Borst, P., 1997. Normal viability and altered pharmacokinetics in mice lacking mdr1-type (drug-transporting) P-glycoproteins. *Proc. Natl. Acad. Sci. U. S. A.* 94, 4028–4033.
- Schinkel, A.H., 1999. P-glycoprotein, a gatekeeper in the blood-brain barrier. *Adv. Drug Deliv. Rev.* 36, 179–194.
- Schneider, J., Efferth, T., Centeno, M.M., Mattern, J., Rodriguez-Escudero, F.J., Volm, M., 1993. High rate of expression of multidrug resistance-associated P-glycoprotein in human endometrial carcinoma and normal endometrial tissue. *Eur. J. Cancer* 29A, 554–558.
- Schoenlein, P.V., 1993. Molecular cytogenetics of multiple drug resistance. *Cytotechnology* 12, 63–89.
- Schrenk, D., Michalke, A., Gant, T.W., Brown, P.C., Silverman, J.A., Thorgeirsson, S.S., 1996. Multidrug resistance gene expression in rodents and rodent hepatocytes treated with mitoxantrone. *Biochem. Pharmacol.* 52, 1453–1460.
- Schuetz, E.G., Beck, W.T., Schuetz, J.D., 1996. Modulators and substrates of P-glycoprotein and cytochrome P4503A coordinately up-regulate these proteins in human colon carcinoma cells. *Mol. Pharmacol.* 49, 311–318.
- Schuetz, E.G., Yasuda, K., Arimori, K., Schuetz, J.D., 1998. Human MD R1 and mouse mdr1a P-glycoprotein alter the cellular retention and disposition of erythromycin, but not of retinoic acid or benzo(a)pyrene. *Arch. Biochem. Biophys.* 350, 340–347.
- Schwab, M., Eichelbaum, M., Fromm, M.F., 2003. Genetic polymorphisms of the human MD R1 drug transporter. *Annu. Rev. Pharmacol. Toxicol.* 43, 285–307.
- Scotto, K.W., Egan, D.A., 1998. Transcriptional regulation of MD r genes. *Cytotechnology*

- 27, 257–269.
- Scotto, K.W., Biedler, J.L., Melera, P.W., 1986. Amplification and expression of genes associated with multidrug resistance in mammalian cells. *Science* 232, 751–755.
- Scotto, K.W., 2003. Transcriptional regulation of ABC drug transporters. *Oncogene* 22, 7496–7511.
- Seebacher, N.A., Richardson, D.R., Jansson, P.J., 2016. A mechanism for overcoming P-glycoprotein-mediated drug resistance: novel combination therapy that releases stored doxorubicin from lysosomes via lysosomal permeabilization using Dp44mT or DpC. *Cell. Death. Dis.* 7, e2510.
- Senior, A.E., al-Shawi, M.K., Urbatsch, I.L., 1995. The catalytic cycle of P-glycoprotein. *FEBS Lett.* 377, 285–289.
- Shang, Y., Zhang, Z., Liu, Z., Feng, B., Ren, G., Li, K., Zhou, L., Sun, Y., Li, M., Zhou, J., An, Y., Wu, K., Nie, Y., Fan, D., 2014. miR-508-5p regulates multidrug resistance of gastric cancer by targeting ABCB1 and ZNRD1. *Oncogene* 33, 3267–3276.
- Shang, Y., Feng, B., Zhou, L., Ren, G., Zhang, Z., Fan, X., Sun, Y., Luo, G., Liang, J., Wu, K., Nie, Y., Fan, D., 2016. The miR27b-CCNG1-P53-miR-508-5p axis regulates multidrug resistance of gastric cancer. *Oncotarget* 7, 538–549.
- Shapira, A., Livney, Y.D., Broxterman, H.J., Assaraf, Y.G., 2011. Nanomedicine for targeted cancer therapy: towards the overcoming of drug resistance. *Drug Resist. Updates* 14, 150–163.
- Shapiro, A.B., Ling, V., 1997. Effect of quercetin on Hoechst 33342 transport by purified and reconstituted P-glycoprotein. *Biochem. Pharmacol.* 53, 587–596.
- Sharom, F.J., 2008. ABC multidrug transporters: structure, function and role in chemoresistance. *Pharmacogenomics* 9, 105–127.
- Sharom, F.J., 2011. The P-glycoprotein multidrug transporter. *Essays Biochem.* 50, 161–178.
- Sharom, F.J., 2014. Complex interplay between the P-Glycoprotein multidrug efflux pump and the membrane: its role in modulating protein function. *Front. Oncol.* 4, 41.
- Shen, D.W., Fojo, A., Chin, J.E., Roninson, I.B., Richert, N., Pastan, I., Gottesman, M.M., 1986. Human multidrug-resistant cell lines: increased *mdr1* expression can precede gene amplification. *Science* 232, 643–645.
- Sheu, Y.J., Stillman, B., 2010. The Dbf4-Cdc7 kinase promotes S phase by alleviating an inhibitory activity in Mcm4. *Nature* 463, 113–117.
- Shibue, T., Weinberg, R.A., 2017. EMT, CSCs, and drug resistance: the mechanistic link and clinical implications. *Nat. Rev. Clin. Oncol.* 14, 611–629.
- Shieh, M.J., Hsu, C.Y., Huang, L.Y., Chen, H.Y., Huang, F.H., Lai, P.S., 2011. Reversal of doxorubicin-resistance by multifunctional nanoparticles in MCF-7/ADR cells. *J. Controlled Release* 152, 418–425.
- Shukla, S., Abel, B., Chufan, E.E., Ambudkar, S.V., 2017. Effects of a detergent micelle environment on P-glycoprotein (ABCB1)-ligand interactions. *J. Biol. Chem.* 292, 7066–7076.
- Silva, R., Carmo, H., Vilas-Boas, V., Barbosa, D.J., Palmeira, A., Sousa, E., Carvalho, F., Bastos Mde, L., Remiao, F., 2014. Colchicine effect on P-glycoprotein expression and activity: in silico and in vitro studies. *Chem. Biol. Interact.* 218, 50–62.
- Silva, R., Vilas-Boas, V., Carmo, H., Dinis-Oliveira, R.J., Carvalho, F., de Lourdes Bastos, M., Remiao, F., 2015. Modulation of P-glycoprotein efflux pump: induction and activation as a therapeutic strategy. *Pharmacol. Ther.* 149, 1–123.
- Sivak, L., Subr, V., Tomala, J., Rihova, B., Strohalm, J., Etrych, T., Kovar, M., 2017. Overcoming multidrug resistance via simultaneous delivery of cytostatic drug and P-glycoprotein inhibitor to cancer cells by HPMA copolymer conjugate. *Biomaterials* 115, 65–80.
- Smit, J.W., Schinkel, A.H., Muller, M., Weert, B., Meijer, D.K., 1998. Contribution of the murine *mdr1a* P-glycoprotein to hepatobiliary and intestinal elimination of cationic drugs as measured in mice with an *mdr1a* gene disruption. *Hepatology* 27, 1056–1063.
- Smith, P.C., Karpowich, N., Millen, L., Moody, J.E., Rosen, J., Thomas, P.J., Hunt, J.F., 2002. ATP binding to the motor domain from an ABC transporter drives formation of a nucleotide sandwich dimer. *Mol. Cell* 10, 139–149.
- Song, R., Zheng, Y., He, G., Yang, L., Luo, Y.F., He, Z.Y., Li, S.Z., Li, J.M., Yu, S., Luo, X., Hou, S.X., Wei, Y.Q., 2010. Development of PLGA nanoparticles simultaneously loaded with vincristine and verapamil for treatment of hepatocellular carcinoma. *J. Pharm. Sci.* 99, 4874–4879.
- Sparreboom, A., van Asperen, J., Mayer, U., Schinkel, A.H., Smit, J.W., Meijer, D.K., Borst, P., Nooijen, W.J., Beijnen, J.H., van Tellingen, O., 1997. Limited oral bioavailability and active epithelial excretion of paclitaxel (Taxol) caused by P-glycoprotein in the intestine. *Proc. Natl. Acad. Sci. U. S. A.* 94, 2031–2035.
- Stark, M., Bram, E.E., Akerman, M., Mandel-Gutfreund, Y., Assaraf, Y.G., 2011. Heterogeneous nuclear ribonucleoprotein H1/H2-dependent unsplicing of thymidine phosphorylase results in anticancer drug resistance. *J. Biol. Chem.* 286, 3741–3754.
- Sugihara, N., Toyama, K., Okamoto, T., Kadowaki, M., Terao, K., Furuno, K., 2007. Effects of benzo(e)pyrene and benzo(a)pyrene on P-glycoprotein-mediated transport in Caco-2 cell monolayer: a comparative approach. *Toxicol. In Vitro* 21, 827–834.
- Sugiyama, T., Frazier, D.P., Taneja, P., Kendig, R.D., Morgan, R.L., Matisse, L.A., Lagedrost, S.J., Inoue, K., 2008. Signal transduction involving the *dmp1* transcription factor and its alteration in human cancer. *Clin. Med. Oncol.* 2, 209–219.
- Sun, S.S., Hsieh, J.F., Tsai, S.C., Ho, Y.J., Lee, J.K., Kao, C.H., 2000. Expression of mediated P-glycoprotein multidrug resistance related to Tc-99 m MI BI scintimammography results. *Cancer Lett.* 153, 95–100.
- Sun, Y., Wang, C., Meng, Q., Liu, Z., Huo, X., Sun, P., Sun, H., Ma, X., Peng, J., Liu, K., 2017. Targeting P-glycoprotein and SORCIN: dihydromyricetin strengthens anti-proliferative efficiency of adriamycin via MAPK/ERK and Ca<sup>2+</sup>–mediated apoptosis pathway in MCF-7/ADR and K562/ADR. *J. Cell. Physiol.* <http://dx.doi.org/10.1002/jcp.26087>.
- Swanton, C., 2012. Intratumor heterogeneity: evolution through space and time. *Cancer Res.* 72, 4875–4882.
- Szakacs, G., Paterson, J.K., Ludwig, J.A., Booth-Genthe, C., Gottesman, M.M., 2006. Targeting multidrug resistance in cancer. *Nat. Rev. Drug Discov.* 5, 219–234.
- Szewczyk, P., Tao, H., McGrath, A.P., Villaluz, M., Rees, S.D., Lee, S.C., Doshi, R., Urbatsch, I.L., Zhang, Q., Chang, G., 2015. Snapshots of ligand entry, malleable binding and induced helical movement in P-glycoprotein. *Acta Crystallogr. Sect. D, Biol. Crystallogr.* 71, 732–741.
- Tabe, Y., Konopleva, M., Contractor, R., Munsell, M., Schober, W.D., Jin, L., Tsutsumi-Ishii, Y., Nagaoka, I., Igari, J., Andreoff, M., 2006. Up-regulation of MD R1 and induction of doxorubicin resistance by histone deacetylase inhibitor depsipeptide (FK228) and ATRA in acute promyelocytic leukemia cells. *Blood* 107, 1546–1554.
- Tada, Y., Wada, M., Kuroiwa, K., Kinugawa, N., Harada, T., Nagayama, J., Nakagawa, M., Naito, S., Kuwano, M., 2000. MDR1 gene overexpression and altered degree of methylation at the promoter region in bladder cancer during chemotherapeutic treatment. *Clin. Cancer Res.* 6, 4618–4627.
- Tada, Y., Wada, M., Migita, T., Nagayama, J., Hinoshita, E., Mochida, Y., Maehara, Y., Tsuneyoshi, M., Kuwano, M., Naito, S., 2002. Increased expression of multidrug resistance-associated proteins in bladder cancer during clinical course and drug resistance to doxorubicin. *Int. J. Cancer* 98, 630–635.
- Takei, Y., Ishikawa, S., Tokino, T., Muto, T., Nakamura, Y., 1998. Isolation of a novel TP53 target gene from a colon cancer cell line carrying a highly regulated wild-type TP53 expression system. *Genes Chromosomes Cancer* 23, 1–9.
- Takwi, A.A., Wang, Y.M., Wu, J., Michaelis, M., Cinatl, J., Chen, T., 2014. miR-137 regulates the constitutive androstane receptor and modulates doxorubicin sensitivity in parental and doxorubicin-resistant neuroblastoma cells. *Oncogene* 33, 3717–3729.
- Tan, Y., Li, G., Zhao, C., Wang, J., Zhao, H., Xue, Y., Han, M., Yang, C., 2003. Expression of sorcin predicts poor outcome in acute myeloid leukemia. *Leuk. Res.* 27, 125–131.
- Taneja, P., Mallakin, A., Matisse, L.A., Frazier, D.P., Choudhary, M., Inoue, K., 2007. Repression of Dmp1 and Arf transcription by anthracyclins: critical roles of the NF-kappaB subunit p65. *Oncogene* 26, 7457–7466.
- ter Beek, J., Guskov, A., Slotboom, D.J., 2014. Structural diversity of ABC transporters. *J. Gen. Physiol.* 143, 419–435.
- Thevenod, F., Friedmann, J.M., Katsen, A.D., Hauser, I.A., 2000. Up-regulation of multidrug resistance P-glycoprotein via nuclear factor-kappaB activation protects kidney proximal tubule cells from cadmium- and reactive oxygen species-induced apoptosis. *J. Biol. Chem.* 275, 1887–1896.
- Thiebaut, F., Tsuruo, T., Hamada, H., Gottesman, M.M., Pastan, I., Willingham, M.C., 1987. Cellular localization of the multidrug-resistance gene product P-glycoprotein in normal human tissues. *Proc. Natl. Acad. Sci. U. S. A.* 84, 7735–7738.
- Thomas, H., Coley, H.M., 2003. Overcoming multidrug resistance in cancer: an update on the clinical strategy of inhibiting P-glycoprotein. *Cancer Control* 10, 159–165.
- Tian, S., Zhang, M., Chen, X., Liu, Y., Lou, G., 2016. MicroRNA-595 sensitizes ovarian cancer cells to cisplatin by targeting ABCB1. *Oncotarget* 7, 87091–87099.
- Tong, W., Sun, D., Wang, Q., Suo, J., 2015. Sorcin enhances metastasis and promotes epithelial-to-mesenchymal transition of colorectal cancer. *Cell Biochem. Biophys.* 72, 453–459.
- Torigoe, K., Sato, S., Kusaba, H., Kohno, K., Kuwano, M., Okumura, K., Green, E.D., Tsui, L.C., Scherer, S.W., Schlessinger, D., Wada, M., 1995. A YAC-based contig of 1.5 Mb spanning the human multidrug resistance gene region and delineating the amplification unit in three human multidrug-resistant cell lines. *Genome Res.* 5, 233–244.
- Trock, B.J., Leonesa, F., Clarke, R., 1997. Multidrug resistance in breast cancer: a meta-analysis of MDR1/gp170 expression and its possible functional significance. *J. Natl. Cancer Inst.* 89, 917–931.
- Tschan, M.P., Gullberg, U., Shan, D., Torbett, B.E., Fey, M.F., Tobler, A., 2008. The hDMP1 tumor suppressor is a new WT1 target in myeloid leukemias. *Leukemia* 22, 1087–1090.
- Tsuruo, T., Iida, H., Tsukagoshi, S., Sakurai, Y., 1981. Overcoming of vincristine resistance in P388 leukemia in vivo and in vitro through enhanced cytotoxicity of vincristine and vinblastine by verapamil. *Cancer Res.* 41, 1967–1972.
- Ueda, K., Cardarelli, C., Gottesman, M.M., Pastan, I., 1987a. Expression of a full-length cDNA for the human MDR1 gene confers resistance to colchicine, doxorubicin, and vinblastine. *Proc. Natl. Acad. Sci. U. S. A.* 84, 3004–3008.
- Ueda, K., Pastan, I., Gottesman, M.M., 1987b. Isolation and sequence of the promoter region of the human multidrug-resistance (P-glycoprotein) gene. *J. Biol. Chem.* 262, 17432–17436.
- Valach, J., Fik, Z., Strnad, H., Chovanec, M., Plzak, J., Cada, Z., Szabo, P., Sachova, J., Hroudova, M., Urbanova, M., Steffl, M., Paces, J., Mazanek, J., Vlcek, C., Betka, J., Kaltner, H., Andre, S., Gabius, H.J., Kodet, R., Smetana, Jr., K., Gal, P., Kolar, M., 2012. Smooth muscle actin-expressing stromal fibroblasts in head and neck squamous cell carcinoma: increased expression of galectin-1 and induction of poor prognosis factors. *Int. J. Cancer* 131, 2499–2508.
- van Asperen, J., Schinkel, A.H., Beijnen, J.H., Nooijen, W.J., Borst, P., van Tellingen, O., 1996. Altered pharmacokinetics of vinblastine in *mdr1a* P-glycoprotein-deficient mice. *J. Natl. Cancer Inst.* 88, 994–999.
- van Asperen, J., Mayer, U., van Tellingen, O., Beijnen, J.H., 1997. The functional role of P-glycoprotein in the blood-brain barrier. *J. Pharm. Sci.* 86, 881–884.
- van Asperen, J., van Tellingen, O., Tijssen, F., Schinkel, A.H., Beijnen, J.H., 1999. Increased accumulation of doxorubicin and doxorubicin in cardiac tissue of mice lacking *mdr1a* P-glycoprotein. *Br. J. Cancer* 79, 108–113.
- van Dekken, H., Vissers, K., Tilanus, H.W., Kuo, W.L., Tanke, H.J., Rosenberg, C., Ijzenga, M., Szuha, K., 2006. Genomic array and expression analysis of frequent high-level amplifications in adenocarcinomas of the gastro-esophageal junction. *Cancer Genet. Cytogenet.* 166, 157–162.
- van der Kolk, D.M., de Vries, E.G., van Putten, W.J., Verdonck, L.F., Ossenkoppele, G.J., Verhoef, G.E., Vellenga, E., 2000. P-glycoprotein and multidrug resistance protein activities in relation to treatment outcome in acute myeloid leukemia. *Clin. Cancer Res.* 6, 3205–3214.
- van der Zee, A.G., Hollema, H., Suurmeijer, A.J., Krans, M., Sluiter, W.J., Willems, P.H.,



- Aalders, J.G., de Vries, E.G., 1995. Value of P-glycoprotein, glutathione S-transferase pi, c-erbB-2, and p53 as prognostic factors in ovarian carcinomas. *J. Clin. Oncol.* 13, 70–78.
- Van der Bliek, A.M., Meyers, M.B., Biedler, J.L., Hes, E., Borst, P., 1986a. A 22-kd protein (sorcin/V19) encoded by an amplified gene in multidrug-resistant cells, is homologous to the calcium-binding light chain of calpain. *EMBO J.* 5, 3201–3208.
- Van der Bliek, A.M., Van der Velde-Koerts, T., Ling, V., Borst, P., 1986b. Overexpression and amplification of five genes in a multidrug-resistant Chinese hamster ovary cell line. *Mol. Cell. Biol.* 6, 1671–1678.
- Van der Bliek, A.M., Baas, F., Ten Houte de Lange, T., Kooiman, P.M., Van der Velde-Koerts, T., Borst, P., 1987. The human mdr1 gene encodes a novel P-glycoprotein homologue and gives rise to alternatively spliced mRNAs in liver. *EMBO J.* 6, 3325–3331.
- Van der Bliek, A.M., Baas, F., Van der Velde-Koerts, T., Biedler, J.L., Meyers, M.B., Ozols, R.F., Hamilton, T.C., Joenje, H., Borst, P., 1988. Genes amplified and overexpressed in human multidrug-resistant cell lines. *Cancer Res.* 48, 5927–5932.
- Varma, M.V., Ashokraj, Y., Dey, C.S., Panchagnula, R., 2003. P-glycoprotein inhibitors and their screening: a perspective from bioavailability enhancement. *Pharmacol. Res.* 48, 347–359.
- Varrin, A.E., Prasad, A.A., Scholz, R.P., Ramer, M.D., Duncker, B.P., 2005. A mutation in Dbf4 motif M impairs interactions with DNA replication factors and confers increased resistance to genotoxic agents. *Mol. Cell. Biol.* 25, 7494–7504.
- Vecchio, S.D., Ciarmiello, A., Potena, M.I., Carriero, M.V., Mainolfi, C., Botti, G., Thomas, R., Cerra, M., D'Aiuto, G., Tsuruo, T., Salvatore, M., 1997. In vivo detection of multidrug-resistant (MDR1) phenotype by technetium-99 m sestamibi scan in untreated breast cancer patients. *Eur. J. Nucl. Med.* 24, 150–159.
- Verdon, G., Albers, S.V., Dijkstra, B.W., Driessen, A.J., Thunnissen, A.M., 2003. Crystal structures of the ATPase subunit of the glucose ABC transporter from *Sulfolobus solfataricus*: nucleotide-free and nucleotide-bound conformations. *J. Mol. Biol.* 330, 343–358.
- Verhalen, B., Dastvan, R., Thangapandian, S., Peskova, Y., Koteiche, H.A., Nakamoto, R.K., Tajkhorshid, E., McHaourab, H.S., 2017. Energy transduction and alternating access of the mammalian ABC transporter P-glycoprotein. *Nature* 543, 738–741.
- Vilaboa, N.E., Galan, A., Troyano, A., de Blas, E., Aller, P., 2000. Regulation of multidrug resistance 1 (MDR1)/P-glycoprotein gene expression and activity by heat-shock transcription factor 1 (HSF1). *J. Biol. Chem.* 275, 24970–24976.
- Wang, Y.C., Juric, D., Francisco, B., Yu, R.X., Duran, G.E., Chen, G.K., Chen, X., Sikic, B.L., 2006. Regional activation of chromosomal arm 7q with and without gene amplification in taxane-selected human ovarian cancer cell lines. *Genes Chromosomes Cancer* 45, 365–374.
- Wang, H., Zhan, M., Xu, S.W., Chen, W., Long, M.M., Shi, Y.H., Liu, Q., Mohan, M., Wang, J., 2017. miR-218-5p restores sensitivity to gemcitabine through PRKCE/MDR1 axis in gallbladder cancer. *Cell. Death. Dis.* 8, e2770.
- Ward, A., Reyes, C.L., Yu, J., Roth, C.B., Chang, G., 2007. Flexibility in the ABC transporter MsbA: Alternating access with a twist. *Proc. Natl. Acad. Sci. U. S. A.* 104, 19005–19010.
- Ward, A.B., Szewczyk, P., Grimard, V., Lee, C.W., Martinez, L., Doshi, R., Caya, A., Villaluz, M., Pardon, E., Cregger, C., Swartz, D.J., Falson, P.G., Urbatsch, I.L., Govaerts, C., Steyaert, J., Chang, G., 2013. Structures of P-glycoprotein reveal its conformational flexibility and an epitope on the nucleotide-binding domain. *Proc. Natl. Acad. Sci. U. S. A.* 110, 13386–13391.
- Watanabe, T., Suzuki, H., Sawada, Y., Naito, M., Tsuruo, T., Inaba, M., Hanano, M., Sugiyama, Y., 1995. Induction of hepatic P-glycoprotein enhances biliary excretion of vincristine in rats. *J. Hepatol.* 23, 440–448.
- Weidner, L.D., Fung, K.L., Kannan, P., Moen, J.K., Kumar, J.S., Mulder, J., Innis, R.B., Gottesman, M.M., Hall, M.D., 2016. Tariquidar is an inhibitor and not a substrate of human and mouse P-glycoprotein. *Drug Metab. Dispos.* 44, 275–282.
- Weinreich, M., Stillman, B., 1999. Cdc7p-Dbf4p kinase binds to chromatin during S phase and is regulated by both the APC and the RAD53 checkpoint pathway. *EMBO J.* 18, 5334–5346.
- Weiss, J., Theile, D., Spalwisz, A., Burhenne, J., Riedel, K.D., Haefeli, W.E., 2013. Influence of sildenafil and tadalafil on the enzyme- and transporter-inducing effects of bosentan and ambrisentan in LS180 cells. *Biochem. Pharmacol.* 85, 265–273.
- Wen, T., Liu, Y.C., Yang, H.W., Liu, H.Y., Liu, X.D., Wang, G.J., Xie, L., 2008. Effect of 21-day exposure of phenobarbital, carbamazepine and phenytoin on P-glycoprotein expression and activity in the rat brain. *J. Neurol. Sci.* 270, 99–106.
- Wen, P.C., Verhalen, B., Wilkens, S., McHaourab, H.S., Tajkhorshid, E., 2013. On the origin of large flexibility of P-glycoprotein in the inward-facing state. *J. Biol. Chem.* 288, 19211–19220.
- Wijdeven, R.H., Pang, B., Assaraf, Y.G., Neefjes, J., 2016. Old drugs, novel ways out: drug resistance toward cytotoxic chemotherapeutics. *Drug Resist. Updates* 28, 65–81.
- Wilkens, S., 2015. Structure and mechanism of ABC transporters, *F1000prime reports* 7, p. 14.
- Wolf, S.J., Bachtar, M., Wang, J., Sim, T.S., Chong, S.S., Lee, C.G., 2011. An update on ABCB1 pharmacogenetics: insights from a 3D model into the location and evolutionary conservation of residues corresponding to SNPs associated with drug pharmacokinetics. *Pharmacogenom.* 11, 315–325.
- Wolking, S., Schaeffeler, E., Lerche, H., Schwab, M., Nies, A.T., 2015. Impact of genetic polymorphisms of ABCB1 (MDR1, P-Glycoprotein) on drug disposition and potential clinical implications: update of the literature. *Clin. Pharmacokinet.* 54, 709–735.
- Wong, K.K., Engelman, J.A., Cantley, L.C., 2010. Targeting the PI3K signaling pathway in cancer. *Curr. Opin. Genet. Dev.* 20, 87–90.
- Wu, Q., Yang, Z., Xia, L., Nie, Y., Wu, K., Shi, Y., Fan, D., 2014. Methylation of miR-129-5p CpG island modulates multi-drug resistance in gastric cancer by targeting ABC transporters. *Oncotarget* 5, 11552–11563.
- Wu, D.D., Li, X.S., Meng, X.N., Yan, J., Zong, Z.H., 2016. MicroRNA-873 mediates multidrug resistance in ovarian cancer cells by targeting ABCB1. *Tumour Biol.* 37, 10499–10506.
- Xu, Y., Ohms, S.J., Li, Z., Wang, Q., Gong, G., Hu, Y., Mao, Z., Shannon, M.F., Fan, J.Y., 2013. Changes in the expression of miR-381 and miR-495 are inversely associated with the expression of the MD R1 gene and development of multi-drug resistance. *PLoS One* 8, e82062.
- Yabuki, N., Sakata, K., Yamasaki, T., Terashima, H., Mio, T., Miyazaki, Y., Fujii, T., Kitada, K., 2007. Gene amplification and expression in lung cancer cells with acquired paclitaxel resistance. *Cancer Genet. Cytogenet.* 173, 1–9.
- Yamagishi, N., Nakao, R., Kondo, R., Nishitsuji, M., Saito, Y., Kuga, T., Hatayama, T., Nakayama, Y., 2014. Increased expression of sorcin is associated with multidrug resistance in leukemia cells via up-regulation of MD R1 expression through cAMP response element-binding protein. *Biochem. Biophys. Res. Commun.* 448, 430–436.
- Yamamoto, Y., Yoshioka, Y., Minoura, K., Takahashi, R.U., Takeshita, F., Taya, T., Hori, R., Fukuoaka, Y., Kato, T., Kosaka, N., Ochiya, T., 2011. An integrative genomic analysis revealed the relevance of microRNA and gene expression for drug-resistance in human breast cancer cells. *Mol. Cancer* 10, 135.
- Yang, Y.X., Chen, Z.C., Zhang, G.Y., Yi, H., Xiao, Z.Q., 2008. A subcellular proteomic investigation into vincristine-resistant gastric cancer cell line. *J. Cell. Biochem.* 104, 1010–1021.
- Yang, L., Li, N., Wang, H., Jia, X., Wang, X., Luo, J., 2012. Altered microRNA expression in cisplatin-resistant ovarian cancer cells and upregulation of miR-130a associated with MD R1/P-glycoprotein-mediated drug resistance. *Oncol. Rep.* 28, 592–600.
- Yang, Y., Li, H., Hou, S., Hu, B., Liu, J., Wang, J., 2013. The noncoding RNA expression profile and the effect of lncRNA AK126698 on cisplatin resistance in non-small-cell lung cancer cell. *PLoS One* 8, e65309.
- Yi, H., Liu, L., Sheng, N., Li, P., Pan, H., Cai, L., Ma, Y., 2016. Synergistic therapy of doxorubicin and miR-129-5p with self-cross-linked bioreducible polypeptide nanoparticles reverses multidrug resistance in cancer cells. *Biomacromolecules* 17, 1737–1747.
- Yuan, Y., Cai, T., Xia, X., Zhang, R., Chiba, P., Cai, Y., 2016. Nanoparticle delivery of anticancer drugs overcomes multidrug resistance in breast cancer. *Drug Deliv.* 23, 3350–3357.
- Yusa, K., Tsuruo, T., 1989. Reversal mechanism of multidrug resistance by verapamil: direct binding of verapamil to P-glycoprotein on specific sites and transport of verapamil outward across the plasma membrane of K562/ADM cells. *Cancer Res.* 49, 5002–5006.
- Zamparelli, C., Macquaide, N., Colotti, G., Verzili, D., Seidler, T., Smith, G.L., Chiancone, E., 2010. Activation of the cardiac Na(+)-Ca(2+) exchanger by sorcin via the interaction of the respective Ca(2+) binding domains. *J. Mol. Cell. Cardiol.* 49, 132–141.
- Zastre, J.A., Chan, G.N., Ronaldson, P.T., Ramaswamy, M., Couraud, P.O., Romero, I.A., Weksler, B., Bendayan, M., Bendayan, R., 2009. Up-regulation of P-glycoprotein by HIV protease inhibitors in a human brain microvessel endothelial cell line. *J. Neurosci. Res.* 87, 1023–1036.
- Zegerman, P., Diffley, J.F., 2010. Checkpoint-dependent inhibition of DNA replication initiation by Sld3 and Dbf4 phosphorylation. *Nature* 467, 474–478.
- Zhang, Y., Wang, J., 2017. MicroRNAs are important regulators of drug resistance in colorectal cancer. *Biol. Chem.* 398, 929–938.
- Zhang, Y.K., Wang, Y.J., Gupta, P., Chen, Z.S., 2015. Multidrug resistance proteins (MRPs) and cancer therapy. *AAPS J.* 17, 802–812.
- Zhao, Y., Qi, X., Chen, J., Wei, W., Yu, C., Yan, H., Pu, M., Li, Y., Miao, L., Li, C., Ren, J., 2017. The miR-/Sp3/ABCB1 axis attenuates multidrug resistance of hepatocellular carcinoma. *Cancer Lett.* 408, 102–111.
- Zhitomirsky, B., Assaraf, Y.G., 2016. Lysosomes as mediators of drug resistance in cancer. *Drug Resist. Updates* 24, 23–33.
- Zhou, G., Kuo, M.T., 1997. NF-kappaB-mediated induction of mdr1b expression by insulin in rat hepatoma cells. *J. Biol. Chem.* 272, 15174–15183.
- Zhou, D.C., Zittoun, R., Marie, J.P., 1995. Expression of multidrug resistance-associated protein (MRP) and multidrug resistance (MDR1) genes in acute myeloid leukemia. *Leukemia* 9, 1661–1666.
- Zhou, S., Schuetz, J.D., Bunting, K.D., Colapietro, A.M., Sampath, J., Morris, J.J., Lagutina, I., Grosveld, G.C., Osawa, M., Nakauchi, H., Sorrentino, B.P., 2001. The ABC transporter Bcrp1/ABCG2 is expressed in a wide variety of stem cells and is a molecular determinant of the side-population phenotype. *Nat. Med.* 7, 1028–1034.
- Zhou, Y., Xu, Y., Tan, Y., Qi, J., Xiao, Y., Yang, C., Zhu, Z., Xiong, D., 2006. Sorcin, an important gene associated with multidrug-resistance in human leukemia cells. *Leuk. Res.* 30, 469–476.
- Zhou, S.F., 2008. Structure, function and regulation of P-glycoprotein and its clinical relevance in drug disposition. *Xenobiotica* 38, 802–832.
- Zhu, H., Wu, H., Liu, X., Evans, B.R., Medina, D.J., Liu, C.G., Yang, J.M., 2008. Role of MicroRNA miR-27a and miR-451 in the regulation of MD R1/P-glycoprotein expression in human cancer cells. *Biochem. Pharmacol.* 76, 582–588.

# Binding of doxorubicin to Sorcin impairs cell death and increases drug resistance in cancer cells

Ilaria Genovese<sup>1</sup>, Annarita Fiorillo<sup>1</sup>, Andrea Ilari<sup>2</sup>, Silvia Masciarelli<sup>3</sup>, Francesco Fazi<sup>\*3</sup> and Gianni Colotti<sup>\*2</sup>

Sorcin is a calcium binding protein that plays an important role in multidrug resistance (MDR) in tumors, since its expression confers resistance to doxorubicin and to other chemotherapeutic drugs. In this study, we show that Sorcin is able to bind doxorubicin, vincristine, paclitaxel and cisplatin directly and with high affinity. The high affinity binding of doxorubicin to sorcin has been demonstrated with different techniques, that is, surface plasmon resonance, fluorescence titration and X-ray diffraction. Although the X-ray structure of sorcin in complex with doxorubicin has been solved at low resolution, it allows the identification of one of the two doxorubicin binding sites, placed at the interface between the EF5 loop the G helix and the EF4 loop. We show that Sorcin cellular localization changes upon doxorubicin treatment, an indication that the protein responds to doxorubicin and it presumably binds the drug also inside the cell, soon after drug entrance. We also demonstrate that Sorcin is able to limit the toxic effects of the chemotherapeutic agent in the cell. In addition, Sorcin silencing increases cell death upon treatment with doxorubicin, increases the accumulation of doxorubicin in cell nucleus, decreases the expression of MDR1 and doxorubicin efflux via MDR1.

*Cell Death and Disease* (2017) 8, e2950; doi:10.1038/cddis.2017.342; published online 20 July 2017

The development of drug resistance is the leading cause of chemotherapy failure in cancer treatment. Elucidation of the mechanisms that confer simultaneous resistance to different drugs with different chemical structures and molecular targets – multidrug resistance (MDR) – has been a primary goal of cancer biologists during the past decades. Chemotherapy is the treatment of choice in metastatic cancer; by limiting drug's effectiveness, MDR represents a major obstacle to this option.

Cancer cells can adopt several strategies to evade death induced by chemotherapeutic agents. These include changes in apoptotic pathways, increased DNA damage repair, drug inactivation, alteration of drug targets and increased expression of ABC transporters, able to pump xenobiotics (such as toxins or drugs) out of cells.<sup>1</sup> Many cancer cells express large amounts of MDR1 (ABCB1, or P-glycoprotein 1), which confers them MDR.<sup>2–4</sup>

Sorcin (SOLuble Resistance-related Calcium-binding protein) gene is located in the same chromosomal locus and amplicon as the ABC transporters MDR1 and MDR3, both in human and rodent genomes, and is highly conserved among mammals. Sorcin was initially labeled 'resistance-related', since it is co-amplified with MDR1 in multidrug-resistant cells.<sup>5,6</sup> While for years Sorcin overproduction was believed to be a by-product of the coamplification of its gene with P-glycoprotein genes,<sup>7</sup> many recent reports have demonstrated that Sorcin plays a role in MDR, and pointed at a possible role as an oncoprotein.

Sorcin is one of the most highly expressed calcium-binding proteins in many tissues, and part of the 5% most expressed

proteins of the human proteome (PaxDb). Importantly, Sorcin is overexpressed in many human tumors and MDR cancers.<sup>8</sup> The level of Sorcin expression in leukemia patients inversely correlates with patients' response to chemotherapies and overall prognosis. In parallel, Sorcin is highly expressed in chemoresistant cell lines and significantly upregulated in doxorubicin-induced MDR leukemia cell line K562/A02 over its parent cells. Sorcin overexpression by gene transfection increased drug resistance to a variety of chemotherapeutic agents in K562 cells, SGC7901 cells, ovarian and breast cancer. On the other hand, several studies have demonstrated that inhibition of Sorcin expression by RNA interference led to reversal of drug resistance in many cell lines.<sup>8</sup>

Recent data indicate that Sorcin participates in several processes that might contribute to MDR in human cancers, such as drug efflux regulation, apoptosis modulation and epithelial-to-mesenchymal transition (EMT) control.<sup>8,9</sup> Conflicting results are in literature on the effect of Sorcin overexpression and silencing on MDR1 expression and activity.<sup>10–13</sup> A complete understanding of the mechanisms and pathways by which Sorcin contributes to the MDR phenotype of tumor cells and an assessment of the overall diagnostic and therapeutic potential of sorcin in MDR are still missing.

Recently we have solved the crystal structure of apo- and calcium-bound human Sorcin, showing the mechanism of activation of the protein.<sup>14</sup> Upon calcium binding Sorcin undergoes a large conformational change that exposes three pockets, hydrophobic surfaces involving the EF loop and EF5

<sup>1</sup>Department of Biochemical Sciences, Sapienza University, Rome, Italy; <sup>2</sup>IBPM-CNR Institute of Molecular Biology and Pathology, Italian National Research Council, Rome, Italy and <sup>3</sup>Department of Anatomical, Histological, Forensic & Orthopaedic Sciences, Section of Histology & Medical Embryology, Sapienza University, Rome, Italy

\*Corresponding author: F Fazi, Department of Anatomical, Histological, Forensic & Orthopaedic Sciences, Section of Histology & Medical Embryology, Sapienza University of Rome. Via Antonio Scarpa 14-16, Rome 00161, Italy. Tel: +39-0649766575; Fax: +39-064462854; E-mail: francesco.fazi@uniroma1.it or G Colotti, IBPM-CNR Institute of Molecular Biology and Pathology, Italian National Research Council, c/o Dept. Biochemical Sciences, Sapienza University, Ple A.Moro 5, Rome 00185, Italy. Tel: +39-0649910910; Fax: +39-064440062; E-mail: gianni.colotti@uniroma1.it

Received 09.3.17; revised 22.5.17; accepted 13.6.17; Edited by J-C Marine

hand (Pocket 1), EF2-EF3 (Pocket 2) and region EF1-EF3 (Pocket 3). This allows Sorcin to bind and regulate target proteins in a calcium-dependent fashion.<sup>15–21</sup>

Here we demonstrate that Sorcin binds doxorubicin directly and with high affinity and that it changes its cellular localization upon doxorubicin treatment and limits the toxic effects of doxorubicin in the cell; the low resolution structure of Sorcin in complex with doxorubicin allowed the identification of at least one chemotherapeutic drug binding site. We also demonstrate that Sorcin silencing increases cell death upon doxorubicin treatment, increases the accumulation of doxorubicin in cell nucleus, decreases the expression of MDR1 and doxorubicin efflux via MDR1.

## Results

### Sorcin binds doxorubicin and other chemotherapeutic drugs with high affinity.

For surface plasmon resonance (SPR) experiments, two types of sensorgrams have been measured. OneStep-SPR experiments show that Sorcin is able to bind doxorubicin, paclitaxel and vinblastine, with high affinity, in the submicromolar range (Figure 1, Supplementary Figure S1); FastStep-SPR experiments (Figure 1a, Supplementary Figure S2) can be fitted with two binding sites, one in the nanomolar range and one in the low micromolar range ( $K_{D1}=10\text{ nM}$ ;  $K_{D2}=1\text{ }\mu\text{M}$  in the presence of calcium;  $K_{D1}=22\text{ nM}$ ;  $K_{D2}=2\text{ }\mu\text{M}$  in the presence of EDTA). Sorcin also binds cisplatin, with a  $K_D=1.7\text{ }\mu\text{M}$  (one binding site, Supplementary Figure S1). Fluorescence titrations (Figures 1b and c, Supplementary Figure S2) were carried out by measuring the fluorescence at 280 nm upon stepwise doxorubicin addition to Sorcin (Figure 1b) and to the Sorcin calcium-binding domain (SCBD, Figure 1c), comprising residues 32–198 of Sorcin. The fitting of fluorescence titrations for both Sorcin and SCBD are compatible with 2 doxorubicin binding sites (Figure 1, Supplementary Figure S2), with affinity constants in the same order of magnitude with respect to those measured by SPR experiments, that is,  $1.4\pm 1$  and  $734\pm 396\text{ nM}$  for SCBD and  $0.9\pm 0.5$  and  $511\pm 140\text{ nM}$  for Sorcin in the presence of EDTA (1.2 and 360 nM; 0.9 and 318 nM for Sorcin, in the presence of 1 and 5 mM magnesium, respectively): doxorubicin binding occurs at the C-terminal calcium-binding

domain, since SCBD retains the binding sites. Signal shift was not detected, indicating that the environment of fluorophores did not change upon doxorubicin binding. The value obtained for  $K_{D1}$  is lower than protein concentration, condition that can cause an overestimation of the constant and large errors. We could not lower protein concentration due to the signal/noise ratio; however it can be assessed that  $K_{D1}$  is not greater than estimated.

Therefore, Sorcin, which was previously shown to increase resistance to a variety of chemotherapeutic agents, is able to bind directly and with high affinity doxorubicin and other chemotherapeutic drugs *in vitro*; this prompted further experiments to understand how such binding may contribute to increase drug resistance in cells as a function of its expression in the cell.

### Crystal structure of the Sorcin-doxorubicin complex.

Addition of 4:1 molar excess of doxorubicin to a clear, transparent solution of concentrated apo-Sorcin determines clouding of the solution, aggregation and precipitation of the protein (similar to the precipitation observed upon calcium addition), with formation of a red precipitate and the slow growth of red-colored crystals (Figure 2a).

Crystals of different intensity of red color grew depending on the amount of doxorubicin used for crystallization, ranging from 0.5:1 (colorless) to 2:1 (pink) to 15:1 (red) molar excesses. Emission spectra of the crystals grown from these solutions were recorded at 100 K in the Bessy facility, exciting at 473 nm. Changes in peaks intensity and a 25 nm red shift of the bands in high-amount doxorubicin (red crystals) were observed with respect to low-amount doxorubicin Sorcin crystals (Supplementary Figure S3). These changes are likely due to doxorubicin stacking to aromatic residues of the protein or doxorubicin dimerization, once bound.<sup>22</sup>

We solved the structure of the complex between SCBD and doxorubicin (doxo-SCBD) at quite low resolution (3.74 Å, PDB accession: 5MRA). The asymmetric unit contains two dimers (A–B and C–D). The structure contains 10  $\text{Mg}^{2+}$  ions (3 bound to monomer A, 2 to monomer B, 3 to monomer C, 2 to monomer D). Doxorubicin is bound to the B monomer. The protein structure is similar to apo-Sorcin and apo-SCBD (PDB accessions: 4UPG, 1 GJY<sup>14,23</sup>) (Figure 2b). The superimposition between the *Ca* trace of doxo-SCBD with the *Ca*

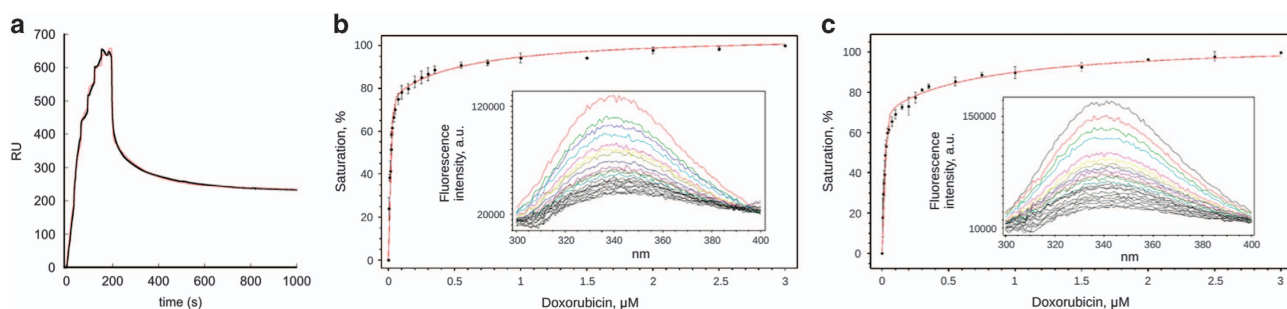


**Figure 1** Sorcin binds doxorubicin with high affinity *in vitro*. (a) SPR titration experiments in the presence of 500  $\mu\text{M}$   $\text{CaCl}_2$  and (b,c) fluorescence titration experiments in the presence of 0.5  $\mu\text{M}$  EDTA: Doxorubicin binding to Sorcin (b) and SCBD (c) monitored by intrinsic fluorescence quenching. Each protein was incubated for 3 min at 25 °C in the presence of increasing concentration of ligand. The bars indicate the standard deviation for three independent experiments. The insets show the whole emission peak for each sample from one representative experiment. Both Sorcin and SCBD contain two binding sites for doxorubicin, with affinities in the nanomolar and low micromolar range



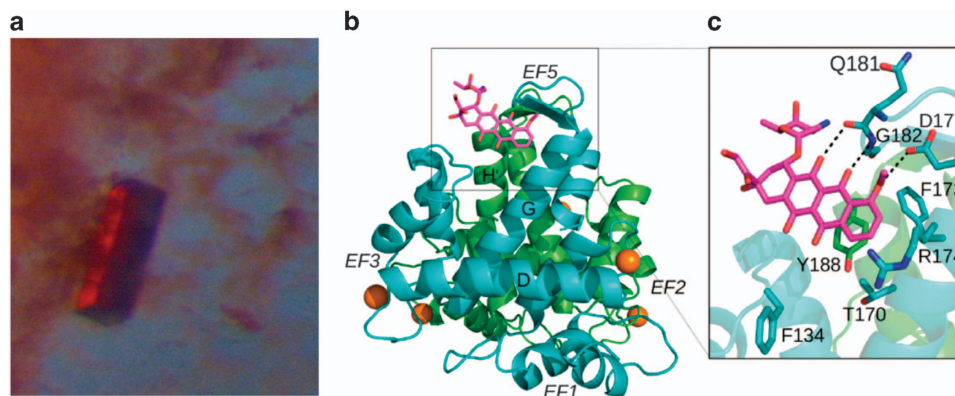


**Figure 2** Sorcin calcium binding domain-doxorubicin complex. (a) Crystal and (b) crystal structure of Sorcin calcium binding domain-doxorubicin complex; (c) doxorubicin binding site at EF5 (pocket 1), stacked to Tyr188

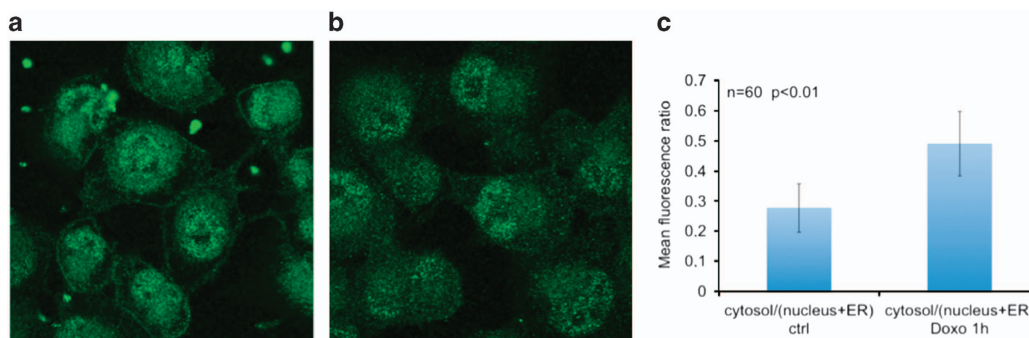


**Figure 3** Sorcin localization changes upon doxorubicin treatment. Sorcin localization (green fluorescence) in (a) control H1299 cells and in (b) H1299 cells treated for 1 h with 0.6  $\mu$ M doxorubicin. (c) ratio between cytosol/(nucleus+ER) fluorescence ( $n = 60$  cells;  $P < 0.01$ )

trace of apo-Sorcin yields an rmsd of 1.11 Å, indicating that the structures are similar and therefore neither  $Mg^{2+}$  ions binding nor doxorubicin binding are able to promote the conformational changes induced by calcium ions in Sorcin. In accordance with binding experiments, doxorubicin binding occurs at two sites. Inspection of the Fo-Fc electronic density map allowed the identification of two peaks (Supplementary Figure S4): one close to the EF5 hand, which does not bind calcium in Sorcin and is responsible for dimer formation, and the other close to the D-helix connecting the EF2 and EF3 sites at the interface between the two dimers. We succeeded in modeling the doxorubicin molecule in the first site (close to the EF5) whereas it was not possible to model the doxorubicin molecule in the second site (close to the D helix) indicating both the low occupancy of the site and the flexibility of the doxorubicin molecule (Supplementary Figure S4). These sites have been previously identified as Pocket 1 and Pocket 2, able to bind protein targets, in another PEF protein, that is, PDCD6 (ALG-2).<sup>24</sup>

The binding of doxorubicin to SCBD in pocket 1 involves a stacking interaction of the drug with the aryl ring of Tyr188 of one monomer and interaction with Asp177, Gly182, Phe173 and Phe134 of the two-fold symmetry related monomer at the dimeric interface (Figures 2b and c). In the second putative site (pocket 2) doxorubicin likely interacts with Trp105 and

Phe134. Probably doxorubicin binding to the second site would be facilitated by the binding of calcium ions which, as previously described,<sup>14</sup> induce a conformational change promoting the movement of the D-helix and the exposure of hydrophobic interfaces.

In the structure, magnesium is bound to EF3 and to part of EF1 and EF2 sites, showing that in Sorcin the first three EF-hands can bind not only calcium, but also magnesium, with rather high affinity, and that EF3 is the site endowed with the highest affinity for divalent cations, responsible for Sorcin cation-dependent activation.

### Sorcin localization responds to doxorubicin treatment.

In H1299 lung cancer cell line, Sorcin (green fluorescence) localizes to cell membrane, nucleus, ER and cytosol, as already observed in other cellular systems.<sup>17</sup> Upon treatment with doxorubicin, Sorcin localization changes with respect to control: after 1-h doxorubicin treatment, cytosolic Sorcin localization increases and nuclear, ER and membrane localization decreases; the ratio of cytosol/(nuclear+ER) Sorcin fluorescence increases by 77% (from 0.278 to 0.491, number of cells = 60,  $P < 0.01$ , Figure 3). This is a clear indication that Sorcin localization responds to doxorubicin treatment and that Sorcin presumably binds doxorubicin also in the cell, upon drug entry.

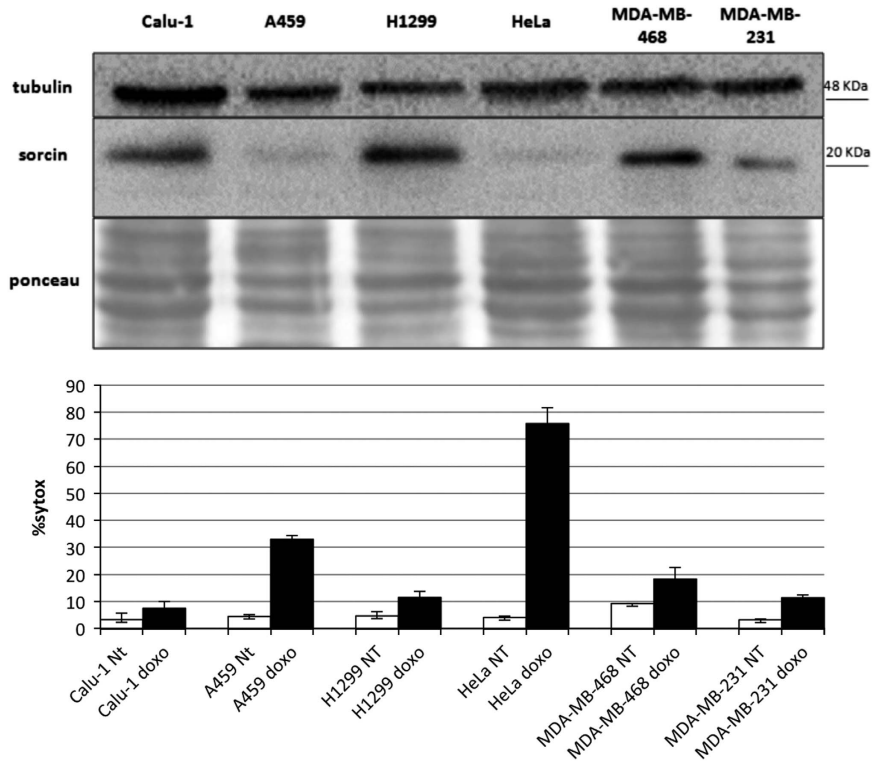


**Figure 4** Sorcin expression versus cell death. (top) Western blot experiment showing the expression of Sorcin in lung carcinoma Calu-1, A459 and H1299 cells; cervix adenocarcinoma HeLa; breast adenocarcinoma MDA-MB-468 and MDA-MB-231. (bottom) Cell death is increased upon 24 h doxorubicin (0.6  $\mu$ M) treatment in A549 and HeLa cells, where Sorcin expression level is reduced by > 80% with respect to H1299 cells

**Effect of Sorcin expression on doxorubicin uptake and toxicity, and cell death.**

Sorcin is expressed at high levels in human and in many cell lines (PaxDB). We have analyzed Sorcin expression in different cell lines from lung, cervix and breast cancers and we evidenced that Sorcin is expressed in all tested cell lines, but the levels differ even by more than one order of magnitude between different lines. In particular, Sorcin is highly expressed in lung cancer cell lines Calu-1 and H1299, that we have selected for further studies, and in breast cancer cell lines MDA-MB-231 and MDA-MB-468, while low Sorcin expression levels were observed in lung A549 and in cervical cancer HeLa cells (Figure 4).

Sorcin high level of expression occurs in cell lines rather resistant to cell death upon treatment with doxorubicin, as H1299, Calu-1 and MDA-MB-468 cells, while A459 and HeLa cell lines, where Sorcin expression is lower by about 90%, are more sensitive to doxorubicin treatment (Figure 4). To support the relevance of Sorcin in doxorubicin treatment response, we proceeded with Sorcin silencing experiments. In all tested cell lines, siRNA cds3 effectively silences Sorcin expression, by at least 85% after 24–48 h (Supplementary Figure S5A). In the H1299 line,  $94 \pm 3\%$  silencing occurs. Interestingly the silencing of Sorcin expression is also maintained upon doxorubicin treatment (Supplementary Figure S5B).

Sorcin silencing by siRNA cds3 (versus control experiments with scrambled siRNA) slightly increases cell death (Figures 5a and b, Supplementary Figure S6), as shown by both cell count and by flow cytometry experiments on cells

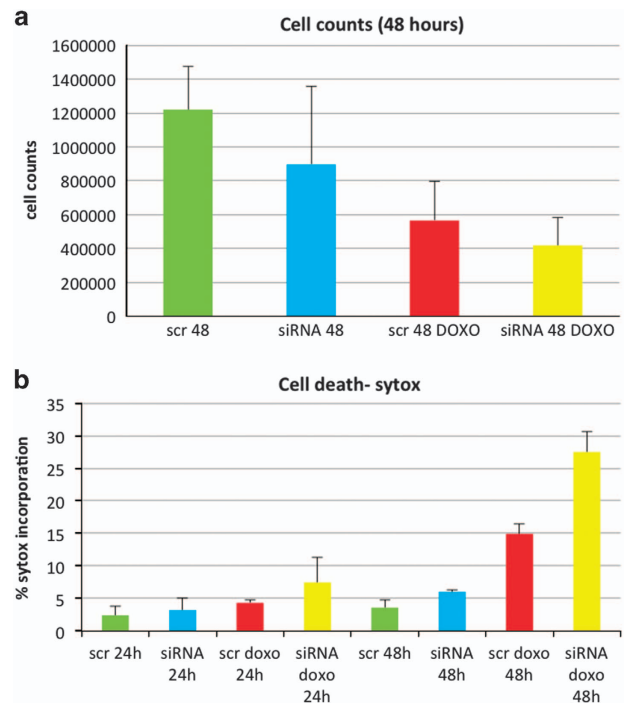


**Figure 5** Sorcin silencing increases cell death upon treatment of H1299 cells with 0.6  $\mu$ M doxorubicin. (a) Cell count and (b) cell death percentage upon treatment of H1299 cells with scrambled siRNA or Sorcin siRNA in control and doxorubicin-treated cells

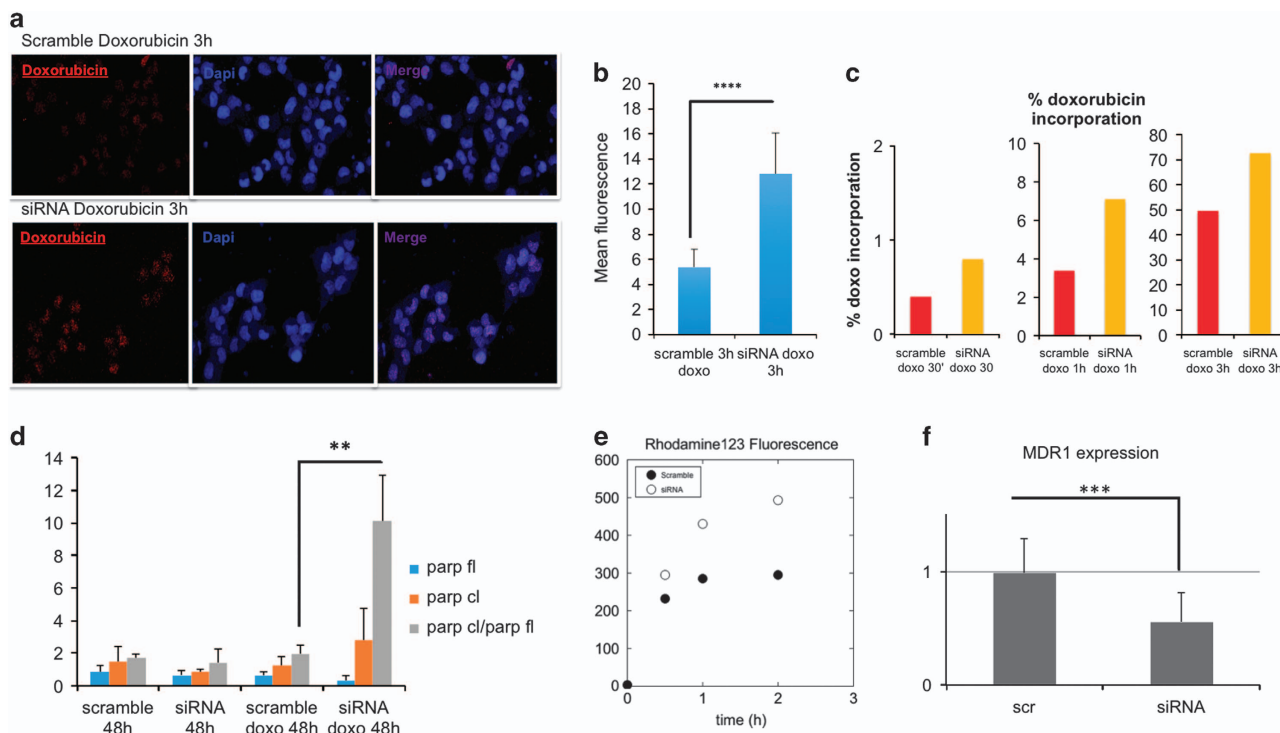


**Figure 6** Sorcin silencing increases doxorubicin accumulation in H1299 cells. (a) confocal microscopy images, showing the nuclear accumulation of doxorubicin upon 3 h treatment in H1299 cells treated with scrambled siRNA (top) or with Sorcin siRNA (bottom); (b) nuclear doxorubicin incorporation by fluorescence quantification ( $n=60$  cells;  $P<0.0001$ ); (c) time-dependent quantification of doxorubicin incorporation in H1299 cells by FACS; (d) upon 48 h doxorubicin treatment, in Sorcin-silenced cells PARP cleavage is increased with respect to control cells ( $n=3$ ,  $P<0.01$ ). Sorcin silencing decreases MDR1 activity and expression with respect to control cells: (e) Rhodamine123 fluorescence is increased (and therefore its efflux is decreased) and (f) MDR1 expression is decreased in Sorcin-silenced H1299 cells with respect to control cells ( $n=3$ ,  $P<0.001$ )

stained with Sytox blue, a cyanine dye that is completely excluded from live eukaryotic cells.

Upon Sorcin silencing, doxorubicin-dependent cell death is markedly increased in H1299 cells (Figure 5): upon treatment with scrambled siRNA and  $0.6 \mu\text{M}$  doxorubicin, the percentage of dead H1299 cells increases from 3.4% (control) to 4.6% and 16.3% (24 and 48 h after doxorubicin treatment, respectively), while upon treatment with Sorcin-directed siRNA and  $0.6 \mu\text{M}$  doxorubicin, the percentage of dead H1299 cells increases from 4.5% (control) to 10.3% and 29.7% (+124% and +82%, 24 and 48 h after doxorubicin treatment, respectively).

Further, Sorcin silencing increases doxorubicin entry in H1299 cell nuclei by 140% as shown by analysis of confocal microscopy experiments (Figures 6a and b). FACS experiments (Figure 6c, Supplementary Figure S7) show that upon treatment with scrambled siRNA and  $0.6 \mu\text{M}$  doxorubicin, the percentage of doxorubicin incorporation increases from 0.4% after 30 min to 3.4% after 1 h to 49.6% after 3 h doxorubicin treatments, while upon treatment with Sorcin-directed siRNA and  $0.6 \mu\text{M}$  doxorubicin, the percentage of doxorubicin incorporation increases from 0.8% after 30 min to 7.1% after 1 h to 72.7% after 3 h doxorubicin treatments (+100%, +109%, +47%, respectively). After 5 h incubation with doxorubicin, the buffering capacity of Sorcin is almost lost (Supplementary Figure S7).

In the presence of high levels of Sorcin, doxorubicin is therefore prevented from entering the nuclei of H1299 cells,

and the cells are protected from drug-dependent DNA damages.

Sorcin protects cells, while Sorcin silencing increases doxorubicin-dependent Poly(ADP-ribose)polymerase (PARP) cleavage (Figure 6d, Supplementary Figure S8), an apoptotic marker. In cells treated with Sorcin-directed siRNA, 48 h after treatment with  $0.6 \mu\text{M}$  doxorubicin, the levels of cleaved PARP are higher than in control cells. An even higher increase of doxorubicin-dependent PARP cleavage upon Sorcin silencing in doxorubicin-treated cells can be measured by calculating the ratio between the intensities of cleaved versus full-length PARP.

**Effect of Sorcin expression on MDR1 expression and activity.** The effect of Sorcin expression on doxorubicin uptake and toxicity can be explained in part by the direct binding of doxorubicin by Sorcin, that may prevent the drug entry in the nucleus. However, doxorubicin is also a substrate of the efflux pump MDR1,<sup>2</sup> whose gene is located in the same amplicon of Sorcin gene.<sup>5</sup> Conflicting results are in literature on the effect of Sorcin expression on MDR1 expression and activity.<sup>10–13</sup>

Figures 6e and f show that Sorcin silencing decreases both MDR1 expression and activity in H1299 cells, as already demonstrated in A549 cells<sup>25</sup> by about 40%. In cells treated with Sorcin-directed siRNA the MDR1-mediated efflux of rhodamine123 is substantially decreased with respect to control cells treated with scrambled siRNA, showing a



decrease of the activity of MDR1 in Sorcin-silenced cells (Figure 6e, Supplementary Figure S9): the level of intracellular rhodamine123 in H1299 cells treated with Sorcin-directed siRNA is increased by 27, 51 and 67% (upon 30 min, 1 h and 2 h incubation with the MDR1 substrate, respectively) with respect to control cells.

MDR1 expression level is also strongly decreased by Sorcin silencing: in cells treated with Sorcin-directed siRNA, a 45% decrease in MDR1 level occurs with respect to H1299 control cells (Figure 6f, Supplementary Figure S10).

## Discussion

The high level of expression of Sorcin in many tumors, especially the MDR ones, the inverse correlation of Sorcin expression with patients' response to chemotherapies and overall prognosis, and reversal of drug resistance upon Sorcin expression by RNA interference have recently struck the attention of many scientists. In particular, Sorcin has been shown to be upregulated in doxorubicin-induced MDR K562/A02 leukemia cells over their parent cells, and Sorcin overexpression has been demonstrated to increase drug resistance to doxorubicin, etoposide, homoharringtonine, vincristine, taxol, cisplatin and 5-fluorouracil in several cancer cells.<sup>6,26–32</sup> Further, many studies have demonstrated Sorcin participation in several processes, such as drug efflux regulation, apoptosis modulation and EMT control, that might contribute to the onset of MDR in human cancers.<sup>8,9</sup>

However, the molecular basis of Sorcin-linked processes that determine MDR has not been elucidated yet.

Here, we show for the first time that Sorcin is itself able to bind directly and with high affinity chemotherapeutic agents able to induce Sorcin-dependent MDR, such as cisplatin, vinblastine, paclitaxel and in particular doxorubicin. SPR and fluorescence titration experiments demonstrated that Sorcin binds doxorubicin with high affinity and that there are at least two doxorubicin-binding sites. The low resolution X-ray structure of the complex allowed the identification of at least one of these sites. Doxorubicin binds to regions that in PDCD6, structurally similar to Sorcin, are involved in ALIX-Abs peptide binding:<sup>24</sup> binding occurs with 100% occupancy and high affinity to Pocket 1 and with lower occupancy to Pocket 2. Sorcin can therefore use the same pockets in different fashions: they not only can bind calcium channels and other proteins (RyR receptors, SERCA, NCX1), and regulate their activity, thereby increasing Ca<sup>2+</sup> accumulation in the endoplasmic (ER)/sarcoplasmic reticulum (SR), and increasing resistance to ER stress,<sup>17,19,20,21,33,34</sup> but can also bind chemotherapeutic drugs with high affinity, decreasing doxorubicin-dependent toxicity and cell death. In addition, the present study shows that in H1299 cells expressing high Sorcin levels, upon doxorubicin treatment Sorcin acquires a more diffused cytosolic pattern, implying that doxorubicin can be bound and sequestered by Sorcin (which is one of the most expressed calcium-binding proteins) in the cytosol, before it can translocate to the nucleus and exert its toxic effects at cellular level.

These experiments contribute to elucidate the mechanisms of drug resistance to chemotherapeutic agents in highly Sorcin-expressing cells. Doxorubicin binds at the D-helix

connecting EF2 and EF3 sites of Sorcin, thereby covering this area and impairing the Trp105-based interaction with its targets located on cell membranes and ER surface<sup>14,16,21,35,36</sup> and at Tyr188 and Arg174 residues, belonging to the putative Nuclear Localization Sequence of Sorcin,<sup>17</sup> thereby hampering Sorcin translocation to nucleus.

Doxorubicin sequestration impairs its chemotherapeutic action, based on drug entry in the nucleus and its intercalation in the DNA, and allows its MDR1-based extrusion. Possibly, in a first phase, MDR may depend predominantly on doxorubicin sequestration. In the longer term, sequestration reaches saturation, and MDR depends predominantly on the higher MDR1-based extrusion.

We also show that when Sorcin expression is decreased, the cells become sensitive to doxorubicin: the chemotherapeutic drug can accumulate in the nucleus, where it exerts cytotoxic effects by inhibiting topoisomerase II, thereby generating free radicals and DNA damages, and activating death pathways via activation of caspases, disruption of mitochondrial membrane potential or mitotic catastrophe accompanied by senescence-like phenotype.<sup>37</sup> Chemotherapeutics binding to Sorcin is a fast process that results in fast cellular response to drug administration: Sorcin, one of the most highly expressed calcium-binding proteins, can act as a buffer for drugs, within a limited time span. Sorcin is a signaling protein, because of its ability to respond rapidly to calcium binding and, as we have demonstrated, to other molecules, such as doxorubicin. In addition, alteration of the cellular levels of Sorcin is a slower process, that impacts on MDR1 expression and that results in another mechanism of Sorcin-dependent drug resistance: Sorcin overexpression induces MDR1 expression via a cAMP-response element (CRE) of the MDR1 gene, and therefore through activation of the CREB pathway, by increasing CREB1 phosphorylation and the binding of CREB1 to the CRE sequence of *mdr1* promoter.<sup>13</sup> Sorcin silencing determines a decrease of activity and expression of MDR1, that pumps doxorubicin and many other drugs outside of the cell, in line with data from other resistant lung carcinoma cells or other tumors.<sup>13,25</sup> Sorcin silencing, combined to doxorubicin treatment, make cells prone to death. Sorcin also participates in other mechanisms related to oncogenesis and MDR onset, since it increases escape from apoptosis, by preventing ER stress and the unfolded protein response, by upregulating Bcl-2 and decreasing Bax expression.<sup>17,33,38–40</sup>

The structure of doxorubicin-bound Sorcin deserves some comments. Doxorubicin binding increases the disorder of the crystal and decreases the resolution of the structure with respect to those from unliganded protein. Addition of doxorubicin to a solution of concentrated apo-Sorcin determines clouding of the solution, aggregation and precipitation of the protein, followed by formation of a red precipitate and the slow growth of red-colored crystals. However, the structure of the Sorcin-doxorubicin complex is very similar to that of the apo protein, possibly because of the presence of magnesium in the crystallization solution. Magnesium binds to EF1, EF2 and EF3, in line with the affinity for calcium, which follows the order EF3>EF2>EF1.<sup>36</sup> While calcium binding to Sorcin determines a large conformational change and protein activation, neither magnesium binding nor doxorubicin binding

alters the structure. This can be due to the smaller ionic radius of magnesium with respect to calcium, and to crystal lattice forces that may favor an apo-like conformation. Generally speaking, calcium-dependent regulation of cellular activities is based on transient and/or local increase of  $\text{Ca}^{2+}$  concentration from 100 nM to low micromolar, while  $\text{Mg}^{2+}$  concentration remains constant at about 0.5–2 mM, that is, 2–4 orders of magnitude higher than  $\text{Ca}^{2+}$ . Usually EF-hand proteins discriminate against  $\text{Mg}^{2+}$ , being evolved to take advantage of the larger ionic radius and the less stringent demands on coordination ligands of  $\text{Ca}^{2+}$ .<sup>41</sup> Sorcin, at least in conditions where  $\text{Mg}^{2+}$  is very concentrated, is able to bind with full occupancy this ion. However, possibly calcium binding can elicit conformational changes that may lead to a better exposure of doxorubicin-binding pockets.

Overall our study demonstrates that Sorcin is able to bind directly and with high affinity doxorubicin and other chemotherapeutic drugs, and that this contributes to the generation of the MDR phenotype. This work, together with other recent papers, shows that Sorcin can be a useful marker of MDR and may represent a therapeutic target for reversing tumor MDR.

## Materials and Methods

**Surface plasmon resonance (SPR) experiments.** SPR experiments were performed with a SensiQ Pioneer apparatus. Wild-type human Sorcin was immobilized via amine coupling onto a COOH5 sensorchip, previously chemically activated by 100  $\mu\text{l}$  injection of a 1 : 1 mixture of *N*-ethyl-*N*'-3-(diethylaminopropyl) carbodiimide (200 mM) and *N*-hydroxysuccinimide (50 mM). Immobilizations were carried out in 20 mM sodium acetate at pH 4.5; the remaining ester groups were blocked by injecting 100  $\mu\text{l}$  of 1 M ethanolamine hydrochloride at pH 9.5.

The amount of immobilized Sorcin was detected by mass concentration-dependent changes in the refractive index on the sensorchip surface, and corresponded to about 5000 resonance units (RU).

Samples of analytes (doxorubicin, cisplatin, vinblastine and paclitaxel) were dissolved in 100% DMSO at a concentration of 10 mM, and subsequently diluted in sterile HEPES 20 mM, pH 7.4, NaCl 150 mM, 500  $\mu\text{M}$   $\text{CaCl}_2$  (or EDTA) 0.005% surfactant P-20 to yield 2% DMSO final concentration (HSP-2%D buffer) and final drug concentration: 200  $\mu\text{M}$ . Further dilutions and all the experiments were carried out at 25 °C in degassed HSP-2%D buffer.

For FastStep experiments, the analytes were automatically diluted in HSP-2%D and injected by seven serial doubling steps (step contact time = 30 s, nominal flow rate = 100  $\mu\text{l}/\text{min}$ ). At the following time points: (1) 0–30 s; (2) 31–60 s; (3) 61–90 s; (4) 91–120 s; (5) 121–150 s; (6) 151–180 s; (7) 181–198 s, analyte concentrations were: (1) 1.25  $\mu\text{M}$ ; (2) 2.5  $\mu\text{M}$ ; (3) 5  $\mu\text{M}$ ; (4) 10  $\mu\text{M}$ ; (5) 20  $\mu\text{M}$ ; (6) 40  $\mu\text{M}$ ; (7) 80  $\mu\text{M}$ . For OneStep experiments, Taylor dispersions were exploited to generate analyte concentration gradients that provide high-resolution dose response in single injections. Full analyte titrations were recorded in HSPC-2%D over four orders of magnitude in concentration, up to 80  $\mu\text{M}$ .

In both FastStep and OneStep experiments, the increase in RU relative to baseline indicates complex formation between the immobilized Sorcin ligand and the analytes. The plateau region represents the steady-state phase of the interaction. The decrease in RU after 198 s in FastStep experiments, or after 350 s in OneStep experiments, indicates analyte dissociation from the immobilized Sorcin after HSP-2%D buffer injection. As a negative control, sensor chips were treated as described above in the absence of immobilized Sorcin. Values of the plateau signal at steady-state ( $R_{\text{eq}}$ ) and full fittings with 1, 2 and 3 sites were calculated from kinetic evaluation of the sensorgrams using the Qdat 4.0 program.

**Fluorescence titrations.** Static fluorescence measurements were performed at 25 °C with a Horiba Fluoromax-4 spectrofluorometer using 1-cm path-length quartz cuvettes (slit width: 5 nm in excitation and emission). Fluorescence measurements were performed on Sorcin and SCBD, a shorter construct missing the first 32 residues, at two different concentrations: 30 nM and 37 nM, in Tris-HCl 10 mM, pH 7.5 and EDTA (0.5  $\mu\text{M}$ ) or  $\text{MgCl}_2$  (1 mM or 5 mM). The excitation

wavelength was set at 280 nm and emission spectra were collected in the 300–400 nm range. Triplicate samples were measured; each figure represents the average of three experiments.

Maximum emission occurs at 340 nm for SCBD and 338 nm for Sorcin. Upon doxorubicin addition, fluorescence quenching was observed to a maximum extent of about 60% in saturating condition. For each sample fluorescence was measured after 3 min of incubation.

Since doxorubicin absorbs light at 280 nm, fluorescence measurements are affected by the inner-filter effect. The following formula was employed for correction:  $F_{\text{cor}} = F_{\text{obs}}10^{(A_{\text{ex}}/2)}$ , where  $F_{\text{cor}}$  and  $F_{\text{obs}}$  are the corrected and observed fluorescence intensities, respectively, whereas  $A_{\text{ex}}$  is the absorbance of each concentration of ligand at 280 nm [IFE-correction]. The effect is negligible at the concentrations of doxorubicin used (5–3000 nM). Data were fitted with the software Qtiplot assuming two independent binding sites. The equation used for data fitting is the weighted sum of two independent binding events:  $K((k+c+x) - \sqrt{((k+c+x)^2 - 4cx)}) / (2c) + H((h+c+x) - \sqrt{((h+c+x)^2 - 4cx)}) / (2c)$ , where  $c$  is protein concentration,  $k$  and  $h$  are the two binding constants,  $K$  and  $H$  are the fraction of signal due to each binding event.

**Crystallization, data collection and structure solution.** Crystallization experiments were performed with both human Sorcin and SCBD. Automated crystallization screening and by-hand optimization were carried out at 298 K by vapor diffusion method.

At first soaking technique was attempted but, while doxorubicin is deep red, the crystals stayed uncolored; then we moved to co-crystallization. Since Sorcin precipitates in presence of doxorubicin excess, trials were set up by adding the ligand to the crystallization drop (0.4  $\mu\text{l}$  of 0.5 mM protein+0.4  $\mu\text{l}$  of reservoir+0.1  $\mu\text{l}$  of 30 mM doxorubicin) to a ligand/protein ratio of about 15. Colored crystals, from light pink to red, grew in many conditions but most of them resulted in poor diffraction. The best data set collected was at 3.7 Å resolution, from a SCBD crystal grown in 0.2 M  $\text{MgCl}_2$ , 0.1 M Tris-HCl pH 7, 2.5 M NaCl. The crystals were cryoprotected by adding 40% w/v glucose to the mother liquor.

A single wavelength (0.9677 Å) data set was collected at ESRF at 100 K on the ID30-A3 MASSIF3 beamline equipped with a Eiger-X-4M detector and processed with XDS.<sup>42</sup> Crystal parameters and data collection statistics are reported in Table 1.

The structure was determined by molecular replacement with the program MOLREP<sup>43</sup> (CCP4 suite) using the structure of the calcium-free human Sorcin

**Table 1** Crystal parameters, data collection statistics and refinement statistics

PDB code	5MRA
Space group	P2 <sub>1</sub> 2 <sub>1</sub> 2 <sub>1</sub>
Cell parameters (Å)	a = 92.36, b = 104.98, c = 113.42
Asymmetric unit, residues	Tetramer, 166 per monomer
N° of bound ions	10 $\text{Mg}^{++}$
<b>Data reduction</b>	
Resolution range (Å)	48.31–3.74 (3.96–3.74)
Unique reflections	11800 (1845)
Completeness (%)	99.0% (97.2%)
Redundancy	6.53 (6.47)
$R_{\text{merge}}$ (%)	10.2 (113.3)
CC(1/2)	99.9 (64.7)
$I/\sigma(I)$	11.81 (1.45)
<b>Data refinement</b>	
Resolution range (Å)	48.31–3.74 (3.83–3.74)
$R_{\text{cryst}}$ (%)	19.6 (35)
$R_{\text{free}}$ (%)	28.5 (37)
rms (angles) (°)	1.324
rms (bonds) (Å)	0.01
Wilson B-factor (Å <sup>2</sup> )	162.2
Residues in core regions of the Ramachandran plot (%)	90
Residues in allowed regions of the Ramachandran plot (%)	10

Values in parentheses are for the highest-resolution shell



(PDB entry 4UPG) as search model. Refinement was performed using the maximum-likelihood method with the program REFMAC<sup>44</sup> and model building with the program Coot.<sup>45</sup>

Fluorescence emission spectra of SCBD-doxorubicin crystals were collected at ESRF ID29S at 100 K and excitation wavelength 473 nm. The experimental setup is described in more detail in a paper by Royant *et al.*<sup>46</sup>

**Cell cultures and western blots.** H1299, Calu-1, A459 human lung carcinoma, HeLa human cervix adenocarcinoma, MDA-MB-468 and MDA-MB-231 breast adenocarcinoma cell lines were cultured in DMEM medium (Gibco, Invitrogen, Thermo Fisher Scientific, Waltham, MA, USA) with 10% FBS (v/v) and 5% Penicillin/Streptomycin (v/v) at 37 °C in a balanced air humidified incubator with 5% CO<sub>2</sub>.

The cells were lysed in a 2% SDS lysis buffer (25 mM Tris-HCl at pH 7.5, 100 mM NaCl, 3 mM EDTA, 7% glycerol) with: NaF 1000 ×, NaVO<sub>3</sub> 100 ×, Na<sub>4</sub>PO<sub>7</sub> 20 ×, Aprotinin 1000 ×, Leupeptin 1000 ×, PMSF 100 × protease and phosphatase inhibitors as final concentrations.

Extracts were sonicated for 10 s and centrifuged at 12 000 r.p.m. for 10 min to remove cell debris. Lysates were quantified in proteins content with Pierce BCA protein assay kit (Thermo Fisher Scientific, Waltham, MA, USA) according to the manufacturer's instructions.

Thirteen percent acrylamide-bisacrylamide SDS gel electrophoreses were run for sorcin, and 7% SDS-PAGE were run for PARP and MDR1. Proteins lysate content was checked by S-Ponceau staining. Western blotting analysis was performed with the following antibodies: rabbit polyclonal anti-human sorcin (home-made<sup>14</sup>), mouse monoclonal anti-PARP (Cell Signalling, Danvers, MA, USA, #9532), mouse monoclonal anti-MDR1 (Santa Cruz Biotechnology, Heidelberg, Germany, sc-13131), mouse monoclonal anti-tubulin (Sigma-Aldrich, Darmstadt, Germany, cat. T5168) and mouse monoclonal anti-βactin (Santa Cruz Biotechnology, sc-81178). Goat secondary anti-mouse and anti-rabbit antibodies conjugated to horseradish peroxidase were used (Bio-Rad, Hercules, CA, USA, cat. 170-6515, 170-6516). Immunostained bands were detected by chemiluminescence (Chemidoc, Bio-Rad).

**Doxorubicin treatment and silencing for sorcin.** We performed a dose-response curve (0.1 μM, 0.3 μM, 0.6 μM, 1.0 μM); 0.6 μM is the dose resulting in the best evaluation of time-dependent accumulation, and is compatible with doxorubicin plasma concentration 15 min to 2 h after treatment of many different types of cancer.<sup>47</sup> Doxorubicin concentration (0.6 μM) was used for most experiments. H1299 cells were transfected with a solution composed by Opti-mem medium (Gibco, Invitrogen, Thermo Fisher Scientific), Lipofectamine RNAi-max (Invitrogen, Thermo Fisher Scientific, Waltham, MA, USA, cat.13778-030) and a final concentration of 500 pM siRNA for sorcin (CDS3 and 3'UTR) (IDT sequence to CDS3-exon3: 5'-GAUAGAUGCUGAUGAAUUGCAGAGA-3'; sequence to 3'UTR-exon8: 5'-AGCUGUACACUUUUAAGUAAGAUCT-3', according to the manufacturer's instructions. CDS3 siRNA silences both sorcin isoforms.<sup>18</sup> After 48 h of transfection, the medium was replaced with fresh DMEM (Gibco, Invitrogen, Thermo Fisher Scientific) containing 0.6 μM doxorubicin. To evaluate doxorubicin incorporation, cells were treated with the drug in time-course experiments (30 min to 3 h incubation for cytofluorimetry, 3 h and 5 h for confocal microscopy). The analysis of biological effects of sorcin silencing was performed 24 h and 48 h after treatment.

**Doxorubicin uptake (confocal microscopy and FACS).** The uptake of doxorubicin was evaluated through confocal microscopy and FACS (Fluorescent-activated Cell Sorting) thanks to the autofluorescence of the molecule (excitation wavelength 470 nm; emission wavelength 585 nm). To avoid cells drug saturation the analysis was performed between 30 min and 5 h incubation.

For confocal microscopy, the medium was removed from the H1299 cells, then washed with PBS. The cells were fixed in 2% paraformaldehyde for 10 min, washed in PBS and incubated 7 min in TO-PRO-3 (Invitrogen, Thermo Fisher Scientific, Waltham, MA, USA, cat. T3605), dilution 1:3000. To avoid fluorophore quenching, samples were covered with Vectashield Mounting Medium (Vector Laboratories, Burlingame, CA, USA, cat. H-1000). Confocal images of slides were acquired at a Leica laser scanning microscope TCS-SP2.

In order to have a quantitative readout on doxorubicin incorporation we performed flow cytometry with CyAn ADP and Summit 4.3 software. The cells were dislodged with trypsin 0.05% (Gibco, Invitrogen, Thermo Fisher Scientific), the emission of doxorubicin was evaluated at 573 nm, and cells were gated as shown in supplementary results. Data were analyzed with FCS4 express software.

**Sytox blue assay and cell counts.** To evaluate cell death we performed assays with Sytox Blue Dead Cell Stain, for flow cytometry (Molecular Probes, Invitrogen, Thermo Fisher Scientific, Waltham, MA, USA, cat. MP34857). According to the manufacturer's instructions, 200 000 cells were sampled for each condition and incubated 15 min at room temperature with Sytox blue 1:1000 dilution. The samples were acquired at CyAn ADP by using Summit 4.3 software. The fluorescence excitation of nucleic acids of dead cells was measured with 405 nm violet laser light. Data were analyzed with FCS4 express software.

Lung, breast cancer cell lines and HeLa cells were treated 48 h with 0.6 μM doxorubicin and the rate of Sytox blue incorporation was evaluated as aforementioned.

Although this assay is very reliable, we evaluated the effect of sorcin silencing on cell death with the traditional method of cell counts. The cells were dislodged diluted 1:1 with Trypan blue dye and counted in triplicates in a burker cell counting chamber.

**Sorcin localization, confocal microscopy.** H1299 cells were treated 1 h with 0.6 μM of doxorubicin and processed as aforementioned for confocal microscopy purpose. After paraformaldehyde fixation, cells were incubated 30 min with a 1:200 dilution of primary antibody against Sorcin and, after PBS 1 × washing steps, 30 min with Alexa Fluor 488 (Molecular Probes, Invitrogen, Thermo Fisher Scientific)-conjugated secondary antibody against rabbit was used at a 1:500 dilution. A Leica laser scanning microscope TCS-SP2 device was used and images were acquired with Leica confocal software.

**Rhodamine123 incorporation.** To ascertain whether sorcin silencing affects MDR1 functionality in pumping out the drugs from the cell, we performed a rhodamine123 accumulation assay. This dye is extruded outside the cells by MDR1/MDR4 pumps. First the cells were silenced for 48 h, as mentioned, then a time course accumulation assay was performed. We considered 250 000 cells each time point (30 min, 1 h, 2 h) and the assay was carried out incubating the samples at 37 °C in RPMI 1640 medium without and with 1 μM rhodamine123.

After incubation the samples were pelleted and washed twice in ice cold PBS 1 ×. Then they were analyzed at CyAn ADP by using Summit 4.3 software. The results were evaluated with FCS4 express software.

## Conflict of Interest

The authors declare no conflict of interest.

**Acknowledgements.** Financial support: Italian Association for Cancer Research (AIRC) StG 4841; FILAS-RU-2014-1020; Sapienza University of Rome 'Progetti di Ateneo' to FF; Ministry of Health RF-2010-2309790; MIUR PRIN 20154JRJPP; CNR Nanomax 'NADINE' Nanotechnology-based Diagnostics in Neurological diseases and Experimental oncology, CNCCS CNR, InterOmics Synlether CNR, PNR-CNR Aging Program 2012–2014 to GC. We thank Fabrizio Padula and Stefania De Grossi for their invaluable technical support.. We acknowledge the European Synchrotron Radiation Facility for provision of synchrotron radiation facilities and we would like to thank the staff for assistance in using beamline ID30-A3 MASSIF3. We also thank HZB where the crystal absorption spectra were recorded for the allocation of synchrotron radiation beamtime. Finally, we acknowledge all the IBPM-CNR biocrystal facility staff (<https://biocrystalfacility.it>) for supporting crystallization experiments. We also thank Antoine Royant for the precious help in collecting crystal emission spectra at ID29S.

## PUBLISHER'S NOTE

Springer Nature remains neutral with regard to jurisdictional claims in published maps and institutional affiliations.

1. Housman G, Byler S, Heerboth S, Lapinska K, Longacre M, Snyder N *et al*. Drug resistance in cancer: an overview. *Cancers* 2014; **6**: 1769–1792.
2. Borst P, Eiferink RO. Mammalian ABC transporters in health and disease. *Annu rev biochem* 2002; **71**: 537–592.
3. Borst P, Schinkel AH. P-glycoprotein ABCB1: a major player in drug handling by mammals. *J clin invest* 2013; **123**: 4131–4133.
4. Pajic M, Iyer JK, Kersbergen A, van der Burg E, Nygren AO, Jonkers J *et al*. Moderate increase in Mdr1a/1b expression causes in vivo resistance to doxorubicin in a mouse model for hereditary breast cancer. *Cancer res* 2009; **69**: 6396–6404.
5. Van der Blik AM, Meyers MB, Biedler JL, Hes E, Borst P. A 22-kd protein (sorcin/V19) encoded by an amplified gene in multidrug-resistant cells, is homologous to the calcium-binding light chain of calpain. *EMBO j* 1986; **5**: 3201–3208.

6. Hamada H, Okochi E, Oh-hara T, Tsuruo T. Purification of the Mr 22,000 calcium-binding protein (sorcin) associated with multidrug resistance and its detection with monoclonal antibodies. *Cancer res* 1988; **48**: 3173–3178.
7. Van der Blik AM, Baas F, Van der Velde-Koerts T, Biedler JL, Meyers MB, Ozols RF et al. Genes amplified and overexpressed in human multidrug-resistant cell lines. *Cancer res* 1988; **48**: 5927–5932.
8. Colotti G, Poser E, Fiorillo A, Genovese I, Chiarini V, Ilari A. Sorcin, a calcium binding protein involved in the multidrug resistance mechanisms in cancer cells. *Molecules* 2014; **19**: 13976–13989.
9. Zheng BB, Zhang P, Jia WW, Yu LG, Guo XL. Sorcin, a potential therapeutic target for reversing multidrug resistance in cancer. *J physiol biochem* 2012; **68**: 281–287.
10. Lee WP. Purification, cDNA cloning, and expression of human sorcin in vincristine-resistant HOB1 lymphoma cell lines. *Arch biochem biophys* 1996; **325**: 217–226.
11. Wang SL, Tam MF, Ho YS, Pai SH, Kao MC. Isolation and molecular cloning of human sorcin a calcium-binding protein in vincristine-resistant HOB1 lymphoma cells. *Biochim biophys acta* 1995; **1260**: 285–293.
12. Xu P, Jiang YF, Wang JH. shRNA-mediated silencing of sorcin increases drug chemosensitivity in myeloma KM3/DDP and U266/ADM cell lines. *Int j clin exp pathol* 2015; **8**: 2300–2310.
13. Yamagishi N, Nakao R, Kondo R, Nishitsuji M, Saito Y, Kuga T et al. Increased expression of sorcin is associated with multidrug resistance in leukemia cells via up-regulation of MDR1 expression through cAMP response element-binding protein. *Biochem biophys res commun* 2014; **448**: 430–436.
14. Ilari A, Fiorillo A, Poser E, Lalioti VS, Sundell GN, Ivarsson Y et al. Structural basis of Sorcin-mediated calcium-dependent signal transduction. *Sci rep* 2015; **5**: 16828.
15. Anthony DF, Beattie J, Paul A, Currie S. Interaction of calcium/calmodulin-dependent protein kinase I $\delta$  with sorcin indirectly modulates ryanodine receptor function in cardiac myocytes. *J Mol Cell Cardiol* 2007; **43**: 492–503.
16. Franceschini S, Ilari A, Verzili D, Zamparelli C, Antaramian A, Rueda A et al. Molecular basis for the impaired function of the natural F112L sorcin mutant: X-ray crystal structure, calcium affinity, and interaction with annexin VII and the ryanodine receptor. *FASEB j* 2008; **22**: 295–306.
17. Lalioti VS, Ilari A, O'Connell DJ, Poser E, Sandoval IV, Colotti G. Sorcin links calcium signaling to vesicle trafficking, regulates Polo-like kinase 1 and is necessary for mitosis. *PLoS one* 2014; **9**: e85438.
18. Landriscina M, Laudiero G, Maddalena F, Amoroso MR, Piscazzi A, Cozzolino F et al. Mitochondrial chaperone Trap1 and the calcium binding protein Sorcin interact and protect cells against apoptosis induced by antiblastic agents. *Cancer res* 2010; **70**: 6577–6586.
19. Matsumoto T, Hisamatsu Y, Ohkusa T, Inoue N, Sato T, Suzuki S et al. Sorcin interacts with sarcoplasmic reticulum Ca(2+)-ATPase and modulates excitation-contraction coupling in the heart. *Basic Res Cardiol* 2005; **100**: 250–262.
20. Meyers MB, Fischer A, Sun YJ, Lopes CM, Rohacs T, Nakamura TY et al. Sorcin regulates excitation-contraction coupling in the heart. *J Biol Chem* 2003; **278**: 28865–28871.
21. Zamparelli C, Macquade N, Colotti G, Verzili D, Seidler T, Smith GL et al. Activation of the cardiac Na(+)-Ca(2+) exchanger by sorcin via the interaction of the respective Ca(2+) binding domains. *J Mol Cell Cardiol* 2010; **49**: 132–141.
22. Changenet-Barret P, Gustavsson T, Markovits D, Manet I, Monti S. Unravelling molecular mechanisms in the fluorescence spectra of doxorubicin in aqueous solution by femtosecond fluorescence spectroscopy. *Phys Chem Chem Phys* 2013; **15**: 2937–2944.
23. Ilari A, Johnson KA, Nastopoulos V, Verzili D, Zamparelli C, Colotti G et al. The crystal structure of the sorcin calcium binding domain provides a model of Ca2+-dependent processes in the full-length protein. *J Mol Biol* 2002; **317**: 447–458.
24. Suzuki H, Kawasaki M, Inuzuka T, Okumura M, Kakiuchi T, Shibata H et al. Structural basis for Ca2+-dependent formation of ALG-2/Alix peptide complex: Ca2+/EF3-driven arginine switch mechanism. *Structure* 2008; **16**: 1562–1573.
25. Gao Y, Li W, Liu X, Gao F, Zhao X. Reversing effect and mechanism of soluble resistance-related calcium-binding protein on multidrug resistance in human lung cancer A549/DDP cells. *Mol med rep* 2015; **11**: 2118–2124.
26. He Q, Zhang G, Hou D, Leng A, Xu M, Peng J et al. Overexpression of sorcin results in multidrug resistance in gastric cancer cells with up-regulation of P-gp. *Oncol rep* 2011; **25**: 237–243.
27. Hu Y, Cheng X, Li S, Zhou Y, Wang J, Cheng T et al. Inhibition of sorcin reverses multidrug resistance of K562/A02 cells and MCF-7/A02 cells via regulating apoptosis-related proteins. *Cancer chemother pharmacol* 2013; **72**: 789–798.
28. Hu Y, Li S, Yang M, Yan C, Fan D, Zhou Y et al. Sorcin silencing inhibits epithelial-to-mesenchymal transition and suppresses breast cancer metastasis in vivo. *Breast Cancer Res Treat* 2014; **143**: 287–299.
29. Kawakami M, Nakamura T, Okamura N, Komoto C, Markova S, Kobayashi H et al. Knock-down of sorcin induces up-regulation of MDR1 in HeLa cells. *Biol Pharm Bull* 2007; **30**: 1065–1073.
30. Liu X, Chen L, Feng B, Liu G. Reversing effect of sorcin in the drug resistance of human nasopharyngeal carcinoma. *Anat Rec (Hoboken)* 2014; **297**: 215–221.
31. Parekh HK, Deng HB, Choudhary K, Houser SR, Simpkins H. Overexpression of sorcin, a calcium-binding protein, induces a low level of paclitaxel resistance in human ovarian and breast cancer cells. *Biochem Pharmacol* 2002; **63**: 1149–1158.
32. Zhou Y, Xu Y, Tan Y, Qi J, Xiao Y, Yang C et al. Sorcin, an important gene associated with multidrug-resistance in human leukemia cells. *Leuk Res* 2006; **30**: 469–476.
33. Maddalena F, Laudiero G, Piscazzi A, Secondo A, Scorziello A, Lombardi V et al. Sorcin induces a drug-resistant phenotype in human colorectal cancer by modulating Ca(2+) homeostasis. *Cancer res* 2011; **71**: 7659–7669.
34. Marmugi A, Parnis J, Chen X, Carmichael L, Hardy J, Mannan N et al. Sorcin links pancreatic beta cell lipotoxicity to ER Ca2+ stores. *Diabetes* 2016; **65**: 1009–1021.
35. Colotti G, Zamparelli C, Verzili D, Mella M, Loughrey CM, Smith GL et al. The W105G and W99G sorcin mutants demonstrate the role of the D helix in the Ca(2+)-dependent interaction with annexin VII and the cardiac ryanodine receptor. *Biochemistry* 2006; **45**: 12519–12529.
36. Mella M, Colotti G, Zamparelli C, Verzili D, Ilari A, Chiancone E. Information transfer in the penta-EF-hand protein sorcin does not operate via the canonical structural/functional pairing. A study with site-specific mutants. *J Biol Chem* 2003; **278**: 24921–24928.
37. Eom YW, Kim MA, Park SS, Goo MJ, Kwon HJ, Sohn S et al. Two distinct modes of cell death induced by doxorubicin: apoptosis and cell death through mitotic catastrophe accompanied by senescence-like phenotype. *Oncogene* 2005; **24**: 4765–4777.
38. Maddalena F, Sisinni L, Lettini G, Condelli V, Matassa DS, Piscazzi A et al. Resistance to paclitaxel in breast carcinoma cells requires a quality control of mitochondrial antiapoptotic proteins by TRAP1. *Mol Oncol* 2013; **7**: 895–906.
39. Marmugi A, Parnis J, Chen X, Carmichael L, Hardy J, Mannan N et al. Sorcin links pancreatic beta-cell lipotoxicity to ER Ca2+ stores. *Diabetes* 2016; **65**: 1009–1021.
40. Qi J, Liu N, Zhou Y, Tan Y, Cheng Y, Yang C et al. Overexpression of sorcin in multidrug resistant human leukemia cells and its role in regulating cell apoptosis. *Biochem biophys res commun* 2006; **349**: 303–309.
41. Malmendal A, Linse S, Evenas J, Forsen S, Drakenberg T. Battle for the EF-hands: magnesium-calcium interference in calmodulin. *Biochemistry* 1999; **38**: 11844–11850.
42. Kabsch W. Xds. *Acta Crystallogr D* 2010; **66**: 125–132.
43. Vagin A, Teplyakov A. MOLREP: an automated program for molecular replacement. *J Appl Crystallogr* 1997; **30**: 1022–1025.
44. Murshudov GN, Vagin AA, Dodson EJ. Refinement of macromolecular structures by the maximum-likelihood method. *Acta Crystallogr D* 1997; **53**: 240–255.
45. Emsley P, Cowtan K. Coot: model-building tools for molecular graphics. *Acta Crystallogr D* 2004; **60**: 2126–2132.
46. Royant A, Carpentier P, Ohana J, McGeehan J, Paetzold B, Noirclerc-Savoye M et al. Advances in spectroscopic methods for biological crystals. 1. Fluorescence lifetime measurements. *J Appl Crystallogr* 2007; **40**: 1105–1112.
47. Kontny NE, Wurthwein G, Joachim B, Boddy AV, Krischke M, Fuhr U et al. Population pharmacokinetics of doxorubicin: establishment of a NONMEM model for adults and children older than 3 years. *Cancer chemother pharmacol* 2013; **71**: 749–763.




**Cell Death and Disease** is an open-access journal published by **Nature Publishing Group**. This work is licensed under a **Creative Commons Attribution 4.0 International License**. The images or other third party material in this article are included in the article's Creative Commons license, unless indicated otherwise in the credit line; if the material is not included under the Creative Commons license, users will need to obtain permission from the license holder to reproduce the material. To view a copy of this license, visit <http://creativecommons.org/licenses/by/4.0/>

© The Author(s) 2017

Supplementary Information accompanies this paper on *Cell Death and Disease* website (<http://www.nature.com/cddis>)

# SCIENTIFIC REPORTS



OPEN

## Structural basis of Sorcin-mediated calcium-dependent signal transduction

Received: 30 May 2015  
Accepted: 20 October 2015  
Published: 18 November 2015

Andrea Ilari<sup>1</sup>, Annarita Fiorillo<sup>1</sup>, Elena Poser<sup>1</sup>, Vasiliki S. Lalioti<sup>2</sup>, Gustav N. Sundell<sup>3</sup>, Ylva Ivarsson<sup>3</sup>, Ilaria Genovese<sup>1</sup> & Gianni Colotti<sup>1</sup>

Sorcin is an essential penta-EF hand calcium binding protein, able to confer the multi-drug resistance phenotype to drug-sensitive cancer cells and to reduce Endoplasmic Reticulum stress and cell death. Sorcin silencing blocks cell cycle progression in mitosis and induces cell death by triggering apoptosis. Sorcin participates in the modulation of calcium homeostasis and in calcium-dependent cell signalling in normal and cancer cells. The molecular basis of Sorcin action is yet unknown. The X-ray structures of Sorcin in the apo (apoSor) and in calcium bound form (CaSor) reveal the structural basis of Sorcin action: calcium binding to the EF1-3 hands promotes a large conformational change, involving a movement of the long D-helix joining the EF1-EF2 sub-domain to EF3 and the opening of EF1. This movement promotes the exposure of a hydrophobic pocket, which can accommodate in CaSor the portion of its N-terminal domain displaying the consensus binding motif identified by phage display experiments. This domain inhibits the interaction of sorcin with PDCD6, a protein that carries the Sorcin consensus motif, co-localizes with Sorcin in the perinuclear region of the cell and in the midbody and is involved in the onset of apoptosis.

Sorcin (Soluble resistance-related calcium binding protein) is a calcium binding oncoprotein expressed at high levels in several human tumours, such as leukaemia, gastric, breast and ovarian cancers<sup>1–5</sup>. Sorcin gene is located in chromosome 7, in the same amplicon of other proteins involved in MDR (multidrug resistance) such as ABCB4 and ABCB1 (Mdr1); Sorcin is highly expressed in different chemoresistant cell lines, and its overexpression confers MDR in several tumors<sup>6–11</sup>. Treatment with antisense oligonucleotides increases cell sensitivity for vincristine and other antitumor drugs, suggesting that sorcin might be a useful marker of MDR and a therapeutic target for reversing tumor MDR<sup>12,13</sup>.

Sorcin is also considered one of the main regulators of calcium-induced calcium release in the heart<sup>4,14–18</sup>. Sorcin is one of the most expressed calcium-binding proteins in human cells, especially in the brain and in the heart (PaxDb). In particular Sorcin is one of the most expressed calcium binding proteins in the amygdala, in the prefrontal cortex, in the hypothalamus and in many brain cancers (GeneAtlas U133A, gcrma), such as anaplastic astrocytoma, oligodendroglioma, glioblastoma<sup>19–21</sup>, and is considered a histological marker for malignant glioma<sup>4</sup>.

The Sorcin mechanism of action is not fully understood. However, we have shown that Sorcin is an essential protein, which activates and regulates mitosis and cytokinesis<sup>22</sup>. Our analysis of the interactome of Sorcin revealed calcium-dependent interactions with kinases playing key roles in cell-cycle progression, including Polo-like kinase 1 that phosphorylates Sorcin. In addition, Sorcin silencing blocks cell cycle progression in mitosis and induces cell death. Sorcin localizes at the nucleus, endoplasmic reticulum

<sup>1</sup>Institute of Molecular Biology and Pathology CNR; Dept. Biochemical Sciences, Sapienza University, P.le A. Moro 5, 00185, Rome, Italy. <sup>2</sup>Centro de Biología Molecular Severo Ochoa, CSIC -Universidad Autónoma de Madrid, Departamento Biología Celular e Inmunología, Cantoblanco; Centro de Investigación Biomédica en Red de Enfermedades Hepáticas y Digestivas (CIBERehd), Madrid, Spain. <sup>3</sup>Department of Chemistry-BMC, Uppsala University, P.O. Box 576, 751 23 Uppsala, Sweden. Correspondence and requests for materials should be addressed to A.I. (email: andrea.ilari@uniroma1.it) or G.C. (email: gianni.colotti@uniroma1.it)

(ER) and cell membranes during interphase, while during mitosis, Sorcin concentrates in the cleavage furrow (late telophase) and midbody (cytokinesis). Upon calcium binding, Sorcin undergoes large conformational changes, presumably involving exposure of hydrophobic surfaces, that allows it to interact with calcium channels, pumps and exchangers like ryanodine receptors (RyRs), sarco(endo)plasmic reticulum  $\text{Ca}^{2+}$  ATPase (SERCA), L-type voltage-dependent calcium channels and  $\text{Na}^{+}$ - $\text{Ca}^{2+}$  exchangers (NCX), and to regulate them<sup>14–17,23,24</sup>. Sorcin regulates calcium homeostasis by binding calcium, binding to and regulating the activity of calcium channels and other proteins; as a consequence, Sorcin increases  $\text{Ca}^{2+}$  accumulation in the endoplasmic (ER)/sarcoplasmic reticulum (SR) and mitochondria. Sorcin prevents ER stress, and its silencing triggers apoptosis<sup>22,25,26</sup>. Knockdown of Sorcin in fact results in major defects in mitosis and cytokinesis, increase in the number of rounded polynucleated cells, blockage of cell progression in G2/M, apoptosis and cell death. ER stress is involved in the accumulation and deposits of misfolded proteins in many neurodegenerative diseases; Sorcin interacts in a calcium-dependent fashion with alpha-synuclein and presenilin 2, two proteins involved in the pathogenesis of Parkinson's disease and Alzheimer's disease, respectively, *in vitro*, in cultured cells and in human brain<sup>27,28</sup>.

From a structural point of view, Sorcin belongs to the small penta-EF-hand (PEF) family<sup>29</sup>. Each monomer of Sorcin homodimer is formed by two domains, i.e. a flexible, glycine-rich N-terminal domain and a C-terminal calcium-binding domain (SCBD), endowed with five EF-hands<sup>30,31</sup>. The SCBD can be divided in two regions: EF1–3 (residues 33–134), which binds calcium with high affinity, and EF4–5 (residues 135–198), which mediates dimerization. Upon calcium binding Sorcin undergoes a large conformational change that allows it to bind and regulate a series of target proteins in a calcium-dependent fashion<sup>32–34</sup>. However, the structural basis of its activation and of its ability to establish calcium-dependent interactions with targets is unclear. In addition, the peptide binding motifs are not known, despite the identification of several target proteins.

To investigate the structural basis of Sorcin activation and of selective calcium-dependent signal transduction, we here solved the structure of the apo Sorcin (apoSor) and, for the first time, the structure of Sorcin in the calcium-bound form (CaSor). The structures have been compared with each other and with those of other PEF proteins evaluating: i) the internal variability of Sorcin; ii) the effect of the calcium binding on the single EF-hands; iii) the effect of the calcium binding to the overall protein fold. The comparison reveals potential surfaces of interaction between Sorcin and its targets. We further established consensus Sorcin-binding motifs in absence and presence of  $\text{Ca}^{2+}$ . Finally, we validated interactions between Sorcin and a molecular partner endowed with such sequences, such as PDCD6 (programmed cell death protein 6, formerly called Alg-2), a PEF protein with similar mechanism of activation but different role in the cell with respect to Sorcin, through Surface Plasmon Resonance experiments and in the fibroblasts by co-localization experiments. Our study shed new light on the molecular basis of Sorcin activation, i.e. the structural changes induced by calcium binding in Sorcin, and on Sorcin mechanism of action, i.e. the interaction of Sorcin with its molecular partners, which leads to regulation of cytokinesis, to protection from apoptosis and to the establishment of MDR phenotype.

## Results

**Overall structures and calcium coordination.** We solved structures of Sorcin in complex with calcium (CaSor) and in the apo form (apoSor), at a higher resolution than the one solved by Xie *et al.*<sup>31</sup>. Structures statistics are reported in Table 1. All the structures have the typical fold of the PEF proteins family. Briefly, the monomer is formed by two domains: a Gly-rich N-terminal domain (residues 1–32), partially visible in both apo and calcium-bound structures (residues 30–32 and 26–32, respectively), and a calcium binding domain (SCBD), containing eight  $\alpha$ -helices (A-H) organised in five calcium binding motifs (EF1–EF5). Two helices are very long and connect two adjacent EF hands: the D-helix (hD) is common to EF2 and EF3, while the G-helix is common to EF4 and EF5 (Fig. 1). EF1 is structurally coupled with EF2, and EF3 is paired with EF4. Sorcin dimerization occurs by pairing of the EF5 of two monomers.

In CaSor,  $\text{Ca}^{2+}$  is bound at EF1, EF2 and EF3 and it is hepta-coordinated in a classical pentagonal bipyramidal configuration (Fig. 2 and Table S1). EF1 and EF2 are coupled by Gln48, which coordinates the EF1-bound  $\text{Ca}^{2+}$ , whereas in EF2 is hydrogen-bound to Thr89.

**Comparison of human Sorcin structures: conformational changes induced by calcium binding.** The comparison between all the known human Sorcin structures (apo human Sorcin, PDB code: 1JÜO; apo-F112L human Sorcin mutant, PDB code: 2JC2; apoSor, PDB code: 4UPG; CaSor, PDB code: 4USL) shows that the EF1–3 region is more flexible than the EF4–EF5 region and that a large conformational change in the EF1–EF2 subdomain and EF3 is visible upon calcium binding to the first three EF hand motifs<sup>16,31</sup>. Indeed, the rmsd values (Table S2) measured by superimposing CaSor to the apoSor clearly indicate that upon calcium binding Sorcin undergoes a large conformational change, mainly involving EF1, EF2 and EF3 (Table S2, Fig. 3). As shown in Fig. 3, calcium binding to EF1, EF2 and EF3, i.e. the three EF hands with the highest affinity for the cation<sup>33</sup>, induces a large displacement (of about 21°) of the D-helix. The comparison between apoSor and the calcium-bound Sorcin structures sheds light on the mechanism of cation-mediated structural changes of Sorcin, which is fundamental for the comprehension of its function. The binding of calcium at the EF3 loop causes the movement of the three ligands Asp113, Asp115 and Ser117 towards the bidentate Glu124 ligand in the E-helix. Thus, the loop



PDB code	apoSor	CaSor
	4UPG	4USL
Space group	I422	C222 <sub>1</sub>
Cell parameters (Å)	a = b = 106.4, c = 77.5 Å	a = 52.4, b = 111.6, c = 60.5
Asymmetric unit (residues)	Monomer (30–198)	Monomer(12–17, 26–198)
N° of bound ions	—	3 Ca <sup>2+</sup>
Resolution ranges (Å)	2.1–50.0 (2.1–2.2)	1.65–50 (1.65–1.69)
Unique reflections	23604 (4375)	41040 (3051)
Completeness (%)	99.7 (98.2)	99.5 (99.6)
Redundancy	6.8 (7)	3.4 (3.3)
R <sub>merge</sub> (%)	11 (59)	4 (66)
CC(1/2)	99.8 (88.2)	99.9 (83.3)
I/σ(I)	14.8 (3.6)	21.57 (3.0)
Resolution ranges (Å)	2.10–40.59 (2.10–2.15)	1.65–37.34 (1.65–1.69)
R <sub>cryst</sub> (%)	18.1 (23.4)	19.1 (32.9)
R <sub>free</sub> (%)	21.9 (30.0)	22.1 (33.3)
rms (angles) (°)	1.46	1.32
Rms (bonds) (Å)	0.01	0.01
Wilson B-factor (Å <sup>2</sup> )	29.3	21.6
Residues in core regions of the Ramachandran plot (%)	98.8	99.4
Residues in allowed regions of the Ramachandran plot (%)	1.2	0.6

**Table 1.** Crystal parameters, data collection statistics and refinement statistics of Sorcin in the apo form (apoSor) and in complex with Ca<sup>2+</sup> (CaSor). Values in parentheses are for the highest-resolution shell.

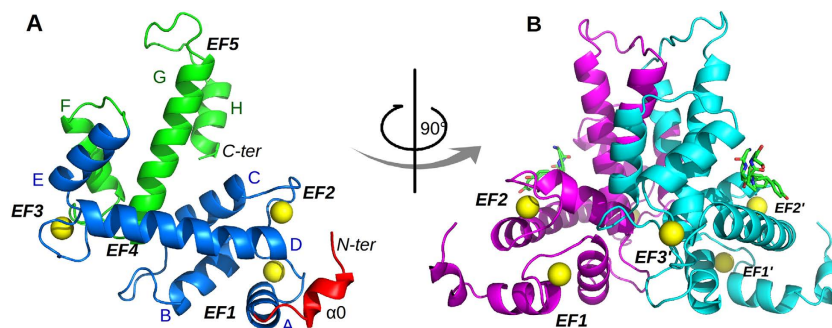


**Figure 1.** Overall structure of calcium-bound human Sorcin. (A) The monomer comprises a part of the flexible N-terminal domain containing an alpha helical region designated  $\alpha 0$  (red) and a calcium-binding domain (SCBD) that can be divided in two region: EF1-3 (blue) and EF4-5 (green). Calcium ions (yellow spheres) are bound at EF1, EF2 and EF3. The helices (A-H) and the EF-hands (EF1-5) are indicated. (B) Dimerization occurs through the pairing of EF4-5 of two monomers (cyan and magenta). The N-terminal hexapeptide modeled in the structure is shown as green sticks.

undergoes a rearrangement and may act as a lever dragging the long and rigid D-helix away from the E-helix. As a result, EF3 acts as a pivot: the first half of the calcium binding domain (formed by A-, B-, C- and D-helices) rotates and moves away from the second half (formed by the E-, F-, G- and H-helices), which is the dimerization subdomain and forms the stable Sorcin dimeric interface.

**Calcium binding and mechanism of activation: comparison with PDCD6 (Alg-2).** Sorcin binds calcium at EF1, EF2 and EF3 hands. In order to investigate the role of each calcium binding site, we analysed each EF hand separately and evaluated the structural variation induced upon ion binding. For the sake of simplicity, the local conformational change has been evaluated by measuring the variation of

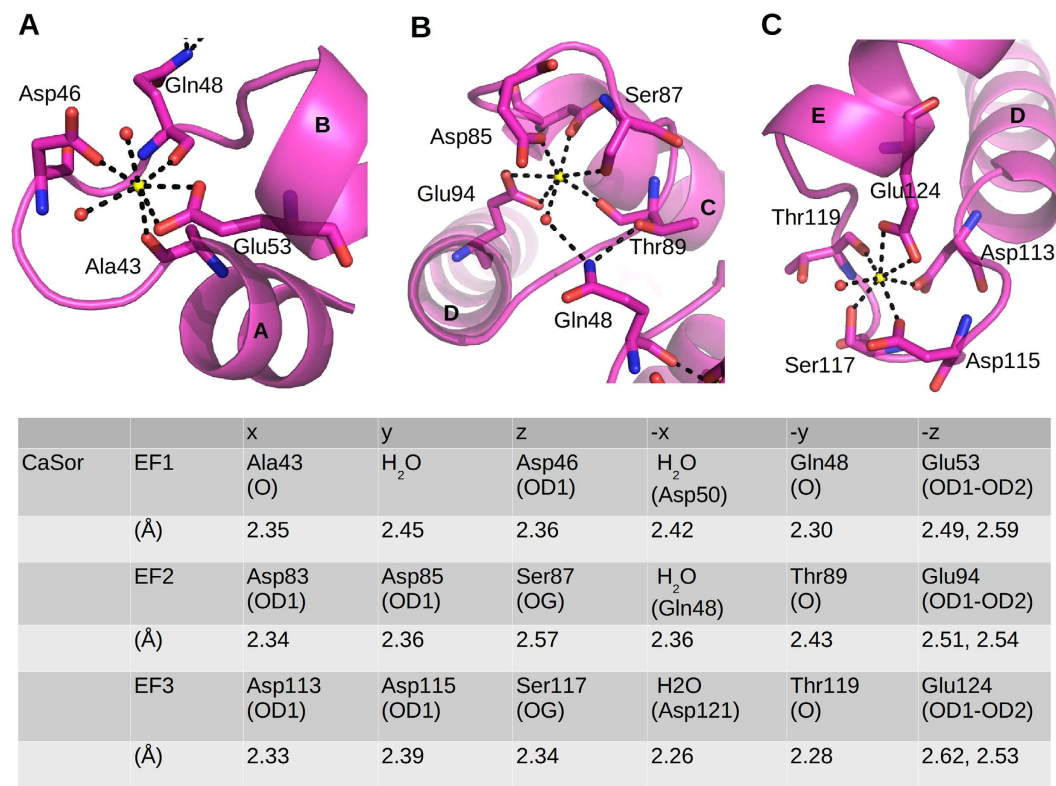


**Figure 2. Calcium coordination in Sorcin.** Close-up of Ca<sup>2+</sup> binding sites in EF1 (A), EF2 (B) and EF3 (C) reveals the classical pentagonal bipyramidal geometry. The involved residues are shown as sticks, water molecules as red spheres and calcium ions as yellow spheres. Ligand positions and coordination distances are listed.

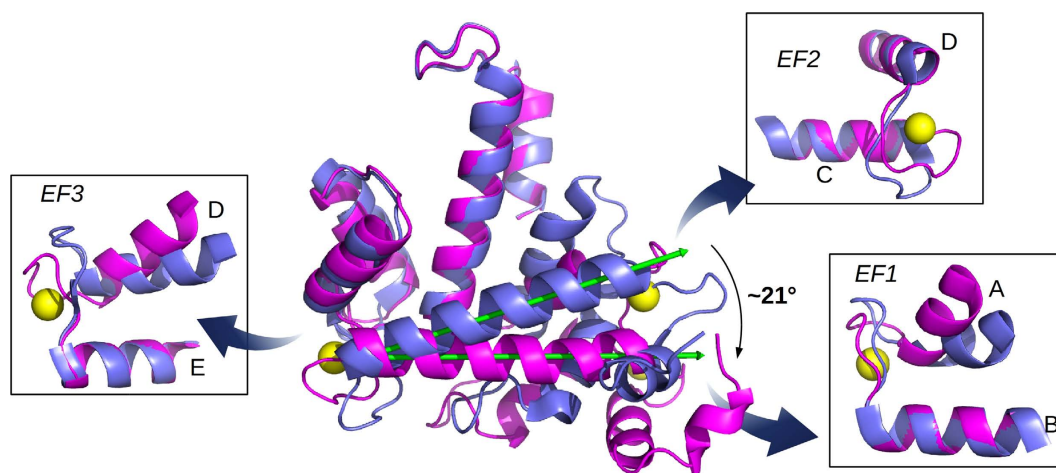


**Figure 3. Conformational changes induced by ion binding.** The superposition of CaSor (magenta) and apoSor (blue) reveals the conformational variation induced by calcium (yellow spheres). The green arrows represent the axis of the D helix in the two structures: the binding of three Ca<sup>2+</sup> to each Sorcin monomer causes a large movement of the D helix that drags the EF1-EF2 region. The panels illustrate the changes of EF1, EF2 and EF3 taken alone, analysed aligning the C-terminal helix for each EF-hand: EF1 and EF3 open upon Ca<sup>2+</sup>-binding, while EF2 is almost unchanged.

the angle between the two helices of each EF-hand motif in the structures of Sorcin and of other PEF proteins, whereas the overall conformational change has been evaluated by measuring the variation of the angle between the D- and G-helices, which takes into account the movement of the EF1-EF2 sub-domain and EF3 with respect to the EF4 and EF5 hands (Table 2).

Prot (pdb)	EF1 ( $\theta$ ) [A-B]	EF2 ( $\theta$ ) [C-D]	EF3 ( $\theta$ ) [D-E]	EF4 ( $\theta$ ) [F-G]	EF5 ( $\theta$ ) [G-H]	D-helix vs G-helix ( $\theta$ )
	$\theta$	$\theta$	$\theta$	$\theta$	$\theta$	
hSorcin						
ApoSor (4UPG)	40.8°	60.7°	52°	47.3°	32.9°	57.5°
CaSor (4USL)	59.2°	57.9°	66.5°	45.9°	29.9°	78.1°
	+Ca	+Ca	+Ca	—	—	
$\Delta$ (+Ca)	+18.4°	-2.9°	+14.5°	-1.40°	-3°	+20.6°
hPDCD6						
PDCD6-apo (2ZND)	68.8°	51.5°	59.2°	56.5°	35.8°	80.2°
PDCD6+Ca (2ZN9) A = B	72°	52.6°	64°	58.4°	27.2°	82.2°
	+Ca	—	+Ca	—	+Ca	
	+3.2°	+1.1°	+4.8°	+2.1°	-8.6°	+2°
hPDCD6-Zn-Alix (2ZNE)	67.2	55.4	62.4	60.5	A = 31.7 B = 36.6	A = 74.5 B = 75.4
	+Zn	—	+Zn x2	—	+Zn	
$\Delta$ (+Zn, +pep)	-1.5°	+4°	+3°	+4°	A = -4°	A = -5.7°
					B = +1°	B = -4.8°
rCalpain-dVI						
apo monA (1AJ5)	40.3°	53.6°	30°	51.5°	28°	47°
apo monB (1AJ5)	41.2°	52° (54°)*	33.6° (28.5°)*	44.5°	20.5°	48.6°
+Ca (1DVI)	61°	63° (71°)*	46.2° (42°)*	49.4°	23.4°	52.3°
	+Ca	+Ca	+Ca	—	—	
$\Delta$ (+Ca)	+20.7°	+9°	+16°	+1.6°	-3°	+5.3°
	+19.7°	+11°	+12°	+3°	+4°	+3.7°

**Table 2. Effect of ion binding on EF-hands in PEF proteins.** The angle between the helices has been calculated with PyMol. The angle between helices D and G is reported ( $\theta$ ), as an indicator of the movement of sub-domain EF1-EF2-EF3 with respect to EF4-EF5.

The PEF proteins are divided in two sub-groups on the basis of the residues present on the EF1 loop; in the group I the EF1 loop is formed by 11 residues whereas in the group II, to which Sorcin belongs, the EF1 loop is formed by 12 residues<sup>35</sup>. The proteins for which both the structures in the apo form and in the presence of a saturating amount of calcium were determined and deposited in the PDB, have been chosen to be compared with Sorcin structures: human PDCD6 (PDB codes: 2ZND, 2ZN9<sup>36</sup>), representative of the group I, and rat m-calpain PEF domain dVI (PDB codes: 1AJ5, 1DVI<sup>37</sup>), representative of the group II.

This analysis shows that in Sorcin both EF1 and EF3 hands are widely opened upon calcium binding (variation of the angle between the helices of the EF hand,  $\theta = +18.4^\circ$  and  $+14.5^\circ$  respectively), while EF2 displays only a minimal variation ( $\theta = -3^\circ$ ).

The comparison with other PEFs is informative and interesting. PDCD6 binds  $\text{Ca}^{2+}$  (or  $\text{Zn}^{2+}$ ) at EF1, EF3 and EF5 but the local conformational changes ( $\theta = +3.2^\circ$ ,  $+4.8^\circ$ ,  $-8.6^\circ$ ) are smaller than those observed in Sorcin. On the contrary calpain-dVI, which binds  $\text{Ca}^{2+}$  at the same sites as Sorcin (plus a fourth  $\text{Ca}^{2+}$  not bound at an EF-hand), shows a similar change for EF1 and EF3 ( $\theta = \sim 20^\circ$ ,  $\sim 14^\circ$ ) and an evident opening of EF2 ( $\theta = \sim 10^\circ$ ). The open question is how the local conformational changes described so far can be transmitted to the overall structure.

As already discussed, in Sorcin the opening of EF3 causes the exposure of a hydrophobic surface with the shift of the EF1-EF2 sub-domain and EF3 with respect to the EF4-EF5 sub-domain (Fig. 3). The variation of the angle between D-helix and G-helix can be used as an indicator of such movement and, as already stated, is of about  $21^\circ$ . As shown by the structural analysis of CaSor the opening of EF1 causes the exposure of an additional hydrophobic surface. The opening of EF1 and EF3 causes the exposure of two distinct hydrophobic surfaces that likely mediate the interaction of Sorcin with its molecular partners.

Calcium binding to PDCD6 does not cause large conformational changes. Indeed, the superimposition between the calcium bound and the apo PDCD6 monomers using the  $\text{C}\alpha$  atoms, yields a  $\text{rmsd} = 1.20 \text{ \AA}$  and the angle between the D- and G-helices varies only by  $2^\circ$ ; the main effect is observed on the EF5 hand where the binding of calcium causes a slight twisting movement and opening of the dimer. Interestingly the hD-hG angle in both the apo and the calcium bound form of PDCD6 has a value similar to that measured in CaSor ( $75^\circ$ – $80^\circ$  vs  $78^\circ$ ) suggesting that the two proteins may share

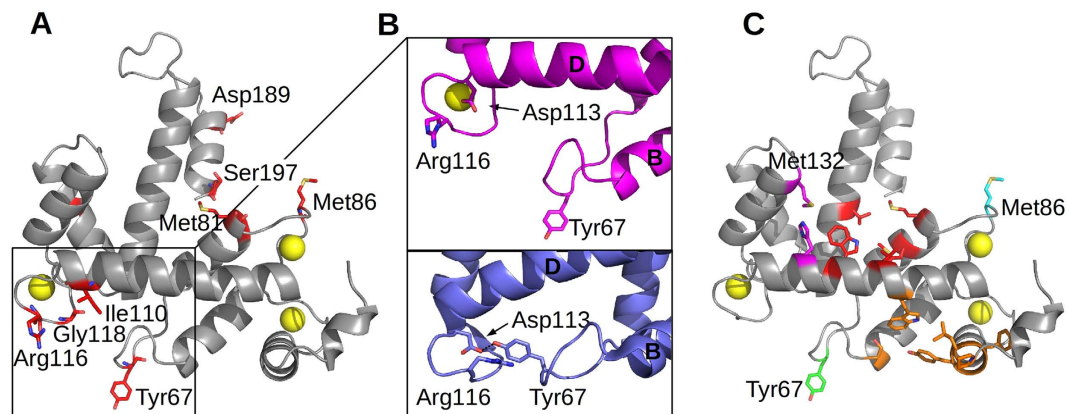


**Figure 4. Solvent accessible surface analysis and hot-spots prediction.** (A) The residues that upon calcium binding become more accessible (SASA increase higher than 30%) are mapped as red sticks on CaSor structure; Tyr67 and Met86 show the strongest variation. (B) In apoSor (blue) Tyr67 forms a hydrogen bond with Asp113. In CaSor (magenta) the hydrogen bond is broken and the loop moves away together with helix B and the EF1-EF2 region. (C) Hotpatch analysis identified 3 pockets (pocket 1, magenta; pocket 2, red; pocket 3, orange) likely mediating protein-protein interactions.

similar target binding sites, with the difference that PDCD6 sub-domains are always in the active overall conformation and therefore only minor variations are necessary to allow target binding.  $\text{Ca}^{2+}$ -dependent activation of PDCD6 is ascribed to the movement of the side chain of Arg125, belonging to the loop between EF3 and EF4, that uncovers and makes accessible the hydrophobic pocket already present in the apo form<sup>36</sup>.

**Analysis of Sorcin solvent-accessible surface areas.** The analysis of solvent accessible surface areas has been performed with areaimol (CCP4 suite, <http://www.ccp4.ac.uk/html/areaimol.html>) and shows that upon calcium binding there is an increase in the exposed surface areas of several residues. The residues with a difference in SASA (Solvent Accessible Surface Areas) higher than 30% between the apo and the calcium bound form of Sorcin are Tyr67, Ser80, Met81, Met86, Ile110, Arg116, Gly118, Ser143 and Ser197 (Table S3, Fig. S1). As shown in Fig. 4A, the residues displaying the highest SASA (higher than 30%) are located in the loop preceding the C helix (hC), in the EF2 loop (which follows the hC), in the C-terminal part of the D-helix and in the EF3 loop; all these structural features present a wide calcium-dependent rearrangement.

Even if, as shown in Table 2, ion binding has almost no effect on the relative position of helices C and D of EF2 hand, upon ion binding there is a reorganization of the last part of the helix C containing Met81 and of the loop 83–91 containing Met86, which become exposed to the solvent. Tyr67 is placed on the loop between helices B and C, and in apoSor it is hydrogen bonded to Asp113 of the EF3 loop and is partially covered by it. Upon calcium binding this interaction is broken since Asp113 participates in ion coordination; the rearrangement of the EF3 loop causes also the exposure of Arg116 (Fig. 4, panel B).

We further analysed the CaSor structure using the Hotpatch server (<http://hotpatch.mbi.ucla.edu/>) in order to identify unusual hydrophobic patches likely mediating protein-protein interactions between Sorcin and its molecular partners<sup>38</sup>. The Hotpatch analysis highlights that besides Met86 (cyan) and Tyr67 (green), each Sorcin monomer has two significant regions consisting of three different zones, shown in Fig. 4C. The pink one includes His108 and Met132 (pocket 1), the red one Met81, Val101, Trp105, Val164 (pocket 2) and the orange one Ala26, Phe27, Pro28, Pro34, Leu35, Tyr36, Gly37, Tyr38, Ser61, Trp99 (pocket 3). Interestingly, these clusters are found in the areas most affected by calcium dependent structural changes, namely EF1 (orange residues) and EF3 (red and pink residues). Moreover, both areas include tryptophan residues (Trp99 and Trp105) strongly conserved among the PEF protein family members. Supporting the importance of these regions in ligands binding, Colotti and coworkers previously demonstrated that mutation of Trp105 impairs the capacity of Sorcin to recognize and interact with RyR2 and annexin 7 at physiological calcium concentrations<sup>39</sup>.

**Analysis of N-terminal peptide-Sorcin interaction and comparison with the PDCD6-Alix structure.** The analysis of the CaSor structure reveals the presence of an electron density peak in the cavity formed upon calcium binding and the consequent tilt of the D-helix. We fitted this electronic density map with the GYYPPG hexapeptide belonging to the N-terminal region of Sorcin (residues 12–17). The same region was thought to interact with PDCD6 N-terminal peptide by Jia *et al.*<sup>40</sup>; Suzuki *et al.* demonstrated that it probably was PEG<sup>36</sup>. We can exclude PEG binding to Sorcin structure: the Fo-Fc and 2Fo-Fc electron density maps shows clearly the presence of a short peptide containing side chains with a very well resolved proline residue clearly visible in the structure (12-GYYPPG-17; Fig. 5, Fig.



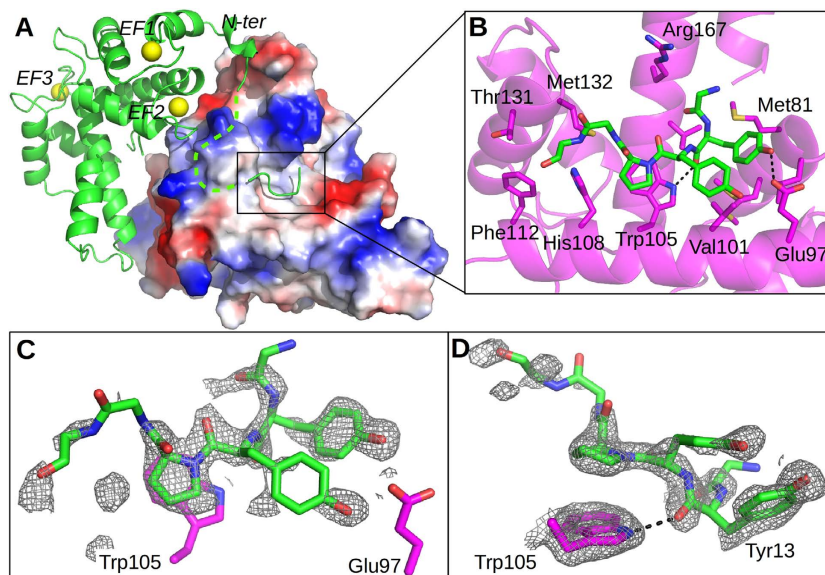


**Figure 5. Interaction between Sorcin and the N-terminal peptide.** (A) The electrostatic surface potential (blue-positive, red-negative) of CaSor dimer is shown. The hydrophobic surface corresponding to pockets 1–2 accommodates the 12-GYYPGG-17 peptide (green) plausibly belonging to an adjacent Sorcin molecule in the crystal (green cartoon); the residues 11–25 are not visible (green dashes). (B) Close-up of the peptide-binding region: the peptide is shown as green sticks, the residues interacting with the peptide are depicted as magenta sticks, and the hydrogen bonds between Trp105–Tyr17 and Glu97–Tyr17 are indicated as black dashes. (C,D) Two views of the electron density map of the peptide (2Fo-Fc, contoured at  $1\sigma$ ).

S2), belonging to a different dimer. The interacting surface between the N-terminal peptide and Sorcin was analysed using the program ePISA ([http://www.ebi.ac.uk/msd-srv/prot\\_int/cgi-bin/piserver](http://www.ebi.ac.uk/msd-srv/prot_int/cgi-bin/piserver)). The residues buried at the interface between peptide and Sorcin are: Met78, Met81, Leu82, Glu97, Ala100, Val101, Gly104, Trp105, His108 placed on the D helix; Phe112 on the EF3 loop; Thr131, Met132, on the EF4 loop; Val164, Arg167, and Asp171 on the G helix. Trp105, Glu97 and Arg167 form hydrogen bonds with Tyr13 and Tyr14 of the peptide (OH Tyr13-OE2 Glu97 = 2.78 Å; O Tyr13-NE1 Trp35 = 2.74 Å; O Tyr14-OE2 Glu97 = 2.90 Å) (Fig. 5B). The residues laying on the D helix play a major role in interacting with the N-terminal peptide; in particular, Trp105 establishes a strong stacking interaction with Pro15 and is hydrogen bonded to the carbonyl group of Tyr13, determining the orientation of the peptide into the pocket which is opposite to that of Alix in PDCD6 (see below). These residues belong to pockets 1 and 2, identified by Hotpatch analysis (Fig. 4C).

The calcium-dependent movements of the EF3 loop determine conformational changes of different extent in the PEF proteins (Fig. S3). As shown in Table 2, the opening of D and G helices opening is quite similar in zinc-bound PDCD6 complexed with Alix and CaSor complexed with the N-terminal peptide (the measured angles between the D and G helices are 78° and 82° respectively). As described by Suzuki and co-workers<sup>36</sup>, the peptide binds to two juxtaposed hydrophobic pockets (1 and 2), which hold PPYP and YP, respectively. The residues lining the pocket 1 are Gly123, Tyr124, Arg125, Thr162, Phe165, Gln172, Gly174 and the residues lining the pocket 2 are Met71, Phe72, Tyr91, Asp94, Trp95, Phe122, Gln159. More recently a third pocket has been identified in PDCD6 (Pocket 3) capable to bind the type 2 motif PXPFG present in Sec31A<sup>41</sup>. Pocket 3 is formed by residues belonging to EF1, the EF1–EF2-connecting loop, EF2, EF3 and EF4 (Phe27, Val31, Val35, Leu48, Ala51, Leu52, Ser53, Gly55, Trp57, Phe85, Val88, Trp89, Ile92, Thr93, Gln96, Phe99, Gly108, Met109, Phe148). Our structures obviously do not contain peptides bound to this pocket, but we cannot rule out the possibility of peptide binding to this site.

The superimposition between Alix-bound PDCD6 and CaSor clearly shows that these pockets are present both in both proteins, and the structural alignment reveals that many of the residues lining the pockets are conserved in Sorcin (underlined residues in Fig. 6D). In particular, relevant conserved residues are: Trp95 (Trp105, Sorcin numbering) which establishes a strong stacking interaction with the proline of the N-terminal peptide and in Sorcin was demonstrated to be necessary for the interaction with its molecular partners; Arg125 (Arg135, Sorcin numbering) whose mutation to alanine caused a loss of binding ability of PDCD6 to Alix; and Met71 (Met81, Sorcin numbering) which was demonstrated to be one of the residues changing more its SASA and that was suggested by Hotpatch analysis to be one of the residues mediating Sorcin interactions. A significant difference concerns Tyr91 that in Sorcin is substituted by Val101, allowing the interaction already described between Trp105 and Tyr13 (Figs 5B–D

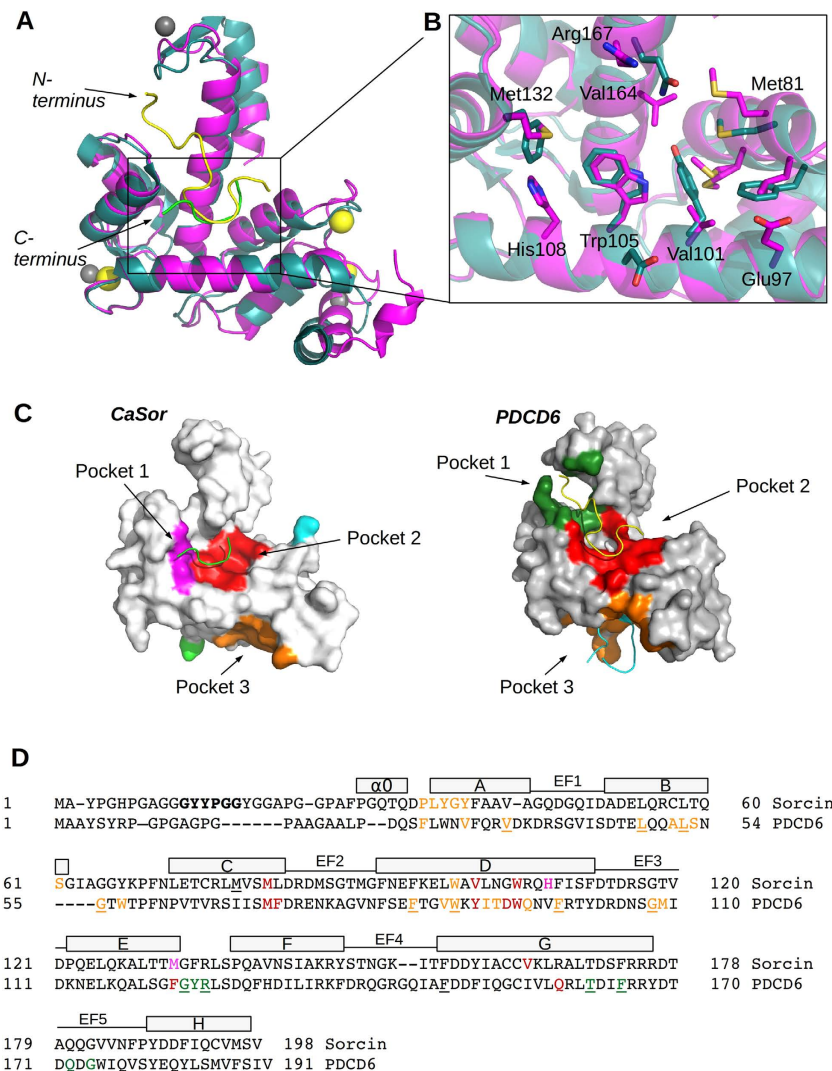


**Figure 6. Peptide binding and pockets comparison in CaSor and PDCD6.** (A) The superimposition of CaSor (magenta; calcium in yellow, peptide in green) and PDCD6 (teal; zinc in grey) in complex with Alix peptide (yellow) shows that the protein have a similar conformation and that both peptides bind in pocket 2 but in opposite direction, as indicated by arrows. (B) The main residues lining pocket 2 are shown (Sorcin numbering); note the presence of Val101 instead of Tyr91. (C) The pockets predicted by Hotpatch in CaSor (left, same color code as Fig. 4C) and the pockets found in PDCD6 (right) by co-crystallization with Alix peptide (yellow) and Sec31A peptide (cyan) are mapped on the surfaces and indicated by arrows. (D) Structural alignment of Sorcin and PDCD6. The residues corresponding to the hexapeptide are in bold. The residues lining the pockets are colored accordingly and the ones present in both sequences are underlined.

and 6B) that partially explains the opposite orientation of the N-terminal peptide in Sorcin with respect to Alix peptide in PDCD6.

Todd and coworkers showed that calpastatin interacts with residues belonging to A and C helices of the calpain-dVI in the open conformation<sup>42</sup>, corresponding to pocket 3 identified by Hotpatch analysis in Sorcin (data not shown). In particular two hydrophobic residues of calpastatin, namely Leu606 and Phe610, were found to be necessary for the interaction with calpain. The pocket where Leu606 binds is lined by several bulky aromatic residues (Phe99, Phe162 and Trp166) and a variety of other hydrophobic residues (Leu102, Leu106, Ile121 and Val125); Phe610 binds to a large hydrophobic pocket formed by the B helix and N-terminal part of the D helix and is in close van der Waals contact with residues His129 and Gln173. Two of the three aromatic residues binding calpastatin belonging to the D helix are conserved in Sorcin (Phe95, corresponding to Phe162 in calpain-dVI, and Trp105 corresponding to Trp166 in calpain-dVI), whereas the residues indicated to line the hydrophobic pocket where Leu606 of calpastatin binds are not conserved but anyway are substituted by hydrophobic residues (Leu106 is substituted by

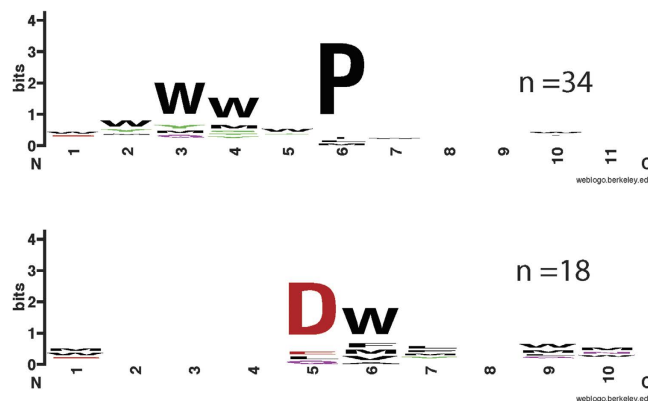


**Figure 7. WebLogo outputs of consensus peptide motifs identified through peptide phage display.**

(A) The  $\Phi$ /Gly/Met- $\Phi$ /Gly/Met-x-P motif is based on 34 unique peptide sequences, of which 20 were obtained from a phage selection performed in the presence of 1 mM  $\text{Ca}^{2+}$ . (B) The acidic- $\Phi$  motif is from 18 unique peptides of which 16 were selected in presence of  $\text{Ca}^{2+}$ .

an alanine residue, Ile121 is substituted by a leucine and Val125 is substituted by a leucine). The residues His129 and Gln173 are not conserved in Sorcin whereas also in Sorcin the B helix and N-terminal part of the D helix are lined by residues forming a hydrophobic pocket, namely Phe156 (Phe224 in calpain-dVI) and Leu102 (substituted by Ile169 in calpain-dVI).

**Phage display selection in presence of EDTA and  $\text{Ca}^{2+}$ .** To investigate if the structural changes conferred by the  $\text{Ca}^{2+}$  binding translate into specificity changes, we used Sorcin as a bait protein against a highly diverse M13 phage display library that displays 16mer peptides on the major coat protein p8. Selections were performed in the presence of EDTA (1 mM) or  $\text{Ca}^{2+}$  (1 mM) and were in both cases successful as judged by pooled phage ELISAs (i.e. signal to background  $>2$ ). Sequencing of individual clones (38 and 20 clones from the selections in presence or  $\text{Ca}^{2+}$  and EDTA, respectively) revealed that the majority of ligands contains a conserved Pro and that the main consensus motif under both conditions is a relaxed  $\Phi$ /Gly/Met- $\Phi$ /Gly/Met-x-P, where  $\Phi$ /Gly/Met is an aromatic residue (Trp, Tyr or Phe) or a Gly or Met residue, and x is any amino acid (Fig. 7A, Fig. S4). The consensus sequence agrees with the GYYPG peptide belonging to the Sorcin N-terminal domain, identified in the Sorcin binding site in our crystal structure. In addition, there is a set of peptides that lack a clear  $\Phi$ /Gly/Met- $\Phi$ /Gly/Met-x-P motif but instead hold an acidic- $\Phi$  motif (Fig. 7). Such peptides are more frequently observed in presence of  $\text{Ca}^{2+}$  (47% of sequenced peptides) than in the presence of EDTA (15% of sequenced peptides). In a cellular context, likely Sorcin can establish interactions with a variety of ligands containing the main  $\Phi$ /Gly/Met- $\Phi$ /Gly/Met-x-P motif, or the acidic- $\Phi$  motif found in intrinsically disordered regions of target proteins. Such interactions might be facilitated by the exposure of hydrophobic binding surface in Sorcin upon  $\text{Ca}^{2+}$  binding, as suggested by the structure. However, peptide binding might occur also in absence of  $\text{Ca}^{2+}$  if the preferred target is readily available as in the high avidity p8 phage display. Indeed, the presence of a high affinity ligand might shift the equilibrium towards the open conformation. Further detailed mechanistic studies should shed light on this issue.

**Selective calcium-dependent interactions between Sorcin and targets.** The interactions between Sorcin and PDCD6 (programmed cell death protein 6) (formerly called Alg-2) a member of the PEF protein family, endowed with Sorcin N-terminal consensus binding motifs was tested by both SPR and colocalization experiments. PDCD6 has a role in the mechanisms of apoptosis onset, and was shown to interact with N-terminal peptide of annexin 11 in the presence of  $50\mu\text{M}$   $\text{Ca}^{2+}$ , with a higher affinity than Sorcin<sup>43</sup>. PDCD6 has 36% identity with respect to Sorcin, displays similar structure and displays residues as Trp95 Arg125 and Met71, conserved also in Sorcin, which allow its interaction with Alix<sup>36</sup> and potentially with the sorcin N-terminal domain. Moreover, PDCD6 displays an N-terminal domain similar to that of sorcin, and containing  $\Phi$ /Gly/Met- $\Phi$ /Gly/Met-x-P sequences identified as Sorcin-interacting motifs.

SPR experiments show that both the whole Sorcin and SCBD are able to interact with PDCD6 in the presence of calcium, with a  $K_D = 3.5\mu\text{M}$  (Fig. 8A). In the presence of EDTA, SCBD interacts with PDCD6 with a  $K_D = 5\mu\text{M}$  whereas the calcium-free Sorcin interacts with PDCD6 with an even lower affinity ( $K_D = 12\mu\text{M}$  Fig. 8B). Both association and dissociation are faster in the presence of calcium than in the presence of EDTA. The N-terminus has therefore an inhibitory activity in Sorcin-PDCD6 interaction at low calcium concentrations. Additionally, both Sorcin and SCBD interact with the N-terminal domain of PDCD6, with  $K_D = 5\mu\text{M}$  for Sorcin and  $K_D = 6\mu\text{M}$  for SCBD (Fig. 8C). Partial colocalization

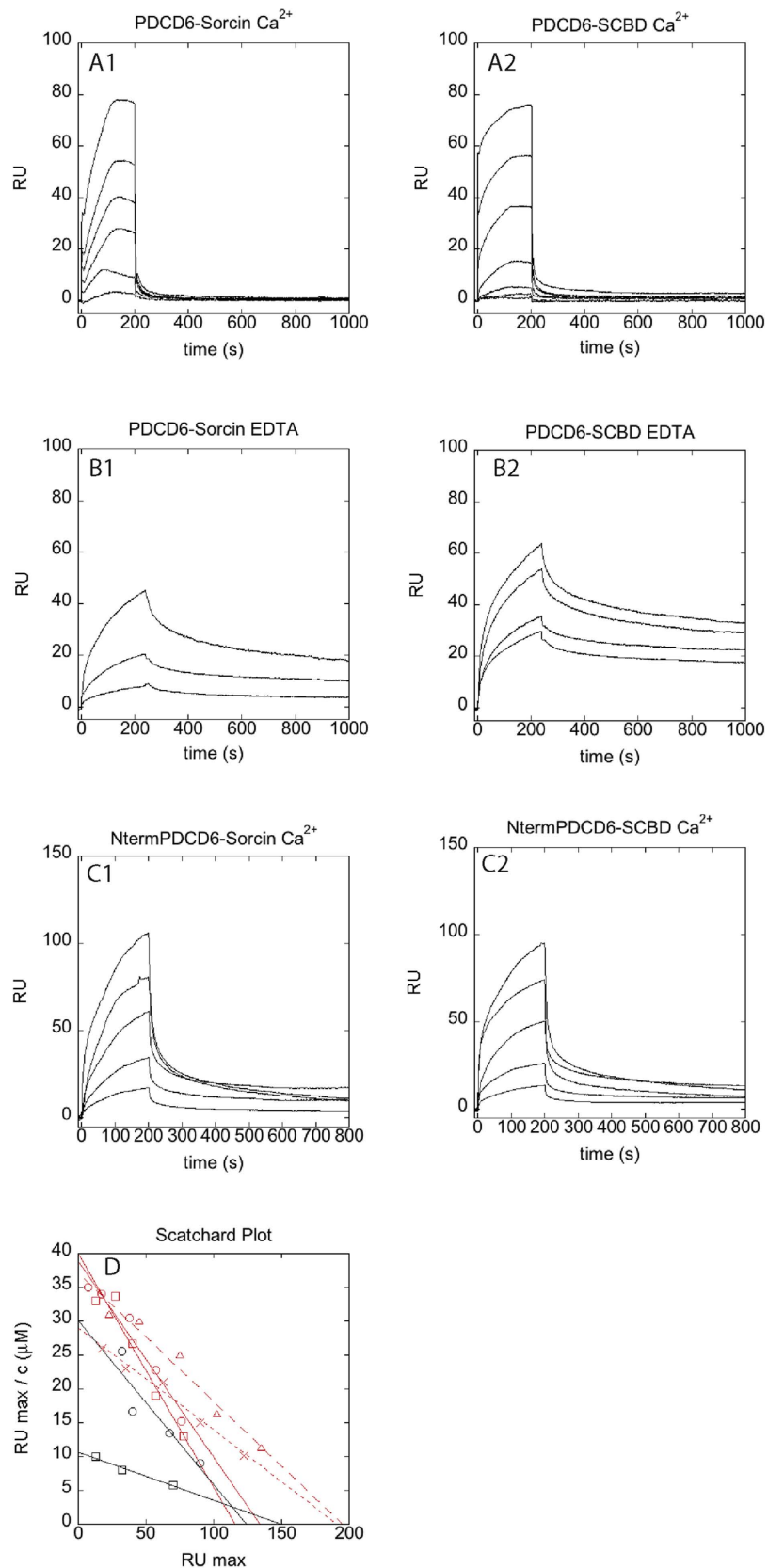


**Figure 8.** Interaction of Sorcin with full-length PDCD6 and N-terminus of PDCD6. (A) Sensorgrams showing the interaction between PDCD6, immobilized on a COOH5 chip and different concentrations of Sorcin (left panel; from bottom to top: 200 nM, 400 nM, 800 nM, 1.5  $\mu\text{M}$ , 3  $\mu\text{M}$ , 6  $\mu\text{M}$ ), and SCBD (right panel; from bottom to top: 50 nM, 100 nM, 200 nM, 500 nM, 1  $\mu\text{M}$ , 2.5  $\mu\text{M}$ , 5  $\mu\text{M}$ ), in the presence of 100  $\mu\text{M}$  calcium. (B) Sensorgrams showing the interaction between PDCD6, immobilized on a COOH5 chip and



different concentrations of Sorcin (left panel: from bottom to top: 1.3  $\mu\text{M}$ , 4  $\mu\text{M}$ , 12  $\mu\text{M}$ ), and SCBD (right panel: from bottom to top: 1.25  $\mu\text{M}$ , 2.5  $\mu\text{M}$ , 5  $\mu\text{M}$ , 10  $\mu\text{M}$ ), in the presence of 1 mM EDTA. (C) Sensorgrams showing the interaction between the N-terminal domain of PDCD6, immobilized on a COOH5 chip and different concentrations of Sorcin (left panel; from bottom to top: 750 nM, 1.5  $\mu\text{M}$ , 3  $\mu\text{M}$ , 6  $\mu\text{M}$ , 12  $\mu\text{M}$ ), and SCBD (right panel; from bottom to top: 750 nM, 1.5  $\mu\text{M}$ , 3  $\mu\text{M}$ , 6  $\mu\text{M}$ , 12  $\mu\text{M}$ ), in the presence of 100  $\mu\text{M}$  calcium. (D) Scatchard plots of the experiments in Fig. 8A–C, and linear fittings. Red squares: PDCD6-Sorcin interaction in the presence of 100  $\mu\text{M}$  calcium; red circles: PDCD6-SCBD interaction in the presence of 100  $\mu\text{M}$  calcium; black squares: PDCD6-Sorcin interaction in the presence of 1 mM EDTA; black circles: PDCD6-SCBD interaction in the presence of 1 mM EDTA; red triangles: N-terminal domain of PDCD6-Sorcin interaction in the presence of 100  $\mu\text{M}$  calcium; red crosses: N-terminal domain of PDCD6-SCBD interaction in the presence of 100  $\mu\text{M}$  calcium.

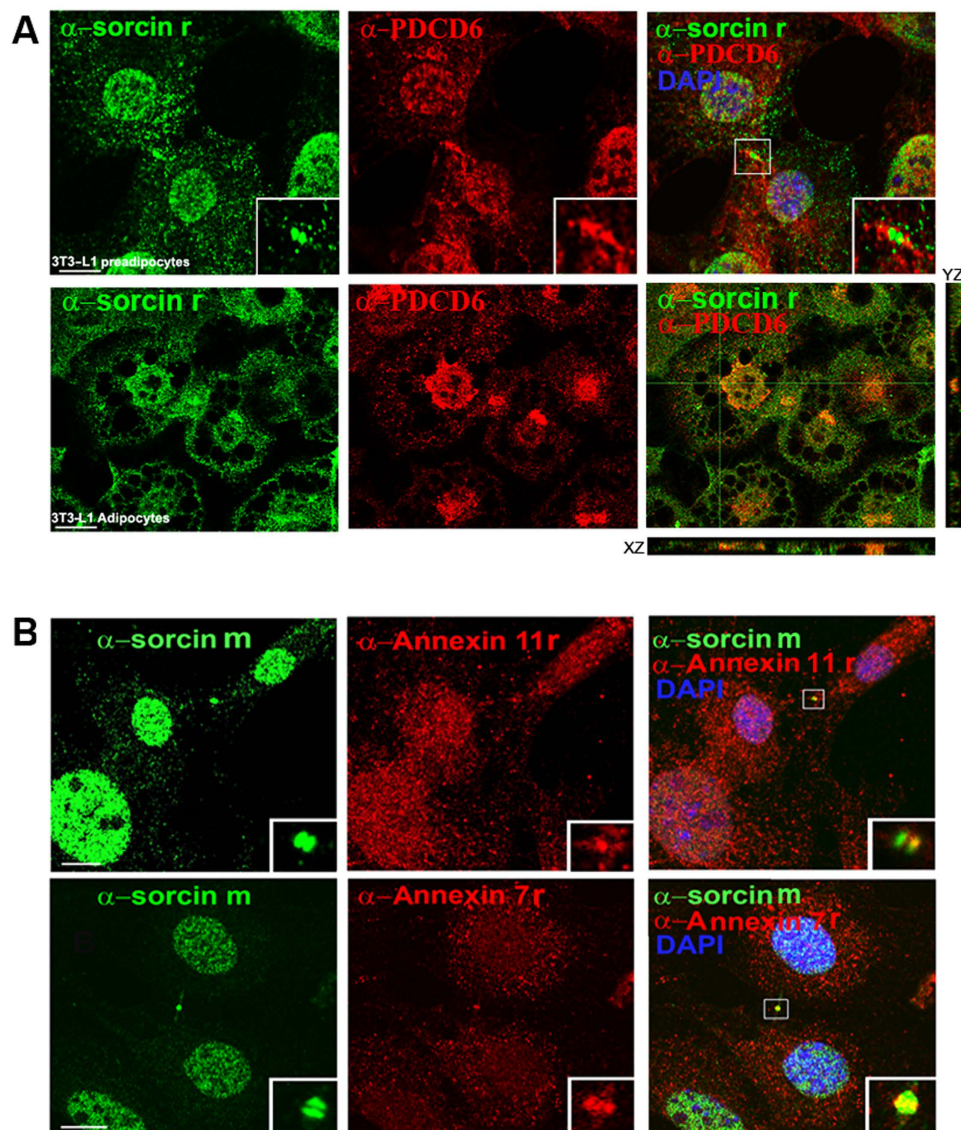


**Figure 9.** Colocalization of Sorcin with PDCD6 and annexins 7 and 11. (A) Experiments showing co-localization between sorcin (rabbit  $\alpha$ -sorcin, green) and PDCD6 (mouse  $\alpha$ -PDCD6, red), in 3T3-L1 preadipocytes in cytokinesis (top panel) and differentiated 3T3-L1 adipocytes (bottom panel) in X and Z axes. Bars: 10  $\mu\text{m}$ . Note the colocalization in the midbody of 3T3-L1 preadipocytes and in the perinuclear region of adipocytes. (B) Experiments showing co-localization between Sorcin (mouse  $\alpha$ -sorcin, green) and annexin11 (top panel: rabbit  $\alpha$ -annexin11, red), or annexin7 (bottom panel: rabbit  $\alpha$ -annexin7, red), in 3T3-L1 preadipocytes in cytokinesis. Bars: 10  $\mu\text{m}$ . Note the colocalization in the midbody (arrows and insets).

between Sorcin and PDCD6 takes place in perinuclear regions of differentiated 3T3-L1 adipocytes and in the midbody of 3T3-L1 preadipocytes (Fig. 9A). Sorcin also colocalizes with annexin 7 and annexin 11, which possess N-terminal domains containing  $\Phi$ /Gly/Met- $\Phi$ /Gly/Met-x-P sequences, in the midbody of 3T3-L1 preadipocytes (Fig. 9B).

## Discussion

Sorcin is overexpressed in several tumor cells as an adaptive mechanism to prevent ER stress and escape apoptosis triggered by chemotherapeutic agents, prompting its further investigation as a novel molecular target to overcome MDR<sup>26</sup>. The present study discloses the structural changes induced by calcium binding in Sorcin and sheds light on the mechanism of interaction of Sorcin with its molecular partners, and thereby on Sorcin-dependent regulation of cytokinesis and establishment of MDR phenotype.

The binding of calcium to Sorcin promotes a large conformational change, which involves a tilt of the D-helix with respect to the G-helix, with EF3 acting as a hinge (Fig. 3). This movement, as displayed in Table 2, is about 21° and is the highest among the PEF family members. Ca<sup>2+</sup> binds to the three high affinity calcium binding sites EF1, EF2 and EF3. Calcium binding to EF1 and EF3 causes a large reorganization of the EF hands and the consequent movement of the EF helices one in respect to the other, whereas calcium to EF2 determines only a local reorganization of the residues of the EF2 loop.

The large D-helix displacement causes the rotation of the EF1-EF2 subdomain (containing A, B, C and D helices) with respect to the EF3-EF4-EF5 subdomain (containing E, F, G and H helices). From the structure it is not possible to understand which is the calcium binding EF-hand endowed with the highest affinity. However, calcium binding studies performed in solution by spectroscopic methods on wt Sorcin and site specific mutants clearly showed that EF3 is the highest affinity site, because when Glu124 (the bidentate ligand in EF3) is mutated the affinity for calcium of the entire protein dramatically decreases<sup>33</sup>. Mutation in the bidentate Glu94 or Glu53 (placed on the EF2 and EF1 loops) has milder effects on overall Sorcin calcium affinity and on Sorcin ability of interacting with target proteins. The superimposition (Fig. 3) between the CaSor and apoSor shed light on the mechanism of Sorcin activation induced by the calcium binding to EF3: the binding of the cation promotes the movement of three calcium ligands (Asp113, Asp115 and Ser117) towards the E-helix where Glu124, the bidentate ligand (Fig. 3), is located and consequently, a large movement of the D helix with respect to the E helix (about 15°, see Table 2). This movement is transmitted to the EF1-EF2 subdomain via the Tyr 67 placed in a strategic position, in the middle of the loop connecting EF1 to EF2, and anchoring the EF1-EF2 subdomain to the EF3 loop. The binding of calcium to EF3 causes the breakage of the hydrogen bond between Asp113 (one of the calcium ligands of EF3) and Tyr67 and consequently the hC and hB helices are free to move.

The structural analysis shows that upon calcium binding there is the formation of two possible interaction sites per monomer. A site (pocket 1 + 2 in the Hotpatch analysis) is lined by residues of the C-terminal part of the D helix and residues of the EF3-hand, which in PDCD6 is the site of interaction with Alix. Another potential site (pocket 3 in the Hotpatch analysis) involves the EF1 and EF2, which in calpain-dVI bind calpastatin and in PDCD6 binds Sec31A<sup>41,42</sup>. Interestingly, the interaction with a N-terminal peptide is similar to that of the peptide bound by PDCD6, and the stacking interaction with the proline of the peptide and Trp105 is conserved between the two structures. It confirms that Trp105 is a residue with a key role in the recognition of hydrophobic Pro-containing peptides in both PEF proteins. The peptide phage display experiments confirm that Sorcin binds preferentially Pro-containing peptides. This analysis further suggests an alternative binding motif (acidic- $\Phi$ ). The interaction with the latter motif appears to be promoted by calcium binding. Positively charged residues located in the EF-loop (Arg135) and at the G-helix (Arg174, Arg175, Arg176), close to pocket 2, or His108 in pocket 1 are possibly responsible for the binding of these peptides.

Thus, Sorcin may interact via both its N-terminal domain and its SCBD domain with proteins containing the  $\Phi$ /Gly/Met- $\Phi$ /Gly/Met-x-P consensus motif, such as TRAP1, a global regulator of tumor metabolic reprogramming<sup>44</sup>, which contains a SIFYVPDMKP sequence that includes the consensus motif. In this framework, the SPR experiments carried out to study the interaction of Sorcin and SCBD with PDCD6 demonstrates that the interaction takes place via sorcin C-terminal domain, because SCBD retains the ability to interact with the target. Moreover, the SPR experiments show that the affinity between SCBD and PDCD6 is higher than between PDCD6 and Sorcin, demonstrating that the N-terminal domain partially inhibits this interaction at low, physiological calcium concentration (in the presence of EDTA). These data shed light on the possible role of different splicing version of Sorcin, which mostly differ for the length of their N-terminus, and can interact in different fashion with different targets: the short, so called mitochondrial 19-kDa Sorcin B-isoform lacks the residues 2–17 (AYPGHPGAGGGYYPGG), which include the region that, in the crystal structure, interacts with the hydrophobic calcium-dependent pocket 1. The Sorcin B-isoform may therefore be able to interact with targets with higher affinity than the A-isoform. The interaction of the N-terminal domain with the C-terminal domain of a neighbouring dimer may also be responsible for Sorcin oligomerization (Fig. 6).

Partial colocalization between Sorcin and PDCD6 takes place in perinuclear regions of differentiated 3T3-L1 adipocytes and in the midbody of 3T3-L1 preadipocytes (Fig. 9). This interaction may be important for the formation of this transient structure in the latest stage of cytokinesis. A competition between Sorcin and PDCD6 for similar targets may also take place, via pockets exposed to solvent upon calcium

binding. Interestingly PDCD6 has a mechanism of activation based on the switch of an arginine residue and this residue is conserved also in sorcin (Arg135, Sorcin numbering)<sup>36</sup>. Calcium-dependent interactions with annexin 7 and annexin 11 in the midbody may also take place with the same mechanism.

In conclusion, in this paper the Ca<sup>2+</sup>-induced conformational change in sorcin has been investigated for the first time. We demonstrate that this change involves a large movement of the D-helix, which takes place in this extent only in sorcin among PEF proteins. Moreover, the study reported here gives the unique opportunity to visualize the interaction between the two sorcin domains: SCBD and the N-terminal domain. Finally, we demonstrate that the interaction between sorcin and its molecular partners may take place via both the SCBD and N-terminal domain and that this latter domain may exert a regulative role by inhibiting in some extent the binding of sorcin to its protein targets.

## Methods

**Protein crystallization, data collection and data reduction.** Recombinant proteins (human Sorcin, SCBD and PDCD6) were expressed in pET vectors (Novagen) in *E. coli* BL21(DE3) cells, purified according to published procedures<sup>18</sup> and dialysed in 20 mM Tris-HCl, at pH 7.5. Automated crystallization screening and by-hand optimization were carried out at 298 K by the hanging-drop vapor diffusion method. Since sorcin precipitates when it is saturated with calcium, we performed the starting crystallization trials with commercial screens adding 5 mM CaCl<sub>2</sub> in the reservoir before mixing the crystallization drops. ApoSor resulted to be rather prone to crystallization even in the presence of calcium; therefore, in order to discriminate between apoSor and CaSor crystals we performed all the crystallization trials in double, with and without calcium. The apoSor crystallization trials were performed using a protein sample concentrated to about 10 mg/ml. Aliquots (1 μl) of the protein sample were mixed with an equal amount of reservoir solution containing 20–22% (w/v) polyethylene glycol 4000, 0.3–0.5 M ammonium sulfate. Crystals grew in 2 weeks and reached dimensions of 0.1 mm × 0.2 mm × 0.3 mm.

Crystals of CaSor were obtained by mixing 1 μl of protein solution, concentrated to about 15 mg/ml, using a reservoir solution containing: 20–25% (w/v) polyethylene glycol 3350, 0.5 M lithium sulfate, 0.1 M Tris-HCl at pH = 8.5 and 5 mM CaCl<sub>2</sub>. For data collection, apoSor and CaSor were cryo-protected in a solution containing 80% (v/v) of mother liquor and 20% (v/v) polyethylene glycol 200. The crystals were mounted in nylon loops and flash frozen by quick submersion into liquid nitrogen and transported to the synchrotron-radiation source. Single-wavelength data sets ( $\lambda = 1 \text{ \AA}$ ) were collected from crystals of apoSor and CaSor at the 5.2R beamline of the Synchrotron Radiation Source ELETTRA (Trieste, Italy), using a Pilatus 2M detector at a temperature of 100 K. The data sets were processed with XDS<sup>45</sup> and scaled with XSCALE<sup>45</sup>. Crystal parameters and data collection statistics for the measured crystals are listed in Table 1.

**Structure solution and refinement.** The structure of apoSor was determined by molecular replacement with the program MOLREP<sup>46</sup> (CCP4 suite) using the structure of the calcium-free human Sorcin (PDB entry 1JUO)<sup>31</sup> as search model.

The case of CaSor was more complex: first we solved the structure of SCBD (Sorcin Calcium Binding Domain) with calcium (Ca-SCBD, data not shown), using the structure of the calcium-free human Sorcin; then we used SCBD monomer to solve CaSor. Ca-SCBD crystallized in orthorhombic space group and the Matthews coefficient calculation indicated a dimeric asymmetric unit. The first attempts to solve the phase problem for Ca-SCBD using the whole apo-Sorcin dimer were unsuccessful, suggesting a wide conformational variation. Based on previous published results we expected that the variation regarded mainly the EF1–2–3 subdomain. For this reason we performed the rotational and translational searches with a truncated apo-dimer including E-F-G-H helices (EF4–5 plus part of EF3), finding a partial solution. We fixed this solution and repeated the search using the rest of the apo-model (helices A, B, C, D). Refinements were performed using the maximum-likelihood method with the program REFMAC<sup>47</sup> and model building with the program Coot<sup>48</sup>. The quality of the models was assessed using the program PROCHECK<sup>49</sup>. The structure of apoSor was refined to 2.1 Å resolution. The final model contains 168 residues (residues 30–198), 73 water molecules, 5 sulfate ions. The structure of CaSor was refined to 1.65 Å resolution. The final model contains 172 residues (residues 26–198), a six residues long peptide, 124 water molecules, 1 sulfate ion, 3 Ca(II) ions with full occupancy and 3 PEG molecules for each monomer.

**PDB accession codes.** The coordinates for apoSor have been deposited in the Research Collaboratory for Structural Bioinformatics (RCSB) PDB with accession code 4UPG. The coordinates for CaSor have been deposited in the RCSB PDB with accession code 4USL.

**Phage Display.** We used a phage library displaying 16mer randomized peptides (diversity  $4 \times 10^{10}$ ) on the p8 protein flanked by spacer linkers at the N- and C- termini (SSSG- and GGGSGG, respectively). The library is similar to the previously established C-terminal library<sup>50</sup>, but displaying internal, instead of C-terminal, peptide stretches. Phage selections were performed in 5 rounds following the detailed protocols in ref. 51. To assess a potential calcium dependence of the interactions selections were performed in parallel using either 1 mM EDTA or 1 mM CaCl<sub>2</sub> during the incubation of the phage library with the



bait protein as well as in all washing steps. Such an approach has previously been successfully used for the identification of calcium-dependent interactions for the calcium-binding protein S100B<sup>52</sup>. Clonal analysis and sequencing was performed as previously described<sup>53</sup>.

**Cell cultures.** Mouse 3T3-L1 preadipocytes (ATCC<sup>R</sup> CL-173<sup>TM</sup>, American Type Culture Collection) and 3T3-L1 adipocytes were grown on plastic dishes or 10-mm glass coverslips using Dulbecco's modified Eagle's medium supplemented with 10% calf serum, 4 mM glutamine, 50 mg/l streptomycin, 100 IU/l penicillin and non-essential amino acids at 37 °C in a humidified CO<sub>2</sub> incubator. 3T3-L1 preadipocytes were differentiated into adipocytes as described by Tafuri, adding 7.5 μM troglitazone in the medium on days 3 and 4 of differentiation<sup>54</sup>.

The mouse α-Sorcin (33–800) was from Zymed, the rabbit α-Sorcin was homemade, the rabbit α-annexin 11 (NB100–78588) was from Novus Biologicals, the rabbit α-annexin 7 (ABIN65268) and the mouse α-PDCD6 (H00010016-M01) were from Abnova.

For immunofluorescence staining, cells were plated and grown on 10 mm glass coverslips, fixed with 2% paraformaldehyde for 20 min, permeabilized with 0.2% Triton X-100 for 10 min and incubated in 50 mM glycine for 30 min more. Primary antibody dissolved in 1% bovine serum albumin was added and allowed to incubate overnight at 4 °C. Primary antibody was removed, wells washed and secondary AlexaFluor 488, 594 or 647 was added and incubated for 1 h at room temperature. Conventional immunofluorescence and confocal microscopy were performed using confocal LSM710 vertical and Axiovert135M microscope (Zeiss).

**Surface Plasmon Resonance experiments.** Surface Plasmon Resonance (SPR) experiments were carried out using a SensiQ Pioneer system. The sensor chip (COOH5) was activated chemically by a 35 μl injection of a 1:1 mixture of N-ethyl-N'-(3-(diethylaminopropyl)carbodiimide (200 mM) and N-hydroxysuccinimide (50 mM) at a flow rate of 5 μl/min. Ligands, i.e. PDCD6 and the N-terminal domain of PDCD6 (KMAAYSYPGPGAGPGPAAGAALP; a lysine residue has been added to the sequence to ensure peptide immobilization principally via the N-terminus), were immobilized on activated sensor chips via amine coupling. The immobilizations were carried out in 20 mM sodium acetate at pH 4.5; the remaining ester groups were blocked by injecting 1 M ethanolamine hydrochloride (35 μl). Proteins interacting with the ligands (in 10 mM Hepes pH 7.4, 150 mM NaCl + 0.005% surfactant P20) were injected on the sensor chip at a constant flow (30 μl/min). The same procedure was set using the buffer with CaCl<sub>2</sub> at 100 μM concentration, or with 1 mM EDTA. The increase in RU relative to baseline indicates complex formation; the plateau region represents the steady-state phase of the interaction, whereas the decrease in RU represents dissociation of Sorcin or SCBD from immobilized ligands after injection of buffer. Regeneration procedures are based on two long (2000 s and 500 s) injections of buffer, separated by a brief (5 s) injection of 10 mM NaOH. The sensorgrams were analysed using the SensiQ Qdat program.

## References

- Colotti, G. *et al.* Sorcin, a calcium binding protein involved in the multidrug resistance mechanisms in cancer cells. *Molecules* **19**, 13976–89 (2014).
- Nagpal, J. K. & Das, B. R. Identification of differentially expressed genes in tobacco chewing-mediated oral cancer by differential display-polymerase chain reaction. *Eur J Clin Invest* **37**, 658–64 (2007).
- Pomeroy, S. L. *et al.* Prediction of central nervous system embryonal tumour outcome based on gene expression. *Nature* **415**, 436–42 (2002).
- Yokota, T. *et al.* Identification of histological markers for malignant glioma by genome-wide expression analysis: dynein, alpha-PiX and sorcin. *Acta Neuropathol* **111**, 29–38 (2006).
- Zhao, P. *et al.* Comparative proteomic analysis of anti-benzo(a)pyrene-7,8-dihydrodiol-9,10-epoxide-transformed and normal human bronchial epithelial G0/G1 cells. *Chem Biol Interact* **186**, 166–73 (2010).
- Deng, L. *et al.* Upregulation of soluble resistance-related calcium-binding protein (sorcin) in gastric cancer. *Med Oncol* **27**, 1102–8 (2010).
- Meyers, M. B., Schneider, K. A., Spengler, B. A., Chang, T. D. & Biedler, J. L. Sorcin (V19), a soluble acidic calcium-binding protein overproduced in multidrug-resistant cells. Identification of the protein by anti-sorcin antibody. *Biochem Pharmacol* **36**, 2373–80 (1987).
- Qu, Y., Yang, Y., Liu, B. & Xiao, W. Comparative proteomic profiling identified sorcin being associated with gemcitabine resistance in non-small cell lung cancer. *Med Oncol* **27**, 1303–8 (2010).
- Van der Bliek, A. M. *et al.* Genes amplified and overexpressed in human multidrug-resistant cell lines. *Cancer Res* **48**, 5927–32 (1988).
- Yang, Y. X., Chen, Z. C., Zhang, G. Y., Yi, H. & Xiao, Z. Q. A subcellular proteomic investigation into vincristine-resistant gastric cancer cell line. *J Cell Biochem* **104**, 1010–21 (2008).
- Zhou, Y. *et al.* Sorcin, an important gene associated with multidrug-resistance in human leukemia cells. *Leuk Res* **30**, 469–76 (2006).
- He, Q. *et al.* Overexpression of sorcin results in multidrug resistance in gastric cancer cells with up-regulation of P-gp. *Oncol Rep* **25**, 237–43 (2011).
- Kawakami, M. *et al.* Knock-down of sorcin induces up-regulation of MDR1 in HeLa cells. *Biol Pharm Bull* **30**, 1065–73 (2007).
- Fowler, M. R. *et al.* Complex modulation of L-type Ca<sup>2+</sup> current inactivation by sorcin in isolated rabbit cardiomyocytes. *Pflügers Arch* **457**, 1049–60 (2009).
- Fowler, M. R., Colotti, G., Chiancone, E., Smith, G. L. & Fearon, I. M. Sorcin modulates cardiac L-type Ca<sup>2+</sup> current by functional interaction with the alpha1C subunit in rabbits. *Exp Physiol* **93**, 1233–8 (2008).



16. Franceschini, S. *et al.* Molecular basis for the impaired function of the natural F112L sorcin mutant: X-ray crystal structure, calcium affinity, and interaction with annexin VII and the ryanodine receptor. *FASEB J* **22**, 295–306 (2008).
17. Matsumoto, T. *et al.* Sorcin interacts with sarcoplasmic reticulum Ca(2+)-ATPase and modulates excitation-contraction coupling in the heart. *Basic Res Cardiol* **100**, 250–62 (2005).
18. Meyers, M. B. *et al.* Calcium-dependent translocation of sorcin to membranes: functional relevance in contractile tissue. *FEBS Lett* **357**, 230–4 (1995).
19. French, P. J. *et al.* Gene expression profiles associated with treatment response in oligodendrogliomas. *Cancer Res* **65**, 11335–44 (2005).
20. Shai, R. *et al.* Gene expression profiling identifies molecular subtypes of gliomas. *Oncogene* **22**, 4918–23 (2003).
21. Sun, L. *et al.* Neuronal and glioma-derived stem cell factor induces angiogenesis within the brain. *Cancer Cell* **9**, 287–300 (2006).
22. Lalioti, V. S. *et al.* Sorcin links calcium signaling to vesicle trafficking, regulates Polo-like kinase 1 and is necessary for mitosis. *PLoS One* **9**, e85438 (2014).
23. Lokuta, A. J., Meyers, M. B., Sander, P. R., Fishman, G. I. & Valdivia, H. H. Modulation of cardiac ryanodine receptors by sorcin. *J Biol Chem* **272**, 25333–8 (1997).
24. Zamparelli, C. *et al.* Activation of the cardiac Na(+)-Ca(2+) exchanger by sorcin via the interaction of the respective Ca(2+)-binding domains. *J Mol Cell Cardiol* **49**, 132–41 (2010).
25. Hu, Y. *et al.* Inhibition of sorcin reverses multidrug resistance of K562/A02 cells and MCF-7/A02 cells via regulating apoptosis-related proteins. *Cancer Chemother Pharmacol* **72**, 789–98 (2013).
26. Maddalena, F. *et al.* Sorcin induces a drug-resistant phenotype in human colorectal cancer by modulating Ca(2+) homeostasis. *Cancer Res* **71**, 7659–69 (2011).
27. Pack-Chung, E. *et al.* Presenilin 2 interacts with sorcin, a modulator of the ryanodine receptor. *J Biol Chem* **275**, 14440–5 (2000).
28. Woods, W. S. *et al.* Conformation-specific binding of alpha-synuclein to novel protein partners detected by phage display and NMR spectroscopy. *J Biol Chem* **282**, 34555–67 (2007).
29. Maki, M., Kitaura, Y., Satoh, H., Ohkouchi, S. & Shibata, H. Structures, functions and molecular evolution of the penta-EF-hand Ca<sup>2+</sup>-binding proteins. *Biochim Biophys Acta* **1600**, 51–60 (2002).
30. Ilari, A. *et al.* The crystal structure of the sorcin calcium binding domain provides a model of Ca<sup>2+</sup>-dependent processes in the full-length protein. *J Mol Biol* **317**, 447–58 (2002).
31. Xie, X., Dwyer, M. D., Swenson, L., Parker, M. H. & Botfield, M. C. Crystal structure of calcium-free human sorcin: a member of the penta-EF-hand protein family. *Protein Sci* **10**, 2419–25 (2001).
32. Colotti, G. *et al.* The W105G and W99G sorcin mutants demonstrate the role of the D helix in the Ca(2+)-dependent interaction with annexin VII and the cardiac ryanodine receptor. *Biochemistry* **45**, 12519–29 (2006).
33. Mella, M. *et al.* Information transfer in the penta-EF-hand protein sorcin does not operate via the canonical structural/functional pairing. A study with site-specific mutants. *J Biol Chem* **278**, 24921–8 (2003).
34. Zamparelli, C. *et al.* Structure-function relationships in sorcin, a member of the penta EF-hand family. Interaction of sorcin fragments with the ryanodine receptor and an Escherichia coli model system. *Biochemistry* **39**, 658–66 (2000).
35. Maki, M. ESCRT and calpain—old and new relationships. *FEBS J* **279**, 1398 (2012).
36. Suzuki, H. *et al.* Structural basis for Ca<sup>2+</sup>-dependent formation of ALG-2/Alix peptide complex: Ca<sup>2+</sup>/EF3-driven arginine switch mechanism. *Structure* **16**, 1562–73 (2008).
37. Blanchard, H. *et al.* Structure of a calpain Ca(II)-binding domain reveals a novel EF-hand and Ca(II)-induced conformational changes. *Nat Struct Biol* **4**, 532–8 (1997).
38. Pettit, F. K., Bare, E., Tsai, A. & Bowie, J. U. HotPatch: a statistical approach to finding biologically relevant features on protein surfaces. *J Mol Biol* **369**, 863–79 (2007).
39. Partha, S. K., Ravulapalli, R., Allingham, J. S., Campbell, R. L. & Davies, P. L. Crystal structure of calpain-3 penta-EF-hand (PEF) domain - a homodimerized PEF family member with calcium bound at the fifth EF-hand. *FEBS J* **281**, 3138–49 (2014).
40. Jia, J., Tarabykina, S., Hansen, C., Berchtold, M. & Cygler, M. Structure of apoptosis-linked protein ALG-2: insights into Ca<sup>2+</sup>-induced changes in penta-EF-hand proteins. *Structure* **9**, 267–75 (2001).
41. Takahashi, T. *et al.* Structural analysis of the complex between penta-EF-hand ALG-2 protein and Sec31A peptide reveals a novel target recognition mechanism of ALG-2. *International journal of molecular sciences*, **16**, 3677–3699 (2015).
42. Todd, B. *et al.* A structural model for the inhibition of calpain by calpastatin: crystal structures of the native domain VI of calpain and its complexes with calpastatin peptide and a small molecule inhibitor. *J Mol Biol* **328**, 131–46 (2003).
43. Satoh, H., Shibata, H., Nakano, Y., Kitaura, Y. & Maki, M. ALG-2 interacts with the amino-terminal domain of annexin XI in a Ca(2+)-dependent manner. *Biochem Biophys Res Commun* **291**, 1166–72 (2002).
44. Chae, Y. C. *et al.* Landscape of the mitochondrial Hsp90 metabolome in tumours. *Nat Commun* **4**, 2139 (2013).
45. Kabsch, W. Xds. *Acta Crystallographica Section D-Biological Crystallography* **66**, 125–132 (2010).
46. Vagin, A. & Teplyakov, A. MOLREP: an automated program for molecular replacement. *Journal of Applied Crystallography* **30**, 1022–1025 (1997).
47. Murshudov, G. N., Vagin, A. A. & Dodson, E. J. Refinement of macromolecular structures by the maximum-likelihood method. *Acta Crystallographica Section D-Biological Crystallography* **53**, 240–255 (1997).
48. Emsley, P. & Cowtan, K. Coot: model-building tools for molecular graphics. *Acta Crystallographica Section D-Biological Crystallography* **60**, 2126–2132 (2004).
49. Laskowski, R. A., Moss, D. S. & Thornton, J. M. Main-Chain Bond Lengths and Bond Angles in Protein Structures. *Journal of Molecular Biology* **231**, 1049–1067 (1993).
50. Tonikian, R. *et al.* A specificity map for the PDZ domain family. *Plos Biology* **6**, 2043–2059 (2008).
51. Huang, H. M. & Sidhu, S. S. Studying Binding Specificities of Peptide Recognition Modules by High-Throughput Phage Display Selections. *Network Biology: Methods and Applications* **781**, 87–97 (2011).
52. Vetter, S. W. Phage display selection of peptides that target calcium-binding proteins. *Methods Mol Biol* **963**, 215–35 (2013).
53. Rajan, S. & Sidhu, S. S. Simplified synthetic antibody libraries. *Methods Enzymol* **502**, 3–23 (2012).
54. Tafuri, S. R. Troglitazone enhances differentiation, basal glucose uptake, and Glut1 protein levels in 3T3-L1 adipocytes. *Endocrinology* **137**, 4706–12 (1996).

## Acknowledgements

The combinatorial peptide phage display library was generously provided by Dr. Sachdev S. Sidhu (The Donnelly Centre, University of Toronto). The X-ray diffraction experiments were supported by the “Italian funded users” program of the ELETTRA-Synchrotron Trieste S.C.p.A. The staff of the XRD1 beamline at ELETTRA (Trieste) where the data have been collected, is gratefully acknowledged. “Quality methods for Design of Experiments in Scientific Research”, in the FaReBio di Qualità Project: Quality and Project Management OpenLab qPMO CNR, CNCCS CNR (National Collection of Chemical Compounds and

Screening Center 2015), the CNR InterOmics Flagship project, the Flagship Project Nanomax: “NADINE: NAnotechnology-based Diagnostic In Neurological disease and Experimental oncology”, and CNR-CSIC Bilateral Italy-Spain to GC are acknowledged. YI was supported by grants from the Swedish Research Council and AkeWiberg’s foundation.

### Author Contributions

G.C., I.G. and E.P. purified the proteins and performed the SPR experiments. A.I. and A.F. solved the X-ray structures and performed structural analysis. G.N.S. and Y.I. performed Phage Display experiments. V.L. performed co-localization experiments. G.C., A.I., Y.I. and A.F. analyzed the data. G.C., A.I. and A.F. wrote the manuscript. All authors reviewed the manuscript.

### Additional Information

**Supplementary information** accompanies this paper at <http://www.nature.com/srep>

**Competing financial interests:** The authors declare no competing financial interests.

**How to cite this article:** Ilari, A. *et al.* Structural basis of Sorcin-mediated calcium-dependent signal transduction. *Sci. Rep.* **5**, 16828; doi: 10.1038/srep16828 (2015).



This work is licensed under a Creative Commons Attribution 4.0 International License. The images or other third party material in this article are included in the article’s Creative Commons license, unless indicated otherwise in the credit line; if the material is not included under the Creative Commons license, users will need to obtain permission from the license holder to reproduce the material. To view a copy of this license, visit <http://creativecommons.org/licenses/by/4.0/>